Gabriel Plank — Dixie Valley thesis draft 1998

TABLE OF CONTENTS

ILLUSTRATIONS

PHOTOGRAPHIC PLATES

ABSTRACT

The Stillwater escarpment is the rugged, southeast-facing flank of the Stillwater Range, between Mississippi Canyon and Fencemaker Pass. It straddles Pershing and Churchill Counties at the north end of Dixie Valley, in north-central Nevada. The Dixie Valley Geothermal Area (DVGA) is the area of Dixie Valley adjacent to the Stillwater escarpment. A heat source of unknown origin manifests itself in the DVGA through fumaroles, hot springs, hot wells, and high heat flow. Since 1988 the area has supported a 62 megawatt geothermal electricity plant, the largest in Nevada. Geothermal fluids which drive the electrical turbines are extracted from the Dixie Valley fault at depths of around 2450 meters and then reinjected at similar depths to areas proximal to the fault.

Above the producing geothermal field in northern Dixie Valley, the geology of the Stillwater escarpment is very well exposed, and reveals a complicated geologic history. Early Mesozoic tectonic contraction, associated with the Fencemaker thrust, placed pelitic rocks of the Fumarole Canyon sequence over Star Peak Group carbonates (D1). A regional penetrative cleavage (S1) formed during this event. The penetrative cleavage is similar in orientation in both the upper and lower plates of the thrust, and is sub-parallel to the ductile shear zone of the Fencemaker thrust. Post-Fencemaker, west-directed tectonic contraction (D2), possibly along the Willow Creek thrust, reoriented D1 structures. A final, unknown deformational event (D3) created a regional crenulation cleavage (S3). During Oligocene and Miocene time, silicic ash flow tuffs, basalt flows, and lake sediments, as well as basaltic dikes, capped and intruded the Mesozoic units. Sometime after the intrusion of the basaltic dikes (≈14.5 Ma), the Mesozoic and Tertiary strata were offset down and to the southeast, by faulting along the Black Canyon fault, and other associated east-to-west-trending faults (D_{4A}). Later, low-angle displacement along the Boyer fault (D_{4B}) truncated, but probably occurred syntectonically with, the Black Canyon fault.

The modern geologic setting of the Stillwater escarpment is dominated by the Dixie Valley fault system. The Dixie Valley fault is the active rangefront fault. The fault lies within a broader zone of active seismicity known as the Central Nevada Seismic

Belt (CNSB). Historic ruptures of the Dixie Valley fault (as well as the Fairview Peak fault to the south, and the Pleasant Valley fault to the north) have occurred within the last one-hundred years. The main faults within the Dixie Valley fault system include the Dixie Valley fault, two semi-active faults (Granite/Gabbro fault, fault V), and a series of inactive fault splays (faults RF2, RF3, RF4, RF5, and RF6). The inactive splays are the oldest faults within the system, and are exposed along the Stillwater escarpment. The semi-active faults are younger than the rangefront splays, but are not exposed at the surface.

The subsurface of Dixie Valley contains the same Mesozoic and Tertiary rocks that are exposed ~~along~~ the Stillwater ~~escarpment.~~ Fluid circulation in the geothermal reservoir, ~~beneath the producing geothermal field,~~ is controlled by ~~permeable faults and fractures, within brittle rocks. The~~ permeable faults include those related to the Dixie Valley fault system, ~~The~~ brittle rocks include Boyer Ranch quartz arenite and gabbroic rocks of the Humboldt igneous complex.

~~The total permeability over a given area of brittle rocks is loosely defined by the number of permeable faults in that area.~~ The ~~total~~ number of faults in a given area ~~are~~ controlled, ~~in turn,~~ by ~~the~~ ramp-flat geometry of the Dixie Valley fault surface. A major fault-flat cuts through incompetent Triassic pelitic rocks ~~that are~~ in the footwall of the Dixie Valley fault. Fault-ramps occur where the Dixie Valley fault cuts across competent rocks of the Boyer Ranch Formation, Humboldt igneous complex, Star Peak Group, and possibly the Koipato Group. The number of permeable subsidiary faults increases in proximity to the major fault-flat. Total permeability is therefore highest in proximity to the fault-flat.

The Stillwater ~~escarpment~~, above the producing geothermal field, contains an uplifted segment of the major fault-flat, ~~that is responsible for the high relative permeability of the northern part of the DVGA~~. Incompetent Triassic rocks, ~~exposed~~ in the rangefront, delineate the maximum exposed extent of the uplifted fault-flat. Inactive, rangefront fault splays also delineate the along-strike length of the flat. Where the uplifted fault-flat dies out, the Dixie Valley fault surface becomes a lateral ramp. This predicts that permeability decreases NE and SW of the exposed Triassic pelitic rocks.

AUTHOR'S PREFACE

Since the oil crisis of the mid-1970's, the Basin and Range Province has been the target of governmentally subsidized industrial development of geothermal electricity plants. The national budget for subsidizing of the geothermal industry peaked at around 200 million dollars in the early eighties, and today hovers at around 20 million dollars. The growth history of the industry has depended mainly on the economics of oil and gas, secondarily on the political stability of the Middle East, and lastly on national concern for the preservation this country's natural resources.

Today in the state of Nevada, geothermal power plants account for about five minutes of every hour of electricity produced. There are ten geothermal power plants ranging in output from around 5 Megawatts (Mw) up to 60 Mw. The sustainability of these plants depends on two factors. First, utilities must be willing to purchase the geothermal electricity for a relatively high price as compared with oil, gas, or coal power. Typically the purchase is subsidized either directly or indirectly by the U.S. government. Secondly, the natural geothermal reservoir from which fluids are extracted must be maintained in volume, pressure, and temperature or wells may cease to produce. Exploration and drilling to acquire new production wells are costly, often beyond the value of the returns. A geothermal company thus must devote a share of funds towards earth science and the understanding of the dynamics of the natural hydrothermal system.

Dixie Valley, Nevada, is a classic example of a typical Basin and Range fault-bounded basin, or graben, which supports a large, long-lived hydrothermal system. The Dixie Valley geothermal power plant, the largest and most remote in Nevada, has drawn and replenished fluids from and into this hydrothermal system since 1988. The fluids are extracted from the subsurface where deep (≈2500 m) wells intersect the Dixie Valley normal fault system. Ideally, a complete understanding of the mechanics of the subsurface geothermal reservoir in Dixie Valley would foster a completely renewable power source. One would know exactly where to extract fluids, how much to extract, and where to reinject them. In practice, more energy is being sapped from the source than is naturally resupplied. Over a period years, all reservoirs typically deteriorate from

geothermal development. The uncertainty which arises in trying to manipulate a complicated natural hydrothermal system is impossible to overcome and results in inefficiency.

In a recent effort to sustain the geothermal resource in Dixie Valley, the industry and federal government have charged many groups of earth scientists with the interdisciplinary task of characterizing this hydrothermal system. This study describes the lithology and fault orientation in the exposed foot wall of the Dixie Valley fault (the Stillwater escarpment); and by doing so, infers the downdip character of the same rocks in the hanging wall of the Dixie Valley fault. However, the work herein presented represents not only the approach and work of one group, but includes the data of many diversified studies.

1 draft 2

STRATIGRAPHY AND STRUCTURAL GEOLOGY OF THE STILLWATER ESCARPMENT, ABOVE THE DIXIE VALLEY GEOTHERMAL SITE

1.1. INTRODUCTION

This chapter presents the detailed bedrock geology of the Stillwater Range, along the section of the range front that lies above the geothermal production field in northern Dixie Valley. As well, it discusses the regional tectonic implications of the geology, based upon new and detailed mapping. In chapter two (2), the surface geology is tied in with the subsurface geology of the Dixie Valley basement, that constitutes the hanging wall of the Dixie Valley fault. Geologic cross sections through both the footwall and hanging wall of the Dixie Valley fault are provided to show the relationships of the geology in both fault-blocks. Chapter two also discusses some aspects of geothermal production that may be influenced by the subsurface geology, with emphasis on the relative permeability of certain rocks and structures.

Project Overview. The success of geothermal power generation depends ultimately on the thermal and hydrostatic conditions of the geothermal reservoir from which fluids are extracted. In monitoring and managing those reservoir conditions, constant attention is given to fluid chemistry, wellhead pressure and temperature, and the state of surface geothermal features. The most useful details of the hydrodynamic properties of a fluid system are yielded by studying the geologic setting of the reservoir. Yet, in the Dixie Valley Geothermal Area (DVGA), the geology has been the least well understood factor. The purpose of this project is, thus, to better characterize the subsurface stratigraphy and structural geology of the geothermal reservoir beneath the DVGA.

Project Scope. The Mesozoic bedrock in the down-dropped block, or hanging wall, of the Dixie Valley fault, contains hydraulically conductive faults and fractured rocks. The distribution of these permeable structures and rocks dictates where fluids circulate, and ultimately controls the shape of the hydrothermal system. By identifying the subsurface

distribution of faults and rocks that are easily fractured, it is the ultimate goal of this project to be an aid in mapping fluid flow; identifying extraction and injection targets; and understanding the natural recharge of the hydrothermal system. In addition, a further objective of this study is to understand better the tectonic processes that, since Early Mesozoic time, have shaped the regional geology.

General Methods. This study combines detailed geologic mapping, surface geophysics, and borehole geology to produce accurate cross sections through both the footwall and hanging wall of the Dixie Valley fault. In theory, the exposed footwall of the Dixie Valley normal fault, along the eastern front of the Stillwater Range, is a mirror image of the down-dropped and buried hanging wall. Structures that are exposed in the footwall can therefore be inferred to exist, down-dip, in the hanging wall of the Dixie Valley fault. This relationship means that knowledge of the surface geology can be used to constrain interpretations of the subsurface geology. The investigation of the surface geology begins with detailed mapping of the footwall, that is the Stillwater Range, at a scale of 1:12,000. Cross-sections of the footwall geology are then created from the map data (Plate 1). To assemble a picture of the geology of the hanging wall, the cross-sections, and structures therein, are projected into the subsurface by moving them (graphically) down-dip, along a system of high angle faults, whose orientations are inferred from seismic reflection profiles and wellbore data. The final cross sections display the footwall geology next to the corresponding subsurface geology (Chapter 2, Plate 2).

Procedures. Geologic mapping of the footwall, or Stillwater escarpment, above the DVGA was accomplished between October 1995 and August 1996. The geology was mapped, with the aid of 1:24,000-scale color-infrared aerial photographs, on four 7.5-minute topographic basemaps at a scale of 1:12,000. Standard cross-sectional analysis of the footwall structural geology followed after completion of the map. Some thin-section analysis—mainly of dikes and small intrusions—followed after completion of the map, so that existing radiometric dates could be applied to a large number of petrographically similar rocks.

Reprocessing of Dixie Valley seismic reflection lines was carried out during the Fall of 1996 and Spring of 1997 by myself and the Consortium for Economic Migration and

Tomography (CEMAT) at the University of Nevada, Reno. The seismic data—and, in addition, borehole lithologic logs, cuttings, and geophysical and survey logs—were also made available by Oxbow Inc. Compilation of borehole geologic data was an ongoing process throughout the course of the study. These seismic and borehole data were assembled into rough geologic cross-sections of the hanging wall. In the final phase, cross-sections from both the footwall and the hanging wall were combined, to demonstrate the geologic relationships between the upper and lower fault blocks.

Acknowledgements. Funding for this research was jointly provided by a private grant from Oxbow Geothermal Inc., and a federal DOE pass through grant via Lawrence Berkeley National Laboratory. For financial support and interest in the project, I wish to thank everyone at Oxbow Geothermal, and Marcelo Lippman, Ardyth Simmons, and Pat Williams at Lawrence Berkeley Lab. For critical reviews and helpful suggestions, I would like to express my appreciation to Richard Schweickert, Dick Benoit, John Louie, John Caskey, and Ardyth Simmons. The completion of this project would not have been possible without the friendship of many people, especially my parents, William and Darrah Plank, my late grandfather, Elmer Link, and Renée Bufkin. Special thanks to Sue Lutz, Ted DeRocher, Ben Sellers, Sergio Chávez-Pérez, Jenn Morgan, Craig Casey, and Don Noble.

Location of the Field Area. The Stillwater escarpment (Figure 1), here defined, is the precipitous section of the rangefront along the southeast flank of the Stillwater Range, from Mississippi Canyon on the southwest to Fencemaker Pass on the northeast. The geographic subdivision is a convenient one for several reasons:

(1) First, the escarpment corresponds with the Stillwater Seismic Gap, or Fencemaker block, of Wallace and Whitney (1984), that extends from the northeast end of the 1954 Dixie Valley surface ruptures, to the southwest extent of the 1915 Pleasant Valley surface ruptures (Caskey and others, 1996).

(2) Second, the escarpment begins at the southernmost exposure of the Middle to Late Jurassic Humboldt igneous complex (Dilek and Moores, 1995), and ends just north of the southernmost exposure of the Lower Triassic Koipato Group, thereby encompassing a corridor of Lower Mesozoic rocks.

(3) Third, the escarpment roughly parallels the DVGA, that begins at Dixie Hot Springs 3.2 kilometers south of Mississippi Canyon and extends northward to Seven Devils Springs in the Sou Hills (Nosker, 1981), 3.2 kilometers south of the 1915 surface ruptures.

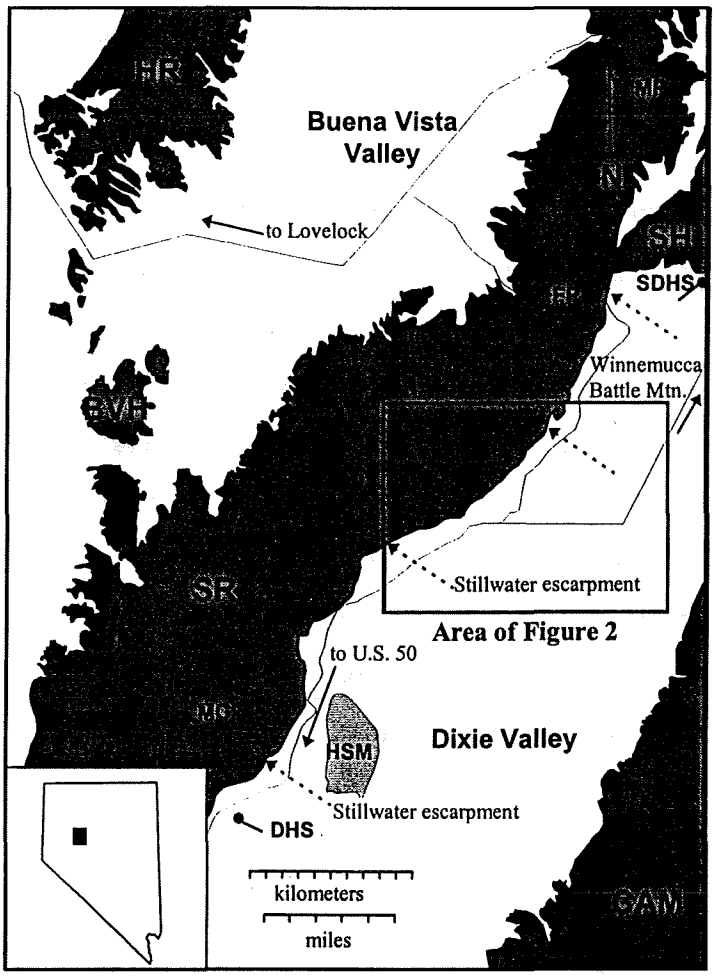

Figure 1. Location of the study area. BVH, Buena Vista Hills; CAM, Clan Alpine Mountains; HR, Humboldt Range; SH, Sou Hills; SR, Stillwater Range; HSM, Humboldt Salt Marsh; DHS, Dixie Hot Springs; SDHS, Seven Devils Hot Springs; MC, Mississippi Canyon; FP, Fencemaker Pass; MP, McKinney Pass.

This study concentrates on part of the Stillwater segment of the Dixie Valley fault, along a northeast trending corridor 8 km long and 5 km wide (Figure 2). The field area is 96 km north of U.S. Route 50, along Nevada State Route 121 through Dixie Valley.

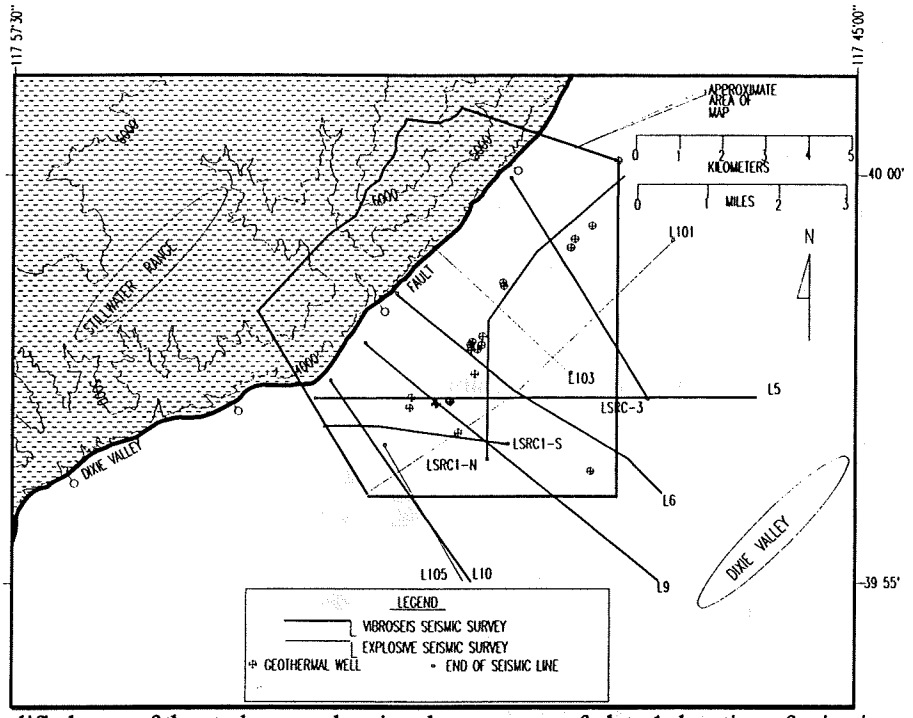

Figure 2. Simplified map of the study area, showing the map area of plate 1, location of seismic surveys, and location of geothermal wells.

Accessibility. The map area is in one of the most remote places in Nevada that are accessible by vehicle; the nearest service station is at least 130 kilometers away. From U.S. Route 50 at the south end of Dixie Valley, Route 121 is paved northward for 40 kilometers, and is graveled the rest of the way to the field area. Sorties to the rangefront exposures should generally be undertaken with a four-wheel drive. Cottonwood Canyon and the mirrors location can be reached with a two-wheel drive. Access to the area from the west is possible by taking the Coal Canyon road east from Lovelock, and then driving northward into Buena Vista Valley. Four-wheel drive vehicles can then reach Dixie Valley via Fencemaker Pass, and cars can continue over McKinney Pass. From Winnemucca, cars can reach the field area by driving from south through Pleasant Valley, or, from Battle Mountain by driving southwest through Buffalo valley. There is no access from the east.

Geography. Dixie Valley is the lowest valley in northern Nevada. The Humboldt Salt Marsh occupies the sink at the lowest point in the valley (elevation ≈1033m), just southwest of the field area. To the west the valley is bounded by the Stillwater Range and to the east by the Clan Alpine Mountains. The majority of Dixie Valley is a low-flight zone for Naval

fighter training flights from Fallon Naval Air Station. Powerful sonic booms occur frequently, especially in the summer. Most of the human occupants of the valley relocated their homes after government designation of the low-flight zone, but some seed and cattle ranches still operate at the north end of the valley and around the town of Dixie Valley. Species of wildlife observed by the author include Desert Bighorn sheep, mountain lion, Mule deer, Great Basin rattler, gopher snake, wild horse, Golden eagle, Turkey vulture, Desert Collared lizard, granite lizard, wood rat, deer mouse, field mouse, tarantula, Black Widow, scorpion, hummingbird, and jackrabbit.

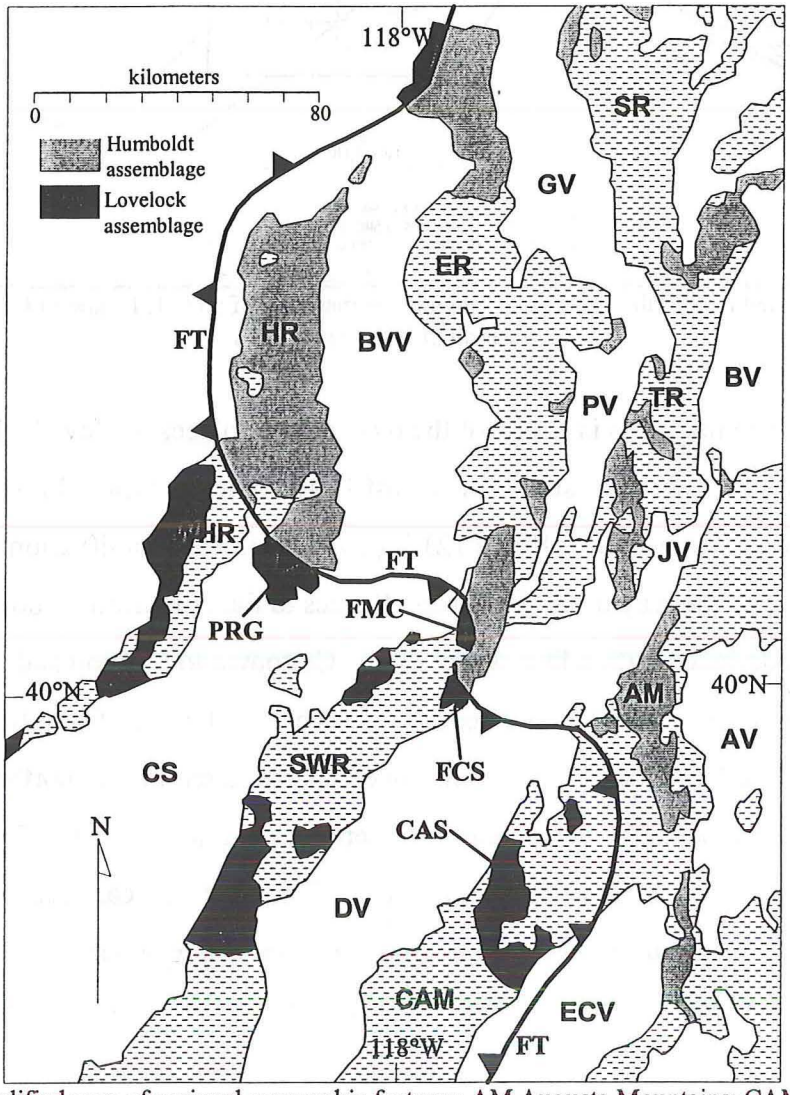

Figure 3. Simplified map of regional geographic features; AM,Augusta Mountains; CAM,Clan Alpine Mountains; ER,East Range; HR,Humboldt Range; SWR,Stillwater Range; SR,Sonoma Range; TR,Tobin Range; WHR,West Humboldt Range; AV,Antelope Valley; BVV,Buena Vista Valley; BV,Buffalo Valley; CS,Carson Sink; DV,Dixie Valley; ECV,Edwards Creek Valley; GV,Grass Valley; JV,Jersey Valley; PV,Pleasant Valley; CAS,Clan Alpine sequence; FCS,Fumarole Canyon sequence; FMC,Fencemaker Canyon sequence; PRG,Pershing Ridge Group; FT,Fencemaker thrust.

1.2. REGIONAL GEOLOGIC SETTING

The Stillwater Range lies in the central part of a region that includes the Tobin, Humboldt, West Humboldt, East, and Sonoma Ranges, and the Augusta and Clan Alpine Mountains (Figure 3). Rocks exposed in the area include: Ordovician and Permian Miogeoclinal rocks; Triassic lithotectonic assemblages; Jurassic intrusive and sedimentary rocks; Cretaceous intrusive rocks; Tertiary intrusive, volcanic, and sedimentary rocks; and quaternary volcanic and sedimentary rocks.

Paleozoic rocks occur in the Humboldt Range, East Range, and Sonoma Range. These rocks are part of the Golconda allochthon, and are widespread in the region, but since they are part of a tectonic regime that is older than the rocks in the study area, they will not be mentioned again.

Triassic lithotectonic assemblages occur predominantly in Pershing County, except for the exposures in the central and southern Stillwater Range and the Clan Alpine Mountains, that are located in Churchill County. The Humboldt lithotectonic assemblage comprises Triassic intrusive, volcanic, carbonate and sandy terrigenous rocks, and lies in the lower plate of the Fencemaker thrust (Figure 3). The Lovelock lithotectonic assemblage consists of Triassic fine-grained argillaceous and quartzose rocks, and lies in the upper plate of the Fencemaker thrust. Most of the Triassic rocks are variably folded and deformed, as a result of tectonic displacement along the Fencemaker thrust, and later, the Willow Creek thrust faults that were active in Early to Middle Jurassic time.

The Triassic assemblages are overlain both depositionally and structurally by Jurassic rocks of the Boyer Ranch Formation. In a few sites, the base of the Boyer Ranch is exposed along a regional angular unconformity. In most places, however, the formation occupies the upper plate of the Boyer fault and structurally overlies Triassic rocks. The Boyer Ranch is regionally restricted in distribution, and occurs only in the Stillwater Range and Clan Alpine Mountains. Jurassic gabbroic rocks of the Humboldt igneous complex intrude the Boyer Ranch Formation in most exposures, and intrude allochthonous basinal rocks of the Lovelock assemblage in the West Humboldt Range. However, the Humboldt complex appears not to intrude rocks that occupy the lower plate of the Fencemaker thrust.

The Cretaceous system is represented regionally by granitic stocks. The stocks intrude Triassic rocks of both the Humboldt and Lovelock lithotectonic assemblages.

Regionally, the stocks crop out only in Rocky Canyon in the West Humboldt Range and in New York Canyon in the Stillwater Range, and are absent from other ranges.

Tertiary volcanic rocks overlie and intrude the Mesozoic rocks in most of the regional mountain ranges. The volcanic rocks comprise rhyolitic tuffs and basaltic to andesitic dikes and lava flows. Regional tuffs generally occupy the southern part of the region, and include the Caetano, Fish Creek Mountains, and New Pass Tuffs. Other tuffs are highly localized or unidentified, such as those in White Rock Canyon in the Stillwater Range and those in the central part of the northern Stillwater Range. Mafic to intermediate lava flows in the region are found in all ranges, but their relative ages and histories are not well known.

The entire stack of Mesozoic and Cenozoic rocks is faulted and dissected by Tertiary normal faults. The largest Tertiary faults have been active since Late Miocene time during the Basin and Range extensional orogeny. The geologically most recent faults bound the regional mountain ranges and are responsible for the morphology of the present landscape.

1.3. REGIONAL STRATIGRAPHIC UNITS

In the following section, I present descriptions of most of the regional stratigraphic units, in order to clarify, for the reader, the names and distribution of rocks in the region. Many of the units are briefly described, and will not be mentioned again. However, the stratigraphy and nomenclature of the Triassic rocks is awkward, and this makes it difficult to understand, later, the regional setting of the Triassic Fumarole Canyon sequence (treated in section 1.5). Therefore, this section places slightly more emphasis on clarifying the stratigraphy of the Triassic lithotectonic assemblages (Figure 4).

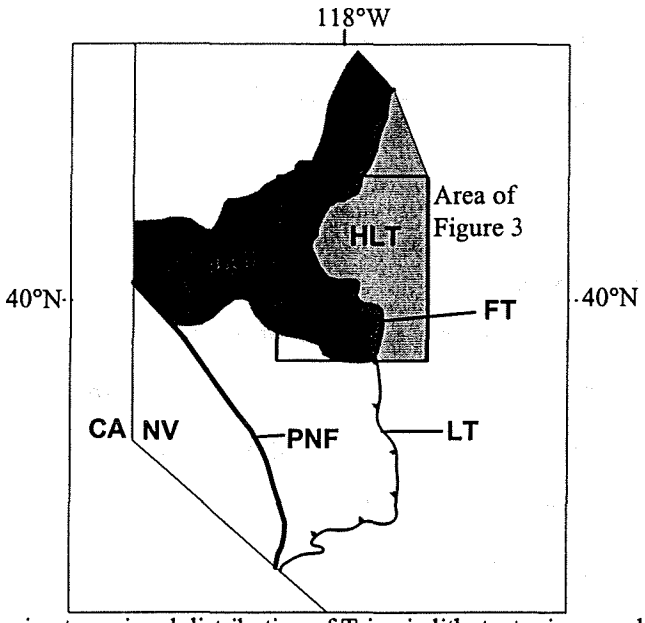

Figure 4. Approximate regional distribution of Triassic lithotectonic assemblages. HLT, Humboldt lithotectonic assemblage; LLT, Lovelock lithotectonic assemblage; FT, Fencemaker thrust; LT,Luning thrust; PNF, Pine Nut fault (modified from Oldow, 1990).

Humboldt Lithotectonic Assemblage (Triassic). The Humboldt lithotectonic assemblage (Figure 4) or platformal assemblage (Oldow, 1984), includes the Koipato Group, the Star Peak Group and correlative rocks, and post-Star Peak siliciclastic rocks of the Auld Lang Syne Group. The post-Koipato units delineate the margins of a widespread Triassic to Jurassic basin known informally as the Early Mesozoic marine province of northern Nevada (Speed, 1978b).

1.3.1. Koipato Group. Lower Triassic continental arc rocks of the Koipato Group (LaPierre and others, 1991) are the oldest rocks exposed in the area. The Koipato Group comprises the Limerick greenstone, Rochester and Weaver Rhyolites, and clastic sedimentary rocks of the China Mountain Formation. Igneous rocks of the Koipato Group were erupted through and deposited upon the Golconda allochthon (Silberling and Wallace, 1967; Burke, 1973). Rocks of the Koipato Group crop out in the Humboldt, West Humboldt, Tobin, East, and Stillwater Ranges, and in the Augusta Mountains. In its type area in the Humboldt Range, the thickness of the Koipato Group reaches 4260 meters (Johnson, 1977).

1.3.2. Star Peak Group and Correlative Rocks. The Koipato arc formed a regional platform upon which Middle to Late Triassic (Upper Norian) shallow marine carbonate sediments and volcanic rocks were deposited. These carbonate and volcanic rocks now constitute the Star Peak Group, as well as units that are correlative with the lower Star Peak,

including the Tobin, Dixie Valley, and Favret Formations. Two additional units, the Augusta Mountain and Cane Springs Formations (Silberling and Wallace, 1969), are correlative with the upper Star Peak Group.

(2a) Star Peak Group. Rocks of the Star Peak Group are exposed in the Humboldt, East, and Stillwater Ranges and in the Augusta Mountains. They comprise the Prida Formation and the overlying Natchez Pass Formation (Silberling and Wallace, 1969). Massive limestones with interbedded andesitic lava flows are the principal units of the Natchez Pass Formation. The Prida Formation, in contrast to the Natchez Pass, is a more terrigenous clastic unit, and generally contains bedded silty limestone, calcareous siltstone and sandstone, and cherty dolomite and limestone. In the type area in the East Range, the thickness of the Star Peak Group is 610 meters. In the Humboldt Range, however, the group is up to 1524 meters thick (Johnson, 1977). The Star Peak Group ranges in age between Spathian (late Early Triassic) and Karnian (Late Triassic) (Silberling and Wallace, 1969).

(2b) Rocks correlative with and similar to the Prida Formation. The Tobin, Dixie Valley, and Favret Formations include calcareous to dolomitic terrigenous rocks and impure limestones that are lithologically similar to and correlative with rocks of the Prida Formation of the Star Peak Group. The Tobin Formation is exposed in the southern Tobin Range, the East Range, and in the Augusta Mountains. In the Augusta Mountains, the formation reaches a maximum thickness of 275 meters where it overlies the China Mountain Formation of the Koipato Group. Ammonites from the base of the Tobin Formation indicate a Spathian age (late Early Triassic) (Burke, 1973). The Dixie Valley Formation overlies the Tobin Formation and is exposed only in the Augusta Mountains and southern Tobin Range. The thickness of the unit ranges from 45 to 244 meters. The Favret Formation overlies the Dixie Valley Formation and is also exposed only in the Augusta Mountains and southern Tobin Range. At the type section in Favret Canyon, in the northern Augusta Range, the Favret formation is 213 meters thick. Ammonites from outcrops in the Tobin Range give an Anisian age (early Middle Triassic) (Burke, 1973).

(2c) Rocks correlative with and similar to the Natchez Pass Formation. The Augusta and Cane Springs Formations include massive carbonate, dolomitic, and volcanic rocks similar to the Natchez Pass Formation (Johnson, 1977). In addition, the rocks are more widespread and apparently extend farther to the north than the Tobin, Dixie Valley, and

Favret Formations; exposures extend westward to the northern Tobin Range (China Mountain area) and southern Sonoma range, and as far north as the northern East Range (Nichols, 1972). In the Augusta Mountains, the Augusta Mountain Formation is 762 meters thick and conformably overlies the Favret Formation. In the same range, the Cane Springs Formation conformably overlies the Augusta Mountain Formation and is 300 meters thick. Although both the Augusta Mountain and Cane Springs Formations are apparently unfossiliferous, their age is bracketed as Ladinian to Karnian (Middle to Late Triassic) by the underlying Favret Formation and the overlying Osobb Formation (described below) (Silberling and Roberts, 1962).

1.3.3. Post-Star Peak Group Siliciclastic Rocks: the Auld Lang Syne Group. Shallow to deep water siliciclastic rocks of the Lower Mesozoic marine province form a sub-province whose stratigraphic and structural geometries are extremely complicated and in some cases poorly studied. The voluminous pelites and sandy terrigenous rocks are sometimes informally called the 'Mud Pile'. Silberling and Wallace (1969) included all the sandy terrigenous rocks exposed in Pershing County as formations within the Auld Lang Syne Group. However, Oldow and others (1990) have more recently demonstrated that some rocks formerly classified as Auld Lang Syne Group are discrete formations within the Lovelock Assemblage, an assemblage of rocks that represents a deep basinal facies of the Jurassic marine province (Speed, 1978b;Oldow, 1984). Furthermore, Oldow (1990) suggested that the name "Auld Lang Syne Group" should be restricted to shallow platformal Upper Triassic rocks that overlie the Star Peak Group; and finally, he suggested that the Auld Lang Syne Group is strictly a part of the Humboldt lithotectonic assemblage.

Formations originally included within the Auld Lang Syne Group (Burke and Silberling, 1974) are, from oldest to youngest, the Grass Valley, Osobb, Dun Glen, Winnemucca, Raspberry, O'Neill, Singas, Andorno, and Mullinix Formations. Oldow (1990) removes the Raspberry, O'Neill, Singas, Andorno, and Mullinix formations from the Auld Lang Syne Group and regarded them instead as part of the Triassic to Jurassic basinal assemblage, or Lovelock lithotectonic assemblage (described below). Oldow's (1990) usage is followed here.

(3a) Grass Valley and Osobb Formations. The Grass Valley and Osobb Formations constitute the lowest part of the Auld Lang Syne Group, and in places they

conformably overlie strata of the Star Peak Group. Regionally, these rocks are exposed in the Tobin, Sonoma, East, Humboldt, and Stillwater Ranges and in the Augusta Mountains. Strata of the Grass Valley interfinger with the Osobb Formation, indicating that they are contemporaneous units. Exposures of the Grass Valley are widespread in the northern East Range. In comparison, the Osobb is confined to more southwestern exposures in the Tobin Range and Augusta Mountains. The Grass Valley Formation consists typically of gray-green, non-calcareous argillite (Oldow, 1990) and wacke. In the East Range, the Grass Valley ranges in thickness from 90 meters in the south to 620 meters in the north. The Osobb Formation, in its type area in the Augusta Range, consists of 550 meters of fine to medium grained sandstone and minor mudstone. The age of these formations is early Norian (Late Triassic) (Johnson, 1977).

(3b) Dun Glen Formation Exposures of the Dun Glen Formation occur in the Sonoma, East, Tobin, Stillwater, and Humboldt Ranges. In all of these ranges, it gradationally overlies the Grass Valley Formation (Oldow,1990). The Dun Glen does not overlie the Osobb to the south and is not present in the Augusta Mountains. The Dun Glen consists predominantly of thick bedded, fossiliferous, fine-grained, gray limestone and dolomite with minor intercalated sandstone. In the Sonoma Range, it attains a thickness of 350 meters, but the formation thins to 30 meters to the south. Ammonites indicate that the age of the Dun Glen is Middle Norian (Late Triassic) (Burke and Silberling, 1974).

(3c) Winnemucca Formation. The youngest unit within the Auld Lang Syne Group is the Winnemucca Formation. The Winnemucca gradationally overlies the Dun Glen in the East and Sonoma Ranges, and is also present in the Tobin and Stillwater Ranges, where the base of the unit is unexposed (Burke and Silberling, 1974). The top of the Winnemucca Formation is nowhere exposed. Rocks in the formation range widely in content, from thin- to thick-bedded sandstone and fine-grained clastic rocks, to bedded dolomite and limestone similar to those in the Dun Glen. In the East Range, the section is 365 meters thick. There are no age-diagnostic fossils, so that the age of the unit is constrained only by the lower gradational contact with the Dun Glen. The age of the Winnemucca is thus younger than Middle Norian.

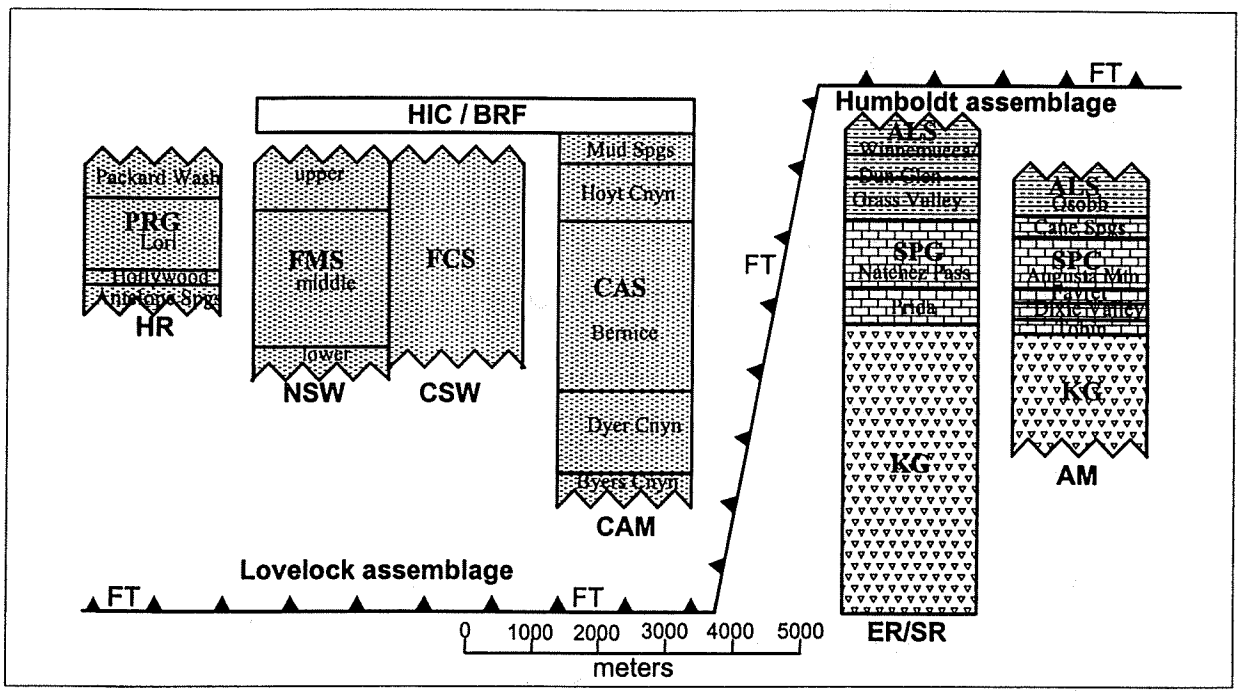

Figure 5. Representative stratigraphic relations within the Lovelock and Humboldt lithotectonic assemblages. HR, Humboldt Range; NSW, northern Stillwater Range; CSW, central Stillwater Range; CAM, Clan Alpine Mountains; ER, East Range; SR, Sonoma Range; AM, Augusta Mountains; PRG, Pershing Ridge Group; FMS, Fencemaker Canyon sequence; FCS, Fumarole Canyon sequence; CAS, Clan Alpine sequence; BRF, Boyer Ranch Formation; HIC, Humboldt igneous complex; KG, Koipato Group; SPG, Star Peak Group; SPC, Star Peak correlatives; ALS, Auld Lang Syne Group; FT, Fencemaker thrust.

Lovelock Lithotectonic Assemblage, or Basinal Assemblage, or Fencemaker Allochthon (Triassic and Jurassic). Lovelock lithotectonic assemblage (Figure 4) comprises deep marine strata of the Early Mesozoic marine province (Oldow, 1984), or basinal assemblage (Speed, 1978b). Because the contact between the Lovelock and Humboldt assemblages is defined by the Fencemaker thrust, the Basinal assemblage is also referred to as the Fencemaker allochthon (Speed and others, 1988).

The Lovelock assemblage is regionally extensive, but poorly studied. Until Oldow's (1990) study, the only part of the Lovelock assemblage that had been described in detail was the "Clan Alpine sequence" in the Clan Alpine Range (Speed,1978b) (Figure 3). Within the Clan Alpine sequence, the Byers Canyon, Dyer Canyon, Bernice, Hoyt Canyon, and Mud Springs Formations are formal units (Figure 5). Oldow (1990) defined the Pershing Ridge Group, at the south end of the Humboldt Range (Figure 3), that comprises the Hollywood, Antelope Springs, Lori, and Packard Wash Formations (Figure 5). In addition, Oldow (1990) defined the Fencemaker Canyon sequence in the northern Stillwater Range (Figure 3)--an

informal succession of siliciclastic sandstone, mudstone, and thin- to medium-bedded limestone. In Oldow's (1990) study, the Raspberry, O'Neill, Andorno, and Mullinix Formations—formerly formations within the Auld Lang Syne Group (Burke and Silberling, 1974) —were also reclassified as part of the Lovelock assemblage (Oldow 1990). In this section, the O'Neill, Andorno, and Mullinix Formations will not be described because they are outside the regional scope of this study. However, the Raspberry Formation, that is exposed in the northern East Range, will be mentioned.

Finally, the Fumarole Canyon sequence in the central Stillwater Range (Figure 3), is a newly defined basinal unit within the Lovelock assemblage. The Fumarole Canyon sequence will be described in detail in this paper.

1.3.4. Clan Alpine Sequence. The Clan Alpine Sequence is a very thick succession (5800 meters) of argillaceous basinal rocks, that are exposed in the Clan Alpine Range, on the east side of Dixie Valley (Figure 6). The sequence is divided into five formations (Speed, 1978b):

(4a) Byers Canyon Formation. The Byers Canyon Formation consists of laminated mudstone with minor, structureless conglomerate and very fine-grained sandstone, and one 60-meter-thick interval of fine-grained limestone. The conglomerate and sandstone have been interpreted as the distal facies of gravity slides, or mass-flow deposits, and indicate a probable outer shelf or slope environment (Prothero, 1989). The Byers Canyon has a minimum thickness of 500 meters; the base is unexposed. Fossils in the lower part of the formation indicate an earliest Norian age.

(4b) Dyer Canyon Formation. The Dyer Canyon Formation gradationally overlies the Byers Canyon Formation. The Dyer Canyon is predominantly mass-flow sandstone with minor (30%) intercalated turbiditic mudstone, with an estimated thickness of 1200 meters. The Dyer Canyon is unfossiliferous.

(4c) Bernice Formation. The Bernice Formation overlies the Dyer Canyon Formation and consists mainly of laminated mudstone and thin, turbiditic sandstone. Oldow (1990) interpreted these rocks as representing a base-of-slope environment. Both the base and top of the formation are exposed, revealing a 2500 meter thickness. The age of the Bernice is middle Norian, as indicated by ammonites.

(4d) Hoyt Canyon and Mud Springs Formations. The Hoyt Canyon and Mud Springs Formations represent a change of depositional environment from slope to carbonate platform (Oldow, 1990). The Hoyt Canyon consists of 850 meters of dark gray to black micritic limestone and orange weathering mudstone and quartz sandstone. The Mud Springs comprises 450 meters of massive limestone with abundant bioclastic material. Both formations contain abundant fauna indicative of the upper Norian. The Mud Springs Formation is unconformably overlain by the Jurassic Boyer Ranch Formation (described below) (Speed and Jones, 1969).

1.3.5. The Pershing Ridge Group. The Pershing Ridge Group resides within the Pershing mining district at the southern tip of the Humboldt Range. The rocks comprise 2295 meters of strongly deformed claystone, siltstone, fine-grained quartzose and calcareous sandstone, micrite, and coarse conglomerate. Mudstone, turbiditic, channel, and gravity flow units indicate a submarine fan environment of deposition. The Pershing Ridge is divided into four formations (Oldow, 1990):

(5a) Hollywood Formation. The oldest formation within the Pershing Ridge Group is the Hollywood Formation. It consists principally of green-gray to tan, clay-rich shale, and subordinately of thin-bedded and fine-grained quartz sandstone. The base of the formation is not exposed, but the apparent thickness is a minimum of 436 meters. Ammonite assemblages indicate that the age is late Norian.

(5b) Antelope Springs Formation. The Antelope Springs Formation immediately overlies the Hollywood. The formation consists of distinctive, well-bedded calcarenite and large carbonate olistoliths at the base of the formation that are traceable throughout the Pershing district. Rocks in the upper unit consist of thin beds of calcarenite with a large fraction of interbedded siliciclastic sandstone and mudstone. Together, the upper and lower units of the Antelope Springs range between 116 and 220 meters in thickness. Ammonites indicate a late Norian age, the same as that of the underlying Hollywood Formation.

(5c) Lori Formation. The Lori Formation conformably overlies the Antelope Springs. The Lori contains chiefly tan to green to reddish-orange shale and thin intercalated turbiditic sandstone. Both the base and the top of the formation are exposed, and the measured thickness is 1059 meters. Conodonts, ammonites, and pelecypods from the Lori indicate a late middle Norian age.

(5d) Packard Wash Formation. The youngest formation within the Pershing Ridge Group is the Packard Wash Formation. The Packard Wash gradationally overlies the Lori Formation, and comprises siliciclastic mudstones and interbedded calcarenite and limestone. Up-section the percentage of carbonate beds increases. The base of the Packard Wash is marked arbitrarily by the first appearance of a calcarenite bed assigned to the Packard Wash. Because the top of the formation is not exposed, the measured thickness of 488 meters is a minimum.

1.3.6. The Fencemaker Canyon Sequence. The road over Fencemaker Pass in the northern Stillwater Range descends westward from the range crest through Fencemaker Canyon. Basinal strata exposed in and around Fencemaker constitute the Fencemaker Canyon sequence (Oldow, 1990). Like the Pershing Ridge Group, the Fencemaker Canyon sequence is complexly deformed. Mudstone, phyllite, and limestone in the sequence are tentatively interpreted (Oldow, 1990) to represent a shallow platform progradational sequence. Three informal members constitute the sequence:

The lower unit consists of 300 meters of dark-green mudstone, with thin interbeds of dark micritic and fine-grained limestone. The lower unit grades upward into a middle, argillaceous unit that is 2000 meters thick. The argillaceous unit is also dominantly a dark-green mudstone, but characteristically lacks calcareous interbeds. Instead, the mudstones are interbedded with fine-grained quartzo-feldspathic arenite. The upper unit abruptly overlies the argillaceous member, and consists of 700 meters of dark gray to black, fine-grained limestone. In the upper unit, distinctive interbeds of massive mudstone and thin, laterally continuous sheets of arenite are also present.

1.3.7. Raspberry Formation. The Raspberry Formation is the only other well-studied unit within the Lovelock assemblage, in addition to those described above. The Raspberry Formation was originally defined as the youngest member of the Auld Lang Syne Group (Burke and Silberling,1974) of the Humboldt lithotectonic assemblage. However, Oldow (1990) regarded the formation as part of the Lovelock assemblage. Indeed, descriptions of the Raspberry Formation by Burke and Silberling (1974) and Johnson (1977) indicate that the Raspberry Formation has a character distinctly different from that of the Auld Lang Syne Group. Exposures at the extreme northern tip of the East Range, are argillaceous rocks with subordinate carbonate-clast conglomerate and very minor sandstone.

The unit has a prominent slaty cleavage that indicates a high argillic content. Neither the top nor the base of the Raspberry is exposed, but the estimated thickness is between 915 and 2430 meters. Ammonites and pelecypods indicate a Late Norian (Late Triassic) age (Burke and Silberling, 1974).

Areally Restricted Rocks: The Boyer Ranch Formation and the Humboldt Igneous Complex (Jurassic). The youngest Mesozoic rocks exposed in the region are Lower to Middle Jurassic quartz arenite, quartzite, limestone, and conglomerate of the Boyer Ranch Formation (Speed and Jones, 1969), and mafic to felsic intrusive rocks of the Middle Jurassic Humboldt igneous complex, that intrudes the Boyer Ranch Formation (Dilek and Moores, 1995; Plank, this study). As discussed in the next section, these Jurassic rocks may represent a tectonic transport regime that was oblique to the east directed contractional deformation (Speed and others, 1988) associated with the Fencemaker thrust.

1.3.8. Boyer Ranch Formation. The Boyer Ranch Formation is exposed only in the central part of the Stillwater Range and the Clan Alpine Mountains (Speed, 1976). The formation consists of two members. The basal member is a coarse- to very coarse conglomerate, with abundant dolomite clasts. Regionally, the basal conglomerate of the Boyer Ranch unconformably overlies folded rocks of the Lovelock assemblage with angular discordance of up to 32 degrees in the Clan Alpine Mountains (Speed and Jones, 1969). In the Stillwater Range the conglomerate is 38 meters thick, but in the Clan Alpine Mountains its thickness ranges from zero (0) to 75 meters.

The upper member consists of well rounded, clean quartz arenite with minor sandy limestone near the base. It gradationally overlies the basal member, and the stratigraphic top is nowhere exposed. The thickness of the upper member reportedly ranges from 30 meters in the Clan Alpine Mountains to 150 meters in the Stillwater Range (Speed and Jones, 1969), though the true thickness of the Boyer Ranch in the Stillwater Range is speculative because it is tightly folded (this study).

The Boyer Ranch Formation is one of several isolated packages of Jurassic quartz arenite in the southwestern Cordillera of the United States. Speed and Jones (1969) suggested the formation was deposited in an isolated trough during foreland contraction. Others (Busby-Spera, 1988) suggested that the formation, and other similar arenitic rocks,

were formed either partly or directly as a result of rifting. Both Speed (1976) and Busby-Spera (1988) postulated that the Boyer Ranch Formation shares provenance with Jurassic sandstones of the eastern Cordillera and Colorado Plateau, such as the Aztec Sandstone. The age of the Boyer Ranch Formation is bracketed between the age of underlying rocks of the Clan Alpine sequence (upper Norian) and intrusive rocks of the Humboldt igneous complex (179- to 157-Ma, K/Ar, Bajocian, or middle Middle Jurassic) (Dilek, 1991).

1.3.9. Humboldt Igneous Complex. The Humboldt igneous complex was mapped in its entirety by Speed (1976) as the "Humboldt Lopolith". His work presents the Humboldt complex as a regional-scale, pancake shaped, layered intrusion, consisting of gabbroic to quartzose dioritic intrusive rocks and superadjacent hypabyssal volcanic rocks. Dilek and others (1988) suggested that the Humboldt complex is part of an ophiolite. Recent, more detailed work by Dilek and Moores (1995) suggests that the geochemistry and structure of the Humboldt complex are more similar to a calc-alkaline volcanoplutonic arc, characterized by multiple phases of complexly intruded—and not necessarily layered—dioritic, monzogranitic, and gabbroic plutons, and basaltic to andesitic dikes. Minor exposures of the Humboldt igneous complex occur in the West Humboldt Range and in the Clan Alpine Mountains, while the majority of the intrusive rocks are in the Stillwater Range. K/Ar hornblende ages from the Stillwater Range suggest the age of the complex lies between 179 and 157 Ma (middle Middle Jurassic to middle Late Jurassic) (Dilek and Moores, 1991).

Cretaceous Intrusive Rocks. Cretaceous granitic plutons occur locally in the Stillwater and Humboldt Ranges, but are few in number. The granite bodies intrude Triassic rocks of both the Humboldt and Lovelock assemblages.

1.3.10. New York Canyon and Rocky Canyon stocks. The New York Canyon stock, on the west side of the central Stillwater Range, consists of equigranular granodiorite containing quartz, K-feldspar, plagioclase, muscovite, biotite, and sphene (Johnson, 1977). The New York Canyon stock has a K/Ar Biotite age of at 69 ± 3-Ma (Silberman and McKee, 1971). In the Humboldt Range, the granodiorite of Rocky Canyon is lithologically similar to the New York Canyon stock. Biotite from the Rocky Canyon stock has been dated at 71 ± 3 - Ma, by K-Ar (Johnson, 1977).

Cenozoic Igneous and Sedimentary Rocks. Cenozoic rocks are exposed in nearly all ranges in the region. These rocks consist of Oligocene to Pliocene granitic intrusions, ash flow tuffs, and basaltic to andesitic dikes and flows.

1.3.11. Caetano Tuff. The Caetano Tuff is the oldest tuff in the region and is exposed in the southern Tobin Range. The unit consists of 100 meters of rhyolitic welded ash flow tuff and basalt (Burke, 1973). K/Ar radiometric ages on sanidine (McKee and others, 1971) give an age of approximately 33-Ma (middle early Oligocene).

1.3.12. Fish Creek Mountains Tuff. The Tobin Range and Augusta Mountains display remnants of the Fish Creek Mountains Tuff. The unit is a crystal rich, welded rhyolitic tuff with a characteristic brick-red, bouldery weathering pattern. McKee and others (1971) obtained a zircon fission-track age of approximately 25-Ma (late early Oligocene) for this unit.

1.3.13. New Pass Tuff. The New Pass Tuff is an extensive ash flow sheet recognized widely in west-central Nevada. Regionally, the New Pass tuff is exposed in the southern Stillwater Range and in the central Clan Alpine Mountains (Hudson and Geissman, 1991; John, 1995). In the Stillwater Range, however, the New Pass Tuff has not been recognized north of White Rock Canyon (Dave John, pers. comm.,1995). The unit is typically a crystal rich, high-silica rhyolitic ash-flow tuff with abundant smoky bipyramidal quartz. Radiometric dating yielded an age of 23-Ma (McKee and Stewart, 1971).

1.3.14. Tuffs in the White Rock Canyon Area. A one-kilometer thick sequence of ash flow tuffs is exposed in White Rock Canyon, that was a major sample location for Hudson and Geissman's (1991) paleomagnetic survey. The tuffs are rhyolitic and are intruded by younger mafic sills and capped by basalt. The youngest ash-flow tuff in White Rock Canyon is the New Pass Tuff (described above). In addition, the Nine Hill Tuff and Tuff of McCoy Mine have also been identified (John, pers. comm., 1995). The rest of the units are unidentified, but because they underlie the New Pass Tuff they must be younger than 23-Ma.

1.3.15. Southern Stillwater Caldera Complex. John (1995) recognized a system of three nested calderas in the southern Stillwater Range. Rocks associated with the caldera system range from sub-caldera plutons, to intracaldera megabreccias tuffs and flows, to regionally extensive ash-flow tuff sheets. The ash-flow sheets extend from the caldera

complex to the south and east, at least as far east as the Clan Alpine Mountains. John (1995) correlated the Tuff of Poco Canyon, associated with the Stillwater caldera complex, with the regionally extensive New Pass Tuff, indicating that the Stillwater caldera complex was the source for that regional ash flow sheet. Radiometric ages (John, 1995) for the complex range from 29- to 23-Ma.

1.3.16. Unnamed Tuffs and Flows Beneath Table Mountain. Tuffs in the north-central Stillwater Range (Speed, 1976) that are overlain by basalts of Table Mountain (Nosker, 1981) are unnamed. Through reconnaissance mapping of the tuffs Hudson (John, pers. comm.,1995) has tentatively identified unit 6 (the tuff of McCoy Mine) and unit 7 of Hudson and Geissman (1991). Because units 6 and 7 of Hudson and Geissman underlie their unit 9 (the New Pass Tuff), the ages of the unnamed tuffs in the Stillwater Range are probably older than 23-Ma.

1.3.17. Rocks of the Sou Hills and the Basalt of Table Mountain. Nosker (1981) identified basalt flows, rhyolite flow-domes, and lake sediments in the Sou Hills, at the north end of Dixie Valley. The lower unit consists of a flat lying rhyolitic ash flow. The ash flow is capped by a the "lower basalt" (Nosker,1981), that in turn is overlain by light beige to pink lake sediments of probable Miocene age. The entire sequence is capped by a flat-topped, olivine basalt flow, the "upper basalt" and younger rhyolite flow dome. The minimum age of the entire package is given by K-Ar ages from the upper basalt, as 18.4- to 13.8-Ma (Nosker, 1981).

The basalt of Table Mountain caps the central and northern Stillwater Range. Whole rock K-Ar ages of Nosker (1981) on the basalt of Table Mountain suggests that it was erupted between 14- to 13-Ma. This age suggests that the Table Mountain basalt may be contemporaneous with the upper basalt in the Sou Hills.

1.3.18. Basin-fill units. Basin-fill units include mainly alluvial, lacustrine, landslide, and playa deposits. The basin-fill units are generally found in the intermontane valleys, but alluvial and landslide deposits can be found at higher elevations within the ranges. Alluvium is the most common constituent in the basin-fill of any given basin, and covers about 45 percent (%) of the regional land area (Johnson, 1977). Alluvial deposits include alluvial fans, stream gravels, and dry-wash gravels. Lacustrine deposits occur in most of the valleys, but are thickest in Buena Vista Valley and Carson Sink (Johnson, 1977). Thick sequences of

sand, silt, gravel, clay, tufa, and saline minerals were deposited in those valleys during the existence of Lake Lahontan, a late Pleistocene (Wisconsinide) pluvial lake. Landslide deposits are most numerous, recent, and recognizable along steep mountain fronts where they have spilled into the adjoining valley(s). Older landslides deposits often occur within the ranges themselves, where they form slope deposits that are sometimes indistinguishable from colluvium. Small playa deposits are present in all of the intermontane valleys. The playa deposits range widely in age; some playas, such as the one in Buena Vista Valley, are Lahontan-aged deposits (Johnson, 1977), while the playa deposits in Dixie Valley (Humboldt Salt Marsh, Figure 1) are presently forming.

Regional Structures. Regional structures pertinent to this study include the Fencemaker thrust, the Willow Creek thrust, the Boyer fault, and the Dixie Valley fault system.

1.3.19. Fencemaker Thrust. The Fencemaker thrust (Speed and others, 1988) is an east-vergent thrust that emplaced Triassic and Jurassic basinal rocks of the Lovelock lithotectonic assemblage upon pene-contemporaneous Triassic rocks of the Humboldt lithotectonic assemblage. The thrust is exposed in the Humboldt, East, and Stillwater Ranges, and its trace approximates the northeastern boundary of the Lovelock assemblage. The Fencemaker is assumed to have moved during the Early Jurassic, but the exact timing is poorly known. The minimum age of Fencemaker displacement is constrained by the minimum age of the Willow Creek thrust, that postdates structures related to emplacement of the Fencemaker allochthon. Regarding its origin, the thrust may have formed along the transition between basinal rocks and platformal rocks of the Early Mesozoic marine province (Elison and Speed, 1989; Oldow, 1990).

1.3.20. Willow Creek Thrust. The Willow Creek thrust emplaced rocks of the Golconda allochthon and overlying strata westward over autochthonous rocks of the Humboldt assemblage (Elison, 1990). The upper plate of the Willow Creek may even have moved over and included parts of the allochthonous upper plate of the Fencemaker thrust. The thrust is only exposed in the East Range. Most of the tectonic fabrics and structures in the East Range are attributed to Willow Creek deformation, and are west-vergent (Elison, 1990). South of the East Range, the trace of the Willow Creek thrust is not exposed, nor is its approximate position suggested by the distribution of upper and lower plate rocks. The

Willow Creek is a Mesozoic structure whose age postdates the Fencemaker thrust. Willow Creek emplacement structures in the East Range are cross-cut by a 155-Ma granitic pluton thrust (Speed, 1988).

3. Boyer Fault. The Boyer fault (Boyer thrust of Speed (1976)) is exposed only in the Stillwater Range. Based on field relations in the Stillwater Range, that are described in the next section (1.4), I postulate that the fault is a Miocene detachment fault. In this text, I refer to the structure by the name "Boyer fault". The Boyer fault generally places rocks of the Humboldt igneous complex and Boyer Ranch Formation over Triassic basinal strata.

4. Central Nevada Seismic Belt (CNSB) and the Dixie Valley Fault. Basin-bounding faults in the region are Tertiary high-angle normal faults. Most of the large normal faults, such as the Dixie Valley, Fairview Peak, Pleasant Valley, Louderback Mountains, and Rainbow Mountain faults, have ruptured in historic time, and many of them show Holocene paleoscarps (Caskey, 1996). They are also part of a north- northeast trending zone of recently active seismicity called the Central Nevada Seismic Belt (CNSB) (Wallace, 1984a).

The Dixie Valley fault trends northeast along the base of the eastern rangefront of the Stillwater Range, and dips steeply (≈67°) to the southeast. The fault is not a discrete surface, but rather consists of a zone of several large and small displacement faults. The zone is delineated mainly by the Stillwater range front, and also by piedmont and bedrock surface ruptures adjacent to the trace of the Dixie Valley fault (Caskey, 1996).

Previous Work. During the 1960's and 1970's, the regional stratigraphic and tectonic relationships were worked out by a handful of geologists. Silberling, Roberts, Wallace, and Burke published many detailed descriptions of the geology of the Star Peak and Koipato Groups. Speed mapped and described Triassic and Jurassic rocks in the Clan Alpine Range, Stillwater Range, and West Humboldt Range, and worked out the detailed stratigraphy of the Boyer Ranch Formation. In addition, Speed was the first to map and describe rocks of the Humboldt igneous complex. Page mapped the southern and central Stillwater Range, including a large section of highly deformed basinal rocks of the Lovelock lithotectonic assemblage.

More recently, in the 1980's and 1990's, a few workers have focused their studies on the finer details of regional tectonics. Elison mapped the East Range in detail, and sorted out the hierarchy of structures related to the Fencemaker and Willow Creek thrusts; Dilek remapped parts of the Humboldt igneous complex, in the Stillwater Range, and speculated anew upon the origin of that group of rocks; Hudson and Geissman discovered important details of Oligocene and Lower Miocene tectonics, in their study of regional paleomagnetic rotations; John re-mapped the southern Stillwater Range, and in doing so discovered an extensive Oligocene caldera system; and, LaPierre, and others, studied the petrology and geochemistry of the Koipato Group. Geologic studies, by the mining and geothermal industries, are interdisciplinary and too plentiful to enumerate.

1.4. STRATIGRAPHY OF THE STILLWATER ESCARPMENT

Stratigraphic Framework. In the Stillwater Range, the contacts between rocks of discrete lithology and age are usually faults. The fault-bounded blocks, or terranes, are internally homogenous and strongly deformed, causing the stratigraphic relations to be obscure. Thus the rocks described in this section are posed in such a way that their tectonostratigraphy is simple, while the primary sedimentary and igneous relationships are complicated. For these reasons, the following presentation of the stratigraphy and structure of the Stillwater escarpment separates the terranes into structural domains.

The structural domains occupy a corridor that is bounded on the southeast by the Dixie Valley fault and on the northwest by the eastern divide of the Stillwater Range. Arbitrary map boundaries to the northeast and southwest have been created in order to confine the map area to a manageable size. The lower plate of the Fencemaker thrust makes up Domain 1. The only formation exposed within Domain 1 is the Natchez Pass Formation.

Domain 2 is the upper plate of the Fencemaker thrust. The rock exposed in Domain 2 includes only the Fumarole Canyon sequence.

Domain 3 is the upper plate of the Black Canyon fault. Rocks in Domain 3 include the basal part of the Boyer Ranch Formation and underlying, unnamed Triassic slate and sandstone. One small sill, associated with the Humboldt igneous complex, is also present in Domain 3.

Domain 4 is the upper plate of the Boyer fault. Rocks in Domain 4 include the Boyer Ranch Formation and the Humboldt gabbroic complex, and these overlie and truncate all rocks and structures within domains 1, 2, and 3. Domain 4a is a piece of Domain 4 that has been down-dropped to a position low along the Stillwater range front, along a splay of the Dixie Valley fault (RF4 fault). Because the rocks in Domain 4a are the same as those in Domain 4, Domain 4a will not be mentioned again until the RF4 fault is described (page 61).

Tertiary rocks do not fit into the domainal scheme, as they are scattered throughout the map area independently of the Mesozoic geology. The Tertiary rocks comprise basaltic to andesitic dikes, travertine deposits, landslides, colluvium, and alluvium. Tertiary volcanic tuffs and flows, that are outlined in the previous section (1.2), crop out at Table Mountain along the backbone of the Stillwater Range, but they are not present in the study area.

Quaternary units include alluvial, lacustrine, playa, and landslide deposits. Generally these units are basin-fill, but some alluvial and landslide deposits occur within the range, along slopes and in the dry wash beds.

Stratigraphy. The following paragraphs describe the rocks that are present in each domain, in order of decreasing age. Tertiary and Quaternary rocks are described separately.

1.4.1. Domain 1 Rocks. Rocks in Domain 1 include part of the Triassic Natchez Pass Formation. The Natchez Pass Formation is the upper of two formations within the Star Peak Group. The formation was named from typical exposures in Natchez Pass in the East Range (Silberling and Wallace, 1969). The section in Domain 1 is the southern-most exposure of the Natchez Pass Formation, and was identified here by Speed (1976). Typically, the Natchez Pass comprises massive carbonate and interbedded volcanic and siliceous detrital rocks, and these rocks increase in thickness regionally from north to south (Silberling and Wallace, 1969). This section, in Domain 1, contains no volcanic rocks, but includes massive carbonate rocks. Reconaissance mapping has shown, however, that volcanic rocks and some fine-grained, quartzose strata exist lower in the section, just north of the map area.

(1a) Black Limestone and Black Schist. The lowest exposed part of the Natchez Pass Formation in Domain 1 crops out at the bedrock/alluvial contact, along the Dixie Valley fault. There, the formation consists of a distinctive, impure, black limestone. In places

where it is not tectonized, the black limestone is very thinly bedded, similar to a shale. Individual beds are very fine grained, and have no distinguishable internal structure. The limestone has a friable, shaly texture, and weathers to a fine flour. The black color of the limestone is due to high carbon content, that causes the rock to be dirty to the touch. To the southeast, the black limestone becomes a calcareous, cordierite schist, as it warps into the ductile shear zone of the Fencemaker thrust. The schist provides a good marker horizon between upper and lower plates of the thrust. The appearance of the schist is similar to that of the limestone, except for the presence of metamorphic porphyroblasts, and strong tectonic foliation and lineation.

(1b) Whitish-Gray to Dark-Gray Marble. The upper boundary of the black limestone is a very distinct and abrupt transition to massive, strongly foliated, whitish-gray to dark-gray marble and marble tectonite. The contact can be seen from a distance, about 200 vertical meters topographically above the mouth of Fumarole Canyon. For the most part, the unit has been completely recrystallized, but small enclaves of less-deformed rock can be found, in which the original limestone texture is recognizable. At the southeast boundary of Domain 1, along the ductile shear zone of the Fencemaker thrust (discussed below), the marble is strongly deformed into a marble tectonite.

Small-scale bedding in the marble is eradicated, but large-scale relict bedding is still visible along some steep-walled ravines. The original strata have given way to thick (2 to 5 meters), alternating bands of grayish-white and dark-gray marble (figure showing picture of black and white marble). The grayish-white marble is completely recrystallized, and consist of flattened lenses of white, sparry calcite in a groundmass of light gray, coarse calcite (plate P1A). Often, the calcite lenses are cored by brown, dolomitic material (plate P1B). The dark-gray marble is finer-grained and fossiliferous (plate P2A). The dark-gray marble, though strongly foliated, is recrystallized to a lesser degree; this is probably a result of there being much less original calcite and more carbonaceous or terrigenous material within the protolith. Fossil tests in the dark-gray marble have been recrystallized and dolomitized, but many retain a recognizable shape. In places, fine scleratinian coral structure is even visible (plate P2B). However the majority of the clastic fragments lack biological structures. In summary, the relict compositional layering and pervasive, dolomitic detritus indicate that the protolith may have consisted of massive white or gray limestone, interbedded with impure,

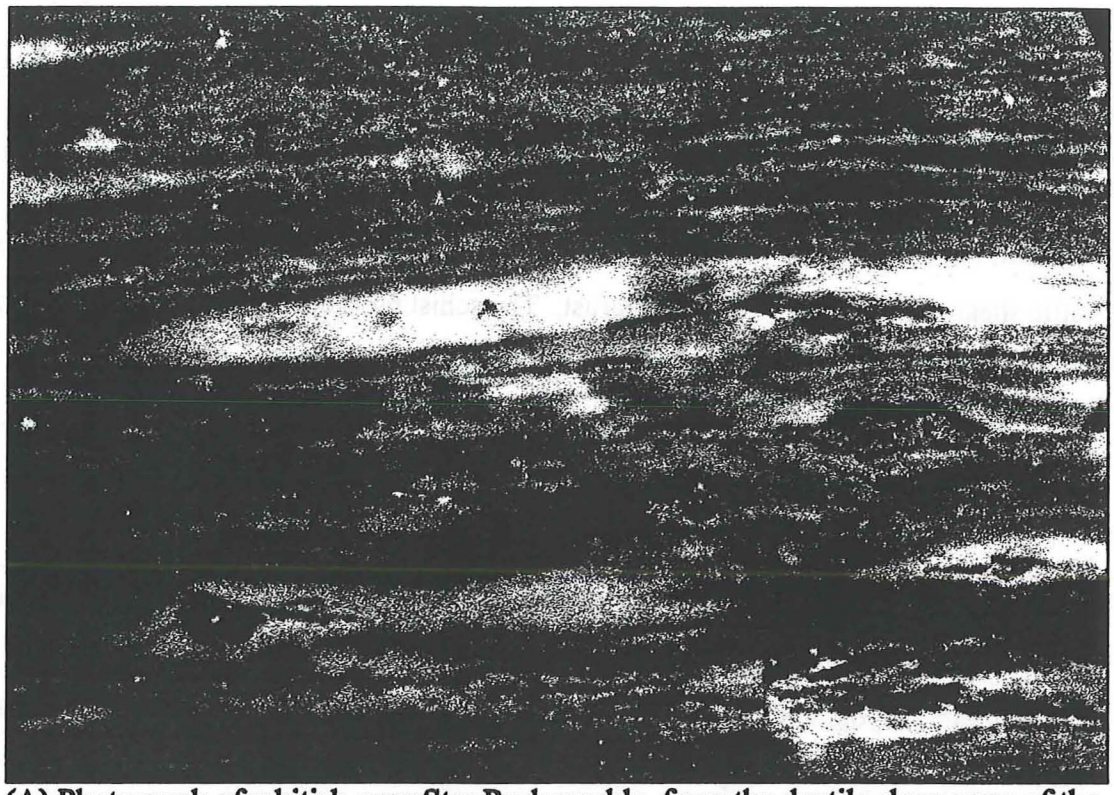

(A) Photograph of whitish-gray Star Peak marble, from the ductile shear zone of the Fencemaker thrust, showing elongated sparry calcite lenses cored by dolomitic material. within a darker calcite matrix.

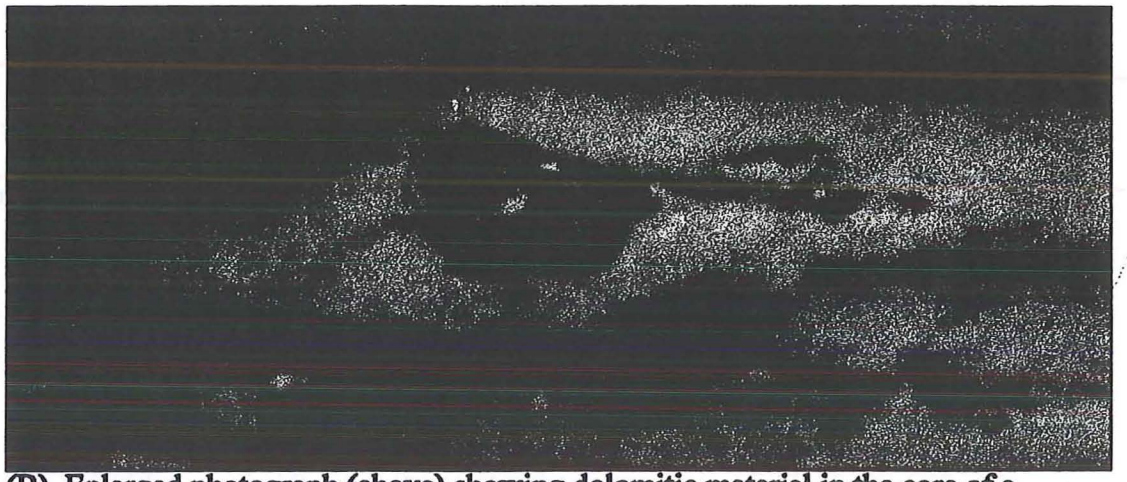

(B) Enlarged photograph (above) showing dolomitic material in the core of a sigmoidally rotated calcite porphyroclast (shear sense is dextral).

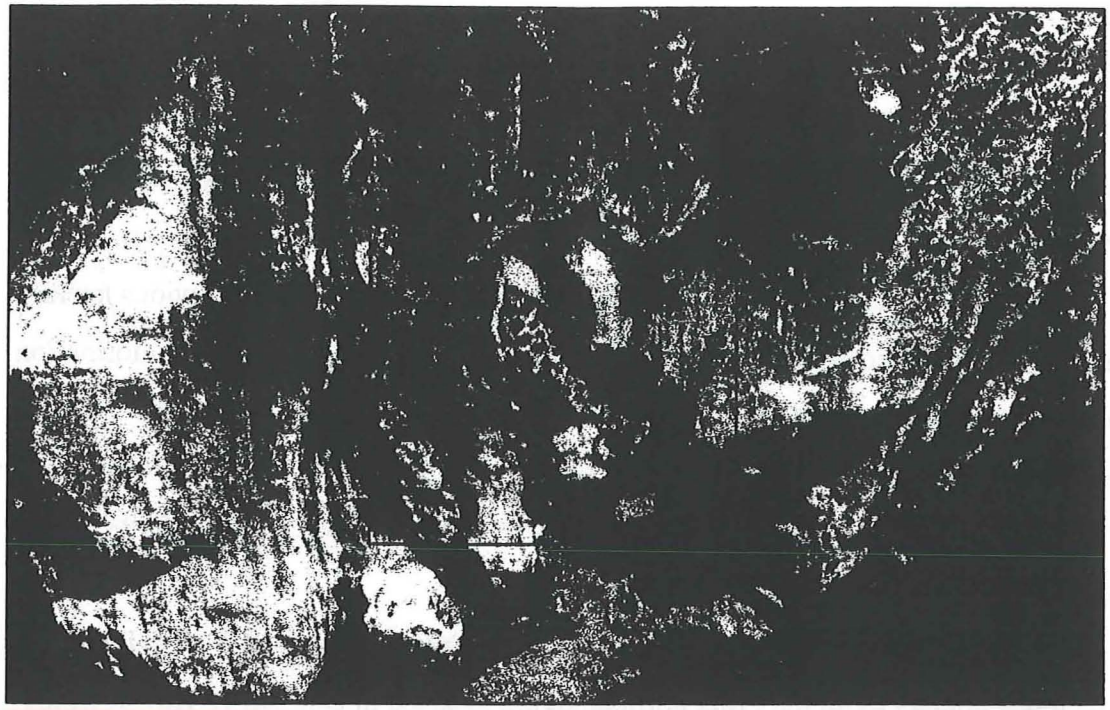

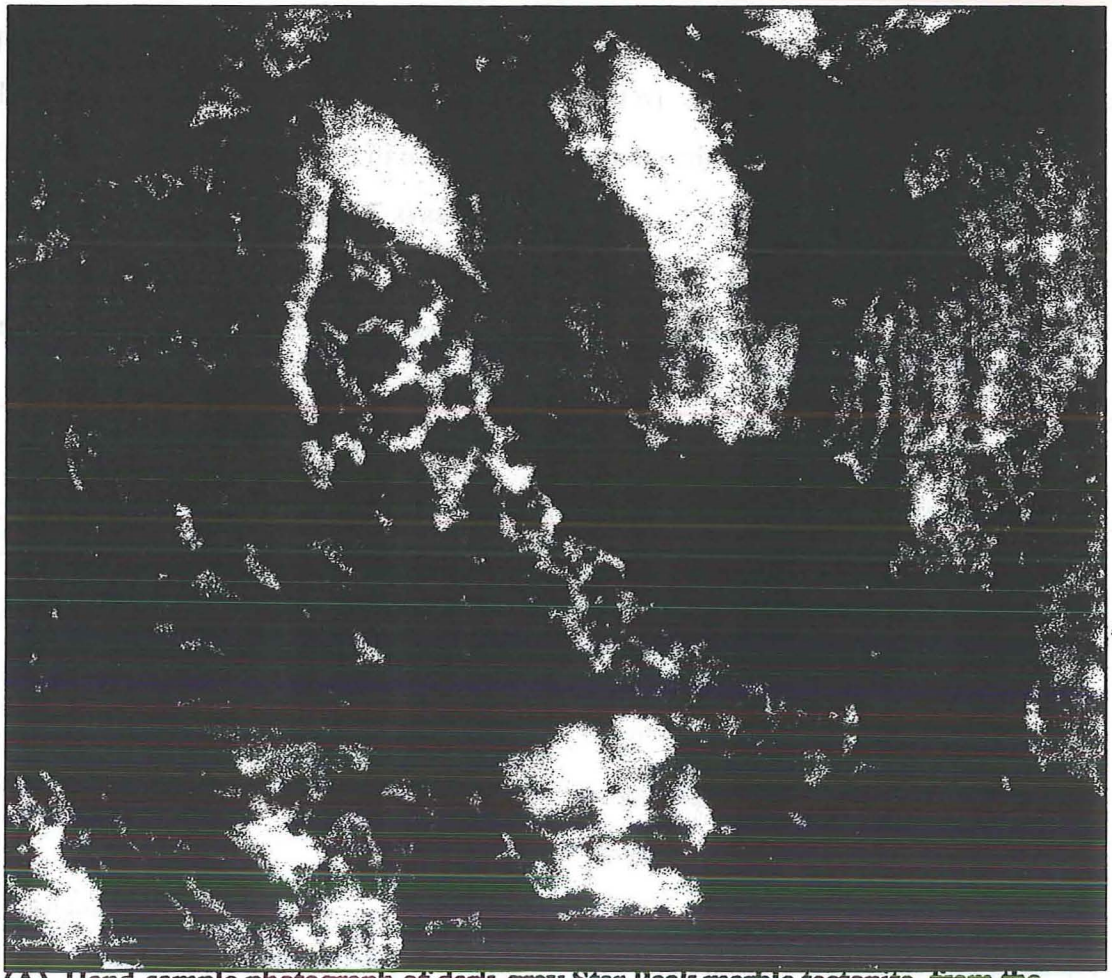

(A) Hand-sample photograph of dark-gray Star Peak marble tectonite, from the ductile shear zone of the Fencemaker thrust. (B) Closeup photo of scleratinian coral structure.

dark gray limestone, both of which were fossiliferous or bioclastic, and which possibly included some dolomitic and calcitic vein material.

Because of the structural complexity in Domain 1, there are no obvious lateral stratigraphic variations in the marble. However, the intensity of structural deformation decreases with distance from the Fencemaker shear zone. In short, the marble tectonite occupies the shear zone, the foliated marble resides along levels structurally beneath the shear zone, and foliated limestone is found along structural levels that are farthest from the shear zone.

Neither the upper contact of the Natchez Pass (with the Grass Valley Formation) nor the lower contact (with the Prida Formation) are exposed in Domain 1. However, the approximate thickness of the Natchez Pass—from an map estimate of the maximum exposed thickness—is at least 580 meters. To the west, in the neighboring Humboldt Range, where exposures of the formation are the most similar to those in the Stillwater Range (Silberling and Wallace, 1969), the thickness of the Natchez Pass is 760 meters. Thus, the thickness estimate in Domain 1 is within reason for the Natchez Pass Formation. Rocks that are similar to the black limestone are found in the Humboldt Range, where they are known to be a lower member of the Natchez Pass Formation (Silberling and Wallace, 1969). As described, that lower member consists of 460 meters of distinctive, impure, massive limestones, complexly interfingering volcanic tuffs and flows, siliceous detrital beds, and a high percentage of dolomitic to sparry calcitic vein material. The lithology and thickness of this limestone in the Humboldt Range is remarkably similar to the portion of the Natchez Pass found in structural Domain 1 in the Stillwater Range. Thus, the section of Star Peak Group that is found in Domain 1 probably represents the lower Natchez Pass Formation. If the rock in Domain 1 is indeed part of the lower Natchez Pass, the age is latest Middle Triassic to early Late Triassic (Ladinian to Carnian) (Silberling and Wallace, 1969).

1.4.2. Domain 2 Rocks. Rocks in Domain 2 include the Fumarole Canyon sequence. The Fumarole Canyon sequence consists of fine-grained quartzose and argillaceous basinal rocks that are part of the Lovelock lithotectonic assemblage. The sequence occupies the entire body of structural Domain 2: a narrow, fault bounded corridor extending from Fumarole Canyon to three (3) kilometers south-southwest of the canyon. The Fumarole Canyon sequence is named from the Senator Fumaroles, that are situated at the

mouth of Fumarole Canyon—a steep walled canyon at the north end of the field area. To the northeast, the formation is bounded by the Fencemaker thrust, and there it structurally overlies the Natchez Pass Formation. To the southwest, the formation is truncated by the Black Canyon fault, and so structurally underlies unnamed Triassic slates that stratigraphically underlie the Boyer Ranch Formation in Domain 3. The formation is capped by rocks of Domain 4, and truncated on the east by a splay of the Dixie Valley fault system (fault RF4).

(2a) Lower Unit of the Fumarole Canyon Sequence. The lower unit of the Fumarole Canyon sequence consists of black to very dark-gray slate. Although the character of the bedding is heavily overprinted by a strongly developed, bedding-parallel, tectonic cleavage, the original bedding most likely consisted of thinly laminated argillite with occasional, thin, quartzose intercalations. The relatively competent quartzose intercalations usually occur as thin, platy boudins. Very thin laminae of hematitic material also indicate bedding.

The slate in the lower unit is composed of very fine-grained quartz, argillaceous minerals, and organic material. These components impart to the rock a homogeneous appearance and texture. The high pelitic content is indicated by ultra-fine cleavage foliation; well developed lineations of stretched micaceous minerals; phyllitic sheens on cleavage planes; and by the obvious incompetency of the rock. The protolith, therefore, was probably a claystone interbedded with thin layers of siliceous mudstones. Because the lower unit is exposed in a profile view (almost cross-sectional) along the face of the Stillwater escarpment, lateral variations in the stratigraphy are not apparent.

(2b) Upper Unit of the Fumarole Canyon Sequence. The upper unit of the Fumarole Canyon sequence gradationally overlies the lower unit. The contact is defined by an upwards increase in the width and number of competent, quartzose interbeds (usually occurring as quartzose boudins). Because of thrust and/or normal faulting, variations in lithology within the upper unit are juxtaposed in a confusing way; thus it is difficult to say exactly how the vertical stratigraphy changes in the upper unit. However, it appears to consist of thinly bedded, brown argillite in the upper part, and laminated, olive-green to bluish-gray, argillaceous siltstone in the lower part (plate P3).

(A) Brown argillite in Little Cottonwood Canyon, showing thin, sandy and siliceous interbeds. Note polyphase fold ($F1_{asw}$), described later.

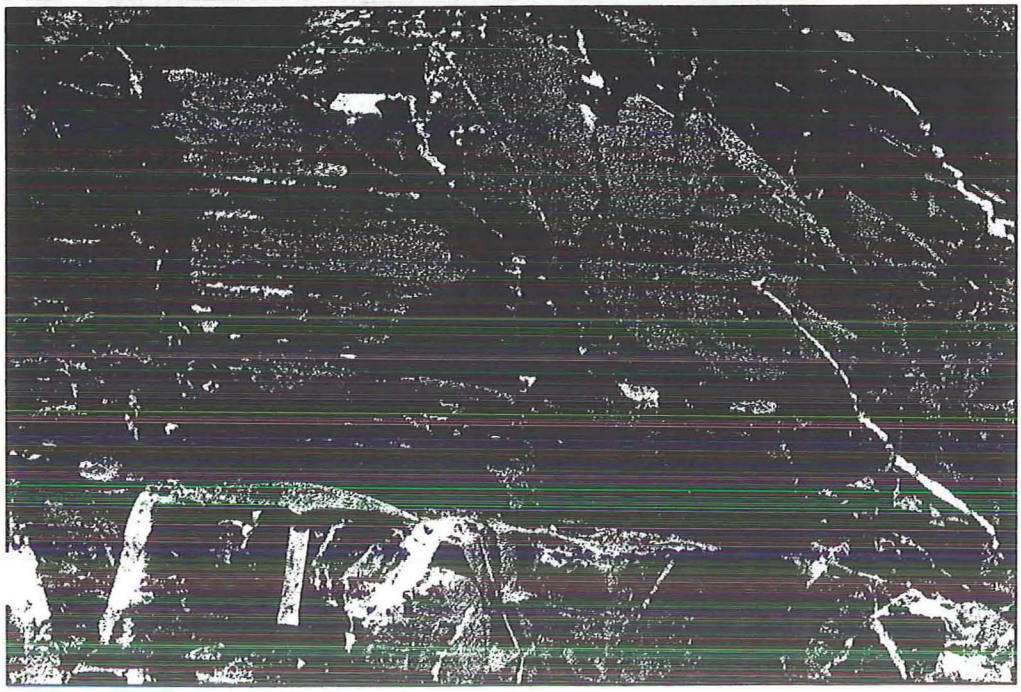

(B) Blue-gray argillite, at the mouth of Black Canyon, showing fine bedding lamination.

Plate P3

Brown argillite is exposed only in the southern one-third (1/3) of Domain 2 (in the back limb of a megascopic anticline in Domain 2, described below). The brown argillite can be distinguished from siliceous argillite solely by the presence of sandy interbeds (plate P3A). The rock is uniformly intercalated with thin, light colored beds of fine turbiditic sandstone, ranging in width from 0.1 to 1.0 centimeters. Thin to thick interbeds of brown, sandy limestone occupy one horizon within the upper part of the upper unit, high in the southeast wall of Little Cottonwood Canyon, but otherwise carbonate beds are absent.

Olive-green to blue-gray argillaceous siltstone, or siliceous argillite, crops out in both the southwestern and northeastern thirds (1/3's) of Domain 2. The siliceous argillite is a competent and overall homogeneous rock, consisting of predominantly of fine-grained quartz, a large amount of organic detritus, and subordinate micaceous minerals, (plate P4A). The rock appears massive, and does not contain interbeds. At a finer scale, however, the bedding is characterized by ultra-fine lamination and wispy, greenish intercalations (plate P3B). The appearance of these intercalations suggests a very low-energy depositional environment, and is reminiscent of current structures in contourites. It should be mentioned that the appearance of the siliceous argillite varies greatly according to the angle between the penetrative tectonic foliation and bedding. The rock can sometimes be penetratively and tightly foliated parallel to bedding, but is only weakly foliated or non-foliated at high angles to bedding.

The upper unit of the Fumarole Canyon sequence also contains rocks of olistostromal or other mass-slide origin. These bodies are intercalated mainly within the olive-green to blue-gray siliceous argillite. Because the Fumarole Canyon sequence is both deformed and restricted in its lateral exposure, the lateral continuity of the olistostromal bodies is not obvious. Locally, their geometries are lensoidal, massive, and lack bedding, and their contacts with the surrounding bedded rocks are indistinct. The matrix of the olistostromal bodies is similar to argillaceous siltstone that dominates the upper Fumarole Canyonsequence, but is slightly more quartzose. Most notably, the olistostromes have a high (≈30%) constituency of pod-like clasts, or olistoliths, that are present in the matrix as suspended blocks. In aspect, the olistoliths are rounded and range in shape from spherical to amoeboid, and they generally, but not always, lack stratification or preferential orientation.

The olistoliths occur in clusters, in which some olistoliths are flow-aligned (plate P5B) while others are chaotically deformed (plate P5A). Ninety (90) percent of the olistoliths are fist- to basketball-sized pods of bioclastic (plate P6A) carbonate and non-bioclastic carbonate sedimentary rock. Other blocks consist of tan to greenish-tan, medium grained sandstone lenses, that range from guitar-sized to car-sized and are usually tabular in aspect. Soft-sediment slump and shear structures also are present around the margins of the olistostromal bodies (plate P6B). This type of soft sediment deformation is commonly associated with mass-slide emplacement (Prothero, 1989) and provides additional evidence that these intercalations have an olistostromal origin.

Domain 2 is part of a megascopic, hanging wall anticline that is overturned to the north. The upper Fumarole Canyon crops out in both the upright and overturned limbs of the megascopic anticline, and the lower unit crops out in the core of the anticline. Although neither the base nor the top of the formation are exposed, an estimate of its thickness, measured from cross-sectional models of the anticline, is approximately 3000 meters. The maximum exposed thickness is akin to 2100 meters. The Fumarole Canyon sequence is non-fossiliferous, except for the bioclastic inclusions or olistoliths within the olistostromal blocks, and therefore it is difficult to put an age to the formation. However, we are currently undertaking uranium/lead (U-Pb) dating of zircons, from within a pre-deformational felsic dike, that may give both a minimum age for the formation and a maximum age for the penetrative deformation. In any case, the similarity of these rocks to the other basinal facies of the Lovelock assemblage, indicates that the age is probably middle to late Norian

The Fumarole Canyon sequence was originally mapped by Speed (1976) as part of an Upper Triassic to Lower Jurassic pelitic sequence in the upper plate of the Fencemaker thrust. Other map compilations of the geology of Pershing and Churchill Counties (Johnson, 1977; Wilden and Speed, 1974), later designated the Fumarole Canyon rocks as undifferentiated phyllites of the Auld Lang Syne Group. Speed (1978a) indicated that the Fumarole Canyon sequence is probably a distal, deeper water member of the Clan Alpine sequence. I correlate the Fumarole Canyon as basinal facies rocks of the Lovelock lithotectonic assemblage, that have affinity toward rocks of both the Clan Alpine sequence (Speed, 1978b) and the Fencemaker Canyon sequence (Oldow, 1990), but that lack evidence for direct correlation to any of those units. Finally, I interpret the facies distribution outlined above to represent a

(A) Photomicrograph of siliceous argillite from the Fumarole Canyon sequence, showing slightly stretched detrital quartz, micaceous minerals, and black carbonaceous material. (Nikon 10x)

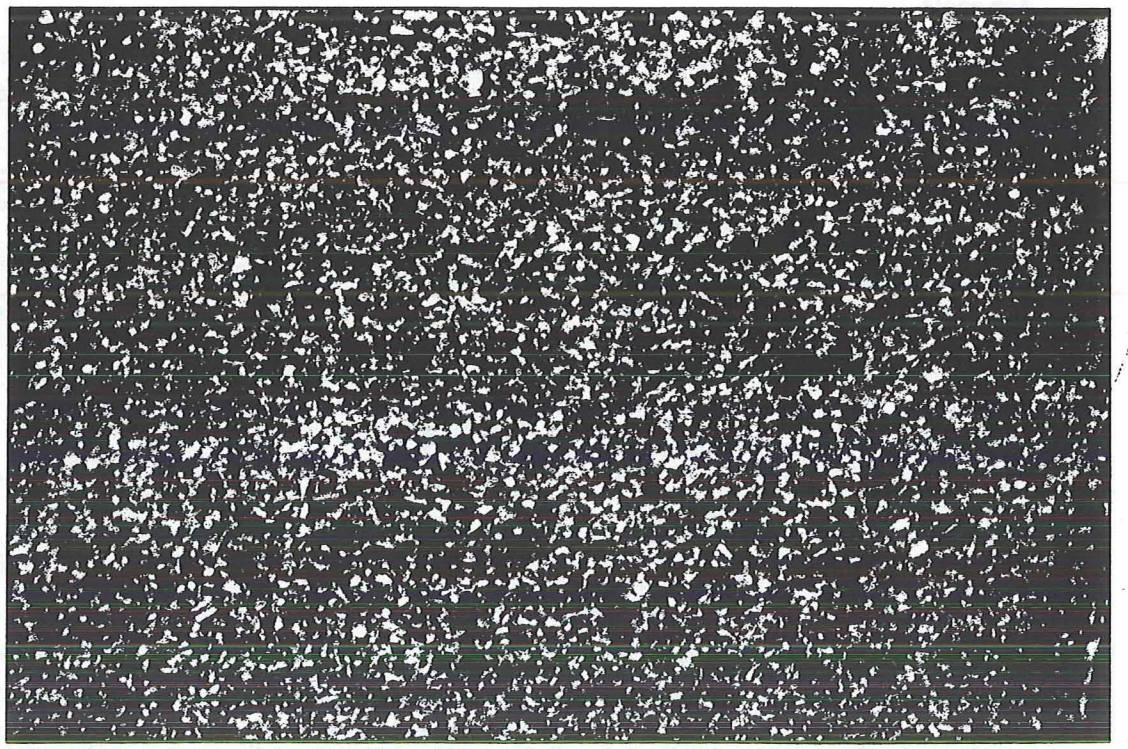

(B) Photomicrograph of pelitic siltstone, from the bottom of the section of green, pelitic, unnamed slates, Cottonwood Canyon. Photo shows horizontal graded bedding (Nikon 5x).

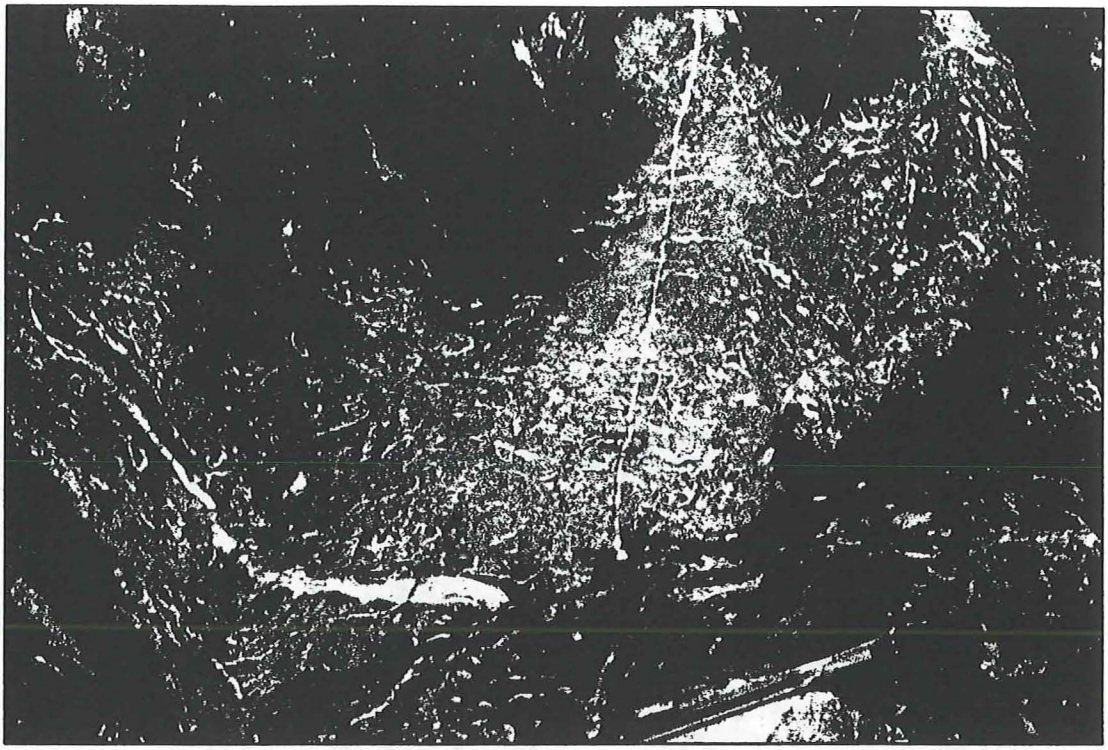

(A) Non-spherical olistolith within the upper Fumarole Canyon sequence showing soft sediment deformation around the margins; Black Canyon. Note ballpoint pen for scale.

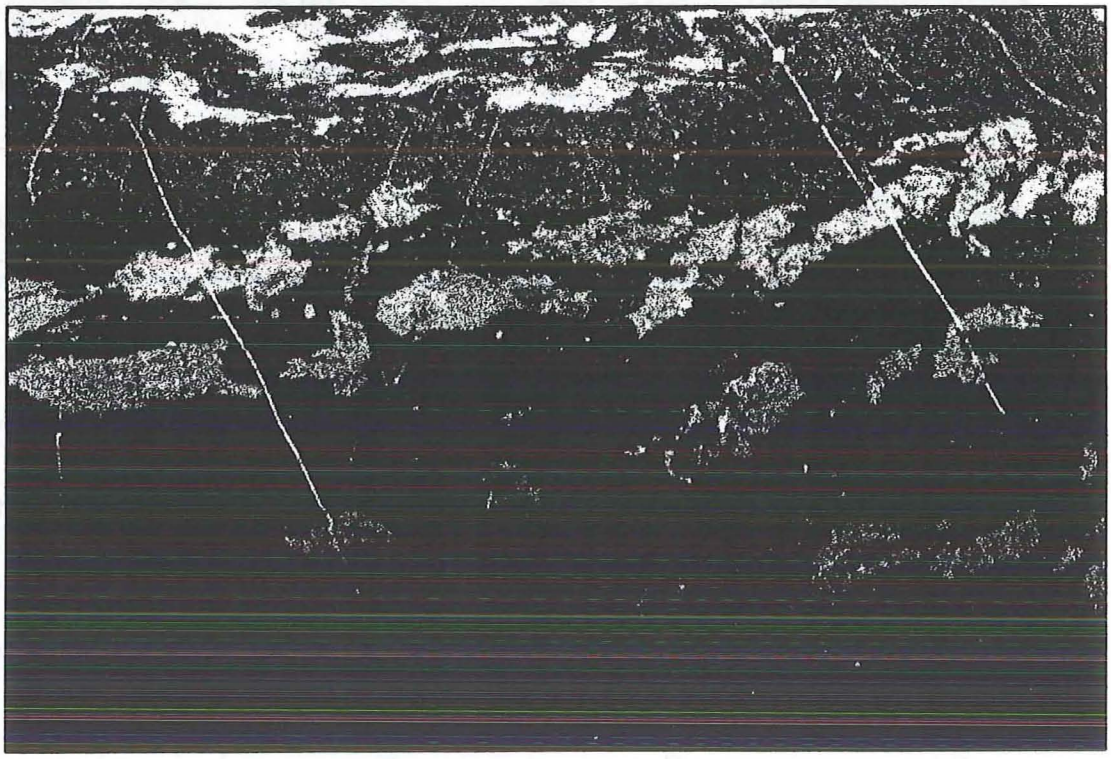

(B) Preferentially aligned, spheroidal olistoliths within the upper Fumarole Canyon Formation showing marginal soft sediment deformation; Black Canyon. Scale is same as above.

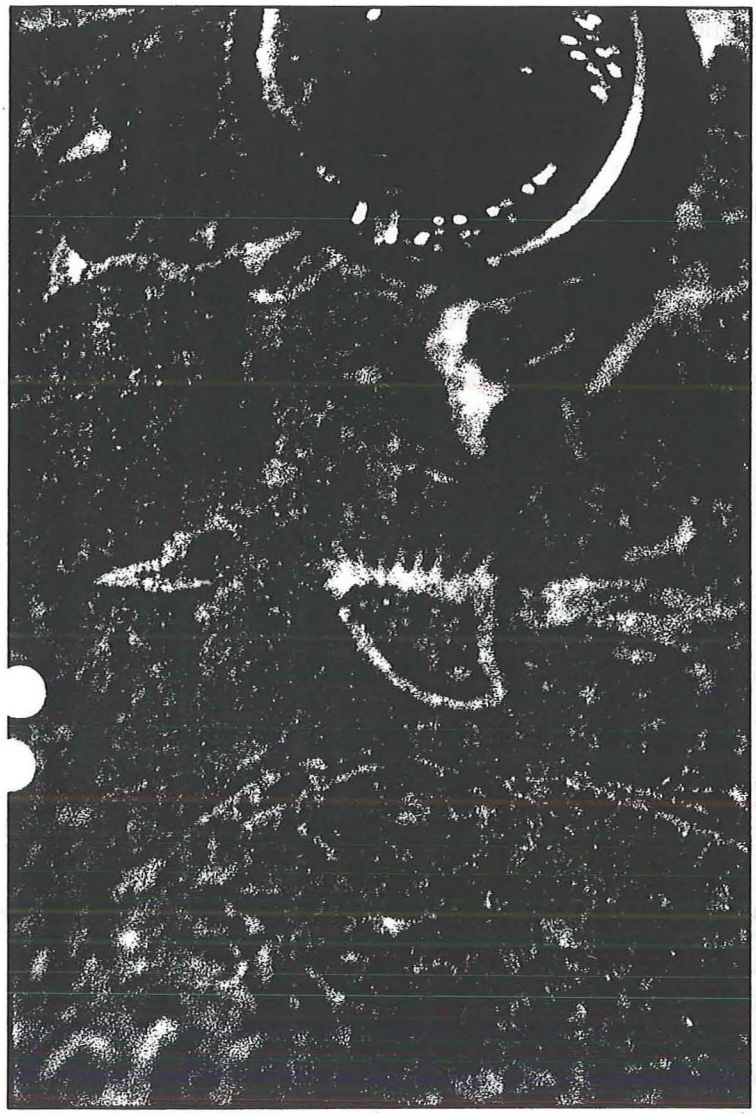

(A) Close-up photograph of fossil hache within bioclastic olistoliths; upper Fumarole Canyon Formation, Black Canyon.

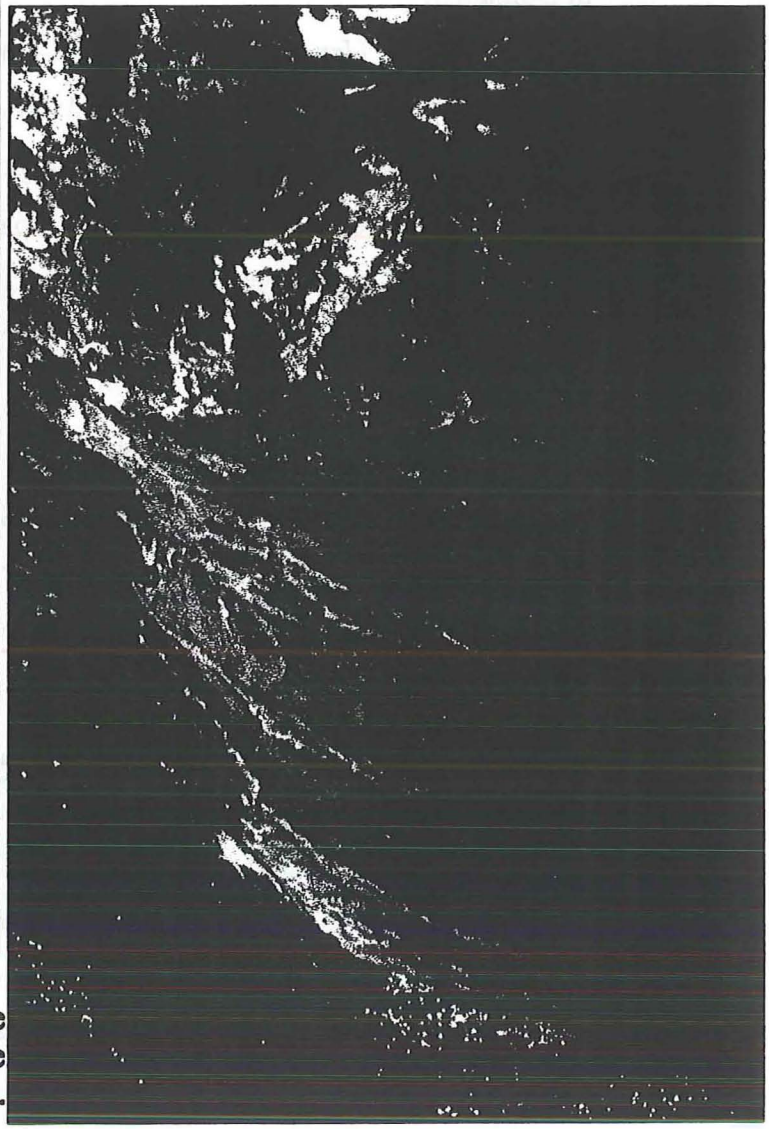

(B) Photograph of soft sediment deformation around the margins of olistostrome bodies; upper Fumarole Canyon Formation, Black Canyon.

Plate P6

continental rise to continental slope environment of deposition, in which fan sedimentation was absent.

1.4.3. Domain 3 Rocks. Rocks in Domain 3, the upper plate of the Black Canyon fault, consist of unnamed Triassic slate and sandstone, and the Boyer Ranch Formation. One gabbro sill, associated with the Humboldt igneous complex, is also present in Domain 3.

(3a) Unnamed Triassic Sandstone and Slate. Unnamed sandstone, sandy siltstone and pelitic siltstone are exposed throughout Domain 3, where they underlie the Boyer Ranch Formation. There are three exposures of the unnamed rocks within the study area. In Cottonwood Canyon, the rocks crop out from beneath the base of the Boyer Ranch Formation. In Black Canyon, they occupy part of the upper plate of the Black Canyon fault. Along the rangefront, south of Cottonwood Canyon, they crop out in a section of strongly hydrothermally altered rock.

The most complete section lies 250 meters north-northwest and upstream from the mouth of Cottonwood Canyon. The section underlies the basal conglomerate of the Boyer Ranch Formation (plate P7) along an angular unconformity. From the unconformity toward the northwest, the slate unit crops out for another 200 meters upstream. The upper part of the unit in Cottonwood Canyon consists of brownish-red, coarse siltstone. The siltstone is interbedded with sheets and lenses of brown, medium-grained sandstone. Stratigraphically down-section, the rock becomes light green, finer grained, and slightly more pelitic (plate P4B); in addition, sandstone beds disappear, and the rock gains a pronounced slaty cleavage. Primary sedimentary structures in the section occur in both the sandstone and siltstone. Symmetric to slightly asymmetric climbing ripples are ubiquitous, and are the most common structures in the siltstone. The ripples are useful in tracing bedding contacts where tectonic cleavage is strong. Loading structures and other soft sediment deformation structures are fewer in number and confined to the coarser grained, red siltstone beneath the unconformity. Sandstone interbeds show cross- and plane-lamination and reactivation surfaces. Approximately 105 meters of unnamed strata are exposed in Cottonwood Canyon; cross sectional analysis suggests, however, that about 210 meters of rock are present at this location between the unconformity and the projected, buried surface of the Black Canyon fault (Plate 2, cross section A-A'). The Cottonwood section is unfossiliferous.

(A) Unconformity (red line) at the base of the Boyer Ranch Formation, on the south side of Cottonwood Canyon. Dolomitic conglomerate of the Boyer Ranch overlies purple, unnamed slates with slight angular discordance.

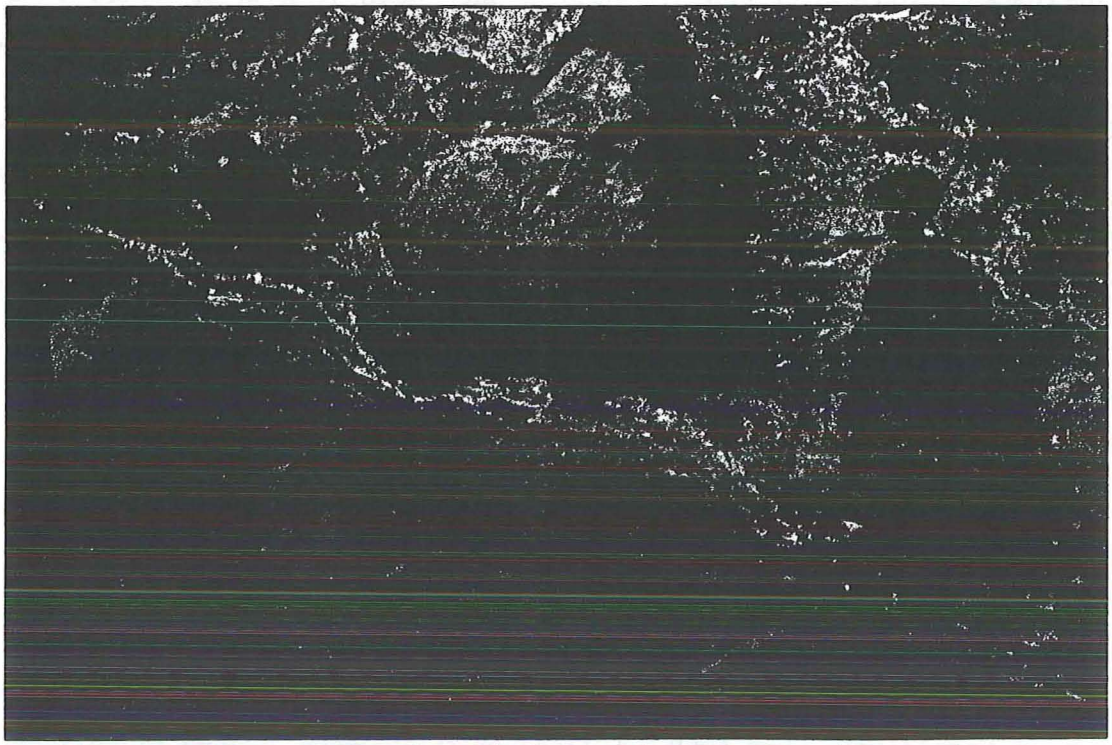

(B) Close-up of the unconformity at the base of the Boyer Ranch Formation, showing dolomitic cobbles of the basal Boyer Ranch lying discordantly above sub-Boyer Ranch slates. Note pencil for scale.

The largest section of unnamed slaty rocks is exposed 1.5 kilometers southwest of Cottonwood Canyon, and crops out beneath the Boyer fault between two large rangefront landslides. Ninety percent (90 %) of the outcrop is heavily hydrothermally altered and friable. Thus, it is not a good location by which to demonstrate the primary character of the rock. Within the wash at the very southwestern tip of the section, however, the alteration is minor, and the rock is discolored but not texturally destroyed. At this location, the rock consists of thinly bedded siltstones, similar to those in Cottonwood Canyon. A host of primary shallow-water bedforms are present, including channel scours with rip-up clasts, algal laminations, bioturbation and burrows, and ripple laminations. Although approximately 380 meters of stratigraphic thickness is exposed at this location, neither the top nor the bottom of the section are exposed.

The third exposure of the unnamed rocks is in Black Canyon, in the upper plate of the Black Canyon fault. The unnamed rocks crop out as a thin seam, above the fault, and along both the southern and northern ridges of Black Canyon. Although they are sheared, the rocks in the Black Canyon area are similar to the green, more pelitic rocks at the bottom of the Cottonwood Canyon section. The rocks lack sandstone interbeds, and are green and highly pelitic, as indicated by their golden, phyllitic sheen, and schistose cleavage. In addition, climbing ripples are present, but are hard to find in the field because shearing has destroyed the delicate bedding. To see the climbing ripples in the Black Canyon outcrops, one must find samples where bedding planes create an intersection lineation with cleavage surfaces. Once bedding is found in this way, the sample can be fractured perpendicular to the bedding, and then the climbing ripples are vague, but visible. In the laboratory, smooth, shorn surfaces of a these types of samples can reveal the climbing ripples very nicely.

The unnamed rocks were first mapped by Page (1964) as being a unit unlike any other in the central and southern Stillwater Range. Speed (1969) also mentions these rocks as being unmatched in the Stillwater Range, but suggests their possible similarity to rocks near the top of the Triassic rocks of the Clan Alpine sequence. I presume that the "similar" rocks to which Speed (1969) refers, are those of the highest terrigenous member of the Hoyt Canyon Formation of the Clan Alpine sequence. There are three reasons for the tentative correlation with the Hoyt Canyon Formation: first, in the Clan Alpine Mountains north of Hoyt Canyon, the Hoyt Canyon Formation underlies the unconformity at the base of the

Boyer Ranch Formation. Second, the exposures of the base of the Boyer Ranch Formation north of Hoyt Canyon are the nearest, to Cottonwood Canyon, of all the regional localities in which the base of the Boyer Ranch is exposed. Third, Speed's descriptions of the upper terrigenous member of the Hoyt Canyon (Speed, 1978b, p.247) fit very generally with my observations in Cottonwood Canyon; in particular, the upper terrigenous unit of the Hoyt Canyon contains "...symmetric ripples...in current laminated fine-grained sandstones". Because of these similarities, the sub-Boyer Ranch rocks exposed in Domain 3 are quite possibly correlative with the upper Hoyt Canyon Formation. Assuming that the unnamed rocks are correlative with the Hoyt Canyon Formation, the age is upper Norian (Speed and Jones, 1969).

(3b) Boyer Ranch Formation. The Boyer Ranch Formation is named from the old Boyer Ranch, that lies three (3) km to the southeast of the mouth of Cottonwood Canyon. The type area lies across Dixie Valley, low in the Clan Alpine Mountains and two miles due north of Shoshone Creek (Speed and Jones, 1969). Within Domain 3, the Boyer Ranch Formation is the most widely exposed unit, and constitutes over half of the outcrops. The Boyer Ranch rocks in Domain 3 include basal conglomerate, a small piece of basal limestone, and a large section of near-basal quartz arenite. The rocks are exposed within a structural window, that is framed on the northwest by the Boyer fault and on the east by the Dixie Valley fault. The basal conglomerate crops out 250 meters inside Cottonwood Canyon, where it unconformably overlies unnamed Triassic siltstones (described above). The outcrop is a southeast dipping wedge of mottled, purple-brown, poorly sorted conglomerate, that is capped conformably by a lens of grayish-brown, sandy limestone. At the very base of the conglomerate, along the unconformity, the conglomerate is very coarse and moderately sorted (plate P8). The larger size fraction of clasts consists of sub-rounded to sub-angular, pink, gray, and tan dolomitic cobbles, that range in width from two (2) to twenty (20) centimeters along the long axis, and average about 12 centimeters in length. Subordinate size fractions are composed of dolomite, chert, and quartzite pebbles that are relatively more rounded and average 2 to 3 cm in diameter. Upward in the section, the conglomerate clasts become finer-grained, more poorly sorted, and more calcareous. In addition, the larger size fraction of cobbles disappears. Along the upper contact of the conglomerate, the univariant size fraction consists of angular to sub-rounded limestone, dolomite, chert, and quartzite

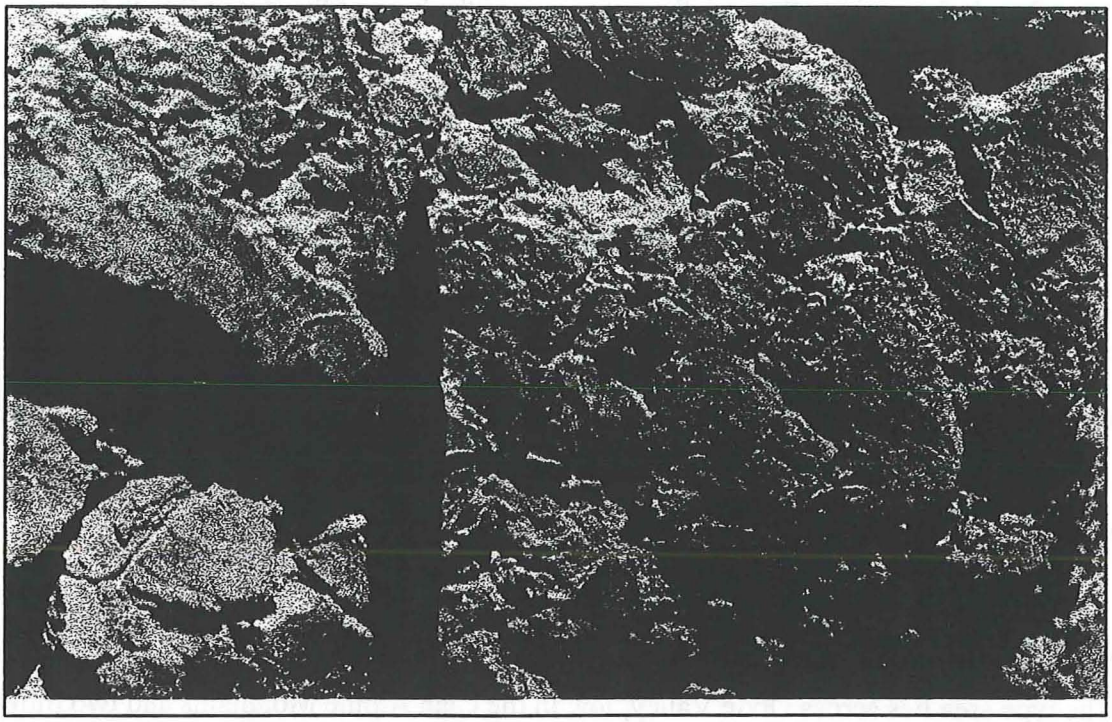

(A) Photograph of dolomite pebbles; basal member of the Boyer Ranch Formation, Cottonwood Canyon. The interlocking texture, called solution pitting, is the result of high strain in the limb of a megascopic F2 anticline.

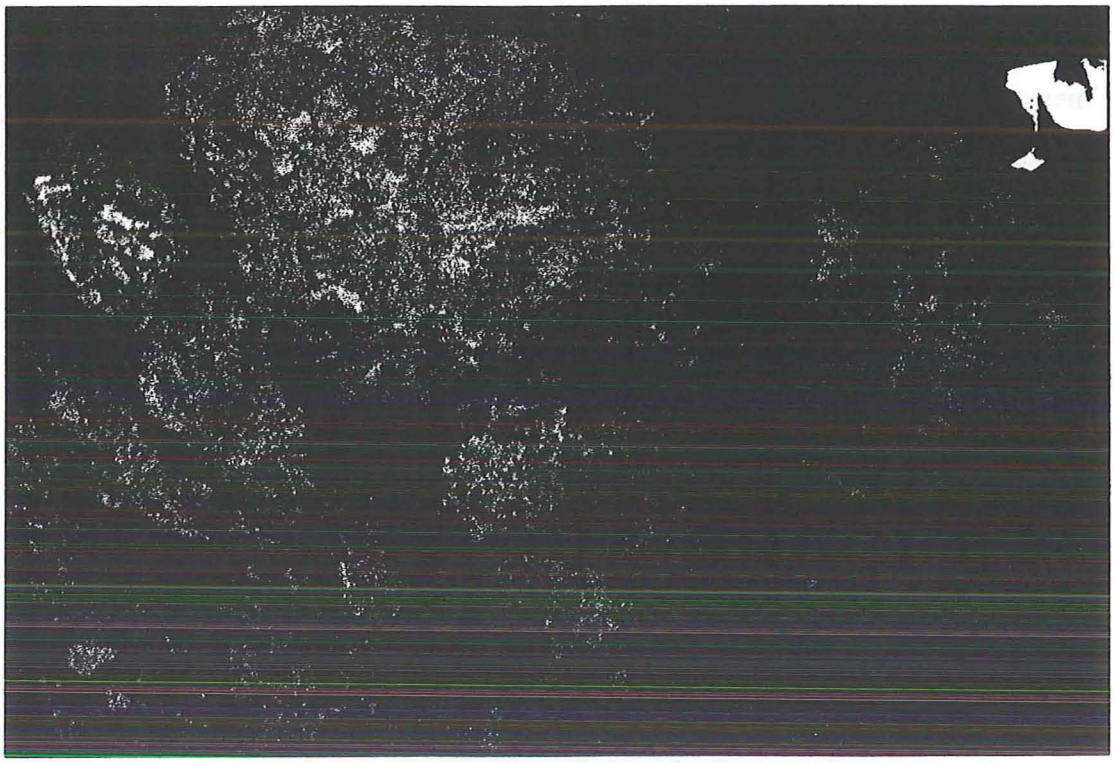

(B) Photograph of the larger size fraction of clasts in the basal Boyer Ranch conglomerate. Again, note the interlocking solution pits around the margins of the clasts.

pebbles that average between 1 and 3 centimeters across their long axes (plate P9B). In addition, the matrix composition changes upward in section from dolomitic to predominantly calcareous and quartzose. At the base of the conglomerate, the matrix is a coarse, moderately sorted dolomitic sandstone. Matrix at the top of the section is coarser grained, very poorly sorted, highly calcareous sandstone.

Along the upper part, the conglomerate is matrix supported, whereas the base of the section is clast supported. Finally the conglomerate is roughly 30 meters thick.

A lens of internally folded, gray limestone conformably overlies the conglomeratic unit (plate P10). From a standpoint within Cottonwood Canyon, the outcrop is almost indistinguishable from the underlying conglomerate, but truly is a distinct and homogenous rock. The exposure consists of gray, massive limestone that is chaotically intercalated with fine, cross bedded brown sandstone. Because the limestone is strongly deformed, larger scale bedding characteristics are not apparent. The limestone is roughly ten (10) meters thick.

Boyer Ranch quartz arenite crops out in Domain 3, from above the basal conglomeratic wedge, to the mouth of Cottonwood Canyon, and then to the northeast as far as the Black Canyon fault. The regularity of bedding contacts in this section is notable. Beds are generally between ten (10) and thirty (30) centimeters thick, and fine upwards, so that the base of each bed to be slightly darker than the top. Between the thick beds, very thin (.1- to 1 centimeter) fine-grained sandstone intercalations are often present. Internally, the sedimentary structure in the arenite beds is homogeneous. Planar, microfine, and parallel laminations permeate the individual beds—and can be used to indicate bedding where the bedding contacts are obscured by fracturing—but constitute the only bedforms Also notable in this near-to-basal section are thick, irregular layers of interbedded conglomerate and coarse sandstone (plate P9A). These layers appear to be present only in the near-to-basal part of the Boyer Ranch quartz arenite. They are internally stratified by cross-bedded sandstone and calcareous, matrix supported conglomerate. The presence of reactivation surfaces, discontinuous lensoidal bedding, and flow alignment of elongate clasts, indicate that these strata were deposited in a turbulent environment. I interpret these interbeds, therefore, as channel deposits. In some cases, however, the order of stratification resembles an incomplete Bouma sequence. An alternate interpretation could be that the coarse strata are of a gravity slide or possibly of a turbiditic origin. Quartz grains are the single constituent of the arenite.

(A) Photograph of conglomeratic mass-flow or channel deposit, interbedded within quartz arenite in the lower Boyer Ranch Formation; Domain 4, upper Little Cottonwood Canyon. Note hammer for scale.

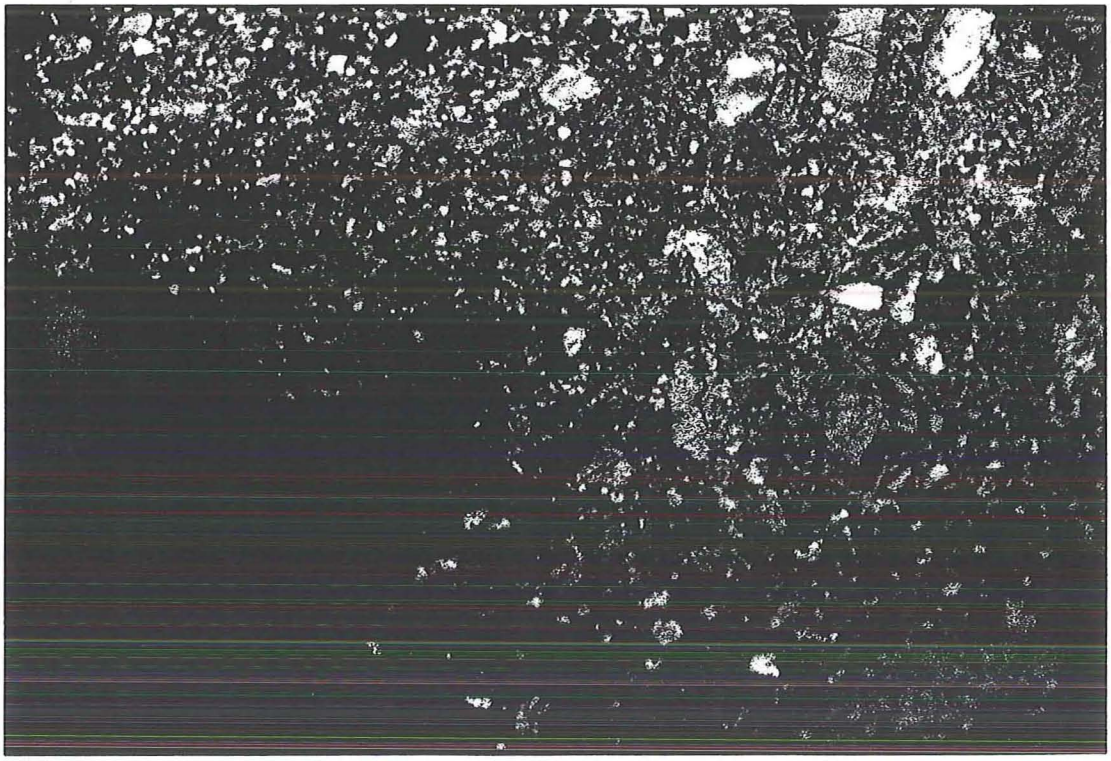

(B) Close-up photograph of matrix supported, calcareous conglomerate near the top of the basal Boyer Ranch conglomerate. Note the smaller size and more varied types of clasts, as compared with the base of the conglomerate (plate P8); Cottonwood Canyon.

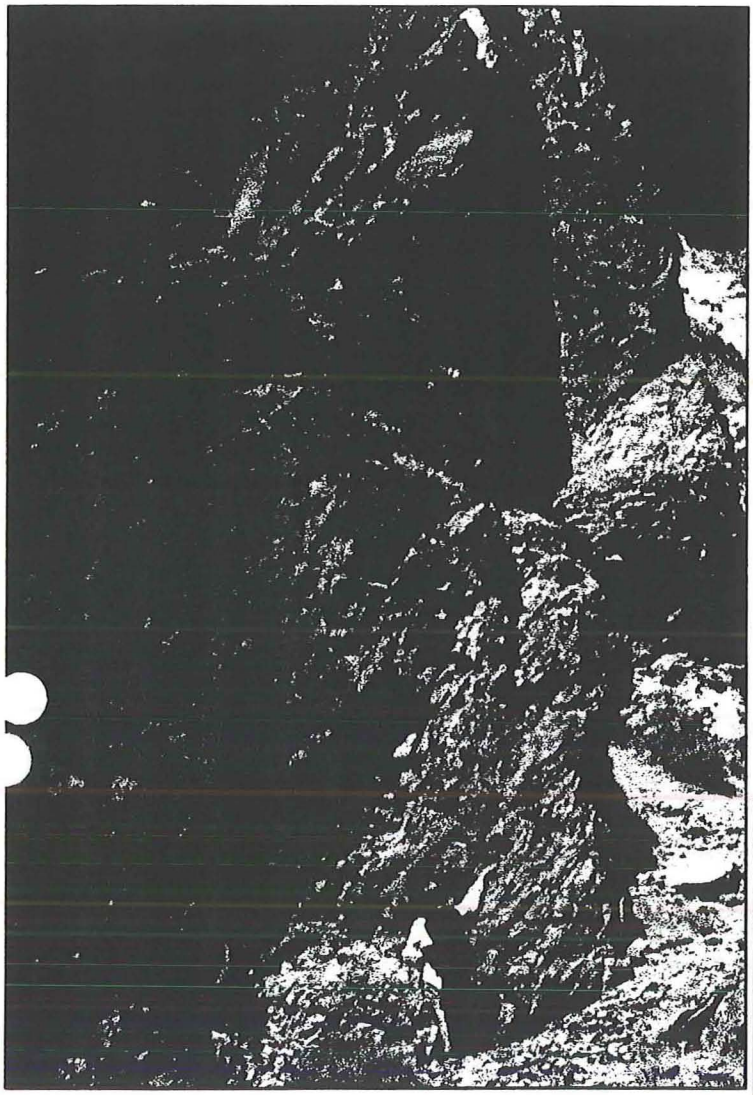

(A) Photograph of a lens of highly internally folded limestone, located between the basal conglomerate and the upper quartz arenite members of the Boyer Ranch Formation; Cottonwood Canyon.

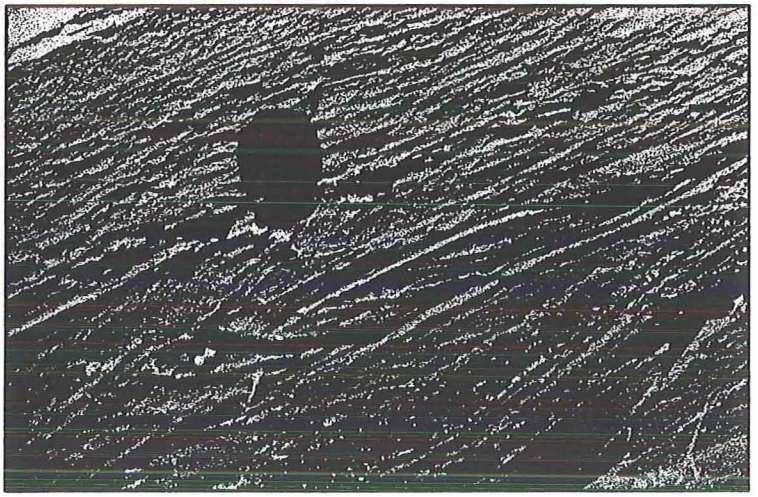

(B) Close-up photograph of light-brown, sandy interbeds, within the gray, Boyer Ranch limestone; Cottonwood Canyon.

The grains are, without exception, rounded and medium-fine to fine-grained, and very well sorted.

The section of Boyer Ranch in Domain 3 thus comprises forty (40) meters of basal conglomerate and limestone, below approximately 120 meters of a near-basal portion of more typical quartz arenite. All of these rocks are unfossiliferous. The lower age of the Boyer Ranch is constrained by Late Triassic (Norian) rocks, that underlie the Boyer Ranch Formation in the Clan Alpine Mountains below an angular unconformity. The upper age is constrained by a range of dates from the Humboldt igneous complex, that intrudes the Boyer Ranch. Potassium/argon (K-Ar) dating of the Humboldt complex (described below) indicates that its age is between 179 and 157 Ma. The Boyer Ranch must therefore be older than about 157-Ma.

(3c) Sills Associated with the Humboldt Igneous Complex. In Domain 3, a sill of orthopyroxene gabbro is exposed around the mouth of Cottonwood Canyon. The sill crops out on the southwest side of Cottonwood Canyon, and strikes southwest for another 300 meters along the face of the Dixie Valley fault scarp. The sill was originally mapped as "microgabbro" (Speed,1976), however the rock has a microgabbroic texture only along the chilled margins of the sill, while in the center it is very coarse grained. In the coarse grained gabbro, purple orthopyroxene oikocrysts and bright green, poikilitic olivine crystals are visible to the un-aided eye. The microgabbro along the margins is dense and green, with a sugary texture, and mafic minerals are too fine grained to be visible.

1.3.4. Domain 4 Rocks. Rocks in Domain 4, the upper plate of the Boyer fault, include the Boyer Ranch Formation and the Humboldt igneous complex.

(4a) Boyer Ranch Formation. In Domain 4, exposures of the Boyer Ranch Formation consist entirely of quartz arenite. In some exposures adjacent to the Boyer fault, the presence of matrix-supported conglomeratic beds, like those described above, suggest that the stratigraphic position represented at the level of the Boyer fault may be near-to-basal. Along the Boyer fault, bedding is obscure and disturbed, because of brittle fracturing and drag folding (see the discussion of structural geology, below). In the areas of Domain 4 that are structurally most distant from the Boyer fault, bedding in the arenite is very regular, similar to that in Domain 3. Furthermore, in the southern three-quarters (3/4), where the arenite is intruded by the Humboldt complex, the bedding contacts are obscured and/or

completely eradicated by fracturing, and by calcium and silica metasomatism. In the aureolae of smaller intrusions, the arenite has a baked, rusty appearance and often contains large, euhedral secondary magnetite and lesser pyrite. In the contact zone of the larger volume of crystalline rock, the Boyer Ranch ranges in appearance from a baked arenite, to a brecciated arenite, to a completely unrecognizable siliceous microbreccia or crackle breccia.

Cross-sectional analysis of the Boyer Ranch Formation in Domain 4 indicates that its thickness may be as much as 975 meters. This figure contradicts an estimated maximum thickness of 150 meters (Speed and Jones,1969); however, a percentage of the relatively large thickness in the study area is probably a result of large structural thickening by megascopic folding. The Boyer Ranch Formation is isolated, and does not correlate with any regional sequences.

(4b) Humboldt Igneous Complex. The Humboldt igneous complex occupies the southwestern three-quarters (3/4's) of Domain 4, and extends from the southwest corner of the map, to the northeast as far as Black Canyon. The complex consists of a continuous volume of mafic and intermediate to felsic plutons, and subordinate small plutons, dikes, sills, and pod-like stocks. Intermediate, volcanic rocks overlie the plutonic rocks. The volcanic rocks have been treated as hypabyssal (Speed, 1976) and are associated with the Humboldt complex; however they will not be discussed in this section.

The largest plutons within the complex are mafic, dark green to greenish-gray diorite and gabbro, and are the dominant crystalline rock in the complex. These rocks are exposed (and easily accessible) in Cottonwood Canyon. The large plutons are not foliated or stratified, though some facies of the Humboldt igneous complex, in other areas, do show layering (units Jg2 and Jg3 of Speed, 1976). The rocks consist of plagioclase and varying amounts of hornblende and olivine, and are generally dioritic; however, enclaves, where the mafic concentration is high enough to produce gabbro, are common. Subordinate mafic and intermediate/felsic plutons intrude randomly into the larger plutons and the surrounding country rock. The largest of these subordinate intrusions is a small pluton, located on the ridge southwest of Cottonwood Canyon, that consists of pinkish-weathering anorthosite. There is some primary foliation along the base of this anorthositic pluton, but otherwise it shows no internal layering. The anorthosite is felty textured and equigranular, consisting wholly of fine- to very medium-grained plagioclase.

The smaller-sized, subordinate intrusions include mainly mafic sills and small, pod-like stocks. These lesser intrusions commonly intrude the country rock (in this case, Boyer Ranch quartz arenite) peripherally to the larger plutons. Almost all of these peripheral intrusions were originally mapped as "microgabbro" (Speed, 1976; Dilek, 1995), and indeed many of the intrusions, especially the sills, are very a fine-grained, dark-green microgabbro. A percentage of the lesser intrusions, however, are coarse-grained gabbro with cumulate hornblende and/or olivine, and are microgabbroic only along their chilled margins. Therefore, not all of the microgabbro, as mapped by Speed (1976), has a microgabbroic texture. In addition, the style of contact metamorphism appears to differ between the cumulate pods and the microgabbro sills. The style of metamorphism around the cumulate bodies is, as described above, baking, staining, and metasomatism, without significant brecciation. Sills, on the other hand, are often accompanied by a unique brecciation of the country rock, in which quartz arenite has been shattered in-situ, and the fragments rounded by the transport of fluids and rock material through the breccia (plate P11). Most of the microgabbro sills and cumulate gabbro pods are exposed in Domain 4, within and to the northeast of Black Canyon. Along the upper part of Black Canyon, the microgabbro sills are crosscut by a large diorite pluton to the south, indicating that the sills are an older phase of the Humboldt complex.

Cross sectional analysis of the Humboldt complex suggests that at least 1500 meters of intrusive rock are present in Domain 4, above the Boyer fault. However, neither the mafic nor the felsic rocks are foliated or well layered within the field area, and therefore it would be difficult to measure their true stratigraphic thicknesses. The first radiometric dating of the Humboldt complex, from exposures in the West Humboldt Range (Wilden and Speed, 1974), constrained the age of the complex to between 165 ± 5-Ma and 145 ± 4-Ma (K-Ar, hornblende and biotite). In the Stillwater Range, a similar, published radiometric date places the age of the complex at 157 ±4-Ma; however, unpublished dates from geochronological studies done by Dr. Mark Elison (Dilek, 1995) give ages of 179- to 165-Ma. The age of the complex is thus bracketed between middle Middle Jurassic and middle Late Jurassic.

1.4.5. Tertiary Rocks.

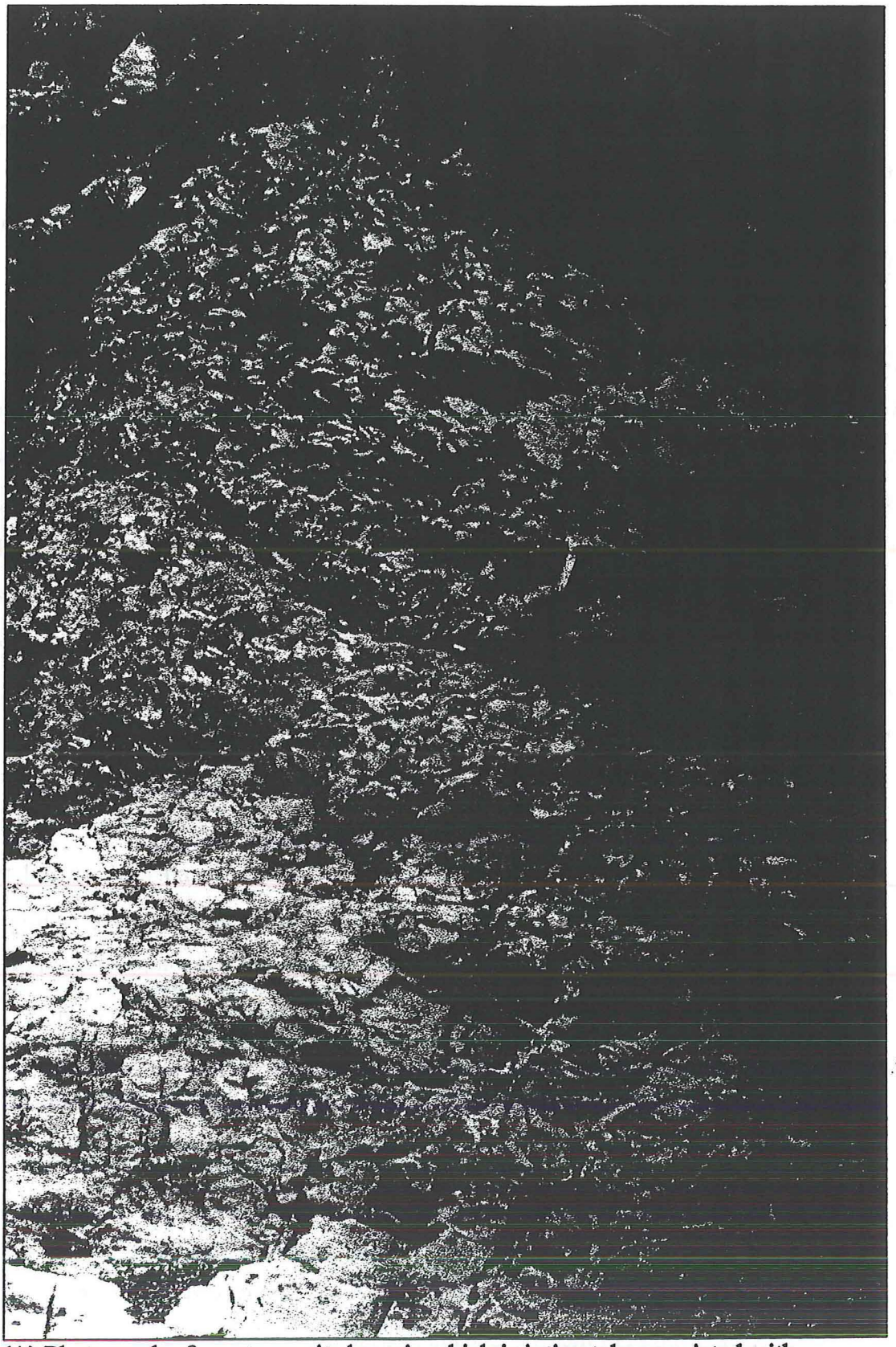

(A) Photograph of quartz arenite breccia which is intimately associated with microgabbro sills. The rounded, yellow clasts are quartz arenite. The green matrix is an altered, punky, chloritic material. Note hammer for scale.

(5a) Miocene Basaltic to Andesitic Dikes. Basaltic to andesitic dikes in the study area were first mapped and described by Dilek (1995). The dikes stem southward from a pluton-sized complex of sheeted dikes located at the extreme northeast end of the map (Plate 1), and intrude the Mesozoic rocks, described above, in all domains.

The larger and greater number of dikes are exposed in domains 1 and 2, where they are nearer to the massive sheeted dike complex, that lies to the north of Fumarole Canyon. These dikes trend consistently toward the northeast, and dip moderately to steeply westward. The larger dikes can be as much as 120 meters in width and are composites of smaller, sheeted intrusions. These sheeted dike swarms are coarse-grained to aphanitic, and equigranular. The cores of the coarse-grained dikes are brownish-green and altered, while their margins are chilled and aphanitic, and weather to a dark reddish-brown color. Coarse surfaces often show a unique pattern of localized spherical exfoliation, that causes pillow-shaped, basketball-sized spheres to differentially weather out of the homogeneous dike mass. Generally, fresh surfaces of coarser-grained dikes are highly altered, though round clinopyroxene or altered clinopyroxene usually stands out. In addition, the large dikes are highly fractured by contact-parallel cooling joints.

A lesser number of smaller dikes are exposed in domains 3 and 4. In general, they have a more inconsistent trend than dikes in domains 1 and 2, probably due to faulting along the Black Canyon and Boyer faults. These dikes are isolated and much narrower, ranging between 15 centimeters and four (4) meters in width, with an average width of one (1) to two (2) meters. In external appearance the isolated dikes are, like the chilled margins of larger dike swarms to the north, weathered to a dark, reddish-brown color. Freshly broken surfaces are black, glassy, and usually aphanitic, though the dikes that are slightly more coarse have visible microlitic plagioclase, round phenocrysts of bottle-green clinopyroxene, bronze biotite, and occasional acicular hornblende. Although some of the isolated dikes clearly show chilled margins, they tend to lack internal contact-parallel cooling joints.

The composition of the Miocene dikes is slightly variable, but not so different as to be indicative of separate intrusive phases. Most of the dikes are well represented, compositionally and texturally, by the large sheeted dike complex that is exposed at the extreme north end of the map (Plate 1). Rocks in that complex consist of fine- to coarse-grained basaltic andesites, that contain intergranular plagioclase and clinopyroxene and/or

orthopyroxene, biotite, a little quartz, and euhedral magnetite and pyrite (plate P12A). The few dikes that take exception to this typical composition contain acicular hornblende. In hornblende-bearing dikes, the hornblende is usually fresh, while the pyroxenes are completely altered to (plate P12B).

Tertiary dikes in the study are have been dated from two different radiogenic elements. Potassium-argon (K-Ar) whole rock dating (Dilek, 1991) gave ages of between 14.9 ± 0.5 and 21.1 ± 1.0-Ma. Argon-argon (Ar-Ar) dating of hornblende from dikes in the southwestern part of Domain 2 (Dilek, pers. comm.) gives an age of 14.5-Ma. Because whole rock dates have a range of roughly 7-Ma, it is conceivable that in Early Miocene time the rocks in the field area were subjected to a long lived episode of basaltic magmatism. It is probable, therefore, that the variance in petrology of the dikes represents multiple but indistinct stages of intrusion from a basaltic magma source.

(5b) Travertine and Sugary Limestone. A unit of travertine and sugary limestone is exposed 1.5-km upstream from the mouth of Cottonwood Canyon. The entire exposure is located around the juncture of a northeast-striking normal fault (the RF5 fault), and a set of north-striking vertical faults(the N-S fault set). The RF5 fault bounds the unit on the east, while the vertical faults cut right through the middle of the unit. The entire unit dips moderately to steeply towards Cottonwood Creek.

The lower part of the unit, exposed along the jeep trail in Cottonwood Canyon, consists of travertine. At its base, the travertine depositionally overlies both Boyer Ranch quartz arenite and rocks of the Humboldt complex, or entrains colluvium. Larger scale characteristics of the contacts are obscure, and large scale bedding is chaotic. The travertine is typical: very thinly bedded, flaky, and vessicular, with abundant plant fossils.

Topographically higher exposures consist of a dense, sugary-textured limestone. The limestone is sub-vertically foliated, and forms resistant, vertical ledges, that stand out in relief. In addition, the ledges appear to delineate the vertical faults that cut through the unit. The vertical foliation and resistance to erosion probably are the result of the movement of hydrothermal fluids, that have recrystallized and/or metasomatized the travertine and destroyed its original texture. Limestone that is recrystallized in this way is sometimes called "sanded" limestone. Additionally, open-space calcite can be found in the carbonate

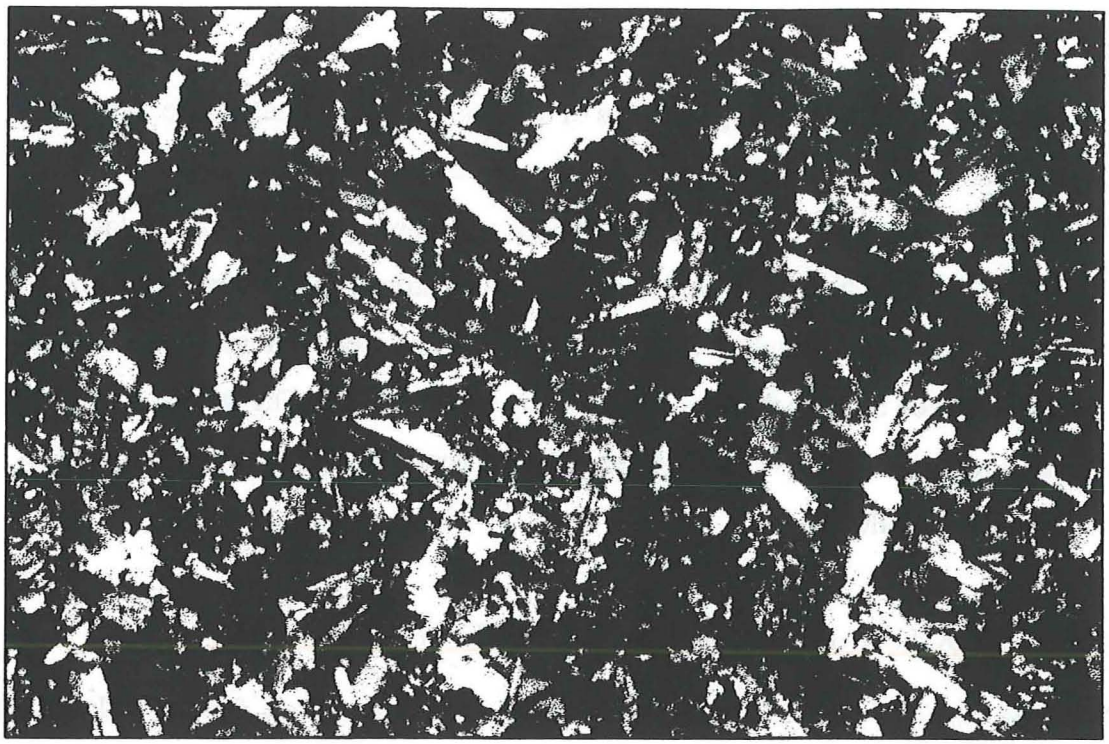

(A) Photomicrograph showing the typical texture and composition of basaltic Miocene dikes. Sample is from a sheeted dike complex north of Fumarole Canyon.

(B) Photomicrograph showing the atypical composition of some basaltic Miocene dikes. Note brown hornblende and round, altered pyroxene. Sample is from Black Canyon.

unit. The RF5 fault contains large crystals of dogtooth spar and other calcite spar. The vertical faults that cross-cut the show no open-space calcite.

The entire unit thickens toward the southeast, attaining a maximum thickness of approximately forty (40) meters, within the ephemeral stream channel that delineates the northeast-striking normal fault. The age of the unit is relatively younger than the local colluvium, as well as older than the cross-cutting vertical faults. The unit may have originated as a spring deposit during the late Pleistocene, during which period a pluvial lake occupied Dixie Valley.

1.5. STRUCTURAL GEOLOGY OF THE STILLWATER ESCARPMENT

Structural Framework. Cross-cutting relationships between folds, fabrics, faults, and other tectonic structures are used to determine the relative ages of those structures. A single deformation event, or phase, that results in the formation of the oldest tectonic suite of structures is referred to as "D_1". Correspondingly, folds formed during a phase are referred to as "F_1"; cleavage or foliation as "S_1"; and mineral and other lineations as "L_1". D_2 is a younger deformation phase than is D_1, and so on. A description of all structural features, organized thus, can be useful in reconstructing the tectonic history of a geologically complicated area. In the following section (1.5), I develop such an organization of structural features.

Folds and fabrics are treated according to a scheme of structural domains, as outlined earlier (section 1.3, page 17), that are broken out on the basis of their having distinct lithologies and discrete, faulted boundaries. I will describe consecutively younging phases of folds as they occur in each domain. Also, I will present individual generations of folds in order of size, as megascopic (wavelength ≈ 1000m), macroscopic (wavelength ≈ 100m), mesoscopic (wavelength ≈ 10m), or outcrop-scale (wavelength ≈ 1m). Faults are presented last, for the reason that their descriptions draw upon knowledge of previously established folds and fabrics.

Folds. Folds within the four domains constitute four main phases of deformation: D_1, D_2, D_3 and D_4. F_1 folds are folds within bedding, in domains 1, 2, and 3. F_1 is represented, for

the most part, by a megascopic, north-vergent syncline in the lower plate of the Fencemaker thrust (Domain 1). The F_1 phase may also include a complementary, overturned, megascopic anticline in the upper plate (Domain 2). Smaller scale second- or third-generation F_1 folds are rare; for example, they occur as intrafolial fold hinges in the Fencemaker shear zone. F_{1A} folds occur in the back limb of the megascopic F_1 anticline. This sub-notation applies to certain folds that fold S_1 cleavage, and that also have an axial planar cleavage that is nearly co-planar with the folded S_1 foliation.

F_2 folds are oblique to F_1 folds and reorient S_1 cleavage. These folds verge generally to the west, plunge gently to steeply to the south-southeast or south-southwest, and are present as both mesoscopic and outcrop-scale folds.

F_3 folds are west vergent, upright to overturned, kink bands. They are generally axial planar to a map-area-wide crenulation cleavage (S_3). Without exception, F3 folds are present only in outcrop-scale.

F_4 folds are drag folds associated with both the Black Canyon (F_{4a}) and Boyer (F_{4b}) faults. These folds are localized along and restricted to the shear zones of these faults.

1.5.1. Structural domain I - Folds in the lower plate of the Fencemaker thrust.

Domain 1 contains folds of phases F_1 and F_2. F_3 folds are apparently not present.

Megascopic F_1 folding in Domain 1 is represented by an overturned footwall syncline. The syncline is expressed by the abrupt contact, between black limestone in the lower part of the Natchez Pass Formation, and massive gray limestone in the upper part. At the north end of the map, the attitude of the contact strikes 094°, 45°N. Toward the southern end of Domain 1, the contact is pulled into the shear zone of the Fencemaker thrust. Exposures of the contact, within the shear zone, are parallel to S_1 foliation, and dip moderately to the southeast. The contact thus delineates an northward-overturned footwall syncline that has an interlimb angle of just over 90° degrees. The minimum wavelength of the syncline is approximately 500 meters, but only a small part of the fold is exposed. Cross-sectional analysis suggests that the fold wavelength may be on the order of 1000 meters. Smaller, outcrop-scale F_1 folds occur within the shear zone of the Fencemaker thrust, as dismembered, intrafolial hinges. These folds are exposed in narrow canyons that dissect the shear zone, and occur predominantly in the darker, more competent marble.

F_2 folds in Domain 1 comprise macroscopic, mesoscopic, and outcrop-scale structures, that reorient D_1 structures. Macroscopic F_2 folds are not well preserved in Domain 1, but their existence is implied by scattered erosional remnants of their limbs. The erosional remnants occur along the wide, steep slope on the northeast wall of Fumarole Canyon (Figure 7). Furthermore, Pi (π)-diagram analysis of S_1 cleavage (Figure 6) indicates that the penetrative S_1 foliation is macroscopically folded around a moderately south-southwest plunging F_2 hingeline. Mesoscopic and outcrop-scale F_2 folds are localized and most intensely developed along the Fencemaker shear zone. F_2 folds are best defined where calcareous schist crops out against marble tectonite. The smaller-scale F_2 folds bear out the south-southwest hingeline trend that is demonstrated by Pi-analysis.

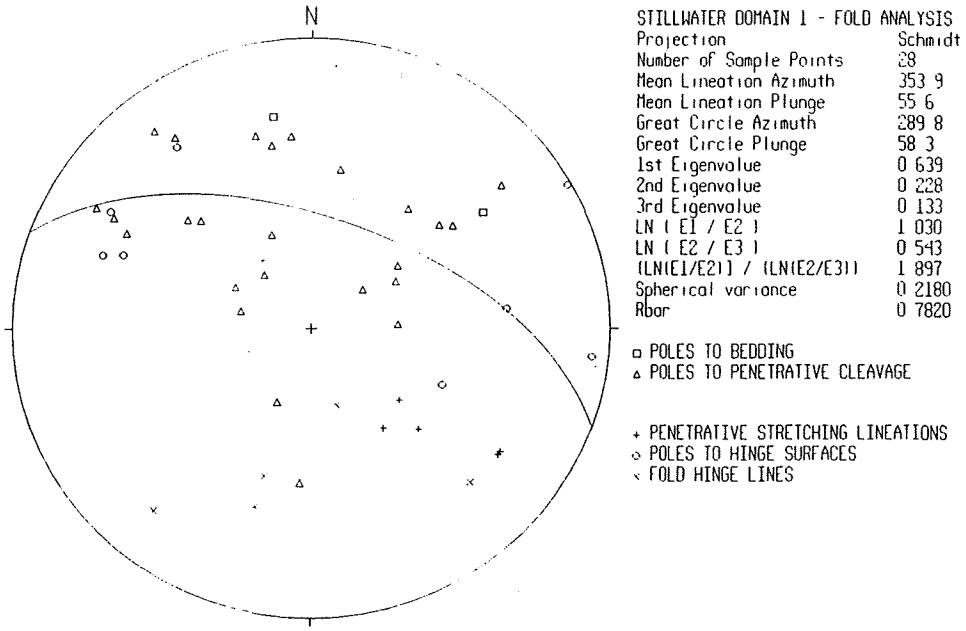

Figure 6. Pi (π)-diagram of poles to S1 foliation, and other data, from Domain 1. The poles define a weak girdle around a south-southwest trending F2 hinge line.

Mesoscopic and outcrop-scale F_2 folds are actually second- and third-generation folds in the limbs of macroscopic F_2 folds. These subordinate generations of F_2 folds consist of upright to overturned, moderately plunging, open to tight folds in S_1 cleavage. The more tightly appressed F_2 folds in Domain 1 have a weak axial planar cleavage (S_2), but more often the F_2 folds lack S_2 cleavage.

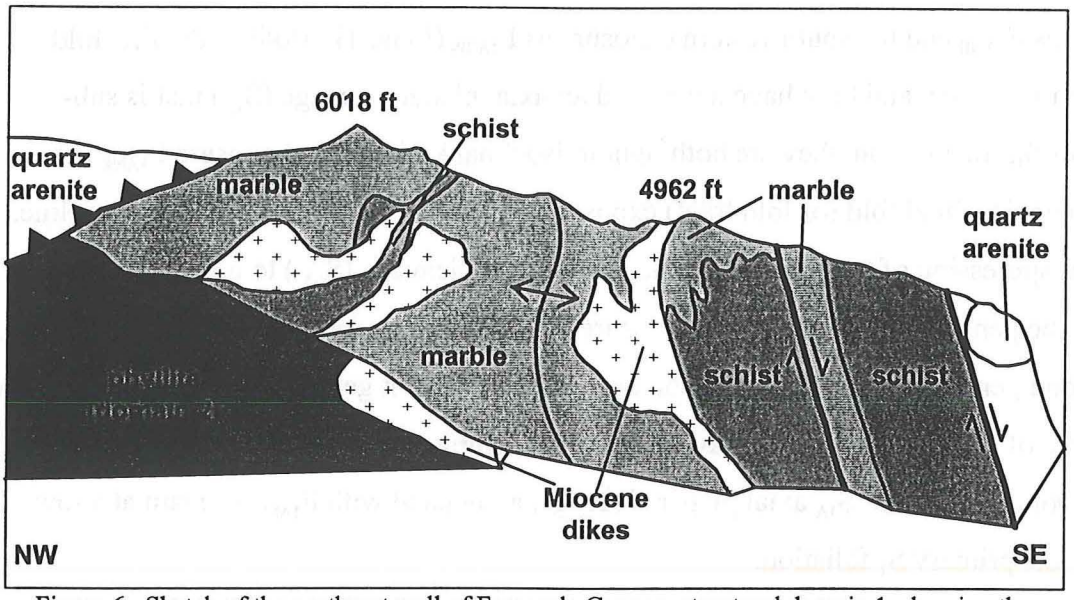

Figure 6. Sketch of the northeast wall of Fumarole Canyon, structural domain 1, showing the location of schist outcrops in the limbs of one or more macroscopic F2 folds.

1.5.2. Structural domain II - Folds in the upper plate of the Fencemaker thrust. As in Domain 1, Domain 2 contains folds of phases F_1 and F_2. In addition, the most dense population of the F_3 folds, in the map region, are found in Domain 2.

Megascopic F_1 folding is present in Domain 2 as one hanging wall anticline, that is overturned to the north. The existence of this megascopic structure is substantiated, but not proven, by the repetition of olistostromal rocks and siliceous argillite of the upper Fumarole Canyon sequence. Siliceous and olistostromal strata in the overturned limb of the fold occupy the ductile shear zone of the Fencemaker thrust. These same strata appear again to the southwest, at approximately the location of Little Cottonwood Canyon, and occupy the upright, back-limb of the anticline. The limbs of the fold thus define an anticline that has an apparent wavelength of at least 1200 meters. The fold is further defined by the anticlinal core, in which pelitic rocks of the lower Fumarole Canyon sequence are highly strained and very strongly foliated. Cross-sectional analysis suggests that the fold has a minimum amplitude of 1500 meters, measured vertically from the projected surface of the Fencemaker thrust. Mesoscopic and outcrop-scale F_1 folds are apparently present in Domain 2 only in the Fencemaker shear zone (described below). Other folds, whose axial surfaces are sub-parallel to the penetrative foliation (S_1), are given the sub-notation F_{1A}. F_{1A} folds are rare and I have only identified two of their exposures. I will therefore refer to the northeastern

exposure as F_{1ANE} and the southwestern exposure as F_{1ASW} (Plate 1). Both of the F_{1A} folds deform S1 cleavage, and both have developed an axial planar cleavage (S_{1A}) that is sub-parallel to S_1. In addition, they are both tight to isoclinal kink folds. Exposure F_{1ANE} is a mesoscopic, isoclinal fold (or fold train) exposed in the core of the megascopic F_1 anticline. The tight appression of the fold causes the axial planar cleavage (S_{1A}) to be always at a low angle to the penetrative S_1 cleavage. Exposure F_{1ASW} is a single, polyphase fold (plate P3A). The second generation, chevron folds, on the limbs of the first generation, are F_{1A} folds. The first phase of this polyphase fold may be the only example, so far, of an outcrop-scale F_1 fold in Domain 2. Faint S_{1A} axial planar cleavage, associated with F_{1ASE}, is again at a low angle to the primary S_1 foliation.

F2 folds are exposed throughout Domain 2. This phase consists of steeply inclined, moderately plunging, gentle to close folds that deform S_1 cleavage. All of the F_2 folds in Domain 2 have been, to my observation, mesoscopic and outcrop-scale structures. However, π-diagram analysis of the S_1 cleavage, in Domain 2, shows that poles to S_1 cleavage form a girdle around a shallowly south-southwest plunging hinge line (Figure 8).

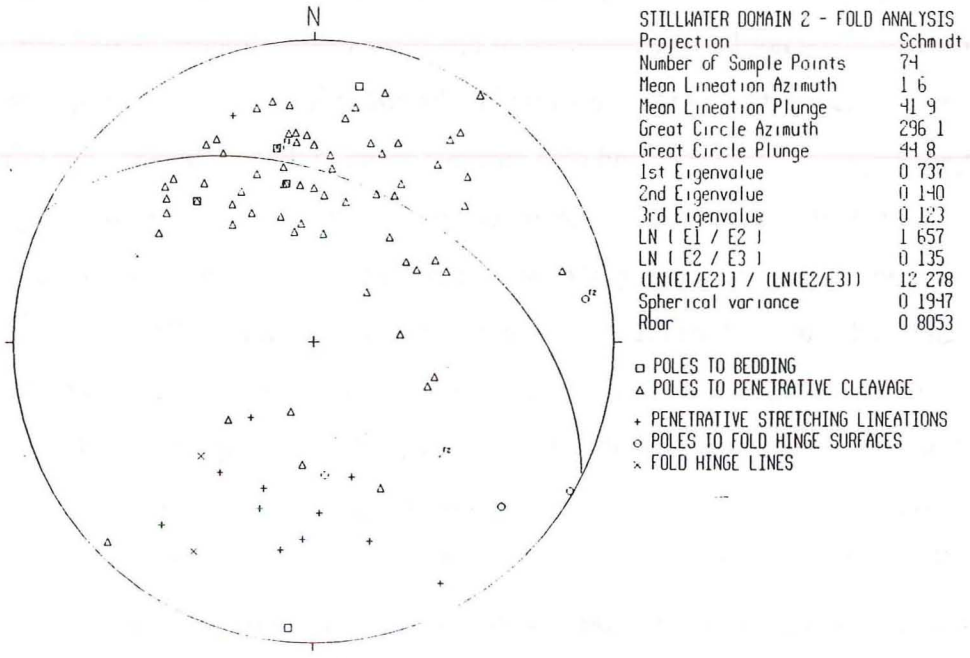

Figure 8. Pi (π)-diagram of poles to S_1 foliation, and other information, in structural Domain 2. The poles define a girdle about the F_2 hinge line.

This stereographic evidence indicates that, as in Domain 1, the penetrative foliation is folded into macroscopic F_2 folds. Mesoscopic and outcrop-scale F_2 folds always plunge moderately to the south or southwest, thereby reflecting the same F_2 hinge orientation demonstrated by the π-diagram girdle (Figure 8). F_2 axial surfaces, in mesoscopic and outcrop-scale folds, dip steeply to the southeast or northwest. In contrast to F_2 folds in Domain 1, F_2 folds throughout Domain 2 tend to lack axial planar cleavage, and are less tightly appressed.

F_3 folds in Domain 2 are small, outcrop-scale folds that range in amplitude from one (1) centimeter to thirty (30) centimeters. They are genetically related to a regional crenulation cleavage (S_3), and occur only in conjunction with S_3 surfaces. The F_3 folds (and cleavages) occur where the pre-existing planar anisotropy of S_1 is the strongest. For example, in Domain 2 the F_3 folds are most numerous in the overturned limb and core of the dominant F_1 anticline. In that limb, S_1 cleavage is strongly developed parallel to bedding and therefore planar anisotropy is strong. F_3 folds are, more or less, kink bands. Typically, the kink bands are asymmetric, and occasionally overturned, to the west. The axial surfaces are co-planar with S_3 crenulation cleavage.

1.5.3. Structural domain III - Folds in the upper plate of the Black Canyon fault.

Domain 3 contains abundant F_2 and F_3 folds, and isolated F_4a folds along the Black Canyon fault. Whether F_1 folds are present in this domain is uncertain.

Macroscopic and megascopic F1 folds are not present in Domain 3, but their existence is loosely suggested by smaller-scale bedding folds, and cleavage, in the unnamed Triassic slates. Mesoscopic bedding folds in the slates can be found in the lowest part of the section, on the south side of Cottonwood Creek. At that location, vertical bedding planes can be found at right angles to the penetrative cleavage. Although the rollover in bedding is not perfectly traceable, through the strongly foliated slate, the bedding roughly defines a west vergent S-fold, with an interlimb angle of approximately 45° degrees. Other S-type bedding folds are found near the stratigraphic top of the slate, just below the Boyer unconformity, where they clearly demonstrate that the penetrative cleavage in Domain 3 is axial planar to bedding folds. Because the penetrative cleavage in Domain 3 is both axial planar to bedding folds, and of a similar orientation to S_1 cleavage in Domains 1 and 2, it is possible that bedding folds in Domain 3 belong to phase F_1 or F_{1A}. Intuitively, one might

expect all bedding folds in the Upper Triassic rocks to be F_1, and axial planar cleavage to be S_1. On the other hand, the bedding folds trend southward, much like typical F_2 folds. In addition, we know that the slates must have been co-folded with Boyer Ranch Formation, that depositionally overlies the slates, and that is permeated by F_2 folds (described below). Thus it is possible that bedding folds in the slates are also F_2 folds. In any case, the slates must have been gently folded, prior to the deposition of the Boyer Ranch, in order to have given rise to the regional angular unconformity that underlies the Boyer Ranch Formation (Speed, 1969). Thus, it is necessary to conclude that pre-unconformity folding exists in Domain 3, and therefore that it may represent F_1.

The entire body of Domain 3 is deformed into a train of megascopic F_2 folds. Megascopic F_2 folds are never completely preserved, but mesoscopic second- and third-generation folds, in the Boyer Ranch Formation, validate their existence. Cross sections through Domain 3 (Plate 1) also require the existence of megascopic and macroscopic F_2 folds in order to explain the distribution of conglomerate at the base of the Boyer Ranch. Furthermore, Pi-(π)-diagram analysis of bedding in quartz arenite (Figure 9) shows that all arenite bedding in Domain 3 is folded around a moderately south-southeast plunging F2 hinge line.

The most tangible evidence for large-scale F_2 folding is found in Cottonwood Canyon. Second- and third-generation folds, and evidence of high strain—in the Boyer Ranch conglomerate, and in the surrounding limestone and slate—indicate that the monoclinal wedge of conglomerate, in Cottonwood Canyon, is part of the back-limb, near the hinge zone, of a megascopic F_2 anticline. The anticline has a very large radius of curvature, and is west-vergent. The sense of vergence is indicated by two, west-vergent synclines in quartz arenite that overlies the conglomerate. The larger syncline is a macroscopic, nearly recumbent syncline that is exposed in the north wall, and near the mouth of Cottonwood Canyon (plate P13). Both Pi-(π)-diagram analysis, and field inspection of the fold, indicates that it plunges moderately to the south-southeast, and therefore that it is an F_2 fold. The lower limb of the fold occupies a section of well bedded, moderately-dipping quartz arenite that crops out at the level of Cottonwood Creek. Sub-vertical strata, in the upper limb of the fold, are exposed along the finger-like ridge on the

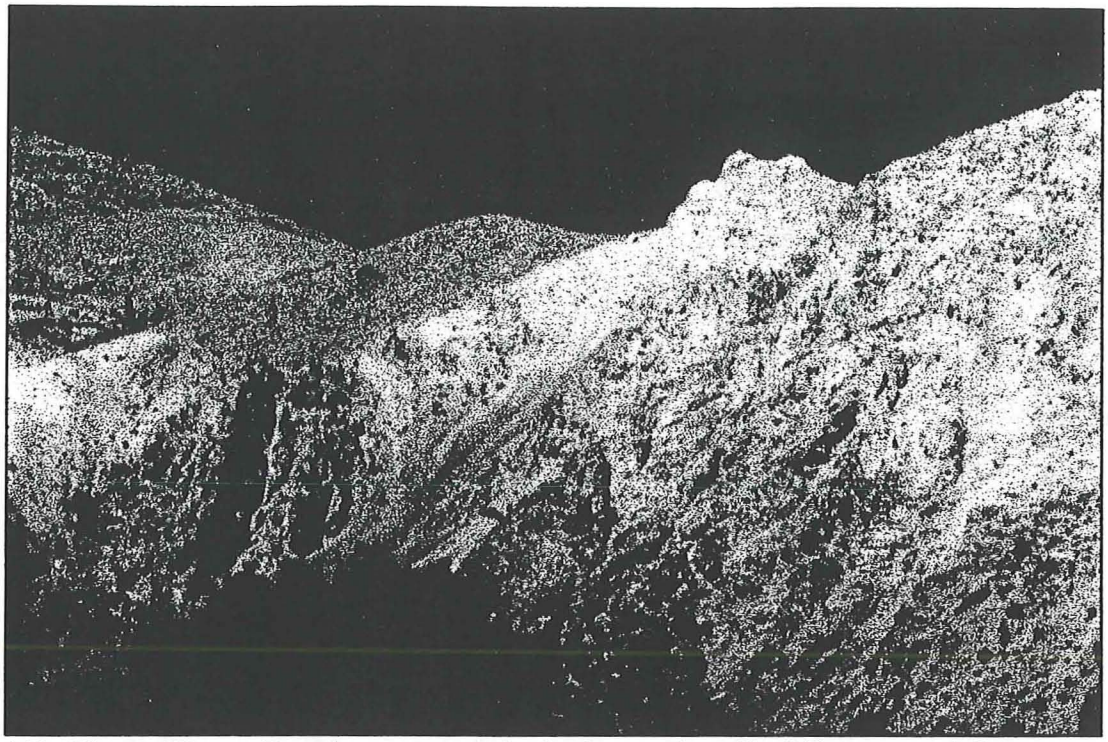

(A) View of Boyer Ranch quartz arenite in the north wall of Cottonwood Canyon, structural domain 3.

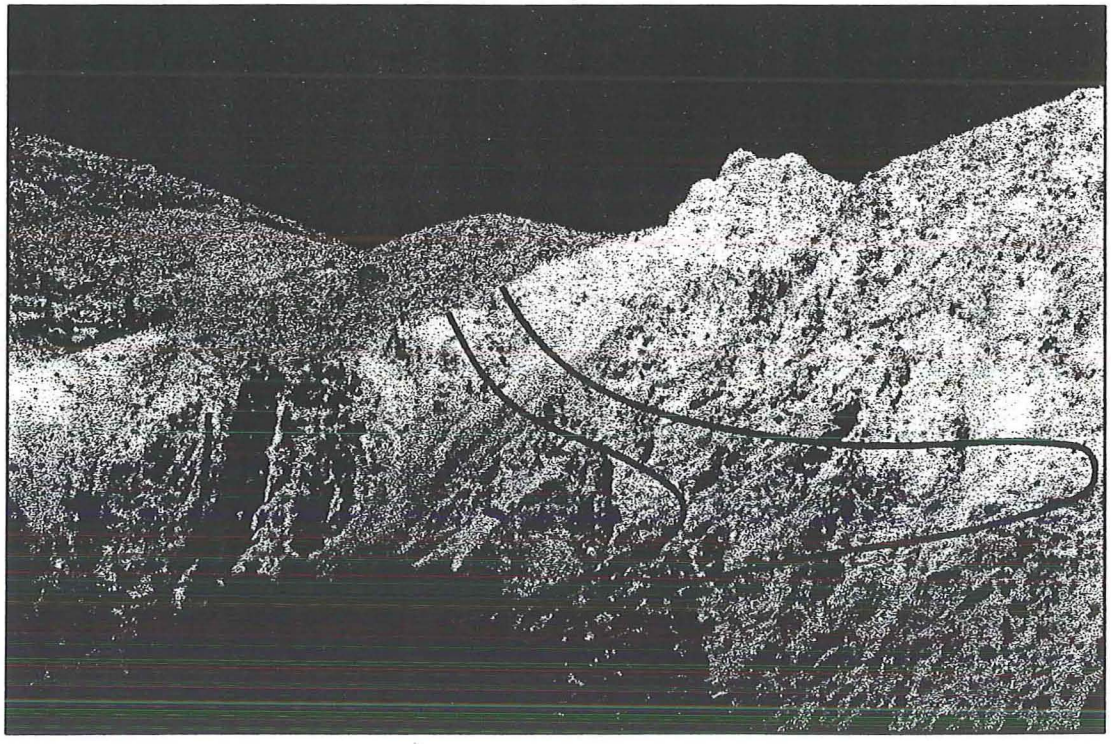

(B) Same view of Boyer Ranch quartz arenite in the northeast wall of Cottonwood Canyon, structural domain 3, showing approximate profile views of mesoscopic and recumbent, macroscopic F2 synclines.

northeast lip of the canyon. In late summer daylight, it is possible to make out the tight hinge of the fold, about midway up the slope on the northeast side of the canyon. The smaller syncline is exposed about 10 meters eastward of the lens of Boyer Ranch limestone (plate P13). This syncline is overturned to the west and moderately inclined. The hinge of the mesoscopic syncline forms a rough pinnacle and is well illuminated in late summer daylight.

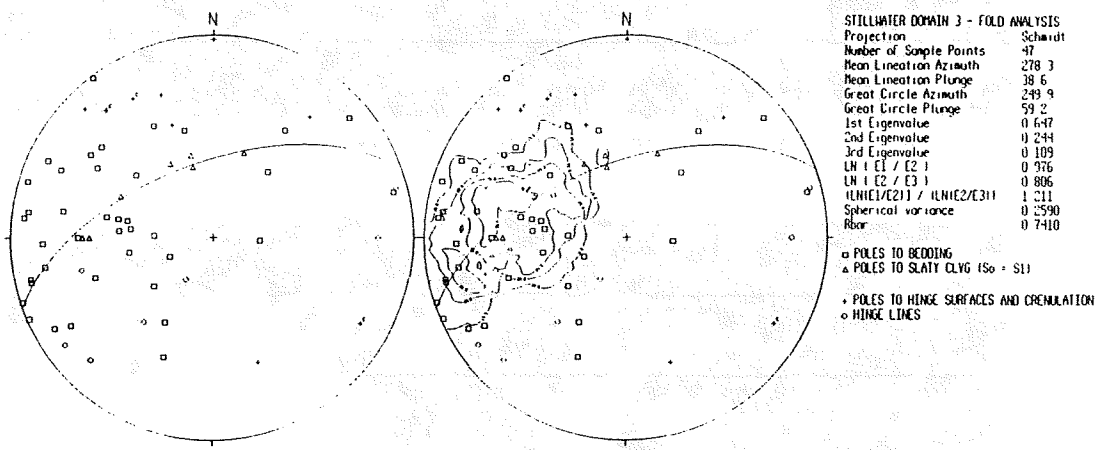

Figure 9. Pi (π)-diagram of poles to Boyer Ranch bedding in structural Domain 3. The poles form a partial girdle around a southeast-trending hinge line, that probably is an F_2 hinge line. The probable reason for the partiality of the girdle is that Domain 3 is located on one limb of a megascopic F_2 fold.

The character of strain within the megascopic F_2 anticline that is partially exposed in Cottonwood Canyon, presents a classic example of fold mechanics around a single competent layer (Ramsay and Huber, 1987). The conglomerate has been folded on a macroscopic or megascopic scale. Penetrative strain in the conglomerate—a highly competent rock—is reflected as solution pitting of the clasts and in extensional fracturing, instead of as small-scale folding or cleavage development. As an effect of the contrast in competence between the conglomerate and the surrounding incompetent rocks, strain in the quartz arenite and limestone is manifested as disharmonic mesoscopic and outcrop-scale folds. The lens of Boyer Ranch limestone that lies above the conglomerate and below the quartz arenite is highly internally deformed by outcrop-scale and mesoscopic folds. The folds are moderately inclined to recumbent, tight to isoclinal folds, that plunge moderately

to the southwest. Within the limestone the folding appears to be disharmonic, giving the impression that the carbonate has been plastically deformed. Given the position of the limestone between two much more competent rock types, the extent and appearance of its deformity suggest that the limestone acted as a high strain or high slip zone, possibly as a detachment surface, between the quartz arenite and the conglomerate. I interpret the deformation in the limestone as evidence for layer parallel shear in the limbs of a megascopic F_2 anticline.

F_3 folds in Domain 3 comprise mainly outcrop-scale folds in the unnamed Triassic slates (plate P14). Gentle, mesoscopic buckle folds and tighter, outcrop-scale kinks within the Boyer Ranch quartz arenite may also be F_3 folds. The F_3 folds are generally of greater frequency and amplitude in Domain 3 than they are in Domain 2. In other respects, such as preferential formation within anisotropic foliation, and adjunct crenulation cleavage, the F_3 folds are exactly the same in all domains where they are exposed.

F_4 folds in Domain 3 are localized along the shear zone of the Black Canyon fault (described below). I give these folds the sub-notation, F_4a. F_4a folds reorient penetrative cleavage. The folds are asymmetric to overturned to the northwest, and generally not more than one to five centimeters (1-5cm) in amplitude.

1.5.4. Structural domain IV - Folds in the upper plate of the Boyer fault. The upper plate of the Boyer Fault is devoid of two phases of folds, F_1 and F_3, that are common in Domains 1 and 2. However, the whole block is folded into tight or isoclinal, megascopic F_2 folds. F_4 (F_{4b}) folds are common in the quartz arenite, within and along the margins of the shear zone of the Boyer fault.

Pi (π)-diagram analysis of bedding in the Boyer Ranch Formation reveals that quartz arenite in Domain 4 is folded around an F_2 hinge line (Figure 10) trending 223° southwest and plunging 62°. Sporadic outcroppings of near-basal Boyer Ranch conglomerate beds, that appear in Domain 4 along the Boyer Fault, suggest that the Boyer fault may be cutting across megascopic F_2 folds. In addition, sills of microgabbro, that are associated with the Humboldt complex, are often oriented parallel to bedding in the Boyer Ranch Formation. The outcrop pattern of the sills, determined by Speed (1976) (see geologic map, Plate 1), suggests that the microgabbro is folded along with the quartz arenite, while the gabbro/diorite

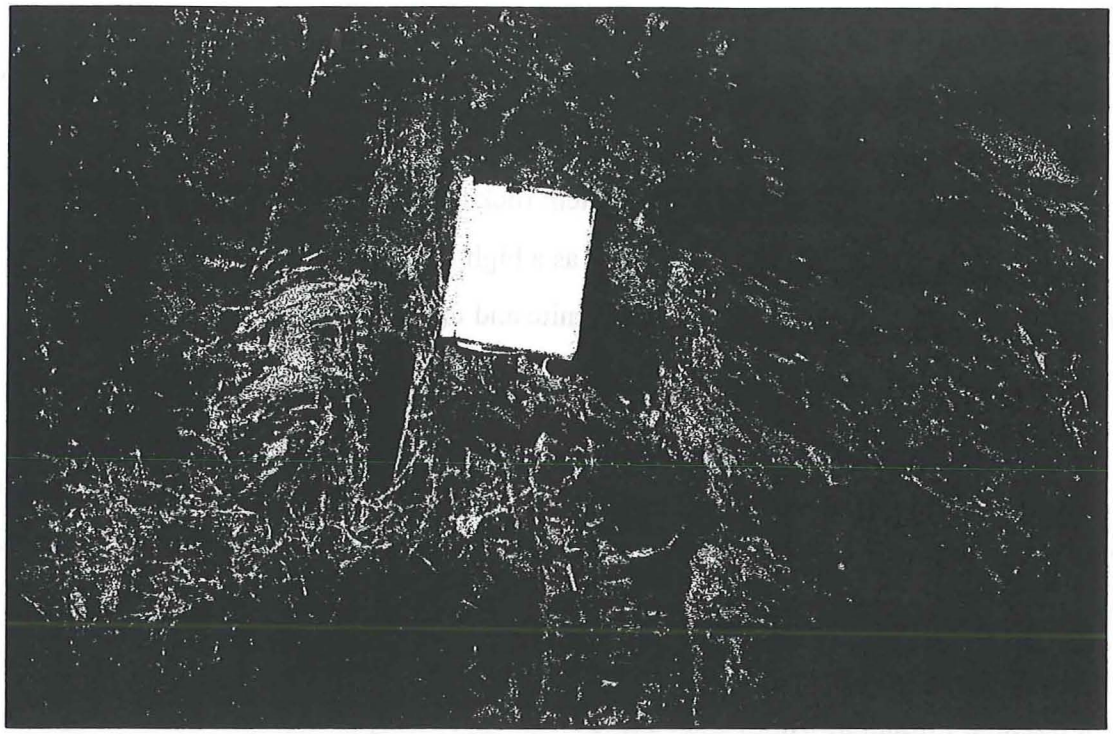

(A) Photo of S3 crenulation cleavage showing crosscutting relationship with S2 axial planar cleavage; unnamed pelitic siltstone, Cottonwood Canyon

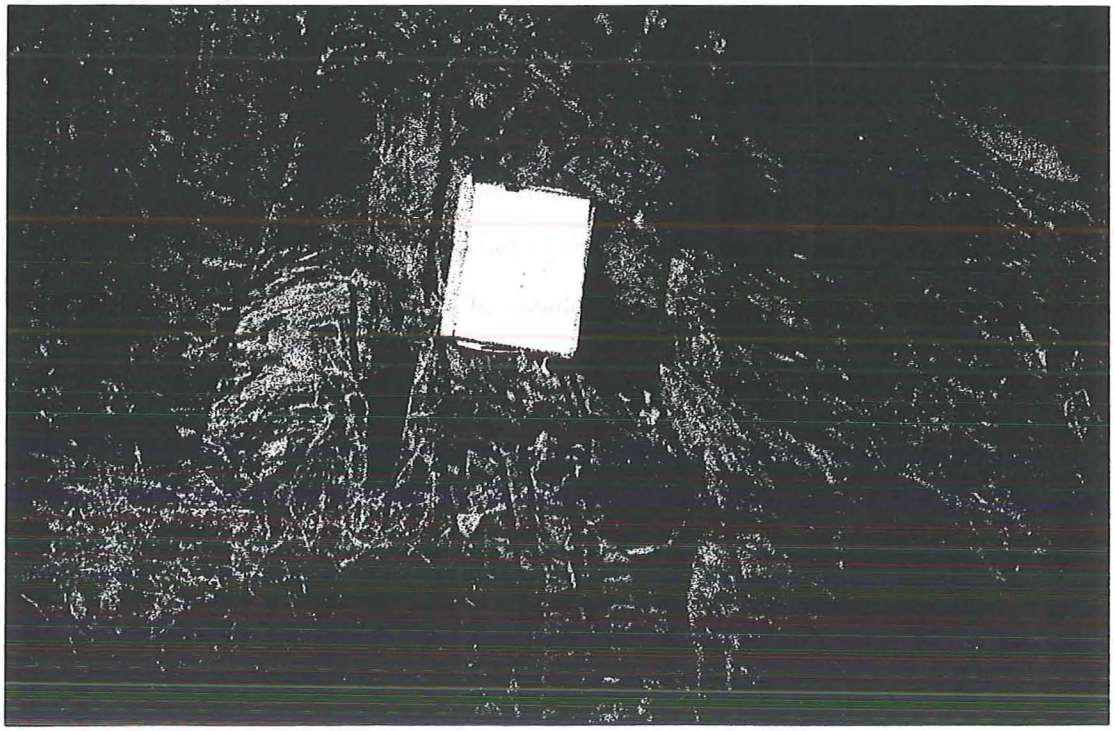

(B) Photo, same as above, with S3 crenulation cleavage highlighted.

pluton to the south of upper Black Canyon is clearly not co-folded. More detailed mapping of the sills is necessary, however, to resolve their structural relationship to folds in the Boyer Ranch Formation.

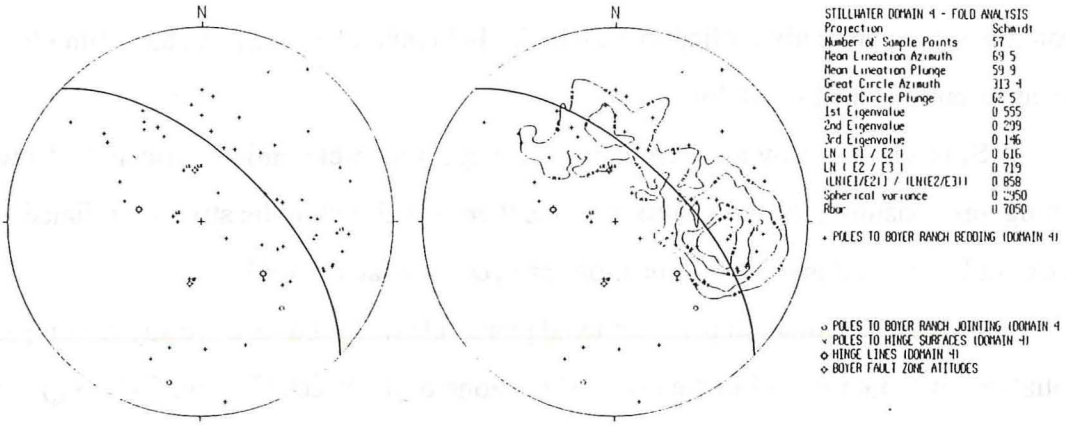

Figure 10. Pi (π)-diagram of poles to Boyer Ranch bedding in structural Domain 4. The poles form a girdle around a southwest-trending F_2 hinge line.

Mesoscopic F_4b folds in the upper plate of the Boyer fault are localized in and along the Boyer fault. These folds are drag folds that are probably associated with displacement along the Boyer fault (D_4). Exposures of F_4b folds in the upper plate, that are directly adjacent the fault, show many different orientations. Sometimes the folds trend parallel to the strike of the fault. Other exposures show crushed, dismembered, limbs and/or hinge surface traces that are inconsistent with the orientation of the fault. House-sized fragments of mesoscopic close- and open-folds are littered throughout the fault zone. The impression thus given, by these seemingly chaotic fold orientations, is that rigid blocks have been tectonically rotated. The origin of some F_4b folds may be therefore pre-tectonic to the Boyer fault (perhaps dismembered F_2 folds). Other F_4b folds may be drag folds, that originated during displacement along Boyer fault, and were subsequently dismembered by progressive brittle deformation.

Fabrics and Strain. Tectonic fabrics in the map area constitute axial planar cleavages, mineral stretching lineations, and shear surfaces. S_1 foliation is the penetrative tectonic foliation in domains 1, 2, and perhaps Domain 3. S_1 is axial planar to megascopic F_1 folds and roughly axial planar to smaller-scale F_{1a} folds. L_1 lineations comprise prolate rods of

calcite in Domain 1, needles of aligned micaceous minerals in Domain 2, and are absent in Domain 3.

S_2 cleavage is axial planar to F_2 folds. In Domains 1 and 2, S_2 cleavage is rare and is confined to tightly appressed, outcrop-scale folds along the Fencemaker shear zone. In Domain 3, the penetrative foliation may be S_2, but could also be S_1. L_2 stretching lineations are apparently absent in all domains.

S_3 is a map-area-wide crenulation cleavage, that preferentially affects rocks with a strong, pre-existing planar anisotropy. S_3 is therefore found in the strongly foliated pelitic rocks in Domains 2 and 3. No lineations are yet associated with L_3.

Finally, S_4 foliation is not an axial planar cleavage, but is a weakly developed shear foliation, or C-fabric, within the brittle shear zone of the Black Canyon fault (S_{4a}) and the Boyer fault (S_{4b}). Because these fabrics are restricted to the fault shear zones, their descriptions are left to the presentation of the individual faults.

1.5.5. Structural domain I - Fabrics and strain in the lower plate of the Fencemaker thrust. Fabrics in Domain 1 are characterized by strong tectonic foliations and lineations. S_1 foliations in Domain 1 dip moderately to the southeast and southwest. Pi (π)-diagram analysis of Domain 1 indicates that the S_1 foliation is broadly folded around an F_2 hinge line (Figure 6) that trends approximately 199° degrees and plunges 53° degrees. L_1 stretching lineations in the foliation planes are aligned more or less in the down-dip direction of S_1 foliation, but are reoriented by F_2 folds. Consequently L_1 lineations are often observed to trend at shallow angles to the dip direction of S_1 foliation.

S_2 cleavage is axial planar to F_2 folds and oblique to the S_1 foliation. However, only tight, outcrop-scale F_2 folds in black schist show a developed S_2 axial planar cleavage. Mesoscopic F_2 folds are less tightly appressed and apparently have no axial planar cleavage. To my observation, S_3 crenulation cleavage does not exist in Domain 1.

The northwestern two-thirds (2/3's) of Domain 1 occupy structural levels that are far from the Fencemaker shear zone (discussed below). At these levels, the rock is an S-type tectonite, in which S_1 cleavage is strongly developed. At structural levels farthest from the shear zone, the tectonite degrades to a highly foliated limestone.

1.5.6. Structural domain II - Fabrics and strain in the upper plate of the Fencemaker thrust. S_1 foliations in Domain 2 dip moderately to the southeast and southwest. Pi (π)-diagram analysis of the S_1 foliation indicates that it is broadly folded around an F_2 hinge line (Figure 8) that trends 206° and plunges 45°. In these aspects, the penetrative foliation in Domain 2 is very similar to that in Domain 1. L_1 lineations are well developed in Domain 2 only where the rock was originally pelitic. The more pelitic rocks in the Fumarole Canyon sequence core the primary, megascopic F_1 anticline, and therefore show the strongest L_1 development. Siliceous argillite is generally non-lineated.

S_2 axial planar cleavage is absent in Domain 2. Mesoscopic and outcrop-scale F_2 folds in Domain 2 are gentle- to close-folds, and strain in the fold cores has not been sufficiently large to form S_2 cleavage. F_2 folding of S_1 causes L_1 lineation trends to be rotated away from the down-dip direction of S_1. In the field, therefore, L_1 lineations are usually found to trend at shallow to moderate angles to the dip direction of S_1 foliation.

S_3 crenulation cleavage permeates rocks of Domain 2 where there is a strong pre-existing S_1 foliation. Crenulation planes are irregularly spaced from two(2) centimeters to as much as three(3) meters, and dip steeply to the east or west. The S3 cleavages are especially well developed in the upper reaches of Fumarole Canyon.

In Domain 2, tectonic fabrics are most strongly developed in the core of the primary, megascopic (F_1) anticline. Cleavages, mineral stretching lineations, and microboudinage structures in the core of the primary F_1 anticline suggest large flattening strains. The rock between cleavage planes, or microlithons, are perfectly flat and highly continuous. Outcrops weather into terraces of thin, pliable rock sheets. The cleavage surfaces are saturated with coarse needles of micaceous minerals. The minerals impart to the rock a phyllitic sheen, and are aligned lengthwise, forming mineral stretching lineations. Competent interbeds of siliceous strata have been stretched apart to form boudins and microboudins that are oriented parallel to the penetrative foliation. These boudins crop out in exposures perpendicular to S_1, and occur as plates in trains with large (10:1) interboudin distances. Finally, macroscopic rotational structures (σ- or δ-porphyroclasts) are absent. I interpret the fabric development and the lack of rotated structures to indicate that simple shear was minor as a deformation

mechanism in the fold core. Instead, flattening caused by the contraction of the anticlinal limbs around the fold core, appears to have been the primary deformation mechanism.

In the limbs of the primary F_1 anticline, the tectonic fabric is different from that in the core. The upright, backlimb of the fold is moderately but relatively weakly foliated. The weaker foliation may be a function the competence of the rock, the large structural distance from the Fencemaker shear zone, and/or the structural distance from the fold core. In contrast, rocks in the overturned limb lie, structurally, between the core of the megascopic F_1 anticline and the Fencemaker shear zone. The rocks are therefore sandwiched between two high-strain zones. Both the upper unit of the Fumarole Canyon sequence, and transitional rocks that lie between the upper and lower unit, occupy the overturned limb. Siliceous argillite, is in the upper unit, dominantly shows tightly spaced, regular, bedding-parallel cleavage. The transitional rocks— pelitic strata, like those in the lower part of the Fumarole Canyon sequence, interbedded with strata of siliceous argillite—have a strong bedding-parallel cleavage (S_0), and usually show a cleavage (S_1) at shallow angles to bedding, especially in the pelitic horizons. S_1 partings in the pelitic horizons are asymptotic to, but do not refract through, the more competent siliceous strata; S_0 may therefore be a C-fabric, or shear fabric, along which some layer-parallel shear has taken place. I interpret the shallow cleavage in the pelitic layers as evidence that simple shear is was the dominant deformation mechanism in the overturned limb.

The tectonic fabrics in Domain 2 define three zones of strain. In the northeast part of Domain 2, the overturned limb of the primary F_1 anticline occupies a zone that is dominated by simple shear, and that is proximal to the Fencemaker shear zone. In the central portion of the domain, the core of the anticline constitutes a second zone that is dominated by pure shear, and that is more distal to the Fencemaker shear zone. The southwest part of the domain makes up a third zone that is moderately foliated, completely lacks blastic mineral growth, and is structurally farthest from the Fencemaker shear zone.

1.5.7. Structural domain III - Fabrics and strain in the upper plate of the Black Canyon fault. Unlike rocks in Domains 1 and 2, the different rocks in Domain 3 do not share a common penetrative fabric. Although the unnamed slates and sandy siltstones beneath the Boyer Ranch Formation have a penetrative tectonic cleavage, the Boyer Ranch

does not have a penetrative cleavage (S_1), or, despite the numerous F_2 folds in that formation, an axial planar cleavage (S_2). In the unnamed Triassic slates, penetrative cleavage is generally a bedding-parallel cleavage—at the top of the section in Cottonwood Canyon, for example—and is sometimes axial planar to bedding folds. The entire slate unit is strongly foliated, and the strongest development occurs in pelites at the bottom of the Cottonwood Canyon section.

It is difficult to ascertain whether penetrative cleavage in the slates formed as an older phase (S_1 or S_{1A}) or a later phase (S_2). Stratigraphically up-section from the slates, penetrative cleavage does not refract through the Boyer Ranch Formation, but instead appears to be sub-parallel to the Boyer unconformity. The lack of continuity of fabric between the slates and the Boyer Ranch suggests two possibilities: (1) that the formation of penetrative cleavage in the slates pre-dates the deposition of the Boyer Ranch, or (2) that the penetrative cleavage in the slates postdates Boyer deposition but does not affect the competent quartz arenite. As described previously, there is evidence that the entire Cottonwood Canyon section is situated in the limb of a megascopic F_2 anticline. If the penetrative cleavage in the slates is assumed to be axial planar (S_2) to that F_2 anticline, it would make sense to expect the cleavage to be sub-parallel to the fold limbs, and therefore sub-parallel to the Boyer unconformity. Axial planar (S_2) cleavage would not be required to develop in the competent fold limbs, as long as there was incompetent rock in the fold core to absorb strain. Perhaps if we could see the entire F_2 anticline, there might be some type of axial planar cleavage developed in the Boyer Ranch rocks, along the hinge zone of the fold.

S_3 cleavage strongly affects rocks throughout Domain 3. In Boyer Ranch quartz arenite, S_3 is spaced between four (4) and ten (10) centimeters, and is easily mistaken for a vertical joint set. S_3 crenulation cleavage is very strongly developed in the slates of Domain 3 where the pre-existing penetrative cleavage is the strongest. The S_3 cleavage planes in all rocks strike to the south-southwest and are steeply inclined to the east or west (plate P14).

1.5.8. Structural domain IV - Fabrics and strain in the upper plate of the Boyer fault. The upper plate of the Boyer Fault is devoid of tectonic fabrics, excepting joints. Joints are ubiquitous in quartz arenite, but they seem to form as sets only in isolated or localized circumstances, and are not continuous in orientation throughout the domain. It is possible that some of the joints are S_3 cleavage. More detailed mapping of the joints will have to be

done, however, in order to establish their relation to other cleavages. Joints in the Humboldt igneous complex in the upper plate are similar to those in the Boyer Ranch quartz arenite. There are restricted exposures in which regularly oriented joint sets occur, but generally there does not appear to be a single penetrative joint set. One exception can be found in Cottonwood Canyon, where a widespread and regularly spaced joint set occurs in the Humboldt complex. Greenish-gray diorite and gabbro in the upper plate of the Boyer fault crops out 750 meters northwest and upstream from the mouth of Cottonwood Canyon. The exposure occupies the stream bed, and both the northeast and southwest walls of the canyon. At this location, there is a regularly spaced, penetrative fracturing that dips 45° degrees to the southeast. The fracturing influences drainage pattern in the diorite and can be seen in air photos. Some of the fractures are sheared, while the majority lack evidence of motion and hence are joints.

Faults.

1.5.9. Ductile Faults.

(9a) Fencemaker thrust. The Fencemaker thrust (the boundary between Domains 1 and 2) is the only ductile fault in the study area (plate P15, Plate 1). The Fencemaker thrust is exposed at the north end of the map area, in Fumarole Canyon (plate P16). The Fencemaker places argillaceous rocks of the Fumarole Canyon sequence (Lovelock assemblage, Domain 2) over carbonate rocks of the Natchez Pass Formation of the Star Peak Group (Humboldt assemblage, Domain 1). The thrust is marked by a ductile shear zone that encompasses the southern one-third (1/3) of the area of Domain 1, and a relatively smaller part of Domain 2.

Within the ductile shear zone, whitish-gray limestone (upper Natchez Pass Formation) in the lower plate, has been metamorphosed into a marble tectonite, or an L-S tectonite, in which both strong lineations and foliations are developed (plate P17). L-fabric lineations in the marble tectonite are defined by sparry calcite lenses that have been stretched along the X-tectonic axis. The extreme constriction of the calcite lenses is demonstrated in the photo on plate P17. In the left-hand photo (P17A), an exposure of the YZ tectonic plane shows almost perfectly circular cross sections of the calcite lenses (note arrows). The oblique

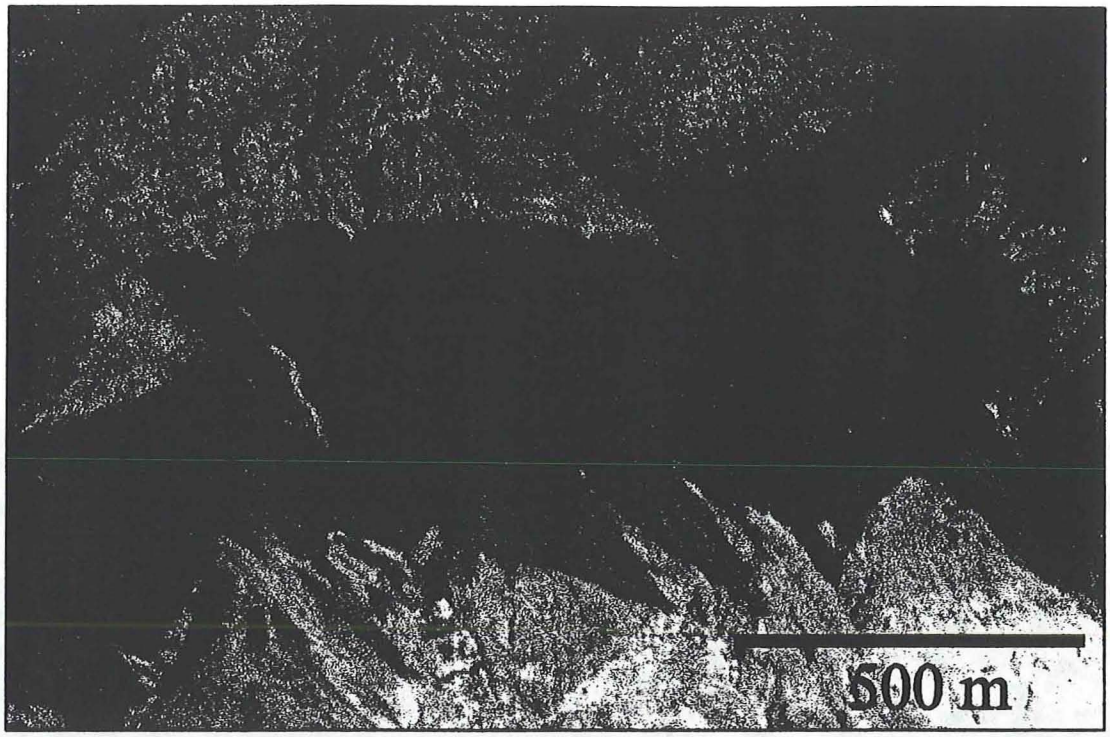

(A) Oblique aerial photograph of domains 1, 2, 4, and 4a. The Fencemaker thrust is the color change on the far right. The Boyer fault is the horizontal contact in the background (see below). The light-colored rocks, in Domains 4 and 4a, are Boyer Ranch quartz arenite, and the dark rocks in Domain 2 are Fumarole Canyon sequence.

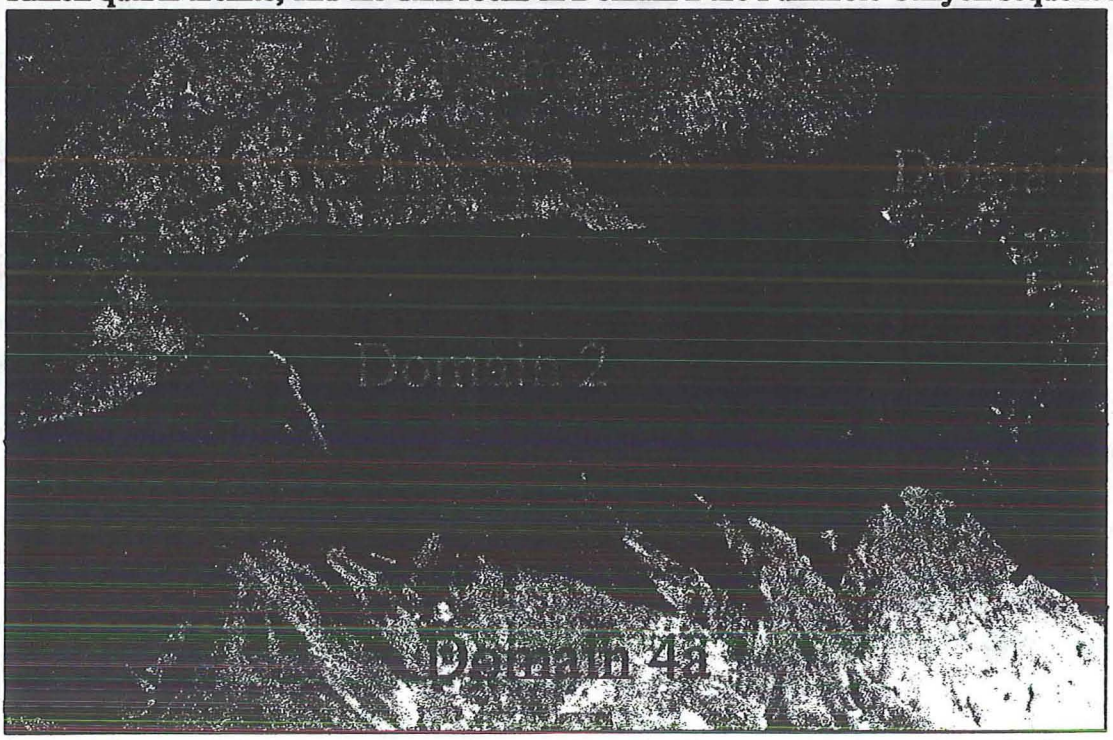

(B) Oblique aerial photograph, as above. Note the Fencemaker thrust (green), the Boyer fault (purple), and a major high-angle splay of the Dixie Valley fault, the RF4 fault (red), that displaces part of Domain 4 down and to the southeast. Also note Miocene dikes in Domain 4 (arrows).

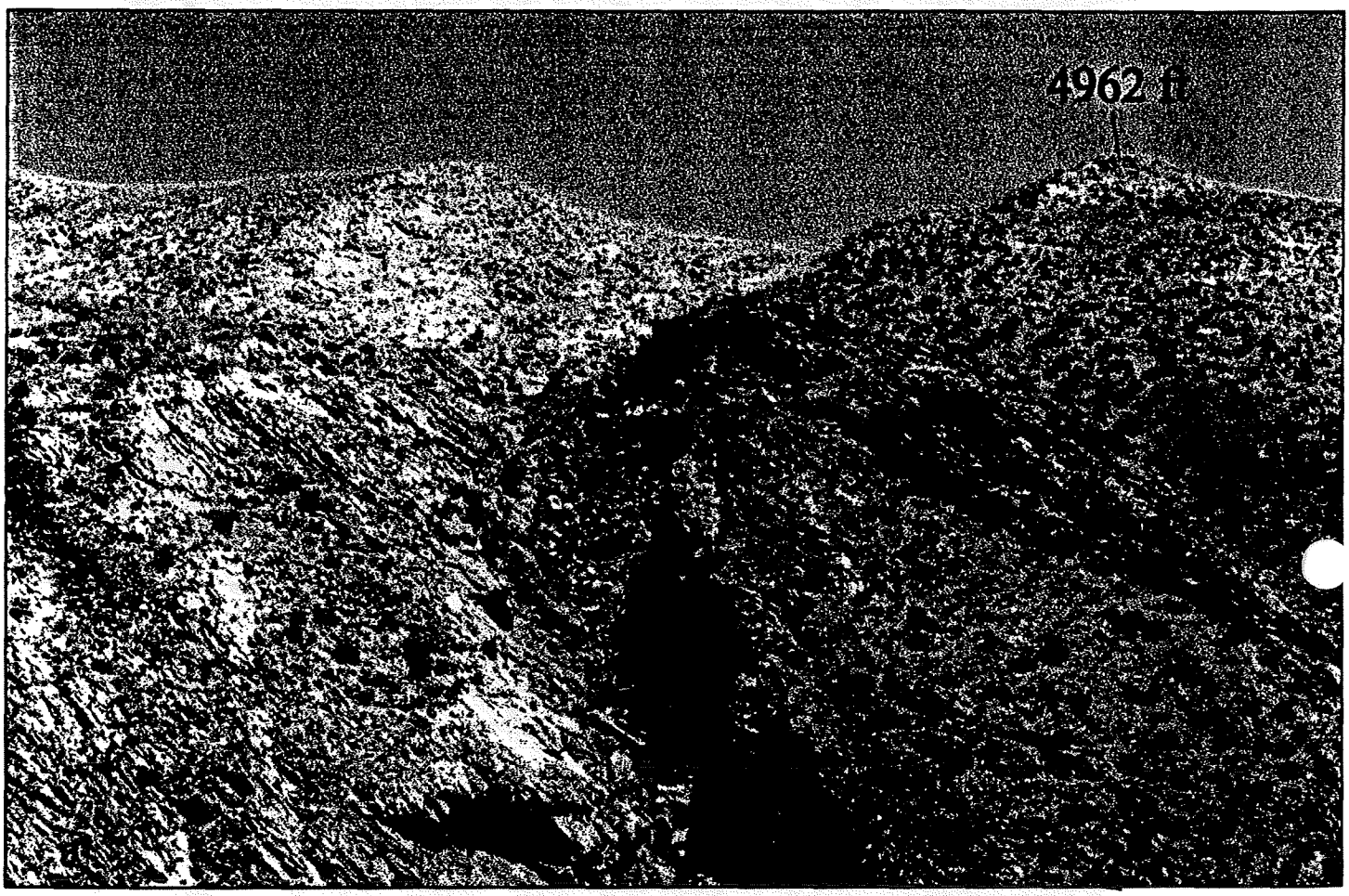

(A) View of the Fencemaker thrust on the northeast wall of Fumarole Canyon. Dark rocks on the right are Fumarole Canyon sequence (upper plate). Light colored rocks to the left are Star Peak Group marble tectonite (lower plate). Approximate trace of the thrust (dashed) is at the top and to the right of the central ravine.

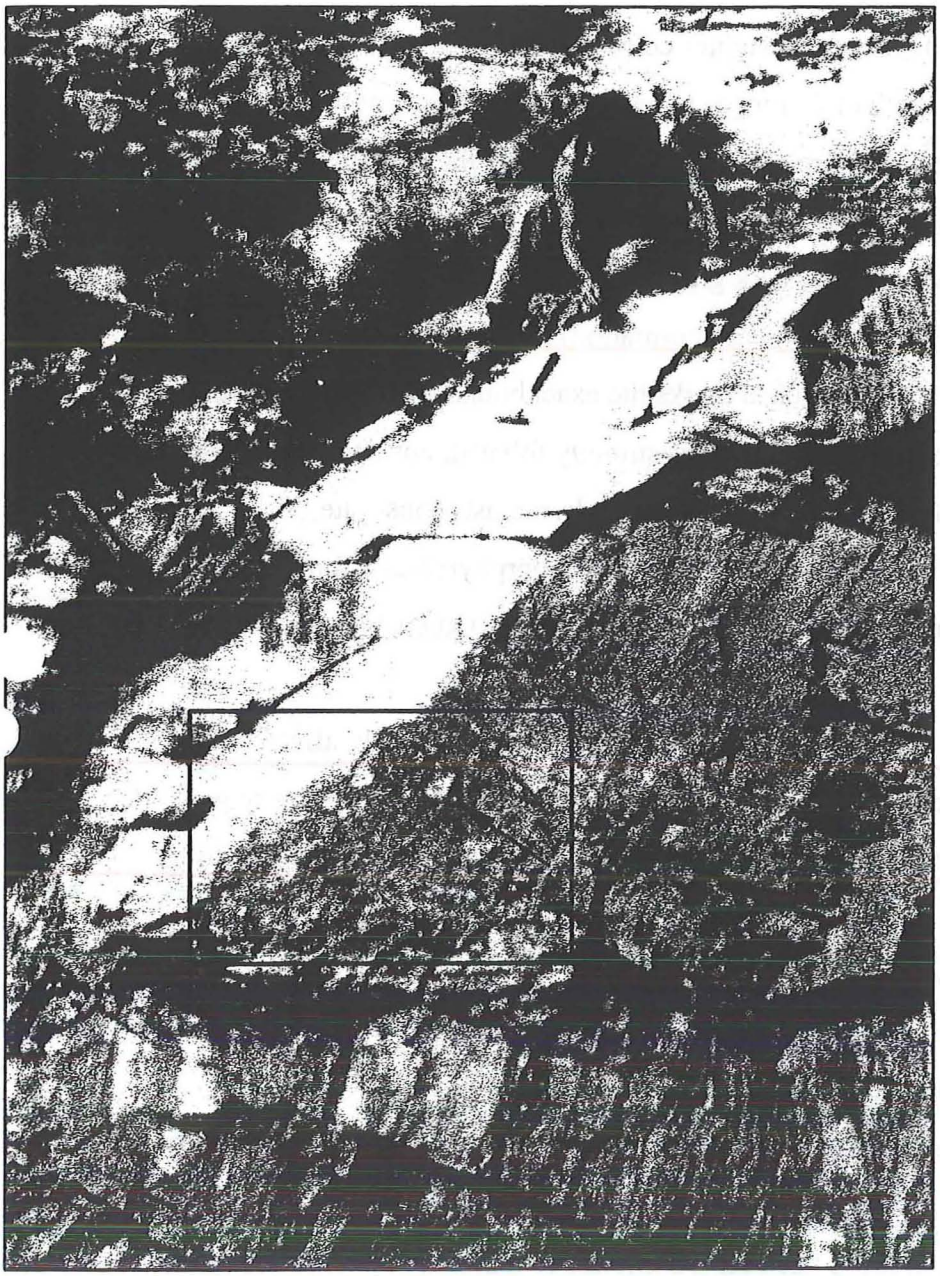

(A) Outcrop of marble tectonite in the ductile shear zone of the Fencemaker thrust shows lenses of sparry calcite in light gray marble. Note circular cross sections of lenses (boxed) in the tectonic YZ plane. Hammer for scale rests on the tectonic XY, or S1, plane.

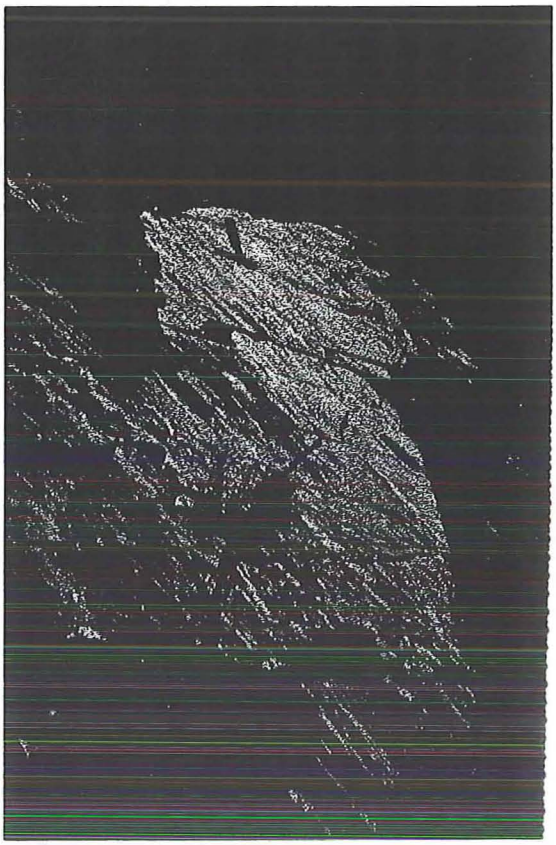

(B) Oblique veiw of marble tectonite in the ductile shear zone of the Fencemaker thrust shows prolate lenses of sparry calcite stretched along the tectonic X axis.

view of the same photo (P17B) shows the stretched, linear nature of the same lenses in the XY tectonic plane. Although this type of lineation dominates the fabric in the center of the shear zone, strongly developed S_1 foliation is always present parallel to the XY tectonic plane (plate P17). Dark gray marble (described on page 24) is slightly more competent and has not been recrystallized to the same degree as the lighter-colored marble. In the shear zone, this competence contrast causes intrafolial fold hinges to be preserved in strata of dark gray marble. The intrafolial hinges in the more competent rock indicate that bedding in the shear zone has been completely transposed.

In addition to the whitish-gray and dark gray marble tectonite, black, carbonaceous limestone in the lower plate (lower Natchez Pass Formation) has been metamorphosed to a black, calcareous, cordierite schist. The schist marks the exact boundary between upper and lower plates of the Fencemaker thrust. The schist is strongly foliated, but linear fabric is much weaker than in the marble tectonite. Cordierite porphyroblasts constitute approximately ten-percent (10%) of the schist. Many of the porphyroblasts form sigma (σ) or delta (δ) structures that are rotated to the southeast (plate P18). Others blasts are not rotated.

Upper plate rocks that occupy the Fencemaker shear zone are weakly affected by ductile deformation. Competent, siliceous argillite of the upper Fumarole Canyon sequence is foliated, but not tectonized to the nearly same degree as footwall rocks in the shear zone. S_1 cleavage in the siliceous rocks is strongly developed parallel to bedding, and very weakly developed at shallow angles to bedding. At high angles to bedding, S_1 foliation is robust, but widely and irregularly spaced.

Upper plate rocks that are transitional, between the upper and lower Fumarole Canyon sequence, are also peripherally involved in the shear zone. In transitional rocks that are nearest to the shear zone, S_1 foliation is strongly developed parallel to bedding, that is, $S_0=S_1$. Strain in the transitional rocks has been partitioned to relatively more pelitic horizons. These beds have been greatly thinned structurally. Metamorphic mineral growth is also partitioned to these less competent pelitic beds. The porphyroblasts within the pelitic beds are micaceous laths, and are oriented parallel to S_1. The siliceous horizons, however, are not foliated or thinned, and the competent (more siliceous) strata weather out in textural relief.

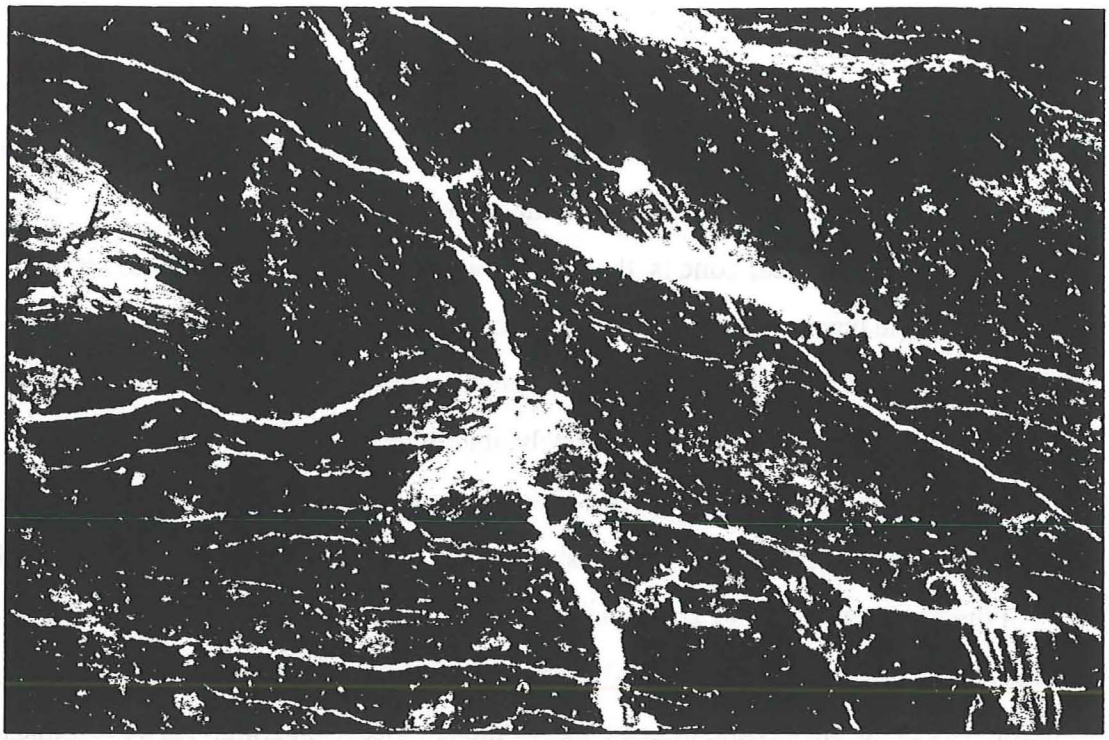

(A) Photomicrograph showing microstructures in black, calcareous schist, within the ductile shear zone of the Fencemaker thrust. Note sigma-structures around porphyroblasts, and double cleavage.

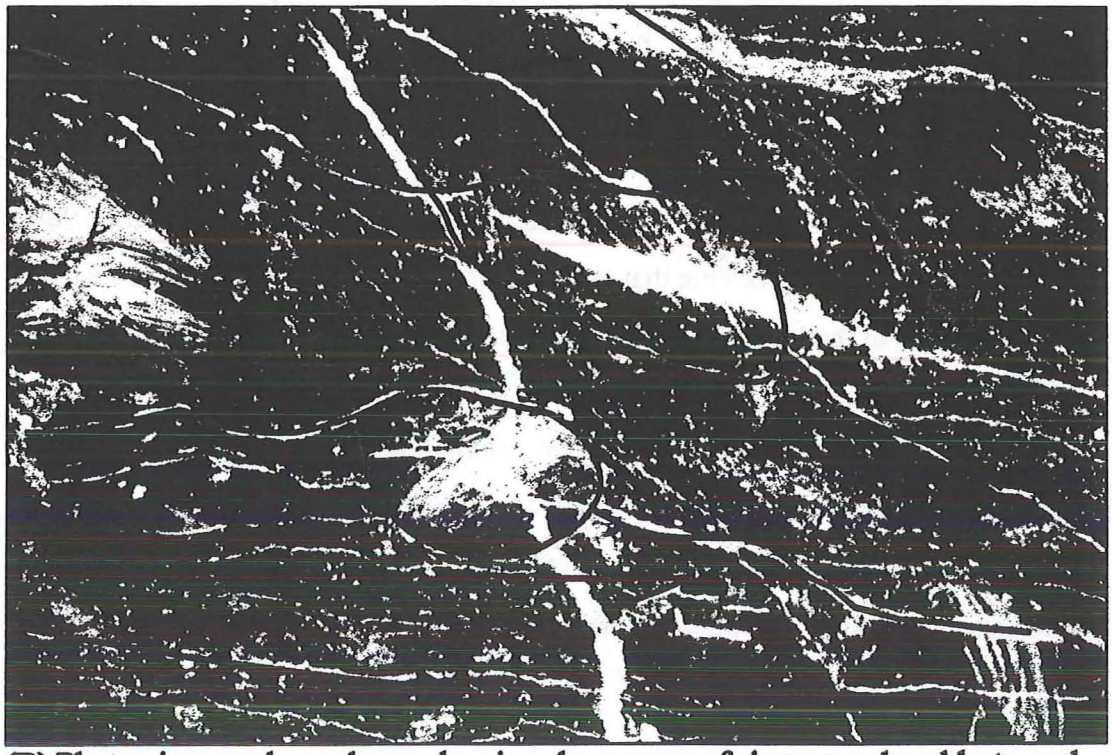

(B) Photomicrograph. as above, showing shear sense of sigma porphyroblasts, and two cleavage sets that intersect at moderate angles (highlighted).

In the competent layers, metamorphic minerals are usually absent, but in cases where they do occur, they are granular and not preferentially aligned.

The Fencemaker shear zone is, thus, broadly characterized by weakly to strongly foliated rocks in the upper plate, resting against highly tectonized rocks in the lower plate (Figure 11). The fault surface is involved in open- to tight-folds (F_2) of varying scales. The F_2 folds trend southward and plunge moderately, and deform the Fencemaker thrust into antiforms and synforms. The thrust surface has a general south-southeast dip, and cross-sectional analysis suggests that the ductile shear zone is roughly 100 meters thick. It is likely that all of the penetrative fabrics and structures in Domains 1 and 2 are the result of the emplacement of the Fencemaker allochthon, along the Fencemaker thrust. Cordierite porphyroblasts in the shear zone indicate top-to-the-southeast shearing. However, this sense of shear is contrary to the northward transport direction of the Fencemaker-B allochthon, given by Speed (1988). The sigma (σ) and delta (δ) structures may therefore be a result of post-Fencemaker (D_2) deformation, for it is possible that the rotation of the blasts occurred because of flexural-slip, layer-parallel shearing in the limbs of F_2 folds.

The Fencemaker thrust may have formed along the transition between basinal rocks and platformal rocks of the Early Mesozoic marine province (Speed and others, 1988; Oldow, 1990). Also, it is possible that the thrust may have been rooted as a decollement between the base of the Lovelock assemblage and the regional basement (Koipato Group or Golconda allochthon), and had perhaps a ramp geometry that cut up-section through the platformal assemblage. Age constraints on thrust displacement are very poorly constrained. The thrust must post-date deformed, Upper Norian strata in the upper plate (225- to 219-Ma). Because the Humboldt igneous complex cuts across F_2 folds, that post-date D_1, the Fencemaker thrust (D_1) also predates the Humboldt igneous complex. Therefore, movement along the Fencemaker thrust happened within a 68 million-year period between 157- and 225-Ma.

1.5.10. Brittle-Ductile Faults.

(10a) Black Canyon fault. The Black Canyon fault is exposed only in the Stillwater Range, 3.2 kilometers northeast of Cottonwood Canyon, in and along the walls of Black Canyon (Plate 1, plate P19A). The fault forms the boundary between Domains 2 and

(A) Photograph of Black Canyon (Plate 1). The Black Canyon fault is exposed in the dry wash in the bottom of the canyon on the right. The Boyer fault (color change at the top of the photo) truncates the Black Canyon fault. Width of view is roughly 400 meters.

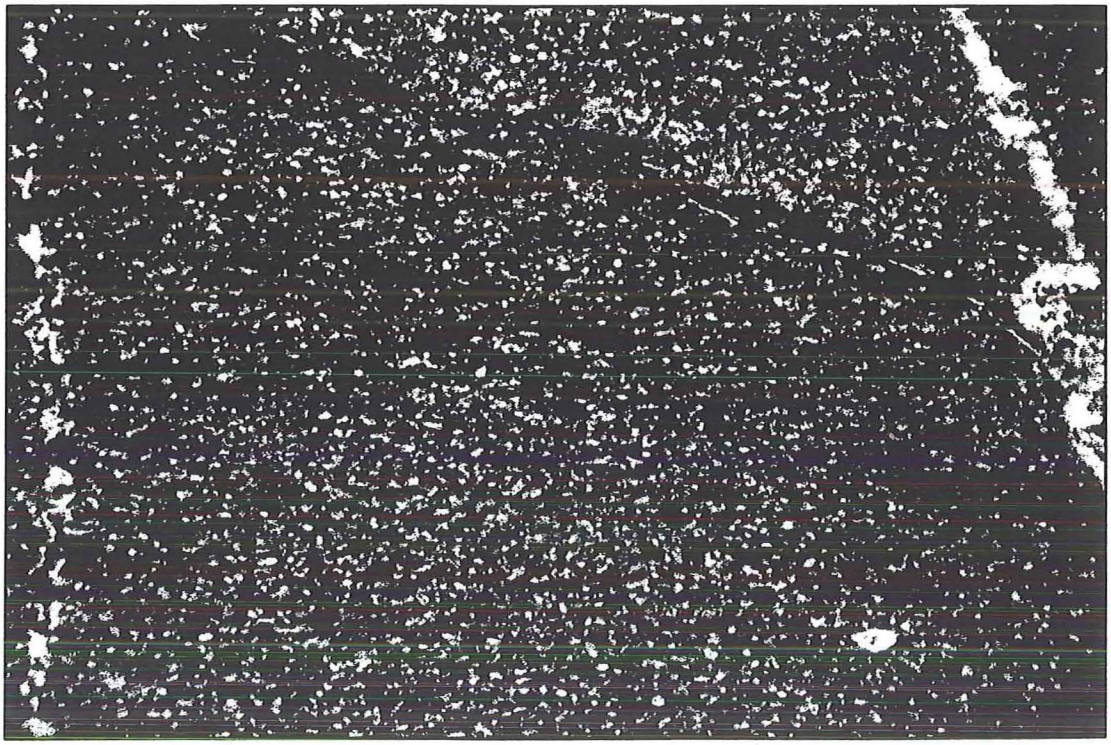

(B) Photomicrograph of unnamed pelitic siltstone in the upper plate of the BCF, from outcrops just to the right of the above photo. Photo shows graded bedding dipping shallowly to the right, and sub-horizontal S4a cleavage developed at a low angle to bedding (Nikon 5x).

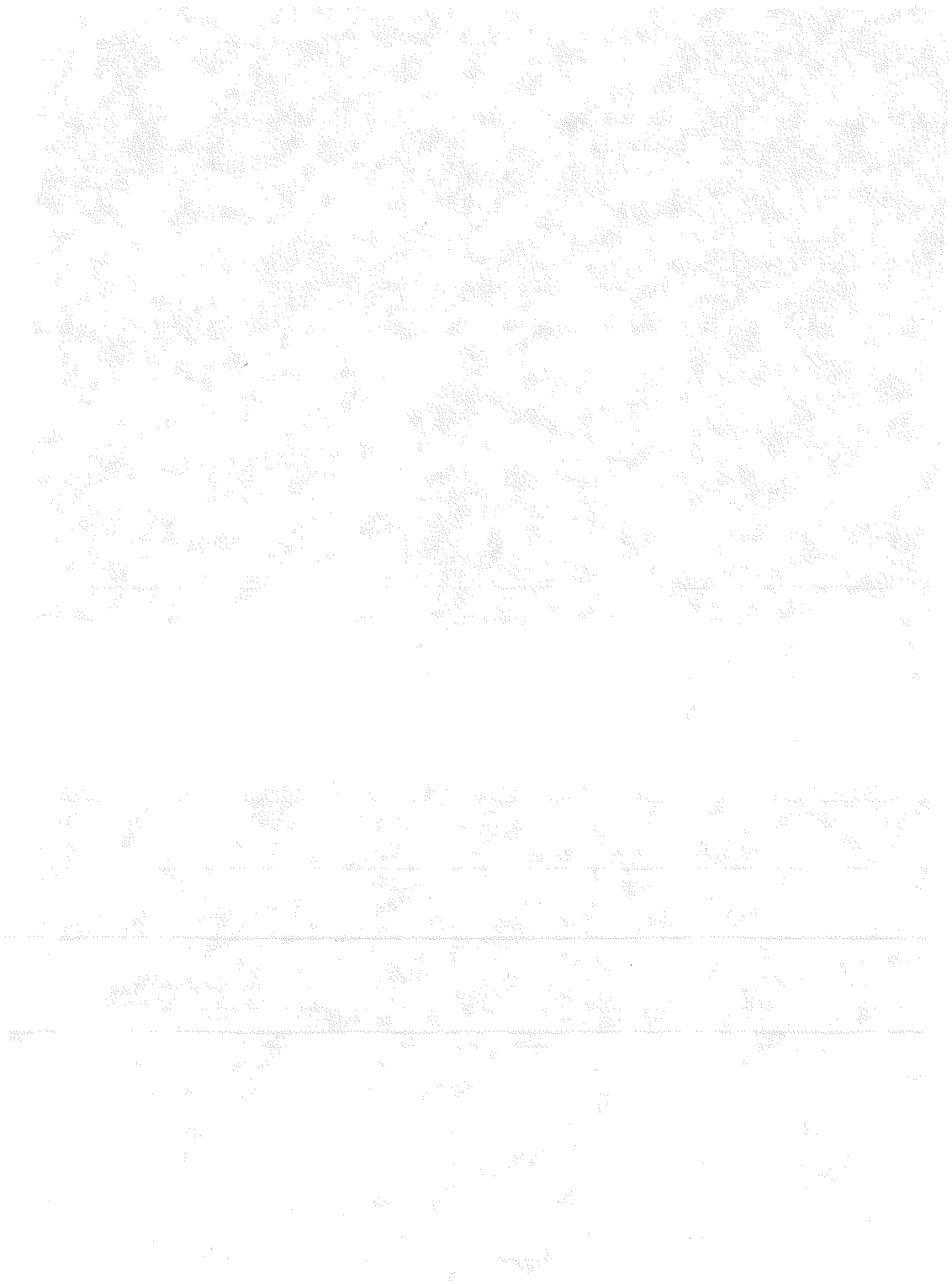

Figure 11. Diagrammatic sketch of structural relations within the ductile shear zone of the Fencemaker thrust.

Figure 11.
Fencemaker thrust

FCS = Fumarole Canyon Sequence

Rnbl = Natchez Pass black limestone (locally schist)

Rnm = Natchez Pass marble (locally marble tectonite)

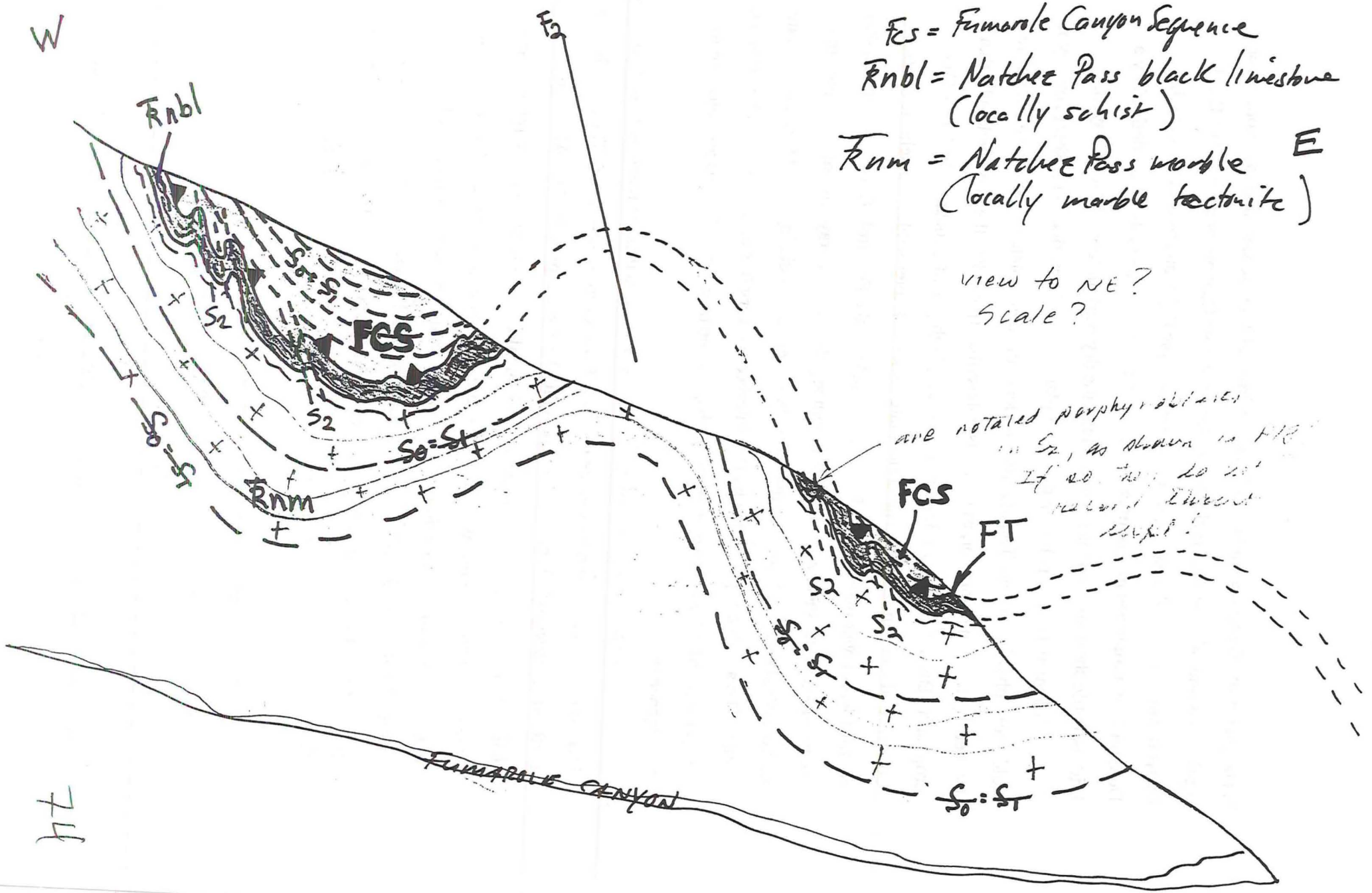

3, and places the Boyer Ranch Formation and unnamed Triassic slate and sandstone, over argillaceous and olistostromal rocks also of the Fumarole Canyon sequence. The Black Canyon fault truncates the back limb of the megascopic (F_1) hanging wall anticline in Domain 2, and truncates megascopic F_2 folds in Domain 3 The fault is best defined by a brittle-ductile shear zone that is exposed along the dry wash in lower Black Canyon.

Unnamed Triassic pelite, in the upper plate, can be identified in the shear zone by its gold-green phyllitic sheen. The unnamed rocks in the upper plate can also be distinguished by their light-green color; for, as previously described (page 30), the unnamed rocks that crop out in Black Canyon are similar to the green, highly pelitic rocks at the base of the Cottonwood Canyon section. The upper plate rocks lack interbedded siliciclastic strata, in contrast with lower plate rocks. Lower plate rocks of the Fumarole Canyon sequence, that are involved in the shear zone, include brown argillite, bluish-gray siliceous argillite, and olistostromal rocks. All three of these lithologies are easily distinguished from upper plate rocks. The argillite is permeated by thin interbeds of very fine sandstone, the olistostromal rocks are mottled by light-colored olistoliths, and the blue-gray siliceous argillite is drab and homogeneous.

The pelitic composition of upper plate rocks causes them to react incompetently, and therefore shear zone structures in the upper plate rocks are semi-ductile. The rocks have a moderate cleavage (S_{4a}) that is confined to the shear zone (plate P19B). Although deformation in the upper plate rocks is semi-ductile, the rocks lack both porphyroblastic mineral growth and mineral stretching lineations. Lower plate rocks in the shear zone are highly competent, and therefore fault-related structures are semi-brittle. Brittle-ductile shears, calcite-filled sigmoidal veins, and both foliation-parallel and perpendicular extensional veins permeate the lower plate rocks in the shear zone (plate P20A). Penetrative foliation (S_1) in the lower plate, is not folded, and is truncated by smaller faults within the shear zone (plate P21)

At all scales, the shear zone is a network of braided shear surfaces (Figure 12). The shears define lensoidal horses and micro-horses, in which the penetrative foliation (S_1?) is fairly internally coherent but is rotated, to varying degrees, with respect to other horses (plate P21). At finer scales, the penetrative cleavage within the micro-horses is often folded into centimeter-scale, top-to-the-northwest, asymmetric folds (F_4a). These folds (F_{4a}) are

Figure 12. Diagrammatic sketch of structural relations within the brittle-ductile shear zone of the Black Canyon fault.

good sketch

Figure 12

schematic sketch of fabrics in the Black Canyon fault zone.

SW?

NE?

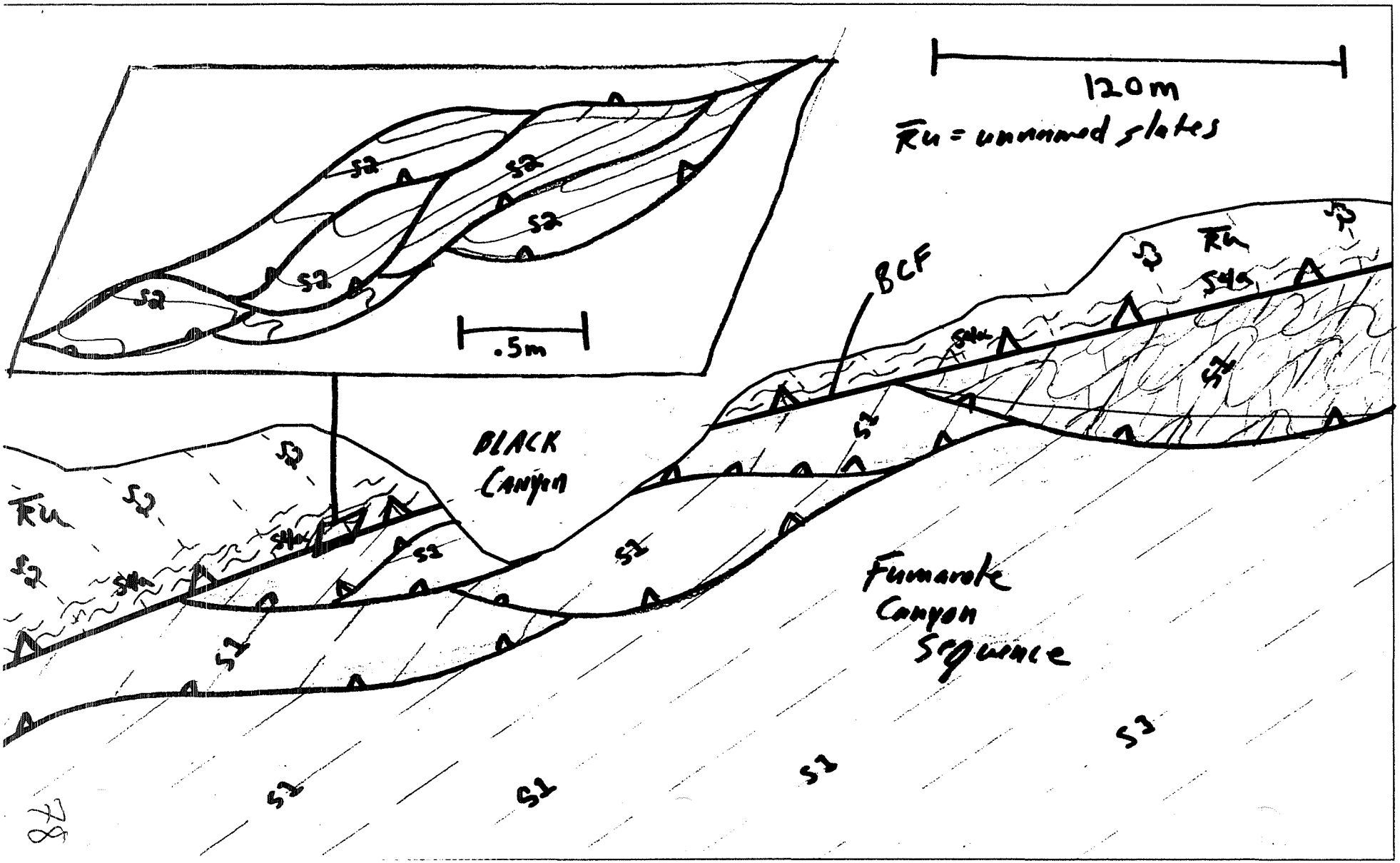

(A) Brittle-ductile shears in the lower plate of the Black Canyon fault, Black Canyon.

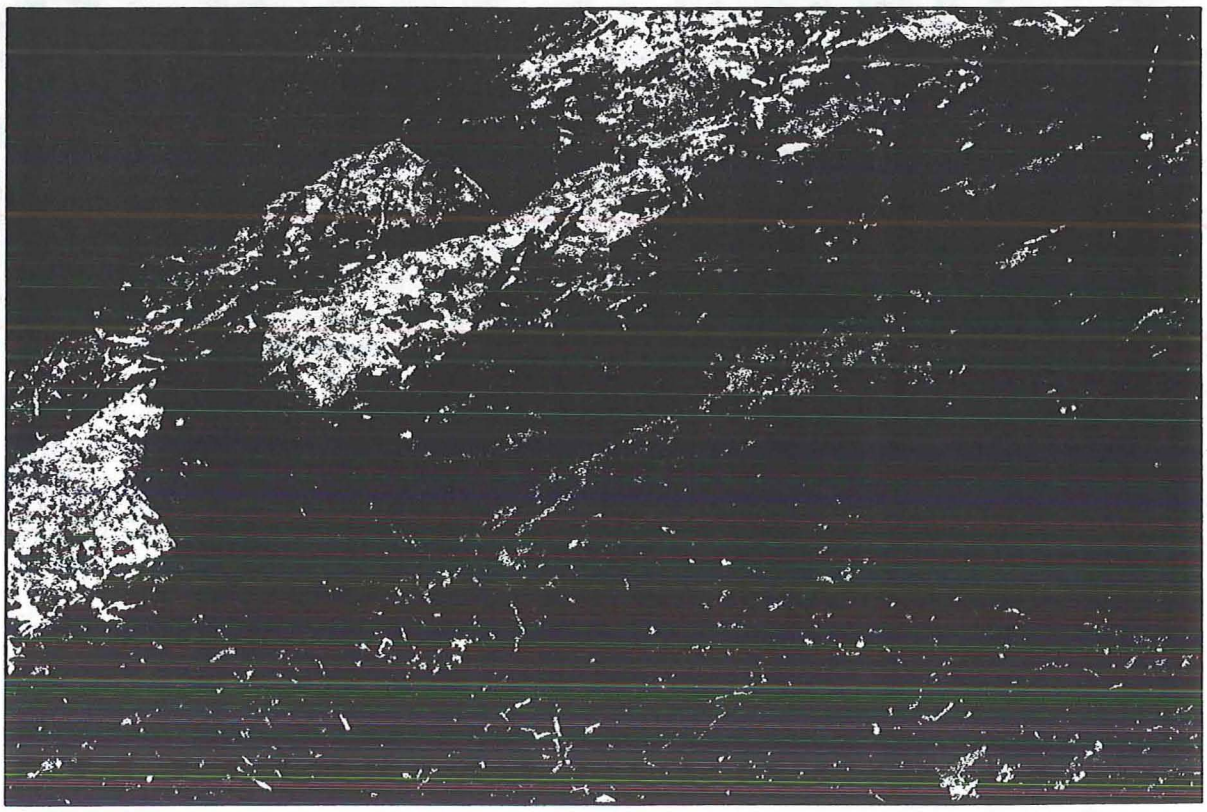

(B) Bedding/S1 perpendicular extensional fractures in lower plate rocks, in the shear zone of the Black Canyon fault, Black Canyon. Note the Miocene dike (highlighted) that is offset in a rather strange way by foliation-parallel shearing.

(A) Subsidiary fault within the lower plate of the Black Canyon fault. The fault trace in the center of the photo separates two large horses within an extensional duplex. Note the slight reorientation of bedding/S1 foliation between the upper block (brown argillite) and lower block (blue-gray siliceous argillite). Both lithologies are part of the Fumarole Canyon sequence in the lower plate of the BCF.

occasionally rootless, and usually occur along, or near, small-offset shear surfaces. At larger scales, shear surfaces are networks of braided, larger faults. These faults occur in rocks of both the upper and lower plates of the Black Canyon fault, and separate larger horses. The faults have large enough offset to cause major changes in dip between the large horses. At all scales, the braided shear surfaces are tight, with no fault gouge.

The Black Canyon fault is broadly characterized, thus, by a braided network of small shears and larger faults, with semi-ductile deformation in upper plate pelitic rocks, and semi-brittle deformation in lower plate siliceous rocks. The fault surface appears to be broadly convex, asymptotic to the Boyer fault, and southeast dipping. Some calcite-filled sigmoidal veins in the footwall of the fault indicate down to the southeast slip, while others are inconclusive. Although F_{4a} folds within the shear zone are asymmetric to the northwest, I interpret these to be the result of antithetic block rotation (Gross and others, 1997), in which a fault block rotates in the direction opposite to that of slip along a basal fault. The sense of displacement along the Black Canyon fault is, therefore, down to the southeast. The fault truncates 14-Ma Miocene dikes, in the footwall (plate P20B), and in turn the fault is truncated to the northwest by the Boyer Fault. The age of the Black Canyon fault therefore postdates dike emplacement, but predates the Boyer Fault.

1.5.11.. Brittle Faults. The brittle faults in the field area the result of extension since Oligocene time. Most of the faults are probably related to late Cenozoic Basin and Range extension, and have been formed since Middle Miocene time (≈ 15-Ma).

(11a) East-West-Striking Faults. East-West (E-W) striking faults in the field are few, but represent an interesting and distinct set of structures. Note that although the Black Canyon fault shows some brittle-ductile features, its orientation is also east-to-west, and therefore it may be a larger-scale example of the E-W fault set. Besides the Black Canyon fault, the E-W set includes two faults within Domain 2: the Little Cottonwood fault and the Rat Wash fault (Plate 1). These faults dip directly to the south at angles of forty to fifty degrees (40° - 50°) and strike east-west. In Domain 1, another top-to-the-south normal fault, the 6018 fault, is a third example of the E-W fault set.

In addition to the distinctive orientation of these faults, they also have a unique set of structures. In all cases, rocks in the hanging walls or footwalls of the faults contain at least

one tight to isoclinal fold of S_1 foliation. Fold F_{1asw} is in the hanging wall of the Little Cottonwood fault. Fold F_{1ane} is in the footwall of the Rat Wash fault. As previously described, F_{1a} folds are folds in S_1 that have a weak axial planar cleavage that is sub-parallel to S_1. In the footwall of the 6018 fault, on the 6018 (ft) summit, there is a tight, overturned synform that folds S1. This fold does not have an axial planar cleavage, and therefore it may be either an F_{1a} or an F_2 phase fold. The axial planar cleavage development, as well as the tightness of the interlimb angles, indicate that these folds formed during ductile, contractional deformation, and, therefore, the folds and faults are probably Mesozoic in age. In contrast, the faults have a number of structures that are characteristic of brittle, Tertiary faults. The fault zones in the E-W set are similar in character to the Black Canyon fault, but have narrow, 0.25- to 0.5-meter-thick gouge zones, and deep, linear grooves and faint slickensides on the fault surfaces, all of which are highly suggestive of Tertiary normal faults.

The orientations of the fault surfaces are, in all cases, nearly identical to the surrounding S1 foliation orientations. Furthermore, the dip directions of the fault surfaces and the trend of the slickensides/grooves differ, in all cases, by at least forty degrees (40°). These observations, as well as the simultaneous presence of ductile and brittle structures, suggest that the faults are Tertiary reactivations of some pre-existing structure, most likely a foliation surface, but also perhaps a fault. Like the Black Canyon fault, the E-W faults are truncated by both the Boyer fault and the Dixie Valley fault. In addition, the Little Cottonwood fault truncates Miocene dikes. Therefore, the E-W faults are the oldest Tertiary faults present in the field area, and are most likely syn-tectonic to the Black Canyon fault.

(11b) Boyer Fault. A 7-km-long segment of the Boyer fault, that marks the eastern boundary of structural Domain 4, crops out along the entire length of the map area. The fault places quartz arenite of the Boyer Ranch Formation, and gabbro/diorite of the Humboldt igneous complex, over the Fumarole Canyon sequence (Domain 2), the Natchez Pass Formation (Domain 1), and the basal part of the Boyer Ranch Formation and underlying units (Domain 3). The Boyer Ranch Formation is therefore present in both the upper plate (Domain 4) and lower plate (Domain 3) of the Boyer fault. The fault is defined by a brittle shear zone that consists of between zero (0) and thirty (30) meters of fault-gouge. In

addition, the gouge entrains blocks of all sizes. Both the gouge and the entrained blocks are derived from the upper and lower plates of the fault.

The shear zone is thickest where fault-gouge is the most voluminous, and this occurs where competent rocks have overridden relatively incompetent rocks. For instance, the shear zone is generally very thick where quartz arenite overlies pelitic rocks of the Fumarole Canyon sequence. In contrast, the zone is relatively narrow where rocks of the Humboldt igneous complex overlie quartz arenite. In places, the fault zone is an abrupt transition between upper and lower plates, and in this case, the upper and lower plate rocks are highly fractured, but the amount of fault gouge is minor. The gouge appears to be derived mainly from rocks in the footwall, as indicated by the color of the gouge. Gouge that is derived from the Fumarole Canyon sequence is clay-rich, and dark gray. Gouge derived from intrusive rocks of the Humboldt complex is chlorite-rich and green. Gouge derived from quartz arenite is sericite-bearing (Sue Lutz, pers. comm.), and is white, to yellowish-brown, to burnt orange.

The largest entrained blocks in the shear zone appear to be derived mainly from the upper plate. Blocks of quartz arenite are tabular and well preserved, and generally longer than 5 meters. The middle-sized fraction of blocks consists of highly altered and sheared, dark green intrusive rocks, that in most cases appear to be pieces of Miocene, mafic to intermediate dikes, derived from the lower plate. The smallest and most strongly deformed blocks are lenses of sheared and chaotically foliated Fumarole Canyon sequence. Intrusive rocks of the Humboldt complex do not tend to occur as entrained blocks. All of the blocks, and especially blocks of quartz arenite, are oriented roughly parallel to the shear zone walls. These blocks form a shape fabric (S_{4b}) that is expressed only at the level of the blocks, and not as a finer foliation. Competent rocks, especially Boyer Ranch quartz arenite and basaltic dike rocks, are often drag folded (F_{4b}) within the fault zone.

In addition to having a variable thickness, the surface of the Boyer fault is highly irregular, as indicated by three-point problems over two-hundred (200) meter sections of the fault (table 1). However, kilometer-scale segments of the fault have a simpler geometry, and an average west-southwest dip.

	Northeast	>>>>>>>>>	>>>>>>>>	Southwest
200m section	080, 06S	231, 16NW	170, 24W	169, 20W
1000m section	029, 79SE	152, 14SW	237, 33NW	062, 10SE

Table 1. Three point orientations of the Boyer fault surface

In map view (Plate 1), the Boyer fault appears to have a west-northwest dip. When the three-point solutions are plotted on a stereonet, the great circles intersect to give a northwest slip line, as well (Figure 13).

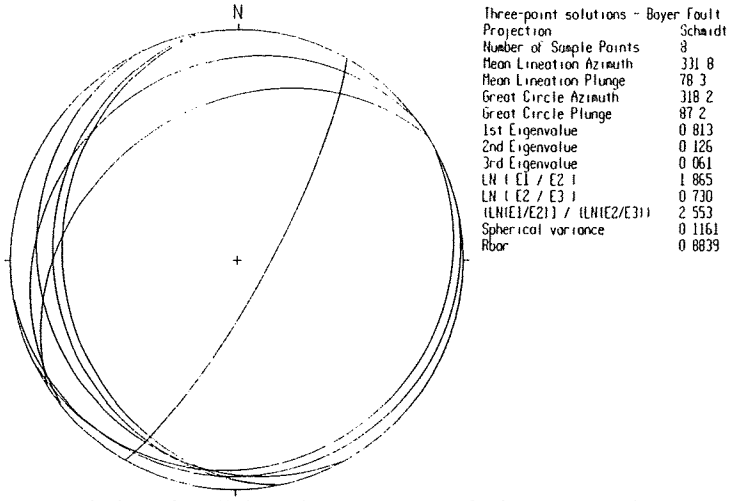

Figure 13. Three point solutions for all dips along the Boyer fault surface. Planes are plotted to show a possible slip line for the Boyer fault. All planes averaged yield a slip direction of approximately N42W, or 318°.

Shear-sense indicators along the Boyer fault are rare, but shear bands at one location within the Boyer fault zone have been rotated toward the west (plate P22). Slickensides are also rare, but occur on some exposures of the footwall surface. In the northern end of the map area, at the 6018 (ft) summit, slickensides at one such footwall exposure plunge 35°, S32W. Another footwall exposure, 250 meters due east of the mouth of Cottonwood Canyon, shows slickensides plunging 55°, N45W. Evidence including the overall dip of the fault surface, the rotated shear bands, and the slickensides suggest that the Boyer fault is a top to the southwest, low-angle normal fault.

The Boyer fault may be broadly characterized as a zone of clay-rich to clay-poor gouge, that entrains sheared lenses of upper and lower plate rocks, and that has a highly irregular surface and thickness (Figure 14). The fault was originally mapped as a thrust fault (Speed,1976; Dilek, 1995); however, Miocene dikes that are truncated by the fault (plate

Figure 14. Diagrammatic sketch of structural relations within the brittle shear zone of the Boyer fault.

Figure 14
Boyer Fault (where?)

good!

; W

NE

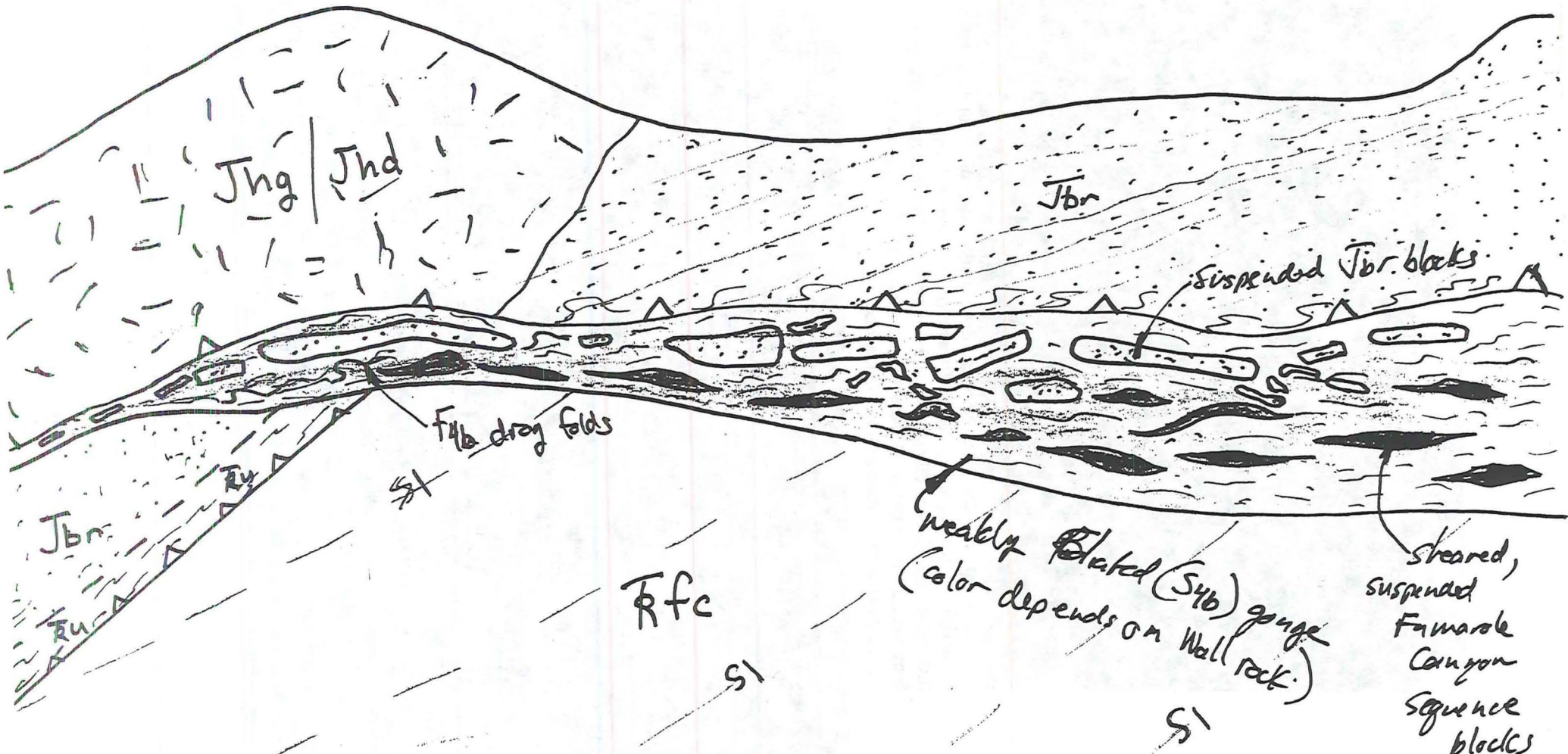

84

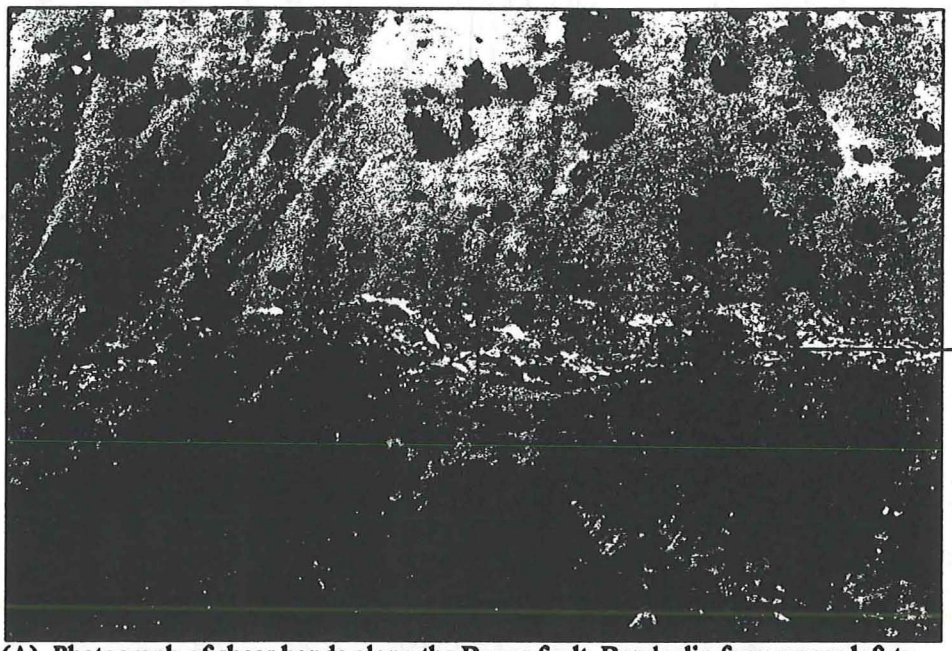

close-up below (B)

(A) Photograph of shear bands along the Boyer fault. Bands dip from upper left to lower right, indicating top-to-the-left (westward) displacement. Brown rocks in the lower plate are Miocene dikes that have been truncated by the Boyer fault. Whitish brown colluvium in the upper plate is weathered diorite. Gray rocks in the shear zone appear to be Fumarole Canyon sequence.

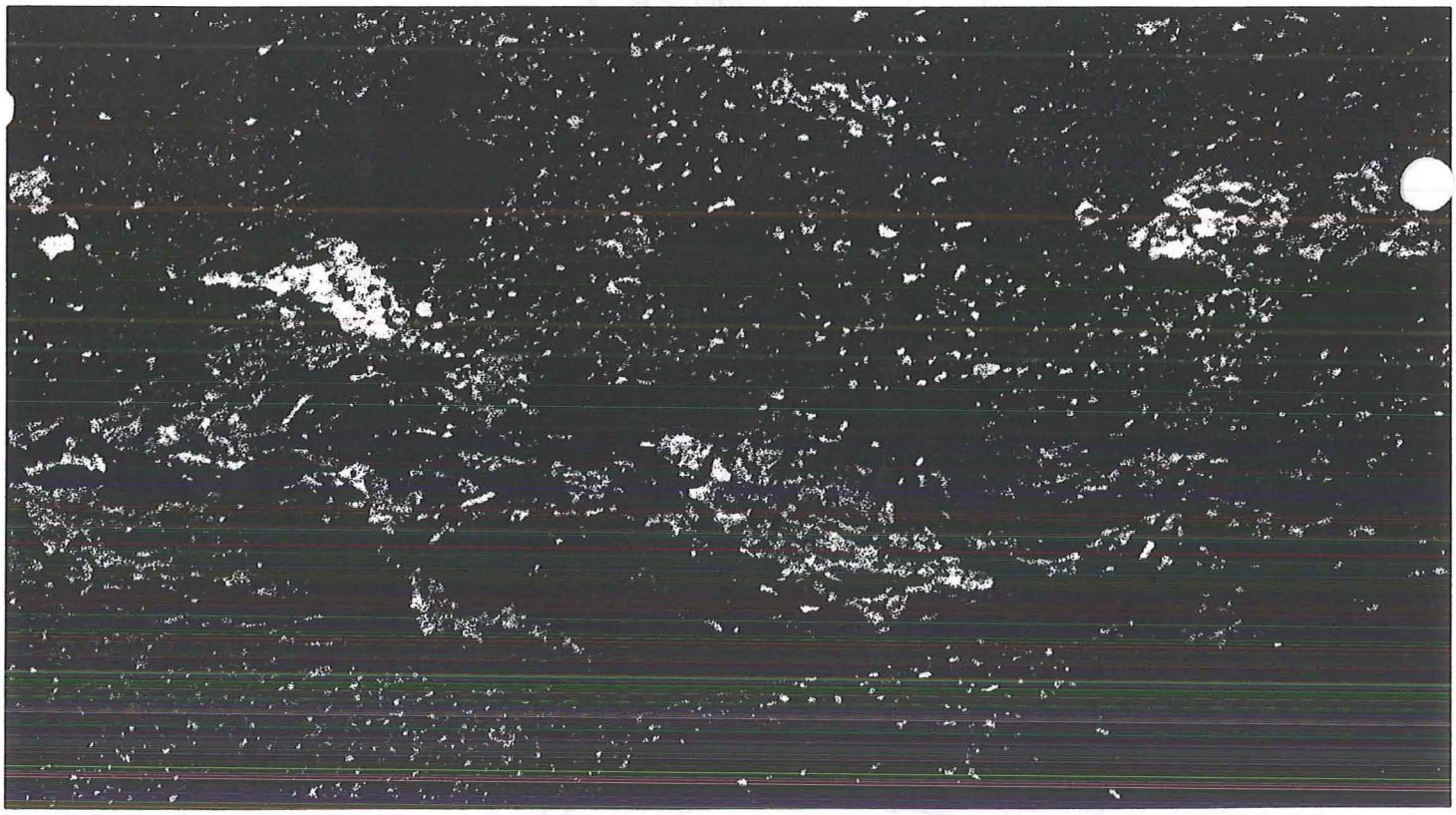

(B) Close-up photograph of shear bands along the Boyer fault, showing bands dipping from upper left to lower right.

P23) are known to be Middle Miocene in age (14.5-Ma, Ar-Ar, Dilek, unpublished data) and therefore the Boyer fault is most probably a Tertiary fault. Another possibility is that the Boyer fault is a reactivated Mesozoic fault, but there is no outstanding field evidence to support an older origin for the fault.

(11c) Dixie Valley Fault and Related Northeast-Striking Faults. The Dixie Valley fault, or range front fault, marks the southeastern boundaries of structural domains 1, 2, and 3. The Dixie Valley fault is not a single fault, but instead is a zone of inter-related, northeast-striking normal faults. The faults have displaced Mesozoic and Tertiary rocks of every domain down and to the southeast, so that the same rocks that crop out along the Stillwater escarpment exist in the subsurface of Dixie Valley, where they are buried by 2300- to 2700-meters of Miocene and Quaternary alluvium. The trace of the rangefront fault (Dixie Valley fault, *sensu strictu*) is defined by a beveled, bedrock scarp along the bedrock/alluvium contact between the Stillwater Range and Dixie Valley. Weakly foliated fault gouge and bedrock shear-bands along the fault dip between 48° degrees and 65° degrees toward the valley. Tectonic and hydrothermal breccias (*fault core* of Caine, 1996) occur in small patches along the fault, but most of the footwall exposures consist of recognizable, but badly damaged, protolith (*damage zone* of Caine, 1996). Exposures of the actual fault surface are rare, but at the mouth of Little Cottonwood Canyon a fault scarp occurs in both the alluvium on the south side of the wash and the bedrock on the north side. In the bedrock, the orientation of the scarp is N50E, 67SE.

Related normal faults—including the RF2, RF3, RF4, RF5, and RF6 faults, and numerous smaller faults—splay from the Dixie Valley fault along the rangefront, and cut through the exposed bedrock of the Stillwater escarpment (Plate 1). These subsidiary fault splays are exposed in bedrock along the escarpment. Other splays continue to the south as alluvial scarps in the piedmont (Caskey, 1996). Still others have been identified in the subsurface, from geophysical data and wellbore data (chapter 2). Footwall, or bedrock, splays that are part of the Dixie Valley system are clearly defined, by abrupt transitions between different rock types, and by well-exposed fault surfaces. However, the cores of the faults are diverse in appearance, depending on the type of rock in the walls. Normal faults that cut through Boyer Ranch quartz arenite dip between 48° and 69° toward the valley.

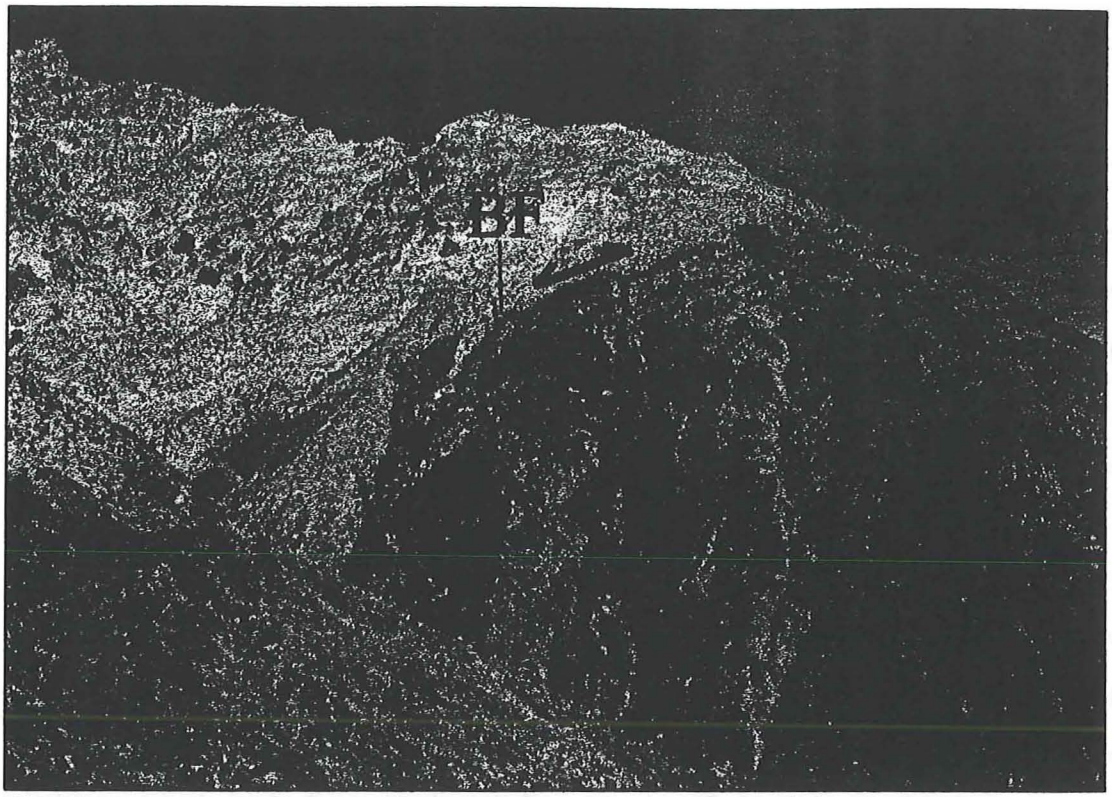

(A) Photograph of Miocene dikes, in the northeast wall of Little Cottonwood Canyon, which are truncated by the Boyer fault. Light-colored rock in the upper plate is Boyer Ranch quartz arenite. Dark gray rock in the lower plate is Fumarole Canyon sequence.

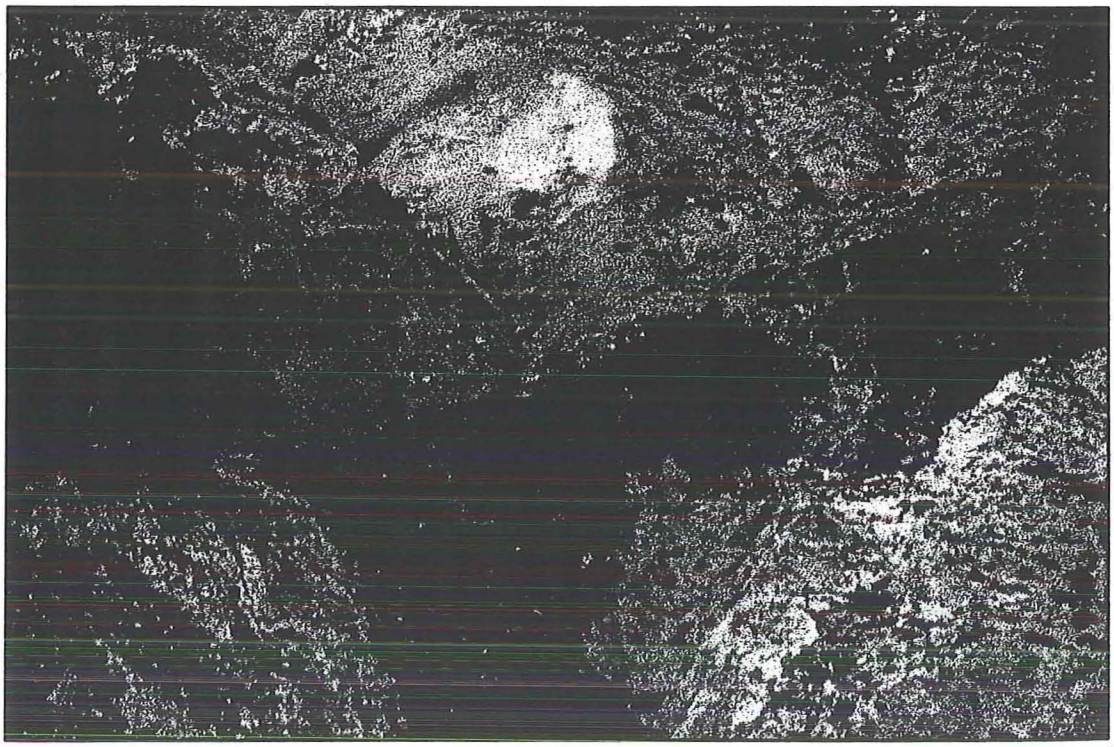

(B) Photograph of Miocene dikes, south of Cottonwood Canyon, which are truncated by the Boyer fault. Dikes and Boyer Ranch quartz arenite are in the lower plate. Mottled colors (arrows) in the upper plate are blocks of quartz arenite and basaltic dikes entrained within clay-rich gouge in the brittle shear zone of the Boyer fault.

They are often perfectly planar, are free of gouge, and are accompanied by large panels of slickensides. In addition, they typically are marked by minor hematite staining and minor hydrothermal breccia. Normal faults that cut through either the Humboldt igneous complex or the Fumarole Canyon sequence are generally marked by zones of gouge up to one meter (1 m) thick. Slickensides on rocks of the Humboldt complex are patchy but well preserved, and in rocks of the Fumarole Canyon sequence slickensides are usually absent. Instead, fault-surface lineations on Fumarole Canyon rocks occur as deep, polished grooves.

Zones in which two or more mapped normal faults coalesce differ from the solitary faults. Within quartz arenite—for instance, where splays rejoin the rangefront fault—the faults have developed relatively large amounts of very colorfully stained cemented gouge, randomly oriented patches of slickensides, and intensely brecciated rock, all of which obscure the exact traces of the faults. Faults in the Humboldt igneous complex and the Fumarole Canyon sequence lack staining and cemented gouge. Unconsolidated gouge is abundant, however, and is so widespread in the coalescent areas, that weathered gouge typically obscures the fault surfaces.

The largest footwall splays are the RF2, RF3, RF4, RF5, and RF6 faults. These faults are all continuous for at least one (1) kilometer. The RF4 fault (plate P24A) is a major fault, that branches from the Dixie Valley fault, 200 meters southwest of Black Canyon, and continues toward the north-northeast for two (2) kilometers, where it splices with the RF5 fault. The trace of the RF4 fault then turns northeastward for one (1) kilometer, until it rejoins the Dixie Valley fault. The RF4 fault, and the Dixie Valley fault, define a lensoidal fault block that is three (3) kilometers long and a maximum of three-quarters (3/4) of a kilometer wide. This fault block, Domain 4a, includes rocks from Domain 4 that have been down-dropped against the rangefront by the RF4 fault. The RF4 fault places quartz arenite of the Boyer Ranch Formation, and gabbro/diorite of the Humboldt igneous complex (Domain 4a), against the Fumarole Canyon sequence (Domain 2). The core of the fault consists of 1 to 2.5 meters of sheared blocks of wall-rock, that are aligned sub parallel to the shear zone walls, and subordinate dark gray fault gouge. Other splays, the RF2 and RF3 faults, are contained within and dissect Domain 4a, and thus contribute to the total offset through the fault block. Since the RF4, RF3, and RF2 faults displace both rocks of Domain 4 and the Boyer fault down and to the southeast, and because the Boyer fault is not exposed in Domain

(A) Photograph of fault RF4, looking north. The fault displaces Boyer Ranch quartz arenite (white to tan rock) and gabbro of the Humboldt igneous complex (dark brown rock), down and to the southeast (right). Fumarole Canyon sequence (dark gray) is in the footwall. Dark rock in the extreme foreground is colluvium shed from the Fumarole Canyon sequence.

4a, the minimum throw across all faults in Domain 4a must equal the vertical distance between the Boyer fault (the base of Domain 4) and the trace of the Dixie Valley fault. Therefore, the RF4, RF3, and RF2 faults have a combined throw of at least 400 meters and a combined heave of at least 800 meters, with most of the displacement having occurred along the RF4 fault. The RF5 fault is a long, low offset fault. From the juncture of the RF5 and RF4 faults, the RF5 fault continues southeastward for three (3) kilometers, until it intersects the N-S fault set (described below) in upper Cottonwood Canyon. The RF5 fault offsets the Boyer fault, and so its vertical and horizontal offset can be measured exactly, at 120 meters and 200 meters, respectively. The RF6 fault begins in Black Canyon, and continues southwest for 3 kilometers. Around Cottonwood Canyon, fault Rf6 offsets both the Boyer fault and the Mesozoic structural window at the mouth of the canyon. The fault re-enters the rangefront at the latitude of the farthest southwestern exposure of unit Tru (undifferentiated sandstones and slaty siltstones).

Thompson and Burke (1973) obtained a first-order approximation of the age of the Dixie Valley fault by multiplying the historic slip rate along the fault with by the total fault offset (the total fault offset was determined from seismic reflection profiles). Although their proposed age of the Dixie Valley fault system, 15-Ma, is reasonable for typical Basin and Range faults, the long term slip and uplift rates for the fault may be poorly represented by slip rates measured from historic fault ruptures.

(11d) North-South Faults. A set of north-south (N-S) striking faults crops out west and northwest of the mouth of Cottonwood Canyon. The faults are sub-vertical structures, poorly exposed, and are most easily seen in air-photographs. They appear in outcrop as groups of closely spaced, subparallel fractures; as headwall scarps above landslides; as color changes or small offsets in colluvium; and as resistant ledges of recrystallized travertine. The dip of the N-S faults varies from steeply west to steeply east dipping. To the north of Cottonwood Canyon, the faults appear dip predominantly westward, while south of the canyon they dip steeply east. There is no indication along these faults that any significant amount of vertical throw (greater than five meters) has occurred. The north-south striking faults near Cottonwood Canyon appear to offset alluvium, and also crosscut a Pleistocene travertine deposit, therefore their age is probably as young as, or younger than, the Dixie Valley fault.

Similar N-S faults to the south, in the area of White Rock Canyon, may have accommodated Oligocene right lateral slip (Hudson and Geissman, 1991), and it is conceivable that the vertical structures around Cottonwood Canyon could related to oblique-slip or strike-slip faulting. However, since the N-S faults around Cottonwood Canyon have been recently active, their relationship to Oligocene faults would have to be one of reactivation.

1.6. GEOLOGIC HISTORY

The stratigraphy and structures, herein presented, establish a loose order of tectonic events that have affected the region of the Dixie Valley geothermal area. At the end of the Late Permian to Early Triassic Sonoma orogeny, the Koipato group (Burke, 1973) was erupted onto the Golconda allochthon as a continental magmatic arc (LaPierre, 1991). These arc rocks are exposed just north of the map area. Shelfal carbonate and terrigenous sediments accumulated on the Koipato platform until Late Triassic time (Silberling and Wallace, 1969). These platformal rocks now comprise the Humboldt lithotectonic assemblage (Oldow 1984). Concurrent with the deposition of the Humboldt assemblage, the Lovelock lithotectonic assemblage was formed in the deep marine basin outboard from the Humboldt platform (Oldow, 1984). Both assemblages collectively make up the Early Mesozoic marine province (Speed, 1978b). Due to the lack of detailed sequence stratigraphy in the marine province, Triassic tectonic phases that affected the Humboldt and Lovelock assemblages are poorly understood. The emplacement of the Fencemaker allochthon (Elison, 1990), in Early Jurassic time, is the oldest Mesozoic tectonic event that is well studied.

In the map area, the first phase of tectonic structures (D1) include penetrative cleavage, folds, and mineral lineations. These structures represent an event of ductile thrusting, that probably corresponded to the emplacement of the Fencemaker allochthon. Penetrative (S_1) foliation, in both the upper and lower plates of the Fencemaker thrust, is parallel to the ductile shear zone of the Fencemaker thrust. L1 lineations plunge down-dip of the foliation, and probably syn-tectonic with S_1. F_1 folds trend east-west, and verge northward on a megascopic scale, while smaller F_1 folds have no apparent vergence. The northward vergence of F_1 folds, and the general southward dip of the S_1 foliation, are

consistent with the northeast transport direction of the Fencemaker (B) allochthon (Speed and others, 1988).

Following the emplacement of the Fencemaker allochthon, another event of contractional deformation (D_2) folded the Fencemaker shear zone and reoriented D_1 structures. The direction of tectonic transport during D_2 was oblique to the strike of S_1 foliation and to the trend of F_1 folds. The vergence of F_2 folds indicate that this transport direction was toward the west. The D_2 event created F_2 folds at all scales not only within the upper and lower plates of the Fencemaker thrust, but also extensively in the Boyer Ranch Formation. A possible source of this deformation was the Willow Creek thrust (Elison, 1987), a west directed thrust that postdates the Fencemaker and was active during Middle Jurassic time. before 155-Ma (Speed 1988). F_2 folds in structural Domain 4 are apparently crosscut by the Humboldt igneous complex, so that the D_2 event must pre-date the intrusion of the complex. Therefore, D_2 must have happened prior to about 165-Ma, which timing lies within the existing constraints for the emplacement of the Willow Creek allochthon. If we assume that D_2 was indeed related to the Willow Creek thrust, the age of the Boyer Ranch Formation can be constrained to post-Fencemaker and pre-Willow Creek deformation, as the Boyer Ranch does not contain D_1 structures. In addition, since D_1 (Fencemaker) structures pre-date D_2 structures, the Fencemaker allochthon was also emplaced prior to 165-Ma.

The D_3 event is associated with a regional crenulation cleavage (S_3). The crenulation crosscuts structures of all previous phases, and so must be younger than 165-Ma. There is not an established Jurassic tectonic event that operated regionally after 165-Ma, and thus it is possible that S_3 crenulation is younger, perhaps Cretaceous or Tertiary in age. On the other hand, S_3 crenulation may be a late stage effect of the Jurassic D_2 event, or an effect of the intrusion of the Humboldt igneous complex.

The next important phase in the geology of the region was the eruption of Oligocene and Miocene tuffs, and the intrusion and eruption of Miocene basalts. The volcanic units capped the Mesozoic rocks in many places, and mafic to intermediate dikes intruded the stack of Mesozoic thrust sheets at all structural levels. Oligocene and Lower Miocene tuffs (23- to 33-Ma) were erupted contemporaneously with an event of rigid block, counter-clockwise, vertical axis rotation. The rotational event affected a discrete but poorly defined area. For example, tuffs in the Tobin Range, forty (40) kilometers north of our study area,

did not experience rotation. However, tuffs in the western Stillwater Range, twenty kilometers west-southwest from our study area, and in White Rock Canyon, 15 kilometers southwest of our study area, show as much as 25° of counterclockwise rotation (Hudson and Geissman, 1991). During Middle Miocene time regional basalt flows and minor tuffs blanketed the older tuffs. The oldest known flows, at Table Mountain and the Sou Hills, range in age from 18.3- to 13-Ma (Nosker, 1981). These flows are not rotated, and therefore vertical axis rotation must have abated, at the latest, by Middle Miocene time (Hudson and Geissman, 1991). At the same time, between 22- to 14.5-Ma (Dilek, 1991), basaltic to andesitic dikes intruded the Mesozoic basement rocks and older tuffs, possibly as feeders to the overlying flows.

The next event of tectonic deformation to occur in the region, D_4, included early extension associated with the Basin and Range. D_4 is represented by two sets of faults: an E-W set and the Boyer fault. East-west striking faults became active (D_{4a}) sometime after the emplacement of Middle Miocene mafic to intermediate dikes. The E-W faults are characterized by brittle and brittle-ductile shearing, slickensides that trend obliquely to the dip of the fault surface, east-west strikes, and by their ages, that are consistently older than the Boyer fault. E-W faults truncate Miocene dikes, at every fault locality in the field area, and are in turn truncated by the Boyer fault. Therefore, their age is post-Middle Miocene but pre-Boyer fault.

The Black Canyon fault, a brittle-ductile fault with large displacement, is the largest example of the E-W fault set. Stereographic analysis of F_2 folds in the upper plate of the fault (Figure 9) show that the average F_2 hingeline in Domain 3 trends 159° to the south-southeast. In contrast, F_2 hingelines, from stereographic analysis of Domains 1 and 2, trend between 206° and 199°. This difference in F2 hinge orientation suggests that the upper plate of the Black Canyon fault may be rotated counterclockwise, with respect to the lower plate, by as much as 47° on a vertical axis. Therefore, the Black Canyon fault, and other E-W faults, may be oblique-slip faults. Slickensides, that trend obliquely to the dip of the E-W fault surfaces, further suggest that some oblique-slip may have taken place on the E-W faults.

D_4 continued with displacement on the Boyer fault (D_{4b}), that coincided with, or post-dated, movement along the E-W faults. The Boyer fault displaced westward the Boyer

Ranch Formation and Humboldt igneous complex. Because the Boyer Ranch Formation is present in both the lower and upper plates of the fault, it is tempting to suggest that the fault has had little displacement. However, the magnitude of the Boyer fault shear zone suggests prolonged slip has occurred along that structure. Furthermore, the bulk of the Humboldt igneous complex resides in the upper plate, while only a very minor mass of related intrusive rocks reside in the lower plate. The distribution of the Humboldt complex therefore loosely suggests that the Boyer fault has experienced large displacement. The significance of the Boyer fault, as it relates to Basin and Range extension, is not yet known. The models of Gross (1997) (discussed below) might suggest that the Boyer fault developed as result of flexural slip within a monoclinal forced fold, above a high-angle normal fault (Gross, 1997; Benoit, 1995). Simply put, the fault was a result of early Basin and Range extension, since there is no question that the fault has moved sometime after the Middle Miocene (14.5 (?)-Ma Dilek, unpublished Ar/Ar dike dates), and prior to the development of the Dixie Valley fault system.

The modern tectonic regime is characterized by active extension along regional Basin and Range normal faults, such as the Dixie Valley fault. The Dixie Valley fault and related faults truncate, and thus postdate, the Boyer fault. First order estimates of the slip rate along the Dixie Valley fault indicate that the fault has been active for the last 8 m.y., since Late Miocene time (Okaya and Thompson, 1985). Presently the fault is seismically active, and last ruptured in 1954. Studies in progress, related to the development of the Dixie Valley geothermal field, are addressing the long term uplift and slip rates of the Dixie Valley fault, using cosmogenic isotopes to obtain exposure ages, and fission track ages to understand the uplift history (Caskey, work in progress).

1.7. DISCUSSION

Structural Relationship between the Black Canyon Fault (E-W set), and the Boyer Fault. The Black Canyon fault and the E-W fault set may be structurally and developmentally related to the Boyer fault. Gross and others (1997), in the Dead Sea rift, recently documented faults, and related folds and fractures, associated with the development of a major, low-angle, brittle detachment. Those structures are very similar to structures found within the shear zone of the Black Canyon fault. The geologic setting of both areas is

similar, as well. The example of Gross and others (1997), suggests that moderately-steep, low-offset faults develop syntectonically and synthetically with high-offset, low-angle detachment faults (Figure 15).

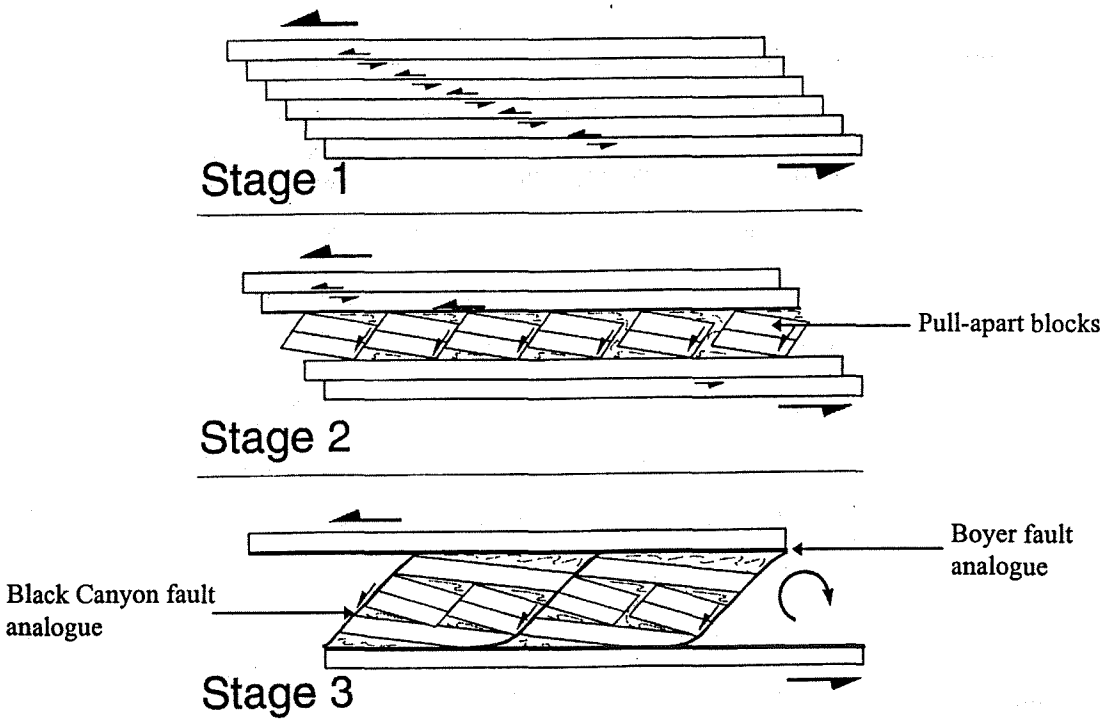

Figure 15. Model of Gross and others (1997) for the development of detachment zones in areas of flexural slip, in the Dead Sea rift. The model offers insight into D4 structures in the Stillwater escarpment, an area with a very similar tectonic setting. Note the horizontal shear zones, analogues to the Boyer fault (and Bolivia fault) and the dipping shear zones, analogues to the E-W fault set (figure modified from Gross and others, 1997).

These moderately-dipping slip zones separate large pull-apart blocks that rotate on a horizontal axis, in a direction antithetic to the overall slip direction. The pull-aparts, and interrelated faults, separate zones of major low-angle displacement. The example of Gross (1997) therefore suggests that the Boyer fault is an analogue to the large-offset, low-angle shear zones, and that the Black Canyon fault is an analogue to the intervening, moderately-dipping faults (Figure 15).

In addition, the Gross (1997) model suggests that Domain 3 may be one large pull-apart. Assuming that Domain 3 is a pull-apart, it is possible that rocks in Domain 3 could have been rigidly connected with Domain 4 well into the evolution of the Boyer fault. Late in the evolution of the Boyer fault, Domain 3 might have been antithetically rotated and then beheaded by continual slip along the overlying Boyer detachment. This fault-mechanical scheme implies that unnamed sandstone and slaty siltstone (unit *Tru*, Plate 1), beneath the

Boyer Ranch Formation, lies much higher stratigraphically—perhaps depositionally—above the Fumarole Canyon sequence. Structurally, unit *Tru* is down-dropped along the Black Canyon fault. It is reasonable to assume, therefore, that strata above the Fumarole Canyon sequence and below unit *Tru* have been faulted-out. If unit *Tru* does correlate with the upper Hoyt Canyon Formation of the Clan Alpine sequence (see page 31), then it is possible that the faulted-out strata include rocks correlative with one or more of the Bernice, Dyer Canyon, and Byers Canyon Formations (Speed, 1978b).

Furthermore, the model of Gross (1997) suggests that more than one, major, low-angle detachment can occur in this type of fault system. As it happens, there is at least one more major, low angle fault in the immediate area of the Boyer fault, herein referred to as the Bolivia fault (not mapped). The Bolivia fault crops out on a low hill on the west side of the abandoned mining town of Bolivia, just off the western edge of the map area. On the Bolivia 7.5-minute topographic quadrangle, the Bolivia fault is delineated by mining adits. In appearance and orientation, the Bolivia fault is very similar to the Boyer fault, but is slightly smaller-scale. I interpret the existence of the Boyer and Bolivia faults as further evidence that the D_4 event involved fault kinematics similar to those outlined in Gross (1997), and that the E-W faults are precursors in the development of the Boyer fault.

2 draft 1 G.P.

SUBSURFACE GEOLOGY OF THE DIXIE VALLEY GEOTHERMAL SITE

2.1. INTRODUCTION

This chapter synthesizes surface geology from Chapter 1, with subsurface geology and geophysics, to ~~create~~ geologic cross-sections through both upper and lower blocks of the Dixie Valley fault. The first section (2.1) briefly reviews the purpose of the project, as it relates to ~~the production of~~ geothermal ~~electricity~~, and then reviews the geologic setting of the geothermal field. The next section (2.2), introduces the various ~~classes~~ of subsurface data that were used to interpret the subsurface geology—a 'data setting'. The third section (2.3) describes how the large volumes of existing data ~~were~~ culled into smaller, pertinent data sets. The fourth section (2.4) presents conclusions that can drawn from the existing data, about the possible ~~behavior~~ of rocks in the subsurface. This section includes all borehole and seismic evaluation. The fifth section (2.5) describes how borehole and seismic interpretations were compiled, and practically integrated into, the geologic cross-sections. The sixth section (2.6), explicitly discusses each of the cross-sections, with attention toward the degrees of confidence that can be placed on various structural features. The seventh section (2.7) summarizes the tectonic development of the Dixie Valley basin, in the area of the geothermal site. The final two sections (2.8, 2.9) speculate on ~~how~~ the tectonic setting and history of faulting ~~influence~~ fluid transport in the geothermal reservoir.

Overview of Problem. Normal faults are important in the mechanics of extensional ~~tectonics in the Basin and Range~~. At mid-crustal levels, normal faults accommodate large extensional strain (Wernicke, 1981). In the shallow crust, faults influence seismogenicity and ~~indicate of~~ the orientation of regional tectonic stress and transport (Zoback and Anderson, 19). In the Basin and Range, shallow faults conduct fluids and are ~~greatly~~ important to the mineral and geothermal industries, ~~whose successes depend upon~~ detailed knowledge of past and present hydrothermal systems.

In the Dixie Valley geothermal area (DVGA), shallow, permeable faults provide the production zone(s) for geothermal fluids (steam and brine). To efficiently extract fluids, therefore, one must know the locations and geometries of these permeable

subsurface faults. The aim of this chapter is ~~this~~ to identify the subsurface locations of permeable faults, and brittle rocks that have a tendency to maintain permeable faults.

Detailed Method. In this study, ~~surface~~ observation has been a fundamental strategy ~~as a source for~~ geologic constraints on ~~the~~ subsurface. One can infer that the same structures and rocks that occur along the Stillwater escarpment are present in the basement ~~of~~ Dixie Valley. In theory, the geology along the footwall escarpment should be mirrored by the slip-face of the down-dropped block. ~~In practice~~, however, this theory must be modified, for three reasons.

REASON 1. A system of both large- and small-offset normal faults, within the Dixie Valley fault system, account for the cumulative ~~downset~~ of the Dixie Valley basement. In addition, the basement rocks ~~are~~ displaced by several ~~additional~~ generations of extensional faults (E-W set, N-S set, Boyer fault) (Chapter 1). Therefore ~~the geology in~~ the down-dropped bedrock ~~is~~ dismembered along high- and moderate-angle normal faults in a complicated way, instead of simply having been downdropped along one fault.

REASON 2. The hanging wall ~~is~~ probably deformed by rollover, a common geologic phenomenon in which the hanging wall of an extensional fault is forced, gravitationally, to sag down against the fault surface (Bally et al., 1981; Dula, 1991). Rollover causes changes in the dips of faults and strata that pre-date the active normal fault system.

REASON 3. Our objectives require a ~~wider cross-sectional~~ area, than just the slip face of the hanging wall, ~~to~~ be understood geologically. However, no structure ~~is~~ perfectly continuous with distance. As the cross-sectional area is ~~widened~~, discontinuities in the geology over distance—for example, structural thickness, stratigraphic thickness, fault orientation, and folding—~~add inaccuracy to~~ cross-sections.

For these reasons, it is apparent that reconstructing the geology of the geothermal reservoir ~~is not simply performed~~ by extrapolating surface geology directly into the subsurface. As this chapter demonstrates, surface geologic relations must be combined with information from geothermal boreholes and seismic reflection surveys. The

products of combining these new and re-evaluated data, are two geologic cross-sections, C-C' and D-D' (Plate 2) that penetrate the deep basement of Dixie Valley. The cross-sections are drawn to depths corresponding to those levels at which geothermal fluid production has been most successful for the last decade.

Geologic Setting of the Dixie Valley Geothermal Area. Dixie Valley is a tectonically active fault-controlled and fault-bounded basin, or graben, in west-central Nevada (Chapter 1). It is a northeast-trending trough roughly 120 km long and 13 km wide, and is the lowest valley in the northern Great Basin. The valley lies between the Stillwater Range, which borders the valley to the northwest, and the Clan Alpine Mountains, on the northeast. In cross-section, the valley is asymmetric, ~~sloping~~ and its floor slopes northwestward toward the Dixie Valley fault.

The basement geothermal reservoir in Dixie Valley lies beneath ~~a~~ 1800 meters of alluvial basin-fill, and includes Mesozoic rocks which are the same as those exposed along the Stillwater escarpment (Chapter 1). In addition, ~~around~~ about 600 meters of Tertiary lacustrine sedimentary rocks, basaltic lava flows, and rhyolitic tuff are present in the ~~basement~~ subsurface, where they depositionally overlie Mesozoic ~~lithologies~~ rocks and underlie the alluvial basin fill. Granite (probably Cretaceous) is also present in the ~~basement~~ subsurface, but it occurs ~~resides~~ only in the footwall of the Dixie Valley fault.

In surface exposures, the Tertiary volcanic units cap Mesozoic rocks high in both the Stillwater Range and in the Clan Alpine Mountains (Speed, 1976). The lacustrine rocks are not exposed anywhere at the surface. Granite, similar to that which occurs in the bottom of the boreholes, is exposed in New York Canyon, on the west side of the Stillwater Range (New York Canyon stock, Chapter 1) (Waibel, 1987). Because neither the ~~igneous~~ volcanic nor the lacustrine rocks are exposed in the map area (Plate 1), they ~~are~~ have not been treated in detail in Chapter 1. Therefore I will briefly outline their stratigraphy, as known from geothermal wellbores:

2.1.1. High-Silica Tuff, Lacustrine Siltstone and Lacustrine Volcaniclastic Sandstone. In most of the wells, lacustrine rocks ~~lie~~ depositionally overlie rocks of the Humboldt igneous complex. However, in well 74-7 (Fig. 2), fifty-five meters (55m) of Oligocene high-silica rhyolitic tuff overlies the Humboldt igneous complex, and this tuff is absent in the other boreholes (Waibel, 1987). Because other wells that ~~are~~ close to 74-7

did
~~do~~ not intersect the high-silica rhyolite tuff, it is ~~possible~~ probable that the tuff unit is an isolated slide block.

The lacustrine sedimentary sequence rocks of includes dark gray siltstone, intercalated with lighter colored (~~often~~ commonly white) tuffaceous and volcaniclastic sandstone. The volcanic components increase in abundance downwards. The thickness of the section ranges from 100 to 420 meters, ~~which~~ the variation probably results mg from normal faulting ~~out~~ pinching out wedges of the section. The minimum age of the lacustrine rocks is constrained ~~to~~ between Middle and Late Miocene by overlying volcanic rocks. The ~~maximum age of the~~ lacustrine rocks ~~is presently constrained~~ date by underlying Oligocene tuffs in well 74-7 (Waibel, 1987). However, as mentioned, the autogenesis of the tuffs in 74-7 has not been established. Furthermore, attempts to obtain fossil dates from the sedimentary rocks have been unsuccessful (Waibel, 1987). Therefore the maximum age of the lacustrine rocks is poorly ~~constrained~~ known.

2.1.2. Miocene Basaltic Rocks. Basalt and minor intercalated volcaniclastic rocks overlie the lacustrine rocks. The basalts are similar to exposed basalts ~~which~~ that cap the Stillwater Range, on and around Table Mountain. However, the stratigraphy of the Table Mountain section has not been worked out, and reconnaissance mapping by the author indicates that the stratigraphy in that area is quite varied. Therefore, it is ~~misleading to say that the subsurface basalts are the same rocks as those on Table Mountain, since it is unknown how exactly they correlate~~ whether the subsurface basalts are correlative with basalts on Table Mountain.

The basaltic rocks ~~around~~ at Table Mountain range from flows to agglutinates, scoria, and palagonitic tuffs (Waibel, 1987). Flows ~~are~~ range from aphanitic and glassy, to porphyritic and oxidized, or zeolitically altered, and typically contain either hornblende or olivine and clinopyroxene. In the boreholes, the basaltic rocks are less texturally varied and are ubiquitously altered. They range ~~greatly~~ in thickness, from 100 to 500 meters. The flows are thickest in boreholes ~~that penetrate~~ in the southwestern part (section 18) of the field, and thinnest in ~~the~~ boreholes to the northeast (sections 7, 5, and 33). The age of ~~the~~ basalt in surface exposures ranges from 17.5± 0.9-Ma (Nosker, 1981, Sou Hills locality), to 13-Ma (Nosker, 1981, K-Ar, Kitten Springs locality) to 8.5 ±0.4-Ma (Waibel, 1987, southern Stillwater Range locality). Basalts were therefore erupted over roughly a nine (9) million-

year period, and it is unknown whether the entire ~~range~~ sequence of basalts ~~are~~ is present beneath Dixie Valley.

2.1.3 The modern setting of Dixie Valley is characterized by active, seismogenic extensional ~~faulting~~ faults. The valley occupies ~~a~~ part of the Central Nevada Seismic Belt, a generally north-northeast trending zone of late Quaternary faulting and historical seismicity that has been the locus of several moderate to large magnitude earthquakes during the past 100 years. These earthquakes include the 1915 Pleasant Valley and 1954 Dixie Valley earthquakes (Savage and others, 1995). The valley is further characterized by a broad geothermal area. At depths of less than 500 meters, water at temperatures greater than 40°C can be found throughout the valley (Trexler and others, 1983). At the north end of the valley, fumaroles and hot springs occur along the Dixie Valley fault. The surface features delineate a known geothermal resource which is located between the endpoints of the 1915 Pleasant Valley and 1954 Dixie Valley surface ruptures (Slemmons, 1954). Within the geothermal area, commercial development of a geothermal field began in 1979 with exploratory drilling, and today the field supports one 60Mw plant which became operational in 1989.

Okaya and Thompson (1985) concluded that Dixie Valley formed over the last 15 million years, since the Early Miocene. As an alternative, Hastings (1979) suggested that Upper Miocene basalts (≈8.5-Ma) were deposited on a surface of low relief, and therefore predate the extensional faulting that caused the formation of Dixie Valley. Variations in the thickness of Middle Miocene lacustrine rocks, indicated by well bores and seismic analysis (this volume), suggest that Middle Miocene lakes formed in fault bounded basins, and therefore that the topography was convoluted. It seems probable that extensional and/or oblique-slip faulting was underway by Middle Miocene time.

2.2. DIXIE VALLEY SUBSURFACE DATA

Data from geothermal boreholes and seismic reflection surveys, from northern Dixie Valley (Figure 1), were made available for this study by Oxbow Geothermal Corporation. The borehole data include well cuttings, and ~~a~~ hard-copies ~~suite~~ of downhole geological and geophysical logs (Table 1). The seismic data include ten (10)

lines, collected as both explosive and Vibroseis reflection surveys (Table 2). These data are archived in SEG-Y format on 9mm magnetic cassettes.

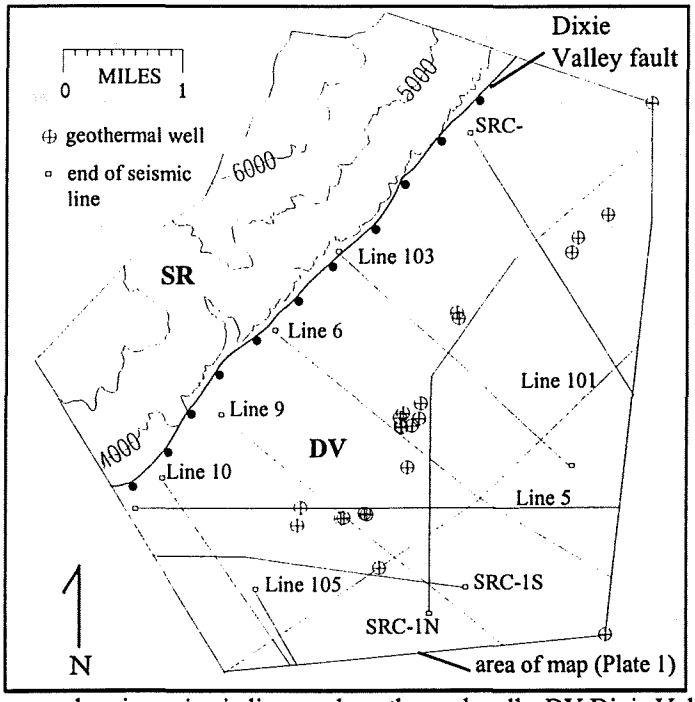

Figure 1. Location map showing seismic lines and geothermal wells. DV,Dixie Valley; SR, Stillwater Range.

Boreholes and Well Logs. Boreholes at the geothermal site ~~act~~ are used as ~~either~~ production or injection wells, or as hydrological observation points. ~~The~~ Some wellheads are ~~sometimes~~ isolated, but usually they are clustered in small groups, and are spaced out along a northeast trend which parallels the Dixie Valley fault (Figures 1, 2).

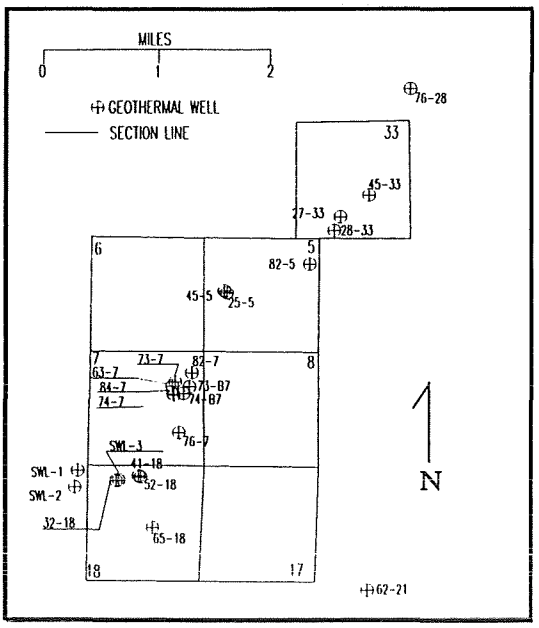

Figure 2. Distribution of wells within the Dixie Valley geothermal field. Note the close spacing within individual clusters, and the northeast trend of the ~~wells~~ field.

From the wellheads, the boreholes usually deviate downward ~~in both the horizontal and vertical directions~~, so that their profiles are not straight in either a horizontal (plan) or vertical (cross-sectional) view. A few wells are, however, almost perfectly vertical. For each borehole, there is a suite of well logs (Table 1).

WELL #	MUD LOG	SONIC LOG	STATIC TEMP LOG	NEUTRON/ DENSITY LOG	INDUCTION ELECTRICAL LOG	DIP METER LOG	GAMMA RAY LOG
45-33	X	X	X	X	X		X
27-33	X		X	X	X		X
28-33	X	X	X	X			X
82-5	X		X		X		
45-5	X	X	X	X	X		
25-5	X	X	X				X
82-7	X	X	X	X			X
73-7	X	X	X	X		X	X
74-7	X	X	X	X	X		
63-7	X	X	X				X
84-7	X		X	X			
76-7	X	X	X				X
41-18	X	X	X	X			X
32-18	X	X	X	X			X
52-18	X		X	X			
65-18	X	X	X	X	X		X
SWL-1	X		X		X		X
SWL-2	X	X	X	X	X	X	X
SWL-3	X		X	X	X		X
62-21	X	X	X	X	X		
76-28	X	X	X		X		

Table 1. Summary of borehole logs from the Dixie Valley geothermal site.

Seismic Reflection Surveys. Sixteen seismic lines span the area of the Dixie Valley geothermal field (Figure 1). The survey lines run either perpendicular or parallel to the Dixie Valley fault, while a few lines are oblique to the fault. From the entire body of ~~Dixie Valley~~ seismic data, ten (10) surveys were ~~provided~~ for study (Table 2). Nine of the seismic surveys—Line 6 excluded—were reprocessed at the University of Nevada, Reno, between the Fall of 1996 and the Fall of 1997, by the Consortium for Economic Migration and Tomography (CEMAT) and myself.

Line #	SOURCE
SRC1-N	Vibroseis
SRC1-S	Vibroseis
SRC3	Vibroseis
101	Explosive
103	Explosive
105	Explosive
5	Vibroseis
6	Vibroseis
9	Vibroseis
10	Vibroseis

Table 2. Summary of ten (10) seismic reflection surveys within the study area, provided and owned by Oxbow Geothermal. The data from Line 6 is lost.

2.3. GEOLOGIC CROSS SECTIONS AND CRITERIA FOR DATA USABILITY

~~The orientations of~~ geologic cross-sections C-C' and D-D' (Plate 1) ~~are severely restricted, for they must be~~ drawn perpendicular to the Dixie Valley fault. ~~The necessity for these cross-sections to be perpendicular to the rangefront is a primary consideration, and is explained as follows:~~ because the sense of slip along the Dixie Valley fault is exactly normal, and not oblique (Caskey,1996), ~~exist~~ directly down-dip from their counterparts in the footwall. Cross-sections through the basement of Dixie Valley must be drawn in the direction of slip, ~~to minimize the distances between displaced structures, and therefore~~ to minimize the error in using exposed geology as an interpretive basis for subsurface geology.

The locations of the cross-sections are ~~also~~ restricted, mainly by the spatial density and distribution of wellbores and seismic lines. Cross-sections must be drawn through the most dense groupings of wells, ~~in order~~ to use the maximum number of boreholes as control points. Therefore, cross-sections C-C' and D-D' intersect wells in sections 18 and 7, respectively (Figure 1). Also, for maximum point control, cross-sections must be drawn along trajectories that are nearly co-linear with, or that intersect, one or more of the seismic sections.

The ~~usability~~ of data depends, therefore, on the ~~nearness~~ of boreholes and seismic lines to the ~~restricted~~ locations of the geologic cross-sections. Many of the boreholes and seismic lines are far from the geologic sections, so they ~~are useless~~ as cross-sectional constraints. In other cases, boreholes and seismic lines lie partially in the planes of sections, and still others lie directly in the vertical planes of cross-sections. Some of the subsurface data is useful, thus, while most of the data must be excluded. Schemes for the proper selection of usable borehole and seismic data are outlined below.

Borehole and Well Log Data Selection: The linear, northeast-trending distribution of individual boreholes (e.g. well 45-33), and groups of boreholes (e.g. section 7 wells), provides very few constraints for the geologic cross-sections. Fault-normal cross-sections intersect far fewer boreholes, than sections ~~otherwise~~ drawn parallel to the

Borehole data was used on the cross-section
borehole trend. ~~This kind of restricted borehole coverage is compensated~~ for in two ways.

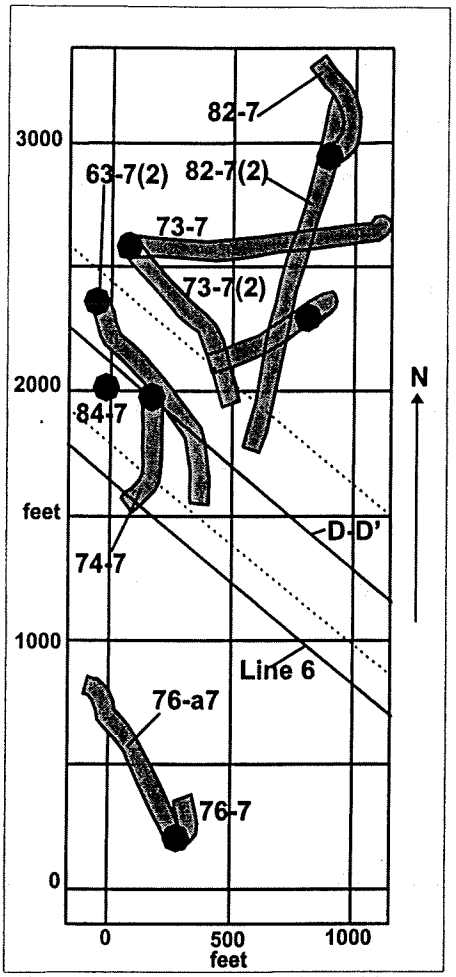

Figure 3. Map view of well profiles in section 7. Wellheads are black circles, deviated well profiles are gray. Note the traces of cross-section D-D' (Plate 3) and seismic line 6. Dashed lines are 250 feet from the traverse line, and encompass the parts of boreholes which ~~are considered to be in~~ were projected into the vertical plane of section D-D'.

held a fairly rigid

First, by very accurately locating the borehole trajectories in both the vertical and horizontal planes, and second, by deciding (albeit arbitrarily) on the distance within which a given datum can be assumed to be in the plane of section. Figure 3 shows the horizontal projections of deviated and vertical boreholes in section 7, and part of the trace of cross-section D-D'. I have arbitrarily assumed that portions of boreholes within 250 horizontal feet (dashed lines) to either side of the geologic traverse can be ~~considered to be in~~ projected into the plane of section. Effectively, therefore, section D-D' has in its plane most of the profiles of wells 63-7(2) and 84-7. In addition, the plane of section includes the upper ~~one~~ half (~~of~~) of borehole 74-7, and the lowermost parts of boreholes 82-7(2) and 73-7(2).

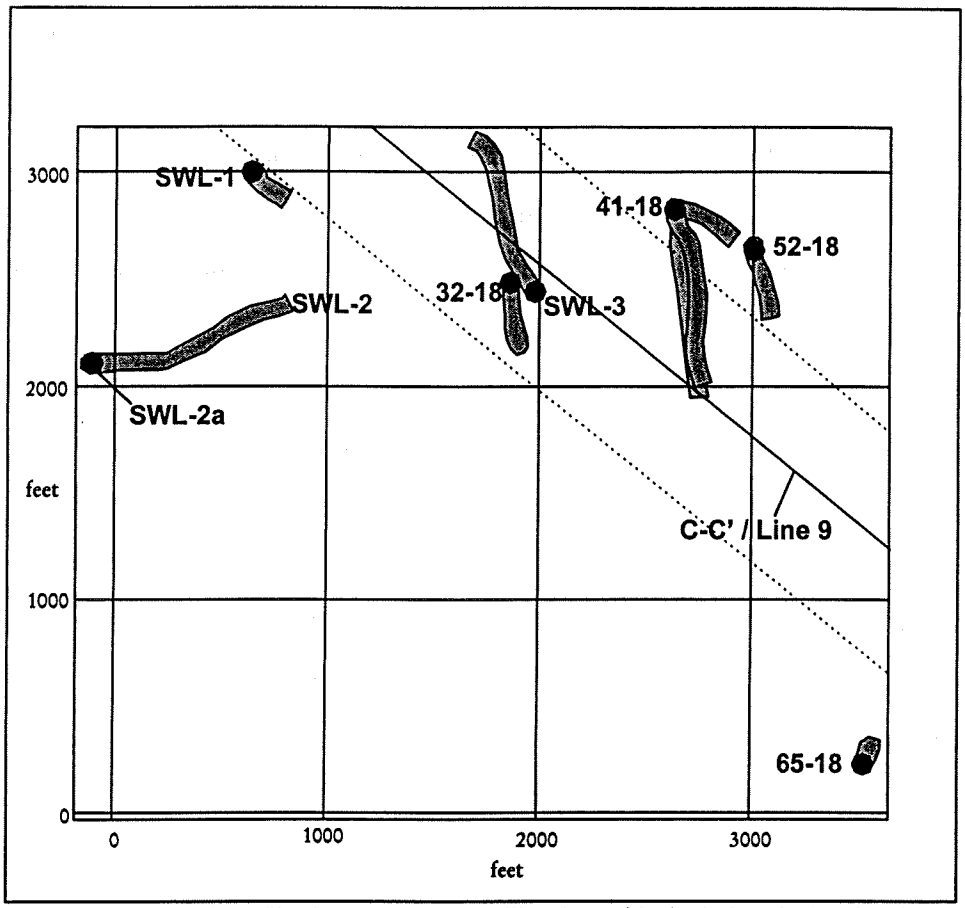

Figure 4. Map view of well profiles in section 18. Wellheads are black circles, deviated well profiles are gray. Note the line of cross-section C-C', which is also the trace of seismic line 9. Dashed lines are 500 feet on either side of the traverse line, and encompass parts of the boreholes ~~which are considered to be in~~ have been projected into the plane of cross-section C-C'.

Like section D-D', section C-C' is also drawn perpendicular to the Dixie Valley fault. Figure 4 shows the horizontal projection of deviated and vertical boreholes in section 18, and the trace of cross-section C-C'. Since the distribution of wells is wider in section 18 than in section 7, I have assumed that parts of boreholes within 500 feet (dashed lines) on either side of C-C' can be ~~considered to be in~~ projected into the plane of section. Effectively, C-C' includes the complete profiles of borehole 32-18, and most of the profiles of boreholes SWL-3, 41-18, and SWL-1.

Of the various well logs, the gamma-ray logs and formation logs were most useful in the interpretation of borehole geology. Gamma-ray logs measure the natural radioactivity, which is proportional to the potassium content, of rocks through which the borehole is drilled. Gamma ray logs were used to pick the precise depths of formation tops, based on sudden changes in the gamma ray signature. Formation logs (mud or lithologic logs) provide two types of data. First, they catalog the types of rocks which are extracted,

in the form of fine cuttings, from the borehole. The mud logs can therefore be used to cross check the gamma logs. In addition, mud logs give information about the state of drilling circulation fluid, or mud. ~~Mud circulation~~ This information is useful, in that open fractures in the subsurface can sometimes absorb the entire column of drilling fluid. These zones are noted on the mud logs as "lost circulation zones", and probably indicate the positions at which the boreholes intersect large, permeable faults.

Seismic Line Selection. The selection of usable seismic ~~surveys~~ lines has been is based partially on the geographic ~~nearness~~ proximity of the ~~surveys~~ lines to the geologic cross-sections, but primarily on the quality of the reprocessed (or previously processed) images. Only the reprocessed images from lines 5, 101, and SRC-3 clearly show faults and stratigraphy. The ~~successes on~~ full reprocessing of these lines ~~were~~ was due primarily to the high volumes of data contained in each of these three surveys. The velocity modeling technique (discussed below) used to reprocess the data requires high data volume for accuracy.

Lines 5 and 101 intersect and/or trend parallel to cross-sections C-C' and D-D', and both of the seismic lines intersect boreholes in section 18. Therefore, lines 5 and 101 are quite ~~useable~~ useful. Line SRC-3 is too far north from C-C' and D-D', so SRC-3 images of these lines are neither included in the geologic cross-sections, nor treated in this chapter. *(Note: other interpretations and discussions of reprocessed lines SRC-3, 5, and 101, can be found in Unruh and others (1997).)*

Hard copies of previously processed seismic images were also available with the seismic data. These were used to constrain interpretations of the reprocessed, depth-migrated images. The post-stack, DMO migration of line 101, ~~done~~ by Simtech Consulting Services for Caithness Geothermal (1994), was particularly useful. Older images, such as those ~~from~~ of Line 5 prepared by Sunmark Exploration (1980), were not as helpful.

2.4. RECONSTRUCTING SUBSURFACE GEOLOGY: CONCLUSIONS FROM EXISTING GEOLOGIC DATA.

Information about rocks and structures in the subsurface can be drawn from ~~existing~~ map and borehole data. For example, structures ~~catalogued~~ mapped at the surface (Chapter 1) ~~suggest that the same~~ structures exist in the subsurface. Boreholes yield stratigraphic information, as well as

the orientations and positions of some fractures and faults. Seismic reflection images yield information about the geometry and relative ages of structures in the subsurface.

Geologic Conclusions from Surface Observations.

2.4.1. Fault Characteristics. The characteristics of subsurface normal faults ~~are~~ demonstrated by exposed footwall normal faults. Observations of exposed faults and related structures—from within the Dixie Valley fault system, the E-W fault set (D_{4a}), the Boyer fault (D_{4b}), and the N-S fault set—give information about the attitudes, kinematics, and relative ages of faults in the subsurface.

Exposed faults of the Dixie Valley fault system (e.g. faults RF2, RF4, RF4), as well as shear bands and foliated fault gouge, strike between N25E and N70E, and dip between 42° and 75° degrees. The higher dips reflect the dips of actual fault surfaces. For example, a bedrock exposure of the range-front fault (Dixie Valley fault, *sensu strictu*), on the northeast side of Little Cottonwood Canyon, dips 67° to the southeast. Shallower dips reflect the dips of minor slickensided surfaces, weakly foliated gouge, fractures, and shear bands, and may not be representative of the true dips of fault surfaces. Surface ruptures constrain the kinematics of the Dixie Valley fault. Modern earthquake ruptures and Holocene paleoscarps, which offset stream channels and other alluvial features, show that the sense of motion along the fault is normal, without an oblique component of slip (Caskey, 1996). These surface observations indicate, thus, that subsurface faults in the Dixie Valley fault system dip steeply to the southeast, are accompanied by a host of lower-angle, related structures, and have normal offset.

The N-S fault set (Chapter 1) comprises a restricted number of isolated faults. These faults may either pre-date the Dixie Valley system or be syntectonic with it. Therefore it is likely, but not certain, that these faults account for some displacement of the basement of Dixie Valley.

The Boyer fault is a major structure along the Stillwater escarpment, above the geothermal field (Chapter 1). The fault dips shallowly to the west-northwest, and truncates the E-W fault set. It is certain that the Boyer fault exists in the subsurface, and also that it is cross-cut by the Dixie Valley fault system.

E-W faults (Chapter 1) pre-date both the Dixie Valley fault system and the Boyer fault. The E-W faults strike west-northwest, ~~trend northwestward on steeply southeast-facing slopes;~~ and dip to the southwest or northeast. One can assume that the same orientation and relative age relations exist in the subsurface, ~~between the E-W and Dixie Valley fault sets~~. ~~Also,~~ since the E-W faults truncate Miocene basaltic dikes, they probably post-date regional basaltic volcanism. Therefore one can assume that southwest- and northeast-dipping E-W faults not only exist in the subsurface, but also that they offset Miocene basalt.

2.4.2. Characteristics of Mesozoic Tectonic Stratigraphy. The tectonic stratigraphy of thrust sheets and fault blocks along the Stillwater escarpment (Chapter 1), is no doubt repeated in the Dixie Valley basement. However, the ~~internal~~ structure of each structural domain may ~~be subject to~~ variation over short distances. For example, in Cottonwood Canyon the Boyer Ranch Formation is infolded with underlying sandstones and slaty siltstones. The macroscopic and megascopic folds/trains (F2) that are partially revealed in the rangefront may be repeated in the subsurface. As a result, the depth to the Boyer Ranch along the hinge crest of a fold may be less than the depth to a hinge trough.

Although the existence of geologic variance is ~~predictable~~, the geometries of folds and other discontinuous structures are not ~~as~~ predictable. Therefore, all of the structures and strata that are exposed in the rangefront, must be ~~imposed on and/or~~ extrapolated into the Dixie Valley basement across faults, ~~and~~ without making inferences about possible geometric changes. For example, the minimum exposed thickness of any unit must be the thickness shown for ~~that unit's~~ down-dip equivalent. Also, the dip of a fault along the rangefront must be equal to the attitude of that fault in the subsurface.

Geologic Conclusions from Existing Borehole Geology.

2.4.3. Characteristics of Borehole Faults. ~~The existing body of~~ subsurface data ~~contains some~~ useful information about normal faulting in the down-dropped block of the Dixie Valley fault system. In boreholes, stratigraphic offsets between formations in closely-spaced wells ~~foster~~ a ~~most~~ simple conclusion: Tertiary faults, other than the Dixie Valley fault, do exist. Downhole investigations have ~~revealed~~ a wide ~~range~~ of details. Borehole televiewer data, coupled with borehole stress and flow tests (Hickman and Zoback,1997; Barton and others,1997), have shown that permeable faults are sub-

parallel to the range-front fault (Table 3). From this condition, one can assume that a lost circulation zone or an inflow zone, within a borehole, marks the location of a fault that strikes to the northeast, and dips steeply to the southeast.

WELL	*RANGE OF FRACTURE/FAULT STRIKE*
37-33	020° to 070°
73-B7	350° to 060°
74-7	012° to 058°
62-21	010° to 050°

Table 3. Summary of orientations of permeable, subsurface fractures, as shown by the high temperature borehole televiewer in selected wells (after Barton and others, 1997).

Borehole televiewer data also reveal the orientations of additional populations of faults or fractures that do not correspond to permeable zones (Table 4). Table 4 shows that ~~there exist~~ a fair number of fractures/faults ~~that~~ strike to the west, northwest, and north. It can be assumed, therefore, that faults indicated by alternative sources—formation-top displacements or seismic profiles, instead of inflow or lost circulation zones—may strike in ~~the range from~~ between approximately 260° to 030°, and may be impermeable or semi-permeable structures.

WELL	*RANGE OF FRACTURE/FAULT STRIKE*
37-33	270° to 320°
73-B7	260° to 335°
74-7	295° to 030°
62-21	*all azimuths, no discrete sub-populations*

Table 4. Summary of orientations of secondary fracture populations that are not correlated with permeable zones, as shown by the high temperature borehole televiewer in selected wells (after Barton and others, 1997).

2.4.4. Characteristics of Borehole Stratigraphy. The Tertiary volcanic and lacustrine ~~stratigraphic order is repeated~~ basin are penetrated in nearly every well. However, the thickness of the Tertiary units differs in each of the wells in sections 18 and 7, ~~is different.~~ Chart 1 shows the variations in apparent thickness ~~for~~ of the Miocene basalt and the Miocene lacustrine rocks, from southwest to northeast.

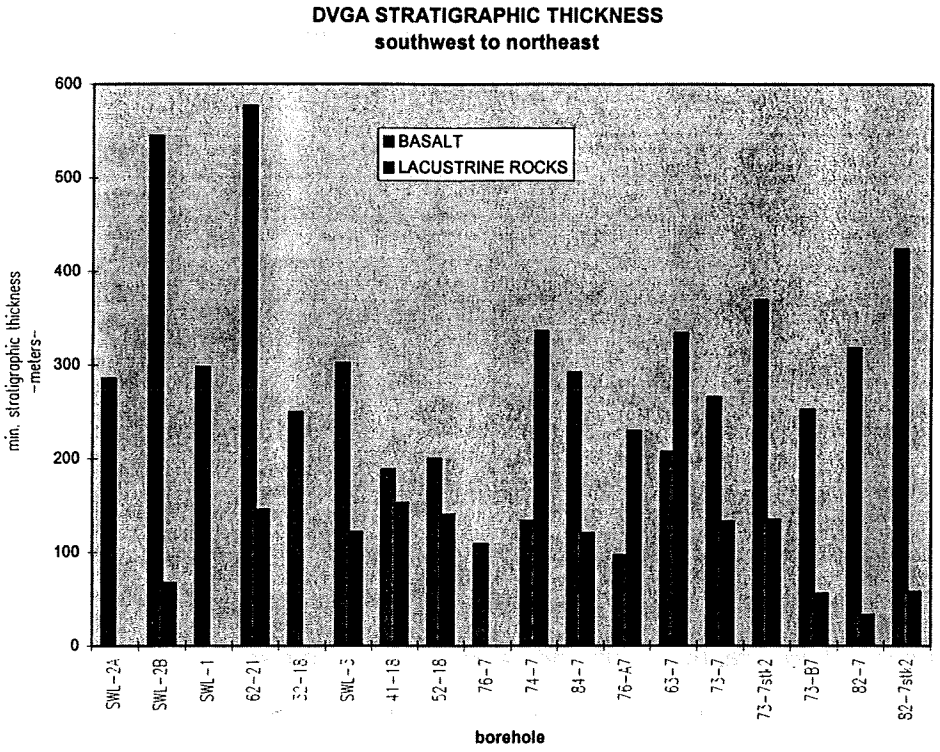

Chart 1. Stratigraphic thickness variations in the Tertiary section.

The great range of thickness ~~variations~~ suggest that both the basalt and the lacustrine rocks ~~are~~ have been structurally thinned, along normal faults. One can assume that the greatest thickness, for each formation, approximates the maximum intact formational thickness. Therefore, the intact thickness of the basalt is approximately 575 meters, and the intact thickness of the lacustrine section is approximately 330 meters. Furthermore, one can ~~conclude~~ infer that boreholes with the greatest thicknesses of rock may intersect the fewest faults. However, Stratigraphic thickness variations could also be due, in part, to primary depositional factors, ~~Formational thickening may have occurred in conjunction with structural thinning~~; i.e. the basalt and/or lacustrine sediments may have pooled in tectonic basins, ~~Formational thinning~~ and may have been thinner ~~occurred~~ along the margins of the tectonic basins.

Geologic Conclusions from Seismic Reflection Interpretation. The accuracy of ~~conclusions about~~ interpretations of geometries of faults and formational ~~geometries~~, drawn from seismic sections, depends on the quality of the interpretation. ~~In turn,~~ interpretive ~~quality~~ depends on three factors. First, the ~~interpreter~~ must have confidence ~~in the good quality of the~~ original

must be of high quality.

data. Second, ~~the interpreter must know something about the~~ processing technique must be understood. Last, ~~the interpreter must understand~~ the geologic setting of the survey area must be understood.

2.4.5. Quality of the Original Data. The Dixie Valley seismic data are generally regarded to be of high-quality. Raw, unprocessed seismic records contain strong hyperbolic reflections from faults and stratigraphy. In addition, the records contain a ~~minimum~~ small amount of noise.

2.4.6. Processing Technique. Our seismic data reprocessing focused on depth imaging, instead of time imaging. Time imaging (Serpa et al., 1988) tends to either flatten or exaggerate the geometry of low angle reflectors and is often insensitive to high-angle reflectors—I call this the 'high-angle fault problem'. Depth imaging, on the other hand, preserves the true geometry of structures, and therefore can be an improvement over time-imaged data (refs.).

(6a) The High-Angle Fault Problem. Seismic imaging of steeply dipping Basin and Range normal faults at all crustal levels has historically been impaired, for two important reasons. ~~Because of faulting~~, In extensional tectonic environments faults juxtapose unconsolidated or poorly indurated alluvium, with crystalline and sedimentary basement rocks. This geologic contrast ~~gives rise to~~ produces large variations in the velocity of seismic waves. Velocities ~~will vary the most laterally~~ variations will be greatest across high-angle faults where the change in lithology is sharp (e.g., between alluvium and basement), while the vertical change in velocity is usually relatively smooth. Typically, time migration methods are unable to incorporate these strong lateral velocity variations into the migration of seismic data. Instead, they incorporate one-dimensional velocity models in which velocities vary only with depth (Okaya and Thompson, 1985). The one-dimensional models inaccurately represent the velocity structure of the subsurface, especially in areas of large extension and rapid sedimentation like Dixie Valley. Therefore, the time-migrated images are distorted or ~~depleted~~ degraded.

The second reason is that many time migration techniques incorporate a Common Midpoint (CMP) stack (so-called "post-stack" migration techniques (refs)). A property of the CMP stack, specifically the Normal Moveout (NMO) correction, causes steep reflections in the raw data, from structures ~~which~~ that have a dip greater than about 15 degrees, to be

filtered out. Consequently, reflections from steep fault surfaces are often eradicated before the data is even migrated. Faults are thus rendered invisible in the seismic image.

Steeply dipping strata are also filtered out by the NMO correction. Typically, the geometry of a fault can be inferred from offsets and truncations of horizontal strata. However, basement rocks and alluvium in the Basin and Range are often deformed, and many times rotated into a greater than 15 degree dip. Thus, in a time migration of a Basin and Range seismic survey, the stratigraphic indicators of a fault may be invisible as well.

An example of the destruction of high angle reflections by the CMP stack/NMO correction is given from Dixie Valley Line 5. Figure 5 shows NMO corrected, stacked data from Line 5. Although shallow reflections from basinal strata are fairly strong, note that the stacked image shows no reflections that dip more than ≈17 degrees (Figure 5a, boxed area). Figure 5b shows the reprocessed image of Line 5, that has left out the NMO correction. In this image, reflections from basin strata attain dips of ≈45 degrees (Figure 5b-S), while one obvious fault reflection (fault B) dips as great as ≈65 degrees.

Figure 5. (A) Seismic image from Line 5, as processed by Sunmark Exploration in 1979, using CMP stack and NMO correction.

(6b) Kirchhoff Pre Stack Migration versus Post Stack Migration.

Migration techniques which do not stack seismic traces before migration are "pre stack" techniques. Pre stack migrations leave out the CMP stack and therefore bypass the NMO correction, so that the image retains the reflections from steeply dipping faults and strata. The depth imaging technique, used to reprocess lines 5 and 101, incorporated Kirchhoff pre stack migration (Louie et al., 1988; Louie and Qin, 1991).

Kirchhoff pre stack migration is a depth migration method. The (X, Y) axes of the final image correspond to distance and depth, instead of distance and travel-time. A migration using the Kirchhoff method is brief, lasting from a few minutes to a few hours, and depending on the size of the seismic data set. The method is technically simple to understand. The migration is based on an amplitude interference scheme. The program searches for amplitude information in the raw seismic records, according to a schedule (the velocity model) (Vidale, 1988). It then adds the amplitude energy into a final image

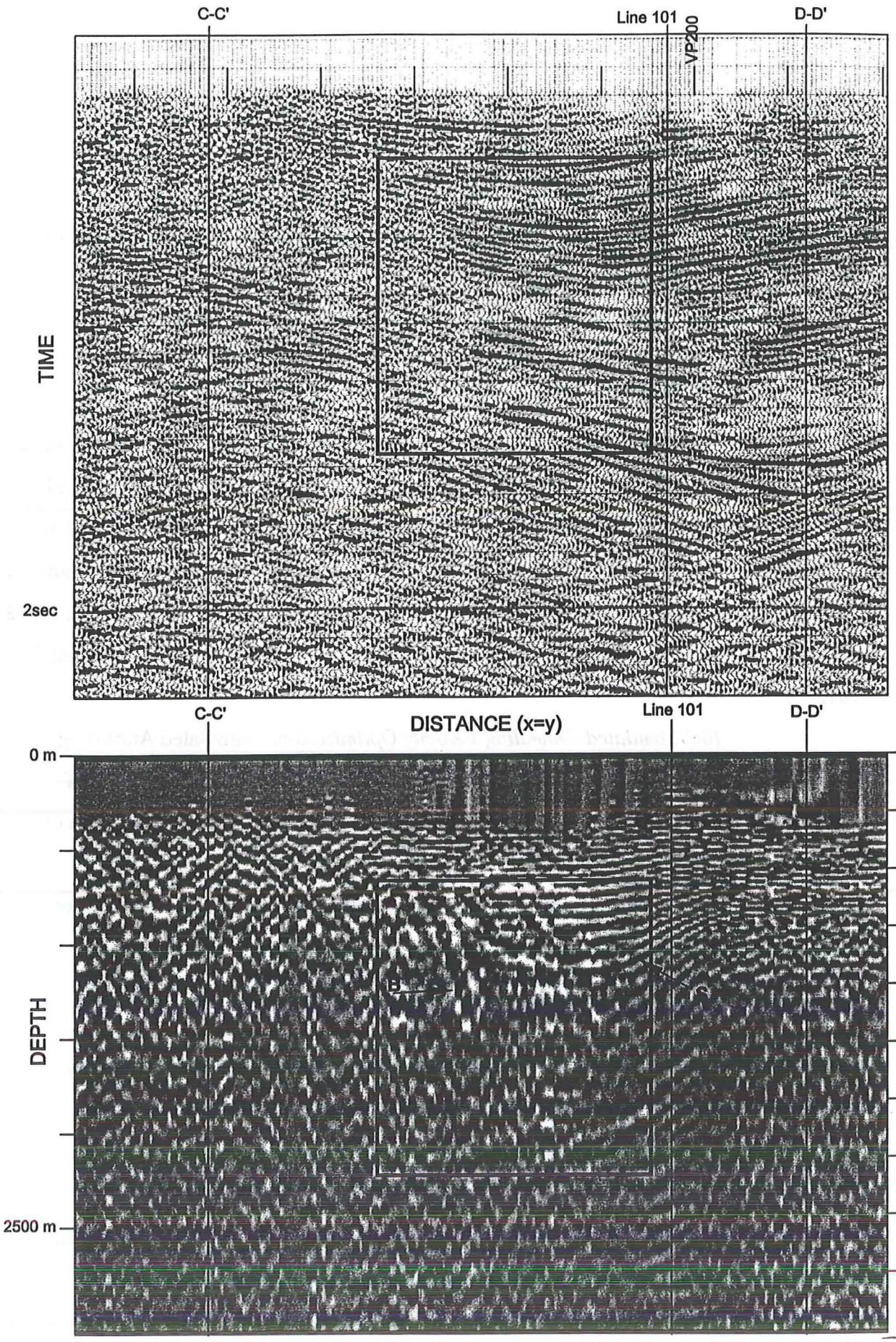

Figure 5. Seismic images from Line 5, as processed (A) by Sunmark Exploration in 1979, using CMP stack and NMO correction. Note the lack of steeply dipping fault and strata reflections (boxed area) as compared with (B), the reprocessed image, showing steeply left-dipping strata, S, and a steeply right-dipping fault, A.

in a way also in accordance with the velocity model. Thus, if the velocity model is accurate, amplitudes from wavelets that occur consistently in each record (i.e., real, reproducible reflections) add together constructively in the final image. On the other hand, amplitudes from wavelets that occur inconsistently (i.e., noise and artifacts) tend to cancel out, or destruct, in the final image.

The success of the Kirchhoff migration relies on the accuracy of the velocity model. Construction of a velocity model can proceed in various ways, but the end product is the same: a mathematical matrix in which the value of each matrix element corresponds to a velocity. The matrix has the same dimensions as each seismic record in the data set. The ~~most~~ simple way of creating a velocity model is to generate a matrix of numbers that are all the same: a single-velocity model. A second-~~order attempt~~ would be to ~~create~~ a geologic cross section, ~~giving~~ each lithology a specific velocity value. A more elegant model would ~~build~~ from direct observation of the raw seismic data. We used one such direct method— simulated annealing optimization— in the processing of lines 5 and 101.

(6c) Simulated-Annealing Velocity Optimization. Simulated Annealing Optimization (SAO) is a process, in the form of a ~~(~~program, that uses ~~observation of~~ unmigrated, or raw, seismic data, to construct a digital model of the velocity structure of the subsurface (Pullamannappillil and Louie, 1994). It is a computationally intensive process which may run from days to weeks, again depending on the size of the data set, and the desired resolution of the model.

SAO is a robust and reliable procedure that operates completely on field observation of P-wave arrival times, and with very few assumptions about unknown geologic structure. The ~~process uses~~ P-wave first arrival times, picked manually from the seismic records, to iteratively deduce the velocity domains through which the P-waves have traveled. SAO has been effective in many studies (Chavez-Perez et cetera). In Dixie Valley specifically, SAO velocity modeling was shown to be sensitive to high velocities in the footwall of the Dixie Valley fault, and ~~the~~ low velocities in the alluvium, to a depth of at least 1KM, using no *a priori* information (Honjas et al., 1997).

2.4.7. Interpretation of Reprocessed Seismic Images. Below, I present my seismic interpretations of ~~various~~ images from lines 5 and 101. Where possible, I provide

reasons and secondary geological evidence for my ~~picks~~. Figures 6, 7, 8, and 9 ~~are interesting for their~~ fine interpretive detail; however, different observers ~~always~~ have slightly different interpretations. Therefore, the profile descriptions concentrate ~~around~~ the obvious ~~and~~ most important structural relations suggested by the profiles, while the subtle geometries are ~~left alone~~. Implications for the tectonic development of Dixie Valley are ~~presented~~ in section 2.6.

(7a) Line 5 interpretation: Line 5 ~~is oblique to~~ the Dixie Valley fault (Figure 1) ~~by~~ an angle of approximately 50°, and oblique to geologic section C-C', by an angle of 38°. Simulated annealing optimization constrained the velocities in line 5 (length=11.82 km) to depths of 1.5 to 2 km. At these depths, the seismic velocity reached 5.8 km/s. Because velocities in the shallow crust do not get much higher than 5.8 km/s, it is assumed that the velocity in the deepest part of the model has reached a maximum. Therefore, it was acceptable to extend the velocity model to 3 km (Figure 6a). *(NOTE: for comparison, ~~shorter~~ lines 9 and 10 (lengths=3.9km and 5.63 km) are constrained only down to 1 km (see Honjas and others, 1997)).*

Figure 6. Reprocessed seismic data from Line 5. A) Velocity model of the subsurface beneath Line 5, created by simulated annealing. B) Kirchhoff pre stack migration of Line 5, based on simulated annealing velocity model. C) Interpretive geologic section.

The image from line 5 (Figure 6b) shows many important structures. Most ~~clearly~~, the image shows ~~the surface of~~ an east-dipping, high angle normal fault, fault B (Figure 6b-B). Steeply dipping and westward-thickening alluvial and lacustrine strata appear as downward bulge in the hanging wall of fault B. The form suggests syntectonic growth of strata in a ~~down-dropping~~ asymmetric graben (Figure 6b-G).

On the western margin of the graben, alluvial strata appear to be truncated by and drag-folded against the steeply dipping ~~surface of~~ fault B. ~~To the east~~, the same strata ~~become thinner~~, but are not obviously truncated. This suggests three possibilities: 1) that strata on the east side of the graben are draped over a topographic irregularity, possibly a rollover fold; 2) that the strata are forced-folded (Benoit, 1996) over a blind normal fault; or 3) that the strata are ~~indeed~~ truncated by a fault with an low apparent dip, and a strike that is almost parallel to the trend of Line 5.

Truncation by a fault (fault V) is the most likely reason for the apparent thinning of the strata on the east side of the graben. In the Line 5 seismic image (Figure 6b-V), the

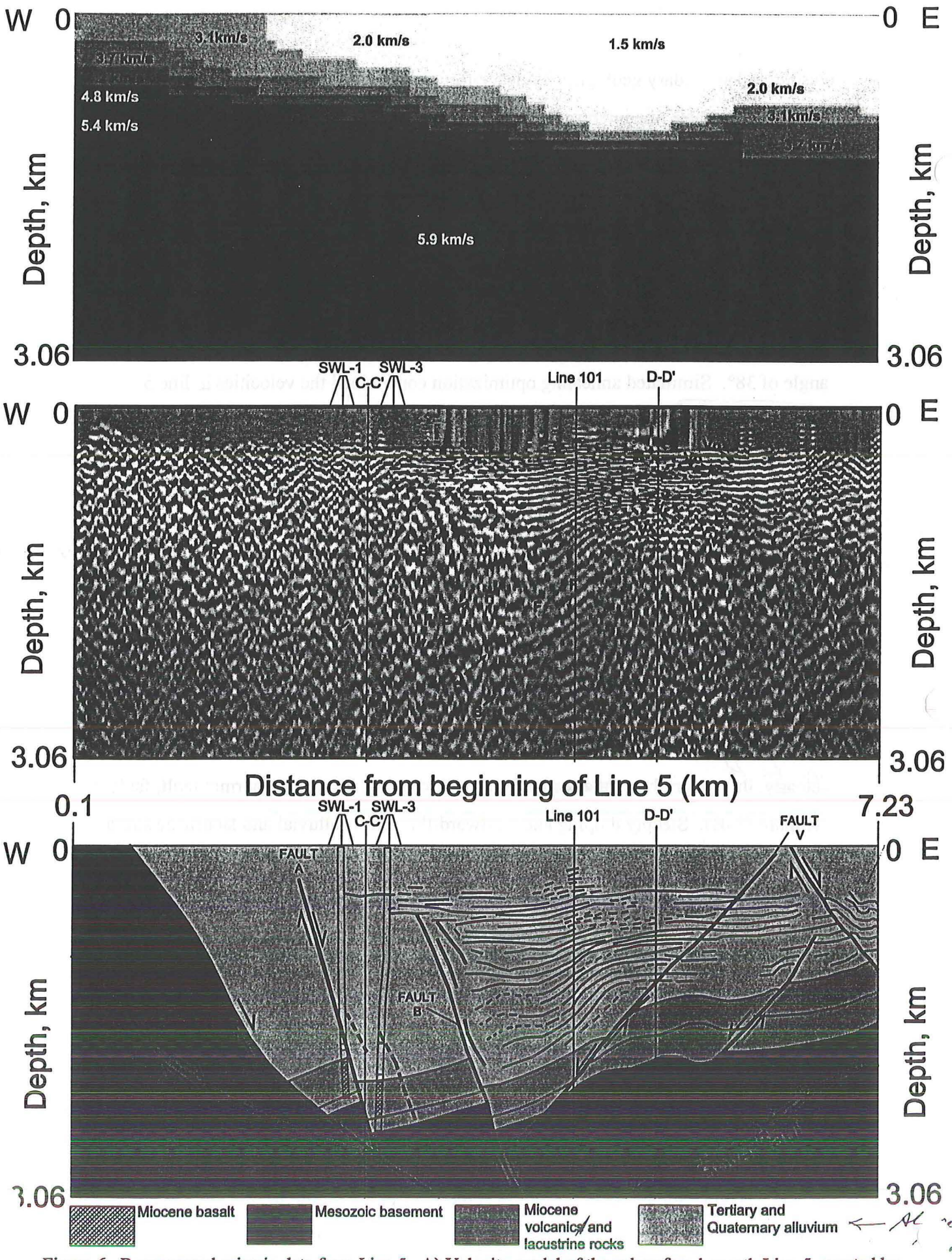

Figure 6. Reprocessed seismic data from Line 5. A) Velocity model of the subsurface beneath Line 5, created by simulated annealing optimization of P-wave arrivals. B) Kirchhoff pre stack migration of Line 5, based on the velocity model above. C) Interpretive geologic section.

~~surface of~~ fault V is faint, but the relative offset of the youngest (highest) quaternary alluvium in the image, by fault V, is fairly clear (Figure 6b-Vo).

Another fault, fault A, is inferred by ~~relative~~ offset of the top of the basalt between wells SWL-1 and SWL-3 (Figure 6b-A). Many steep and closely-spaced, ~~right~~ dipping reflectors in the area of fault A (Figure 6b-R) indicate that the zone to the west of SWL-1 is strongly deformed by a series of sub-parallel, steeply east-dipping normal faults.

In addition to faults, ~~the image from Line 5 faintly~~ reveals the floor of the basin (Figure 6b-F). The top of the ~~basin flooring~~ basalt is pinned at a central location by well SWL-3, which lies almost ~~directly~~ in the plane of Line 5 (Figure ~~6c~~). ~~Laterally~~, the top of the basalt is ~~hard~~ to follow (black arrows). Westward (to the left from SWL-3), the basalt reflection loses coherency, but its position is well constrained by borehole SWL-1. Eastward (to the right of SWL-3), the basalt reflector maintains coherency. At ~~position~~ Q, ~~there even~~ appears to be ~~a~~ slight down-to-the-east ~~offset of the basalt~~ by fault B. ~~Moving farther to the east, just to the right of position Q, the intersection of~~ Line 101 (discussed below) pins the top of the basalt. The relatively shallow basalt depth at this point (1571 m) requires ~~that~~ structural ~~complexity~~ probably down-to-the-west displacement along fault V ~~exists~~ between ~~position~~ Q and ~~the~~ Line 101 ~~intersection~~. The depth of the basalt continues to shallow toward the eastern edge of the profile, probably due to hanging wall rollover and down-to-the-west antithetic faulting.

(7b) Line 101 interpretation. Line 101 runs sub parallel to the Dixie Valley fault (Figure 1), and is oblique to C-C' by 72°. Simulated annealing optimization constrained the velocities in line 101 (length=15.04 km) to depths of 1.5 to 2 km. At these depths, the velocity reached a maximum, and the model was extended to 3 km (Figure 7a). ~~The~~ line 101 ~~migration~~ reveals more subsurface structure than Line 5, ~~for~~ two reasons. ~~First of all,~~ there is ~~more~~ data density in Line 101, because it is longer. Second~~ly~~, line 101 ~~is~~ an explosive-source survey, and therefore the data quality is superior.

Figure 7. Reprocessed seismic data from Line 101. A) Velocity model of the subsurface beneath Line 101, created by simulated annealing. B) Kirchhoff pre stack migration of Line 101, based on simulated annealing velocity model. C) Interpretive geologic section.

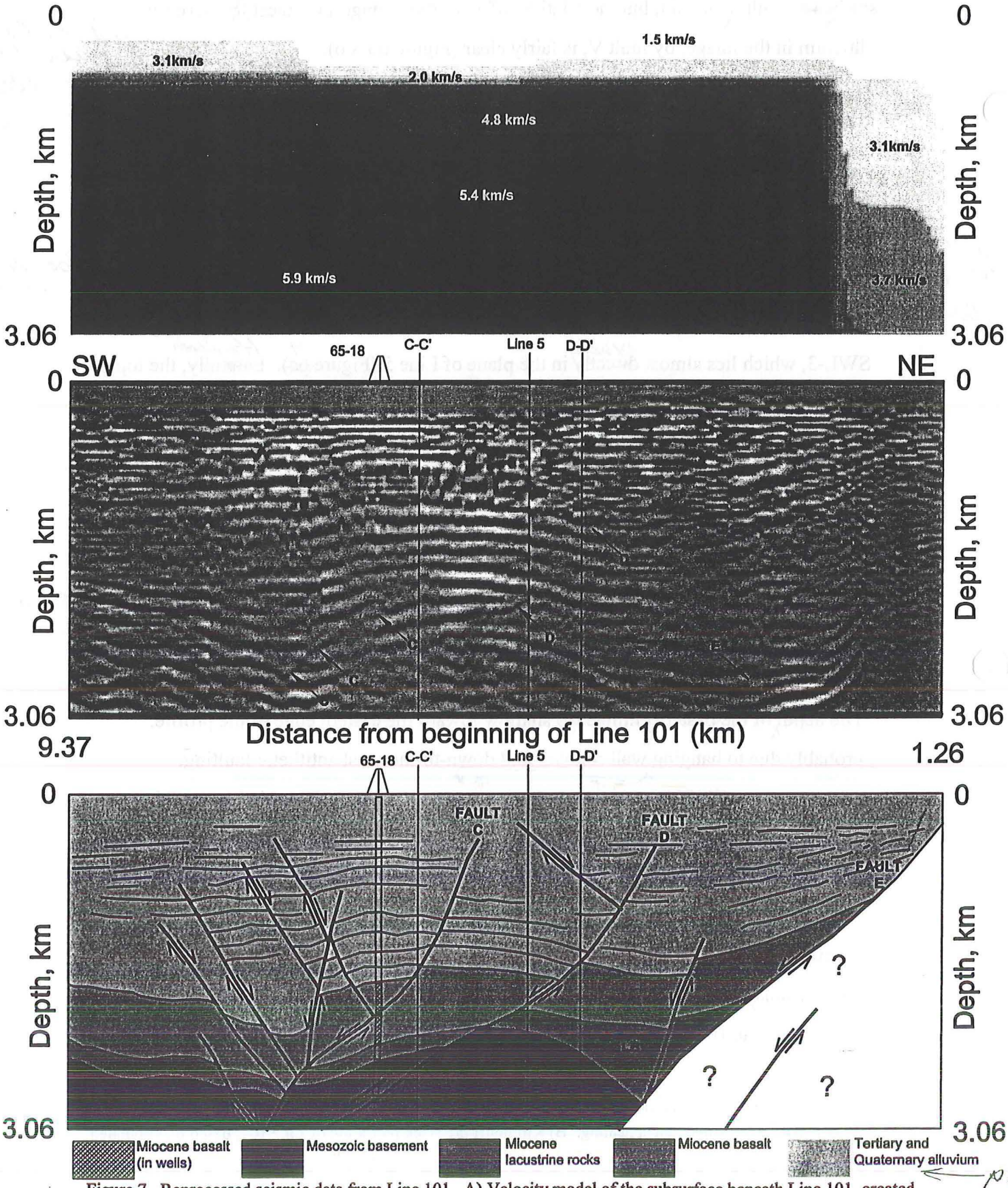

Figure 7. Reprocessed seismic data from Line 101. A) Velocity model of the subsurface beneath Line 101, created by simulated annealing optimization of P-wave arrivals. B) Kirchhoff pre stack migration of Line 101, based on the velocity model above. C) Interpretive geologic section.

Most notably, the image from Line 101 ~~captures~~ shows the basalt at the floor of the basin. The top of the basalt is pinpointed by borehole 65-18, which ~~lies directly along~~ coincides with line 101 and is nearly vertical. Figure 7c ~~shows the projection of 65-18 onto the seismic section, in which the Miocene basalt is patterned.~~ The top of the basalt in the well bore coincides exactly with ~~one~~ a reflection horizon on the seismogram ~~which~~ that I believe ~~to be~~ marks the basalt ~~formation top~~ and the basin floor. The reflector is traceable laterally, and shows considerable topography, suggesting that the surface of the basalt may be an erosional surface, a primary basalt flow surface, or ~~a faulted surface~~ displaced by faults.

I ~~conclude that~~ interpret the topography ~~along~~ of the top of the Miocene basalt is mainly as an effect of down-to-the-southeast normal faulting (Figure 7c). Three southeast-dipping, low- to moderate-angle faults (faults C, D, and E) show up in the seismic image, both as reflectors and ~~as~~ where stratal offset ~~strata~~. The existence of ~~all of~~ these faults (Figure 7b-C,D, E) is corroborated by the post stack migration of Line 101, ~~done~~ by Simtech Inc. (1994) (Figure 8). The three faults displace ~~early~~ older Tertiary alluvium, but are overlain by Quaternary alluvium. Therefore, faults C, D, and E must pre-date the Dixie Valley fault system, and may belong with the E-W fault set (Chapter 1) (discussed below).

Figure 8. Post stack, migrated time image of Line 101, done by Simtech Inc. in 1994. A) CMP stacked image with F-K migration. B) Geologic interpretation. Although the finer details of my interpretations differ between post stack and pre stack (Figure 7b) migrations, the fundamental structural relationships are the same. Faults B, C, and D occur in the similar positions in each seismic profile, and none of these faults penetrate Quaternary alluvium. This cross-cutting age relation indicates that faults B, C, and D are older than the Dixie Valley fault system, and probably correlate to the E-W fault set (Chapter 1).

Offsets of the Miocene basalt along faults C and D explain thickness variations ~~found~~ in boreholes in sections 18 and 7. In section 18, the basalt is thickest in wells 65-18 and SWL-2b ~~at~~ about 570 meters. 65-18 and SWL-2b probably penetrate ~~through~~ nearly intact sections of the basalt, in the hanging wall of fault C (Figure 7c). Other section 18 wells ~~have substantially thinner~~ penetrated smaller thicknesses of basalt ~~around~~ 300 meters. These wells project into Line 101 at approximately ~~the latitude of~~ the intersection of Line 5 (Figure 7c), where the basalt has been structurally thinned along fault D.

In section 7 boreholes, the basalt is generally very thin (~~around~~ about 215 meters). These ~~section 7~~ boreholes project into Line 101 approximately where ~~at the latitude of~~ section D-D', across the line. The basalt thickness along the D-D'/101 intersection is much greater than the thickness at the Line 5/101 intersection. However, when compared with wells 65-18 and SWL2, the ~~low~~ small

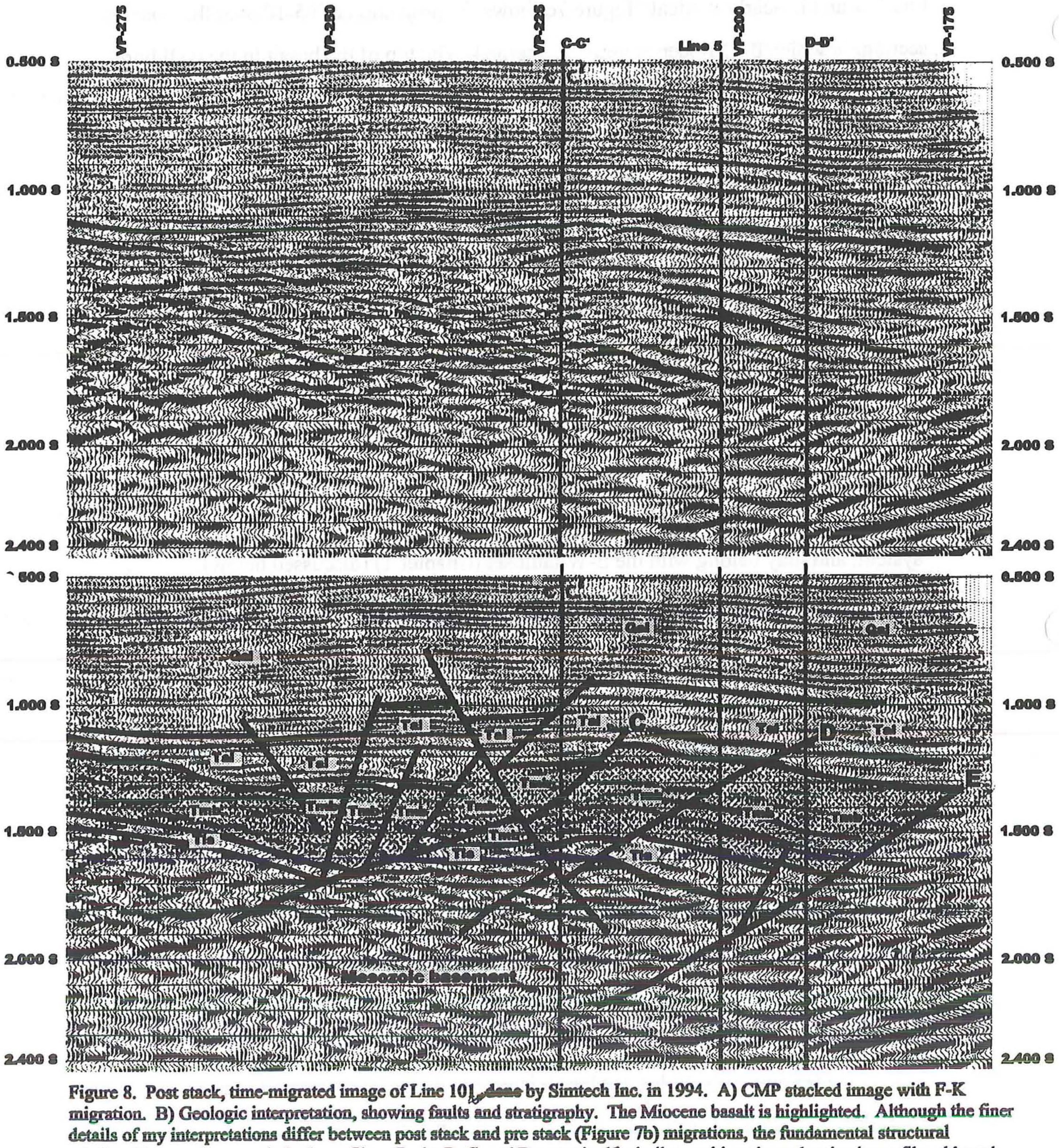

Figure 8. Post stack, time-migrated image of Line 101, done by Simtech Inc. in 1994. A) CMP stacked image with F-K migration. B) Geologic interpretation, showing faults and stratigraphy. The Miocene basalt is highlighted. Although the finer details of my interpretations differ between post stack and pre stack (Figure 7b) migrations, the fundamental structural relationships are the same in both profiles. Faults B, C, and D occur in the similar positions in each seismic profile, although the fault surface geometries vary. Also, a graben structure occurs in both sections, to the west of well 65-18. None of the faults penetrate the alluvium to the surface, and are confined to the Miocene (Tmb, Tls) and later Tertiary (Tvs) section. The relative, cross-cutting age relations indicates that faults B, C, and D are much older than the Dixie Valley fault system, and may belong with the E-W fault set (Chapter 1).

~~relative~~ thickness of the basalt in section 7 still implies substantial structural thinning, probably along fault C (Figure 7c), and perhaps some formational thinning as well.

Large thickness variations also occur in the Miocene lacustrine ~~rocks~~. Lacustrine ~~rocks~~ in section 18 are a maximum of 200 meters thick, while in section 7 they are a maximum of 330 meters thick. I interpret the ~~discrepancy~~ in ~~lacustrine~~ thicknesses both as structural thinning along faults C and D, and as northeastward ~~formational~~ thickening towards a structural basin in the hanging wall of fault E (Figure 7c-LB).

2.5. RECONSTRUCTING SUBSURFACE GEOLOGY: PROCEDURES

There are two necessary pieces of information that allow the geology of the Dixie Valley basement to be reconstructed. The first is an accurate classification of subsurface stratigraphy and/or tectonostratigraphy. This has been treated at length in Chapter 1, and briefly in this chapter. The second—and the focus of this section—is ~~the~~ knowledge of the locations and attitudes of subsurface faults.

~~As I have shown, surface observations give information about the types and~~ relative ages of subsurface faults. Borehole data gives some information about the locations of faults at various ~~one-dimensional~~ points, and the possible range of orientations ~~that~~ faults ~~can have.~~ Seismic data ~~reveal~~ the two dimensional locations and geometries of faults, and ~~constrains~~ the ages of faults relative to basin-fill. Here, I describe my method of integrating these various sources of information, and demonstrate that ~~proper integration can show~~ the ~~rough~~ three-dimensional geometries of faults and formations.

Procedure for Integrating Surface Observations into Geologic Sections. As shown, there are many detailed surface observations that help to constrain the linework in geologic cross-sections. These observations are applied intrinsically, and to describe their explicit use would be redundant. However, the cross sections must account for, and conform with, three fundamental observations:

1) One large-offset (~~fault~~ RF4) and several small-offset (~~faults~~ RF2, RF4) inactive normal faults are exposed in the footwall. ~~Cross-sections must demonstrate some mechanical reason for the existence of these faults.~~

2) The Dixie Valley fault, or rangefront fault, is the active strand of the Dixie Valley fault system. Cross-sections can not place young, large-offset faults basinward from the rangefront, where surface evidence for these faults is absent.

3) Subsidiary normal faults, that may or may not be active, exist and are permeable in the hanging wall. Cross-sections must ~~demonstrate a mechanical reason for~~ the existence of these faults, and a ~~reason for~~ their ~~being permeable~~.

Procedure for Integrating Borehole Geology into Geologic and Seismic Sections.

Data from boreholes that are considered to ~~be~~ in the plane of section (Figures 3 and 4), ~~are superimposed onto deviated~~ well profiles (Figure 9). ~~Figure 9 shows gamma log and mud log data that have been placed along the three dimensional profiles of boreholes from section 7~~. Once these ~~stacked~~ profiles have been constructed, they can be projected into any two-dimensional, vertical or horizontal plane. In Figure 9, for example, the boreholes ~~in~~ have been projected into ~~an arbitrary~~ vertical plane that strikes parallel to the Dixie Valley fault. Figure 4 shows boreholes from section 18 that have been projected into a horizontal plane representing the valley floor. In Figures 6 and 7, ~~section 18~~ boreholes have been projected into the planes of seismic lines 5 and 101, to provide interpretive constraints. The method allows borehole data to be used as accurately as possible, for cross-section drawing and seismic interpretation.

Control points on the borehole profiles are located exactly in the X, Y, and Z dimensions. Therefore, in addition to providing cross-sectional constraints, borehole data can be used to make structural contour maps (described below).

Figure 9. Example of gamma log (formation log) and drilling fluid (mud log) data that have been superimposed onto deviated profiles of boreholes from section 7. Tick marks to the left of the profiles indicate Lost Circulation (LC) zones, and ticks to the right indicate inflow zones. The three-dimensional profiles have then been projected, in this example, into an arbitrary, vertical, two-dimensional plane ~~that parallels the Dixie Valley fault~~.

Procedure for Integrating Seismic Interpretations into Geologic Cross-Sections. In depth sections, it is a simple matter to project a structure up to the surface, or down to the geothermal reservoir. For example, fault A in Line 5 is very well defined between 1 and 1.5 kilometers depth, but is less clear at 3 kilometers. Therefore, in the interpretation of

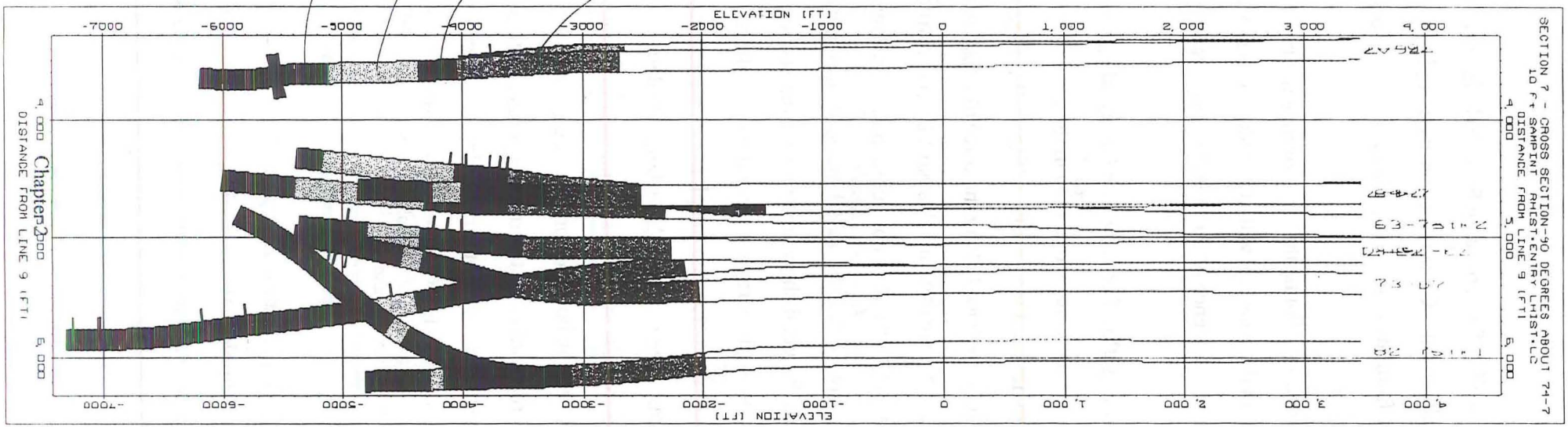

Need a color code -

dotted on

Figure 9. Example of gamma log and mud log data ~~that have been superimposed onto~~ deviated profiles of section 7 boreholes. Tick marks to the left indicate lost-circulation zones, and ticks to the right indicate inflow zones. In this figure, the three-dimensional profiles have been projected into a vertical, two-dimensional plane that pa[illegible] the Dixie Valley fault.

Line 5 (Figure 6c), the lower third of fault B is largely a projection from shallower depths.

A greater problem lies with projecting the faults laterally, into areas where seismic and borehole coverage is relatively sparse. For example, fault-surface images may show apparent dips. Without knowing the true strike of a fault, it would be highly inaccurate to project a planar structure from one section to another. It would be inaccurate, as well, to attempt to correlate faults between seismic profiles based on the semblance of their reflective characters. Three different fault sets, with different orientations (Chapter 1), are known to exist. Without secondary evidence, there is a good chance that a fault correlation—for instance, between Lines 5 and 101—would be wrong.

The problem of lateral fault correlation is dealt with by creating and interpreting structural contour maps (Figure 10a). The maps invoke seismic depth measurements, and secondary evidence, borehole geology, to show the generalized topography along the top of the Miocene basalt. Distinctly steep topographic gradients reveal the rough locations and three-dimensional attitudes of major faults in the subsurface. Therefore, faults can be more soundly projected laterally, between various seismic and geologic sections.

Figure 10a. Structural contour map of the top of the Miocene basalt. Filled circles indicate basalt depths measured from seismic interpretations of lines 5 and 101; triangles indicate depths measured from geothermal boreholes.

The interpretation of structural gradients (Figure 10b) suggests the presence of three different subsurface fault sets: and oldest set (blue), a middle-aged set (green), and a youngest set (red). The faults are labeled to correspond with their counterparts in the seismic sections. The oldest set includes faults C, D, and E. In seismic profiles, these faults do not cut Quaternary alluvium. In addition, the contour map suggests that the blue faults (especially fault D) are cross-cut by fault V, a Quaternary fault. The contour map therefore corroborates the relatively old ages of faults C, D, and E. Because faults C, D, and E belong to the oldest set of Tertiary faults, it is likely that they correlate with the E-W fault set (Chapter 1).

The middle-aged fault set (green) and the youngest set (red) include faults A, B, V, and the Granite/Dixie Valley fault (described below). Faults A and B are shown by seismic line 5 to cut high into the basin. However, these faults do not break the surface

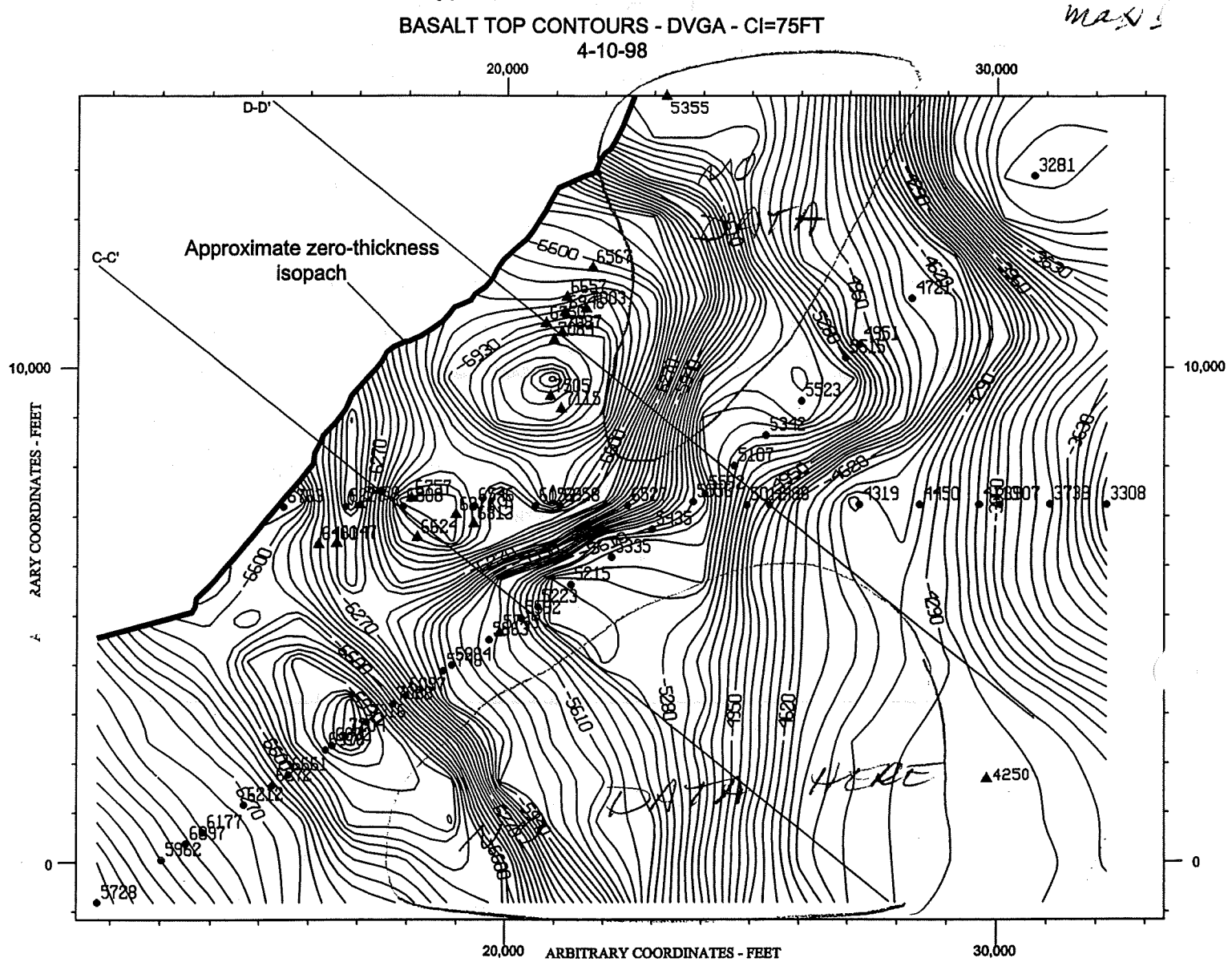

Figure 10a. Structural contour map of the top of the Miocene basalt. Filled circles indicate ~~basalt~~ depths to top of basalt measured from seismic interpretations of lines 5 and 101; filled triangles indicate depths measured from geothermal boreholes.

and are overlain by ~~a maximum of~~ 600 meters of alluvium. Fault V, on the other hand, penetrates the ~~highest~~ Quaternary alluvium (Figure 6B, 6c), and may ~~engender~~ a soil geochemical anomaly (Hinkle, 1995), and a vegetal-spectral anomaly (Nash, 1997) at the surface (Figure 10b). These ~~facts~~ indicate that fault V is a young Quaternary fault and possibly an active fault. The red faults probably correlate with the Dixie Valley fault system, as they are active and young, and have a ~~trend~~ similar to the Dixie Valley fault. The green faults lack a good surface analogue, but may be part of the N-S fault set (Chapter 1).

Figure ~~10b.~~ Structural contour map of the top of the Miocene basalt, as above, showing interpretive locations of large faults (red lines) and smaller faults (blue lines) that displace the top of the Miocene basalt.

2.6. SUBSURFACE CROSS-SECTIONS THROUGH THE GEOTHERMAL RESERVOIR

~~Above~~, I have used ~~direct and indirect observational data~~ borehole logs, surface observations, and seismic profiles ~~to~~ to draw conclusions about subsurface geology. I have also combined the various data, in contour maps, to interpret structural geology where ~~direct observations~~ are ~~completely~~ lacking. Here, I draw on all of these ~~measures,~~ to ~~constrain~~ geologic cross-sections. The geologic sections are based dominantly on stratigraphy from ~~projected~~ borehole ~~profiles, and on~~ faults ~~that are~~ extrapolated ~~downward~~ from the structural contour maps (Figures 10a, 10b). Where possible, ~~the sections invoke~~ surface observations to interpret basement geology at the most poorly understood structural levels.

Compilation and Drafting of Cross Sections. ~~To maintain precision,~~ all borehole and seismic data were manipulated and measured in digital format, using AutoCad (release 14). Cross-sections C-C' and D-D' were also drafted in AutoCad. To show the ~~data origin for~~ each feature in the geologic sections, the linework is color coded. Linework based upon borehole geology is colored red. Linework based upon seismic interpretations and/or structural contour diagrams is dark blue. ~~Black linework is~~ based on observations of exposed geologic relationships in the footwall.

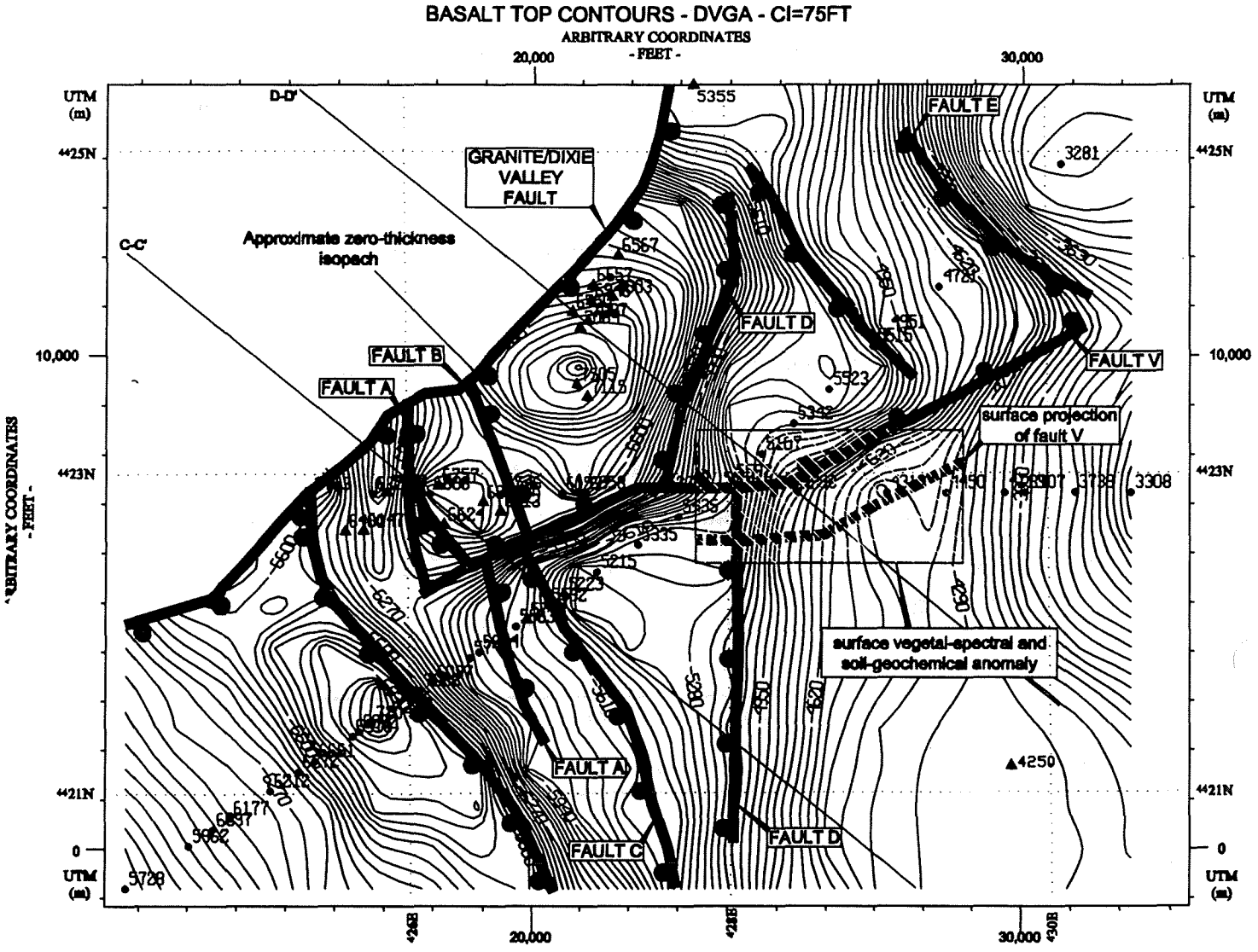

Figure 10b. Structural contour map of the top of the Miocene basalt, as above, showing possible locations and trends of large faults that displace the top of the basalt. Color indicates relative age: blue=oldest, red=youngest. The orientations of the faults agree with the orientations of mapped fault sets in the footwall, and measured fracture sets in geothermal boreholes (Tables 3 and 4). Soil/vegetal anomaly is from Nash (1997).

Elements of Cross-section C-C'. C-C' is the better constrained of the two geologic sections. In addition to four widely-spaced boreholes, ~~structures in C-C' are pinned~~ by ~~the intersections of~~ Line 101 and Line 5.

2.5.1. ~~C-C' Fault~~ Constraints from Section 18 Boreholes

(1a) The Granite fault. A common and predictable ~~horizon~~ in the section 18 boreholes is the structural top of the Cretaceous granite, in the footwall of the Dixie Valley fault. Boreholes ~~that drill~~ through the Dixie Valley fault (SWL-2a, SWL-2b, SWL-1, and SWL-3) penetrate ~~into~~ the granite. From three boreholes, the three-point solution to the structural top of the granite gives the orientation of the top of the granite, ~~herein referred to as~~ the 'Granite fault' (Table 5).

		TOP OF GRANITE	
WELL	*X (arbitrary crds)*	*Y(arbitrary crds)*	*TVD(ft)*
SWL-2a	699893	1895103	7350
SWL-2b	700790	1895350	8200
SWL-3	701700	1896125	~~8675~~
THREE-PT SOL'N, GRANITE FAULT	**→ 032°, 54° SE**	*SURFACE S&D OF DV FAULT*	**→ 034°, 67°SE**

Table 5. Data for a three-point solution to the structural top of the Cretaceous granite (the Granite fault), in the footwall of the Dixie Valley fault, beneath section 18.

The three-point solution indicates that the Granite fault strikes 032°, and dips 54° SE. The strike is exactly parallel with the up-dip, surface trace of the Dixie Valley fault. The dip, however, is thirteen degrees (13°) shallower than surface measurements of the Dixie Valley fault.

As shown in Figure 4, the entire ~~profile of~~ borehole SWL-3 lies within the plane of cross-section C-C'. In C-C', therefore, the Granite fault is ~~drawn according to~~ its calculated dip (Table 5) through the top of the Cretaceous granite in SWL-3 (Figures 11a, 11b). From the SWL-3 tie point, the planar, up-dip projection of the Granite fault intersects the surface 550 meters (1800 ft) southeast (basinward) of the mapped trace of the Dixie Valley fault. This suggests two possibilities:

1) ~~that~~ the Granite fault is the down-dip ~~projection~~ of the Dixie Valley fault, ~~and~~ ~~that the surface~~ geometry ~~of the Dixie Valley fault~~ is highly irregular, ~~Surface~~ ~~measurements of the~~ Dixie Valley fault plane indicate that it dips 67°.

southeastward. To coincide with the mapped dip of the Dixie Valley fault, therefore, the Granite fault would first have to shallow upwards from 54°, and then steepen upwards to 67° at the surface.

2) that the Granite fault is not the Dixie Valley fault, but a subsidiary fault which is parallel to, but basinward of, the Dixie Valley fault. It may be simpler, and more appropriate, to assume that normal faults steepen upwards and become listric downwards (Proffett, 1977; Bally et al., 1981; Wernicke, 1981), and that the fault surface does not have any serious geometric irregularity.

To illustrate the two possible configurations of the Granite fault, C-C' is drawn in two ways. The first model (Figure 11a) shows geometric irregularity along the Dixie Valley fault surface, and concludes that the Granite fault is the down-dip equivalent of the Dixie Valley fault. This model (Figure 11a), allows the Dixie Valley fault to cut at a shallow angle through incompetent Triassic siltstone (Tru) and argillite (Trfc). The fault surface then steepens where it cuts across competent quartzite (Jbr) or marble (Trsp), allowing the fault to correspond with the measured surface dip of the Dixie Valley fault. This model indicates that the Dixie Valley fault has a rheology-dependent, ramp-flat geometry, similar to that of a thrust fault.

Figure 11a. Geologic cross-section C-C', asperity model (see Plate 2 for larger-scale version).

The next model (Figure 11b) shows the surface of the Dixie Valley fault without geometric irregularity, and suggests that the Granite fault is not equivalent with the Dixie Valley fault. In this model, the Granite fault steepens upwards to 67°, to a projected surface trace which lies approximately 850 meters southeast of the Dixie Valley fault. The Dixie Valley fault parallels the Granite fault, and steepens upward to coincide exactly with the Stillwater rangefront. Both faults sole into a regional detachment surface at an elevation of about -2600 meters (-8500 ft).

Figure 11b. Geologic cross-section C-C', listric model (see Plate 2 for larger-scale version).

(1b) Stratigraphic Offset Faults. The position of one fault, fault A, is given by offset of stratigraphic horizons between boreholes SWL-3 and SWL-1. The top of the Miocene basalt (Tmb) in SWL-3 is 186 meters lower than the same horizon in SWL-1. This suggests that the two boreholes are separated by a down-to-the-southeast normal fault.

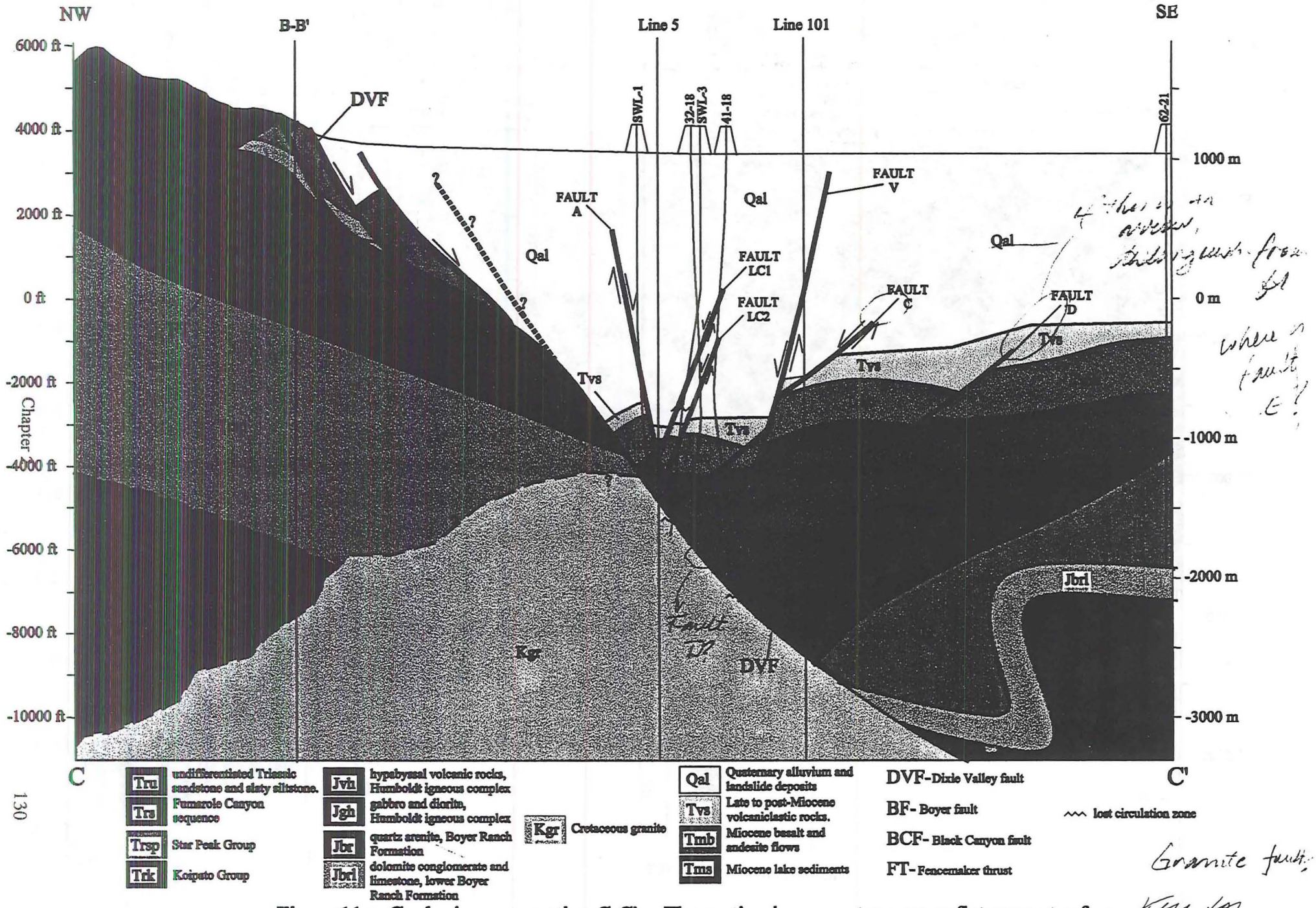

Figure 11a. Geologic cross-section C-C'a. The section incorporates a ramp-flat geometry for the surface of the Dixie Valley fault.

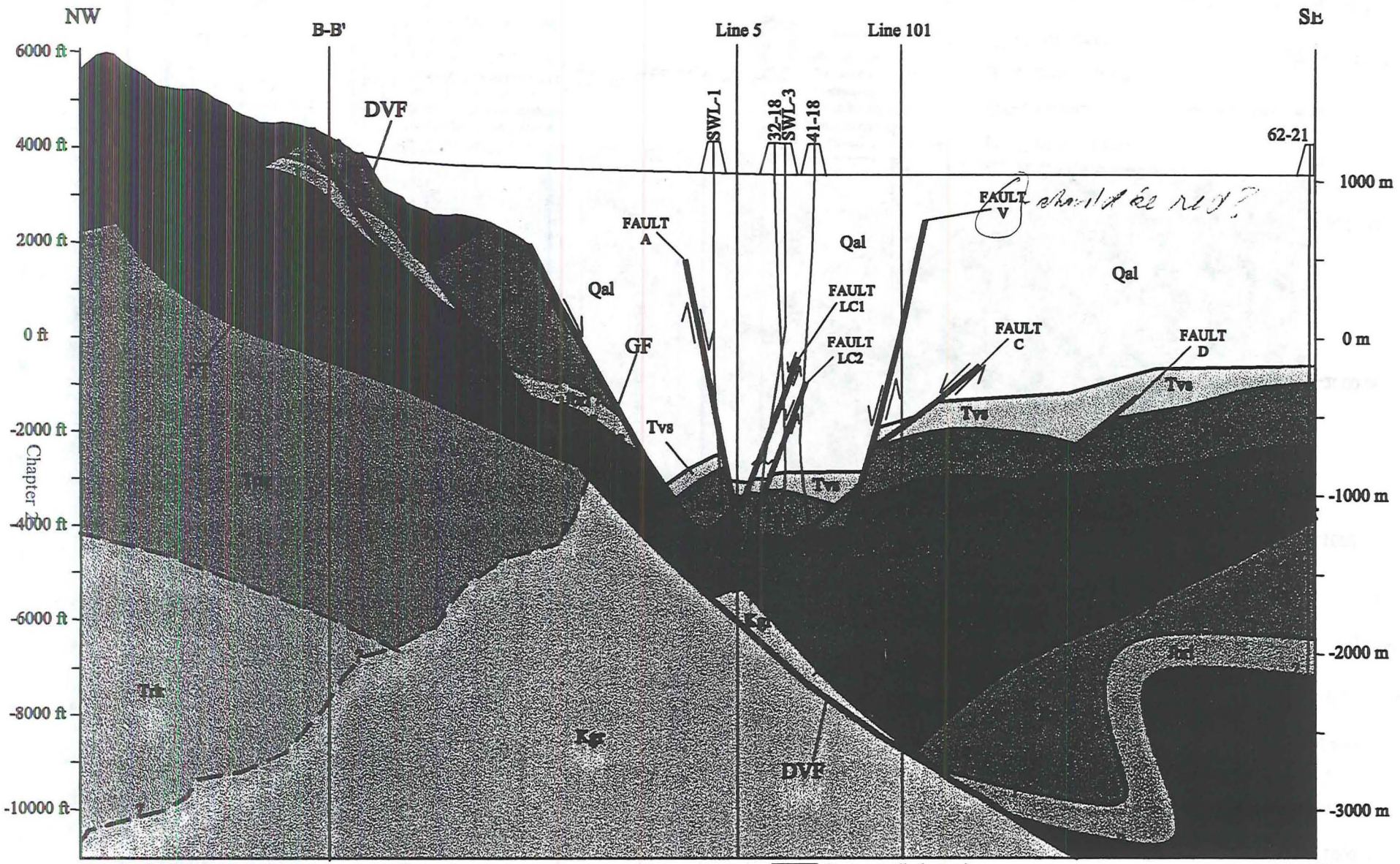

Figure 11b. Geologic cross-section C-C" The section incorporates a listric geometry for the surface of the Dixie Valley fault.

(1c) Lost-Circulation-Zone-Faults. Two faults, LC1 and LC2, are constrained solely by Lost Circulation (LC) zones that occur in well SWL-3. The dip directions of these faults are highly speculative. One or the other, or both, may dip to the SE rather than to the NW. Because permeable faults belong to Dixie Valley system (Hickman and Zoback, 1997), and the Dixie Valley system includes only high-angle faults (Chapter 1), the magnitudes of the dips on LC1 and LC2 are reasonable. Because permeable faults are assumed to strike parallel to the Dixie Valley fault, the faults drawn through these LC zones also reflect a true dip (C-C' is perpendicular to the Dixie Valley fault).

Note that the Granite fault, as well as fault V (discussed below), intersect LC zones at the bottom of SWL-3 and in 41-18. In these cases, the LC zones additionally constrain the orientations of faults that have been identified by other means.

2.5.2. C-C' Fault Constraints from Seismic Images and/or Structural Contour Maps. There are three faults in C-C' that are jointly identified by the seismic reflection images from lines 101 and 5, and the structural contour map of the top of the basalt. These are faults V, C, D, and E.

(2a) Fault V. The existence of fault V is suggested mainly by steep topographic gradients on the top of the Miocene basalt (Figure 10b). Vague traces of the fault V surface and displaced basin strata, in the seismic image of Line 5, also suggests that fault V is real. A third form of evidence, surface soil anomalies, may also verify the existence and age of fault V.

Fault V is a young fault. On the structure contour map (Figure 10a,b), fault V offsets, and therefore post-dates, faults C and D. The Line 5 seismic image shows that fault V offsets the youngest (highest) Quaternary alluvium in the image (Figure 6b, 6c). High soil CO_2 emissions (Hinkle, 1995), and a vegetal-spectral anomaly (Nash, 1997) occur west of section 18 (Figure 10b). The anomalies occur along the surface projection of fault V, and suggest that the tip of fault V is close to the surface. These forms of geological evidence indicate that fault V is a Quaternary to recent fault. Therefore, the fault is shown in cross-section C-C', to offset older faults in the basement, and to penetrate high into the youngest Quaternary alluvium.

(2b) Faults C, D, and E. Faults C, D, and E show up clearly on both seismic images from Line 101 (Figures 7b, 8b). In the reprocessed seismic image (Figure

7b), faults C, D, and E appear to penetrate midway into the Quaternary basin fill. ~~Alternatively~~, the time migrated image of Line 101 (Figure 8) indicates that faults C, D, and E penetrate only the lowest unit of the basin fill (Tvs). ~~Notwithstanding the relative inaccuracy of the interpretations~~, it is clear that faults C, D, and E are older than fault V. Furthermore, the faults are ~~low~~- to moderate-~~angle~~, down-to-the-southeast faults, similar to older Tertiary faults (the E-W set) mapped in the exposed footwall (Chapter 1). From these lines of evidence, it ~~is~~ likely that faults C and D are relatively old faults, perhaps as old as Late Miocene. Therefore, in section C-C', faults C and D are shown to be truncated by fault V, and are overlain by nearly the entire column of basin fill.

2.5.3. ~~C-C' Fault~~ Constraints from Surface Observations. ~~There are only~~ two faults ~~which~~ have been drawn to correspond to surface observations. ~~These are~~ the Dixie Valley fault, and the Boyer fault.

(3a) The Dixie Valley fault and related splays. Surface measurements of the Dixie Valley fault, in at least two ~~sites~~, show that the fault dips about 67° SE. One splay of the fault (Plate 1) dips approximately 45° E. These measurements constrain the shallow ~~geometries~~ of the rangefront faults in section C-C'. The steep, upper part of the Dixie Valley fault is drawn in black, while the lower part of the fault, ~~that~~ is constrained by boreholes (described above), is drawn in red. The footwall splay to the northwest (left) of the Dixie Valley fault (Figure 11a, b) is drawn with a dip that is steeper than 45°, ~~The surface measurement of the fault was taken on a panel of slickensides, that may have been a localized slip surface~~ not representative of the true attitude of the entire fault-surface.

(3b) The Boyer fault. The geometry of the Boyer fault in the deep subsurface is ~~highly~~ speculative. The dip of the Boyer fault, in C-C', is equivalent to the ~~footwall dip, plus~~ an estimate of ~~the degree of~~ hanging wall rollover that occurs along the top of the Miocene basalt. The position of the Boyer fault depends on the thickness of unit Jgh, in the upper plate.

2.5.4. ~~C-C'~~ Stratigraphic Constraints from Section 18 Boreholes. Stratigraphy in the vicinity of boreholes SWL-3, SWL-1, 32-18, and 41-18, is ~~interpreted~~ from ~~formation top data along~~ the well profiles. The stratigraphic tops ~~are~~ projected between boreholes, and forced to honor the faults described above. The stratigraphy in the far-

offset well, 62-21, is very loosely constrained by that well. 62-21 lies approximately 950 meters (3100 ft) from the trace of C-C', but is included in the section because it is the only far-offset control point.

2.5.5. ~~C-C'~~ Stratigraphic ~~Constraints~~ from Seismic Images and/or ~~Basalt~~ Contour Maps. Stratigraphy in the wide area between boreholes 41-18 and 62-21 is constrained by the structural contour map of the top of the basalt (Figure 9a). The ~~profile of the~~ top of the basalt was taken directly from the structural contour map, and then modified to emphasize fault terminations. The geometry of ~~the top of~~ the underlying lacustrine section ~~conforms to the basalt top profile~~, as does the geometry along the bottom of the section. The lacustrine rocks pinch out ~~at the greatest possible~~ southeastern ~~extent~~, because well 65-18 does not penetrate the lacustrine section.

2.5.6. ~~C-C'~~ Stratigraphic ~~Constraints~~ from Surface Observations. Surface constraints are incorporated into C-C' to show the possible ~~stratigraphic~~ geometry of the deepest Mesozoic units. The contacts between Mesozoic rocks are probably ~~rugged~~, but ~~are smoothly drawn to avoid complexity~~. The thicknesses of the units are ~~better~~ known, however. Well 41-18 penetrates the lower ~~boundary~~ of hypabyssal volcanic rocks (Jvh), that are associated with the Humboldt igneous complex. The maximum thickness of Jvh, in cross-section, must equal the distance between the tie point in 41-18 and the ~~lower~~ ~~boundary~~ of the Tertiary lacustrine section (about 655 meters). This thickness is maintained near the wells, but ~~gradually decreases~~ to the southeast (right) of 41-18, ~~in order~~ to meet the minimum thickness constraints provided by well 62-21 (about 425 meters). Note that the ~~minimum, up-dip footwall~~ thickness of Jvh is 264 meters. The ~~great inconsistency in minimum~~ thicknesses may ~~be the~~ result ~~of~~ erosion of Jvh in the footwall ~~over a long period of exposure~~, or ~~perhaps due to my~~ misinterpretation of the Tmb/Jvh contact in 62-21.

The maximum thickness of gabbroic rocks (Jgh) beneath unit Jvh is ~~constrained completely by~~ surface exposures. The ~~up-dip~~ thickness of Jgh in the ~~footwall~~ is approximately ~~782~~ 780 meters. This thickness ~~is~~ has been extrapolated to the subsurface where unit Jgh ~~meets~~ has a cut-off along the Dixie Valley fault, but then decreases southeastward to zero at well 62-21. The lower ~~boundary~~ contact of unit Jgh, as demonstrated ~~in~~ by surface ~~footwall~~ exposures, is the Boyer fault, so that the ~~position~~ depth to of the Boyer fault ~~is~~ depend~~ent~~s on the thickness of unit Jgh.

The most speculative ~~geometries in~~ C-C' ~~occur in~~ the lowest part of the Mesozoic section, where the Boyer Ranch ~~f~~ormation (Jbr, Jbrl) and ~~sub-adjacent~~ sandstones and slaty siltstones (Tru) are shown to be megascopically folded. The thicknesses of these units are partially constrained by well 62-21, but the fold geometries ~~are~~ unconstrained. The presence of large, subsurface folds is ~~assured~~, however, since the same units are strongly deformed into megascopic, west vergent F2 folds at the surface (Chapter 1).

Elements of Cross-Section D-D'. ~~Point controls on~~ D-D' ~~are~~ less well ~~distributed~~ than ~~the controls on~~ C-C'. Boreholes along D-D' are ~~narrowly~~ spaced, and lines 5 and 101 intersect D-D' at nearly a common point. Therefore, D-D' is more of an interpretive section than C-C'. ~~Furthermore,~~ many of the geological and geophysical constraints in D-D' are the same as those outlined for C-C', so in many cases the reader will be referred to previous discussion.

2.5.7. ~~D-D'~~ Fault Constraints from Section 7 Boreholes

(7a) The Gabbro fault. The majority of wells in section 7 terminate within gabbroic rocks of the Humboldt igneous complex. These wells are production wells that tap permeable fractures within the gabbro. Boreholes 74-7, 63-7sidetrack2, and 84-7 each intersect a single fracture within their respective sections of gabbro. In each case, the fracture is similar in width and depth, and is the only large, producing structure in the column. This evidence suggests that the wells intersect the same fracture, herein referred to as the 'Gabbro fault'.

Boreholes 74-7, 63-7 sidetrack2, and 84-7 ~~supply information for a~~ three-point solution ~~to the top of~~ the Gabbro fault (~~Table 6~~).

		TOP OF PRODUCING FRACTURE	
WELL	*X (arbitrary crds, ft)*	*Y(arbitrary crds, ft)*	*elevation(ft)*
74-7	704591	1899061	-5224
63-7stk2	704867	1899130	-5398
84-7	704465	1899515	-4651
THREE-PT SOL'N-GABBRO FAULT	**→ 049°, 53° SE**	*SURFACE S&D OF DV FAULT*	**→ 034°, 67°SE**

Table 6. Data for a three-point solution to the structural top of the producing fracture (the Gabbro fault) in each of the named wells.

The three point solution indicates that the Gabbro fault strikes ~~032°~~ 044°, and dips ~~54°~~ 53° SE. The strike is sub-parallel to the ~~up-dip~~ surface trace of the Dixie Valley fault, while the dip is fourteen degrees (14°) shallower.

As shown in Figure 3, ~~the entire profile of~~ borehole 84-7 (a vertical borehole) lies almost directly within the plane of cross-section D-D'. In D-D', therefore, the Gabbro fault is drawn according to its calculated dip (Table 6) through the producing fracture that lies 75 meters above the ~~terminus~~ bottom of borehole 84-7 (Figure 12; Plate 2). From the tie point in 84-7, the planar, up-dip projection of the Gabbro fault intersects the surface 360 meters (1200 ft) southeast (basinward) of the mapped trace of the Dixie Valley fault. These relations suggest ~~possible~~ a fault geometries ~~that are~~ similar to ~~those~~ that of the Granite fault (page 26). In short, the Gabbro fault may be the down-dip ~~equivalent~~ continuation of the Dixie Valley fault (implying the existence of a fault-surface asperity); ~~or~~ alternatively, the Gabbro fault may be a separate fault ~~(implying listric fault geometry)~~.

The two models ~~represented by~~ for C-C' (Figures 11a, 11b) illustrate the two possible fault ~~surface~~ geometries ~~as if they were mutually exclusive~~. Section D-D' presents the geometries ~~in yet~~ a third ~~fashion~~ way, by incorporating both an asperity on the Dixie Valley fault surface, and a listric ~~fault surface~~ geometry for the Gabbro fault. This model is most appropriate ~~in~~ for explaining the observed properties of the Dixie Valley fault system, especially the configuration of subsidiary faults. The implications of the combined model are treated in detail below, in the discussion section (section 2.8).

(7b) ~~Stratigraphic-Offset~~ Small displacement Faults. ~~Stratigraphic offsets~~ The top of the Miocene basalt (Tmb), between boreholes 74-7, 63-7sidetrack2, and 84-7, ~~apparently do not exist~~ shows no offsets. However, the Miocene lacustrine section, beneath the basalt is displaced, and suggests that a down-to-the-southeast fault must come between borehole 84-7 and boreholes 63-7 sidetrack2 and 74-7. Is this shown?

(7c) Lost-Circulation-Zone-Faults. Two faults, LC3 and LC4, are constrained solely by Lost Circulation (LC) zones ~~that occur~~ in wells 84-7 and 63-7. The dip directions of these faults are again ~~highly~~ speculative (see faults LC1 and LC2, page 27). Fault LC3 may be responsible for the apparent down-to-the-southeast stratigraphic offset of the lacustrine section, mentioned above.

2.5.8. ~~D-D' Fault~~ Constraints from Seismic Images and/or Structural Contour Maps. ~~There are~~ two faults in D-D' ~~that~~ are ~~jointly constrained by the~~ seismic reflection images ~~from~~ lines 101 and 5, and the structural contour map of the top of the basalt. These are fault V and fault D.

(2a) Fault V. Evidence for the existence and relative age of fault V was presented in the previous discussion of cross-section C-C' (page 27). In D-D', the same evidence is assumed to apply. ~~In contrast with C-C',~~ cross-section D-D' ~~dissects~~ the soil-geochemical and vegetal-spectral anomaly of Hinkle (1995) and Nash (1997) that ~~may~~ be associated with fault V. The lateral extent of the anomaly is therefore shown at the top of the Quaternary basin-fill (Figure 12).

The apparent dip of fault V is slightly greater than ~~the~~ dip ~~along the same fault~~ in C-C', because D-D' is less oblique to the strike of fault V. In addition, the ~~total vertical~~ displacement along fault V, in section D-D', is greater than the displacement along the same fault in section C-C'. The discrepancy is caused by ~~my~~ forcing ~~of~~ stratigraphic markers to correspond with seismic interpretations. At the latitude of D-D', seismic lines 101 and 5 are very close together, ~~to either~~ side of fault V. In my attempt to reconcile the interpretations, ~~the~~ inconsistencies between the seismic interpretations have become exaggerated vertically. The estimate of total displacement along fault V ~~is~~ therefore ~~a~~ range between 330 meters (C-C') and 460 meters (D-D').

(2b) Fault D. ~~Again,~~ evidence for the existence and relative age of fault D was presented in the ~~previous~~ discussion of cross-section C-C' (page 28). In D-D', the same evidence is assumed to apply. The difference between the two sections is that D-D' intersects fault D in the ~~footwall~~ of fault V, and at nearly a right angle. As a result, the dip of fault D is greater than ~~its dip~~ in section C-C'. The displacement along fault D, as shown by structural ~~topographic gradients~~ (Figure 9b), increases from south to north. As a result, D-D' shows a ~~total~~ vertical displacement of approximately 550 meters, while C-C' shows only 240 meters of ~~throw~~ along the same fault.

2.5.9. ~~D-D'~~ Fault Constraints from Surface Observations. Faults in D-D' that are constrained by surface observations are ~~entirely~~ the same as those in C-C', except for the Boyer fault (see the preceding discussion of the Dixie Valley fault and related splays, page 28). The position of the Boyer fault is constrained in the subsurface by ~~up-dip~~ stratigraphic thickness of unit Jgh (described below, section 2.5.12).

2.5.10. D-D' Stratigraphic ~~Constraints~~ from Section 7 Boreholes. The stratigraphy in the vicinity of boreholes 74-7, 84-7, and 63-7sidetrack2, is interpreted from ~~formation-top data along the~~ well profiles. As with C-C', the stratigraphic tops are projected between boreholes, and forced to honor known or hypothesized faults. The stratigraphy in the far-offset well, 62-21, is only loosely constrained by that well. 62-21 lies approximately 520 meters (1700 ft) from the trace of D-D', but is included in section because it is the only ~~far-offset~~ control point.

2.5.11. ~~D-D'~~ Stratigraphic ~~Constraints~~ from Seismic Images and/or Structural Contour Maps. Stratigraphic geometry, in the wide area between boreholes 63-7stk2 and 62-21, is ~~constrained by~~ the structural contour map of the top of the basalt (Figure 9a). The ~~profile of the~~ top of the basalt was taken directly from the structural contour map, then modified both to emphasize fault terminations, and to conform with ~~constraints offered by~~ seismic interpretations. The geometry of the top of the underlying lacustrine section conforms with the basalt-top profile, as does the geometry ~~along the bottom of the~~ section. The lacustrine rocks do not pinch out to the southeast, even though well 65-18 does not penetrate the lacustrine section. Evidence from section 7 boreholes, and seismic line 101, indicates that the lacustrine rocks increase in thickness to the northwest. In D-D', I have attempted to ~~demonstrate~~ the northwestward thickness variation as a contrast with C-C'.

2.5.12. ~~D-D'~~ Stratigraphic ~~Constraints~~ from Surface Observations. Surface constraints ~~in~~ D-D' are slightly different from those in section C-C', owing to ~~the~~ variations in mapped thicknesses of ~~the footwall~~ units. Hypabyssal volcanic rocks (Jvh) are absent in the section 7 wells. This observation is borne out by ~~up-dip~~ exposures in the footwall of the Dixie Valley fault (Plate 1). All three of the wells in D-D' terminate in gabbro (Jgh) ~~associated with~~ the Humboldt igneous complex. The ~~up-dip~~ thickness of Jgh in the ~~footwall~~ is approximately 950 meters. This figure represents a minimum thickness, because the upper surface of the gabbro, in the ~~footwall~~, is an erosional surface. The ~~footwall~~ thickness of 950 meters ~~is~~ applied to Jgh in the subsurface, and ~~is~~ measured ~~structurally~~ downwards from the ~~bottom~~ of the lacustrine rocks. Since the Boyer fault is known to ~~subtend~~ unit Jgh in the footwall, the thickness of unit Jgh in the ~~hanging wall~~ constrains the ~~subsurface~~ geometry of the Boyer fault. ~~In other words, the Boyer fault delineates the minimum thickness of unit Jgh at any given point.~~

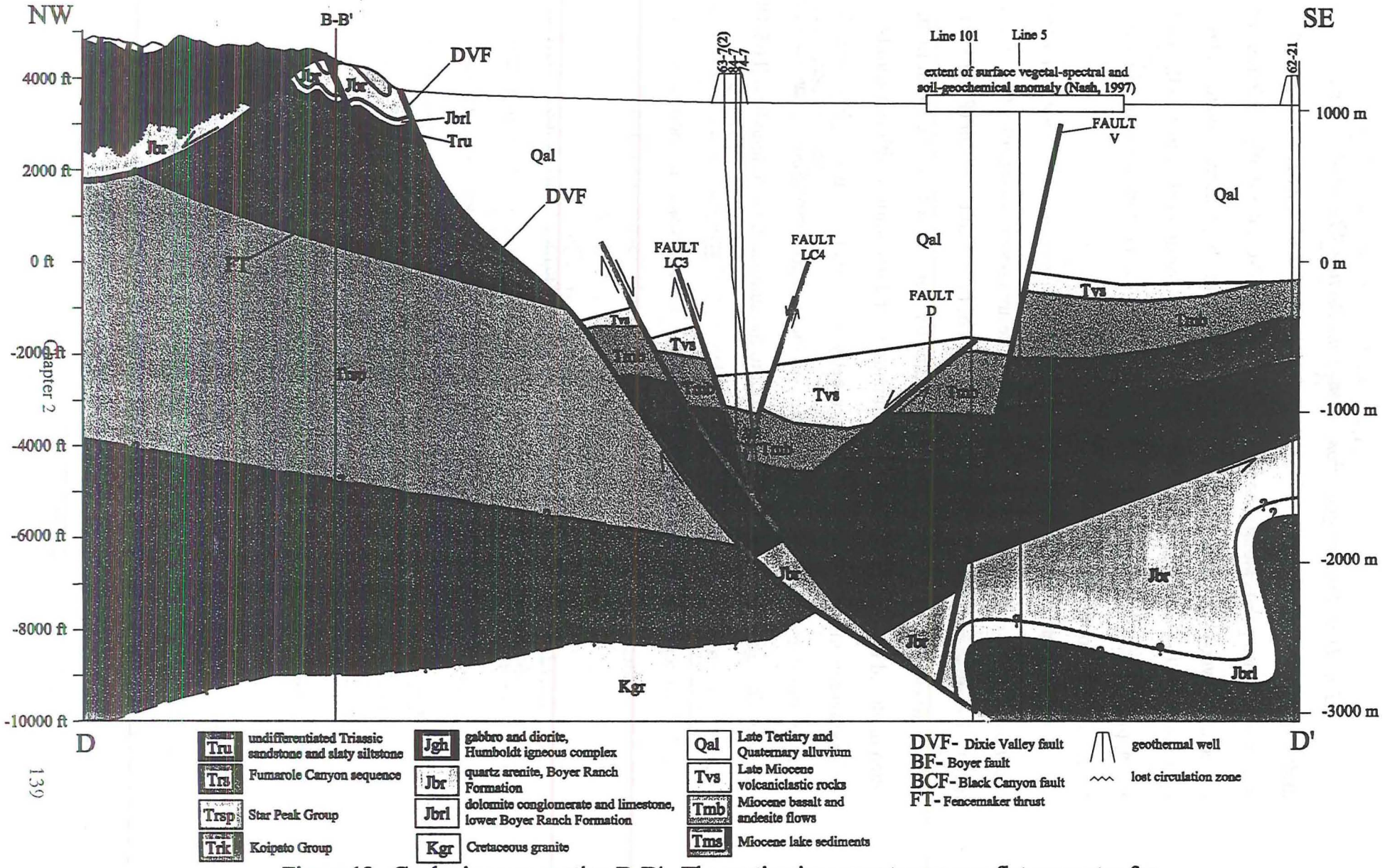

Figure 12. Geologic cross-section D-D'. The section incorporates a ramp-flat geometry for the surface of the Dixie Valley fa[illegible] and listric geometries for the subsidiary faults.

Unit Jgh ~~narrows~~ to 425 meters in well 62-21, in contrast with section C-C', where Jgh is absent in 62-21. The ~~obvious source of error~~ between the two geologic cross-sections is my interpretation of the lithologic/mud log from borehole 62-21. The log indicates that a ~~large~~ section of mafic rocks exist. However, I was unable to determine if the section was Jvh or Jgh, or some other facies of the Humboldt igneous complex, because I did not obtain the well cuttings for a first-hand investigation.

As in section C-C', the subsurface fold ~~geometries~~ in the Boyer Ranch Formation (Jbr) and underlying ~~undifferentiated~~ sandstone and slaty siltstone (Tru) are ~~highly~~ speculative in section D-D'. See page 30 for the treatment of these folds.

Figure 12. Geologic cross-section D-D' (see Plate 2 for larger-scale version).

2.7. GEOLOGIC HISTORY OF THE DIXIE VALLEY BASIN, BENEATH THE DIXIE VALLEY GEOTHERMAL AREA

Geologic relationships within the uplifted and down-dropped blocks of the Dixie Valley fault, establish a loose order of tectonic events. These events were responsible for the development of Dixie Valley as a fault-controlled basin.

The oldest episode of faulting—represented by the E-W fault set (D_{4a})—post-dates regional basaltic volcanism and dike intrusion that occurred before ≈14.5 ma (Dilek, personal communication). The E-W fault set includes a series of west- to west-northwest trending, down-to-the-southeast normal faults in the Dixie Valley footwall (e.g. the Black Canyon fault), and a series of northwest- to north-trending down-to-the-southeast normal faults in the hanging wall. The difference in trend, between fault blocks, may result from reorientation of early structures by later faulting. Tertiary lacustrine rocks may have formed in tectonic basins that were controlled by the E-W fault set, and post-14.5-Ma volcanism may have occurred along with or after displacement on the E-W faults. The E-W faults pre-date the deposition of late Tertiary and Quaternary alluvium, but probably controlled localized deposition of the earliest Tertiary basin fill (unit Tvs, figures 11 and 12)).

The Boyer fault operated with or after displacement on the E-W fault set. Although it is a major structure along the Stillwater escarpment, and although it must exist in the Dixie Valley basement, its effect on the vertical tectonics of Dixie Valley are

unknown. It may have been a shear zone into which the E-W fault sets were rooted (Chapter 1).

The Dixie Valley fault system, and a series of north-to-south-trending faults (N-S set, Chapter 1), developed after displacement along the E-W and Boyer faults ceased. The Dixie Valley fault system includes the Dixie Valley fault, and a series of northwest trending, large- to small-offset normal faults. The faults generally displace basement and alluvium down-to-the-southeast, but antithetic faulting does occur. The N-S faults appear to be sub-vertical faults with down-to-the-east displacement, and may either pre-date or approximate the age of the Dixie Valley fault system.

2.8. DISCUSSION

Development of the Dixie Valley Fault System. Geologic cross-sections C-C' and D-D' s have been constructed around three different fault models. The fundamental difference between each model is the change in fault-surface geometry, of the active, rangefront fault (Dixie Valley fault). Any one of these fault models can be manipulated to fit observational and interpretive geologic data, as the cross-sections demonstrate. However, each fault-surface geometry alters the nature of conclusions that can be drawn, from cross-sections, regarding fault development, offset, and permeability.

2.8.1. Basic Conclusions from Fault Models. The first model, Model A (Figure 11a), gives a ramp-flat geometry to the surface of the Dixie Valley fault. In this model, the Dixie Valley fault is responsible for 100% of approximately 3.9 kilometers of total vertical offset, between the hanging wall and footwall. Model A requires that faulting in the Dixie Valley system evolved in steps toward the center of the basin. Model A also suggests that geothermal fluids, at the level of the geothermal production zone, are mobile because of permeability along the active rangefront fault, or Dixie Valley fault.

The next model, Model B (Figure 11b), gives the Dixie Valley fault a smooth, upward-steepening, listric plane. In this model, the Dixie Valley fault is responsible for 43% of 3.9 kilometers of total vertical offset. Model B suggests that faulting in the Dixie Valley system evolved in steps toward the Stillwater Range. In addition, Model B indicates that fluid mobility at production zone levels is the result of permeability along an inactive strand of the Dixie Valley fault system, the Granite fault.

exposed vertical displacement, as measured from map relations along the same fault (Chapter 1). In domain 4a (Chapter 1), the combined minimum displacement across faults RF2, RF3, and RF4 is at least 400 meters. Therefore, the minimum displacement on fault RF4 must be less than 400 meters. Figure 13 also provides a mechanical reason—a structural flat—for the locking and consequent basinward propagation of the active strand of the fault system.

The progression of events shown in Figure 13 also explain permeability along hanging wall faults, other than along the Dixie Valley fault. It suggests that the fault that doubles as either the Gabbro or Granite fault began to move synthetically with the Dixie Valley fault, around time 4 (Figure 13, TIME 4). At the same time, fault V incurred antithetic displacement. The two faults operated syn-kinematically with the Dixie Valley fault from that time forward, and may be active in the modern setting. This may explain why the Gabbro fault, in particular, is permeable, and why fault V is close enough to the surface to engender a chemical anomaly. Both fault V and the Gabbro/Granite fault are characterized, however, by low displacement over a large time span. Their expression at the surface appears as a subdued topographic low, therefore, instead of as an escarpment or a series of palaeoseismic ruptures. This topographic low channels the highstand playa (Figure 14) as well as the youngest alluvial surface (Qy). Therefore, any palaeo-ruptures, associated with the two minor faults, may have been eradicated by sub-aqueous erosion and rapid alluvial aggradation.

In conclusion, the structural geometries in Figure 13 suggests that Model C is most applicable toward the geologic setting of the geothermal reservoir. The development of the Dixie Valley fault system seems to have been profoundly affected by a ramp-flat geometry along the Dixie Valley fault-surface. A fault-flat is really the only mechanism by which way large fault-splays can be abandoned and uplifted. Fluid mobility, along the subsidiary, listric faults in the hanging wall, is also affected by the ramp flat geometry. The Gabbro fault, for example, is permeable because it is active; but, it is active because it is a late-stage mechanical effect of the last time that the hanging wall of the Dixie Valley fault was temporarily locked against the lower corner of the footwall flat (Figure 13, TIME 4).

Geologic cross-section D-D' gives the most accurate representation of recent subsurface faulting, although is relatively poorly constrained overall. Section C-C'

(Figures 11a,11b) is the best constrained geologic section, but the Dixie Valley and related faults in C-C' may actually resemble the same faults as they are drawn in D-D'. Specifically, the Granite fault should remain a separate fault (as in Figure 11b), while the Dixie Valley fault should retain the ramp-flat geometry (as in Figure 11a).

Structural Controls on Fluid Transport and Permeability.

2.6.2. Inflow Zones, Lost Circulation Zones, and Rangefront Parallel Faults. Hickman and Barton (1997) point out that permeability along extensional faults is a function of the relative orientation of least horizontal stress, S_{hmin} to the dip direction of the faults within that stress regime. Their studies, in Dixie Valley, show that rangefront-parallel faults, which dip parallel to the orientation of S_{hmin}, are both permeable and critically stressed for failure. Their studies also suggest that transverse faults, which do not dip parallel to S_{hmin}, are either semi-permeable or impermeable.

As I and others (Barton, 1996) have described it, the Dixie Valley basement consists of numerous fractures of greatly varied orientations. Barton (1996) uses inflow zones (measured by spinner logs) to connect high fracture permeability with fracture orientation. Lost circulation zones also play an important part in the hydrodynamics of the reservoir, particularly as fluid reinjection points or recharge conduits. Barton (1996) does not specifically describe the stresses or fracture orientations associated with lost circulation zones. However, it is likely that LC zones obey the same permeability rules that apply to inflow zones.

This study has shown that the Gabbro fault, the Granite fault, and fault V are young faults, that strike parallel to or to within approximately thirty degrees (30°) of the surface trace of the Dixie Valley fault. Furthermore, the investigations have shown that these faults are permeable. In contrast, there has been no evidence or suggestion that significant permeability (secondary permeability ?) exists along other faults (E-W faults), that are dissimilar, in their strike and dip, to faults within the Dixie Valley system. Therefore, the conclusions reached by this study corroborate the findings of Hickman, Barton, and Zoback (1996, 1997), but do not preclude the possibility that secondary permeability exists along faults C, D, and E, and other faults belonging to the E-W set.

2.6.3. Fault Development and Spacing, and the Relation to Subsurface Permeability. The geologic cross-sections suggest that the Dixie Valley fault surface follows a ramp-flat geometry. Furthermore, the sections conclude that a flat, through the incompetent Triassic units, influenced the development of major and subsidiary active faulting. However, these fault-mechanical considerations do not readily suggest good reasons for high fluid permeability at the level of the geothermal reservoir. In a simplistic view, a great number of favorably oriented faults may translate to higher overall permeability. If the ramp-flat-related fault mechanics, that we have been discussing, result in the development of many, closely spaced faults, then perhaps the permeability controls are obvious. Certainly, the chances of drilling into a fault get better with an increase in the number of faults.

This simplistic explanation does not proceed far enough to explain the distribution of permeability, laterally, from one end of the geothermal field to the other. In addition, the spacing of faults does not explain, satisfactorily, why the Dixie Valley geothermal area exists where it does. Indeed, to understand the broader controls on permeability is to possess the greater knowledge. For, regarding the successful future development of resources, one should seek foremost to understand what controls the spacing of faults, rather than the quantity of that spacing.

The Stillwater escarpment contains a number of fault-splays, that stem from or are truncated by the Dixie Valley fault. Some of these fault-splays are too small to map. Others—faults RF2, RF3, RF4, RF5, and RF6—are continuous along the rangefront for up to several kilometers (Plate 1). Both the locations and along-strike distances of these splays, exactly coincide with the surface exposure of incompetent Triassic marine rocks (Tru and Trfc). Fault RF6 begins at the farthest southwestern outcrop of unit Tru. Toward the northwest, the splays become more numerous, and cut with increasing distance into the rangefront. The northern splay, fault RF5, rejoins the Dixie Valley fault just north of the apparent zero-thickness isopach (the Fencemaker thrust) of the Fumarole Canyon sequence (Trfc); and, fault RF4 rejoins the rangefront at a position *exactly* coincident with the Fencemaker thrust (Plate 1). The splays thus form a giant scallop, in which faults are numerous and widely spaced at the center of the scallop, and die out at the edges.

Up to this point, surface observations have been used to substantiate and interpret subsurface structural geology. Now that certain models and hypotheses have been presented, let us use those models in reverse, to shed light on one aspect of the Stillwater escarpment. A basic deduction from Dahlstrom's rules, is that the relative angles, between ramps and flats, depend on the relative competency of the host rocks. For example, the angle between a given ramp and flat is more tightly appresed when the ramp-host is highly competent, and the flat-host is highly incompetent. I suggest that nature of the ramp-flat geometry (of the Dixie Valley fault) depends not only upon the position of incompetent Triassic rocks, but also on the condition that strong, Humboldt complex rocks overlie the Triassic rocks. Where gabbroic and dioritic rocks of the Humboldt igneous complex exist in the footwall, the Dixie Valley fault must develop a ramp. When the Dixie Valley fault intersects incompetent Triassic rocks in the footwall, the fault must develop a flat.

Observational supporting evidence for these suggestions is prevalent in the Stillwater rangefront. Fault-splays develop, according to the model in Figure 13, in proximity to flat geometries. Therefore, splays directly above the producing geothermal field (Plate 1) may delineate a partially uplifted and partially buried fault-flat. Figure 13 suggests that the uplifted portion of the flat is the exposed face of unit Trfc (Figure 13, PRESENT), and that the buried part of the flat is not far beneath the modern valley floor.

Similarly, in accordance with the model in Figure 13, splays die out in proximity to ramps. Therefore, in the Stillwater rangefront, a fault-ramp may extend southwestward from the junction between the Boyer and Dixie Valley faults (Plate 1). That junction marks the southwestern-most extent of exposed incompetent rocks (Tru) and the terminus of major fault-splay formation (RF6 fault). As well, a fault-ramp may extend northwest from the junction of fault RF4 and the Fencemaker thrust (Plate 1). That junction marks the northeastern-most extent of pelitic, incompetent Triassic rocks (Trfc) and the terminus of major fault-splay development (RF4 fault).

The fault-ramp that extends northeastward from the Fencemaker thrust, may be slightly different from the ramp that extends southwestward from the Boyer/DV fault junction. To the northeast, the Dixie Valley fault surface may become less convoluted, or nearly planar, because incompetent Triassic rocks (Trfc) do not exist in the footwall of the Dixie Valley fault. To the southwest, however, Triassic rocks are present, beneath the

Humboldt igneous complex, and tectono-stratigraphic competence contrasts are preserved in the footwall. Southwestward form the Boyer/DV junction, therefore, the buried surface of the Dixie Valley fault maintains an angular ramp-flat conversion.

2.9. CONCLUSIONS

In the Dixie Valley geothermal area, surface geology and subsurface geology correlate quite well. Mapped surface fault-sets recur, with similar orientation and relative age, in the Dixie Valley basement. Also, the thickness of and presence of lithologic units—especially Jvh and Jgh—are mirrored across the Dixie Valley fault. The correlation of these structures and strata allow the geometry of the Dixie Valley fault to be modeled in geologic cross-sections. The models suggest that the surface of the Dixie Valley fault follows a ramp-flat geometry. The flat(s) occur through incompetent Triassic pelitic rocks, while ramps form across competent rocks of the Humboldt igneous complex, Boyer Ranch Formation, and Star Peak group.

The ramp-flat geometry of the Dixie Valley fault-surface directly influences the development of major and minor faults, some of which are permeable. The number and spacing of these permeable faults may ultimately determine total subsurface permeability over a given area. Tectono-stratigraphic competence contrasts in the footwall, created fault surface irregularities. These irregularities ultimately influence the evolution, distribution and, indeed, the existence of permeable faults. The along-strike position of a fault-surface irregularity may be identified by exposed geology, though the exact geometry may not be obvious. However, the very existence of such an irregularity suggests that total subsurface permeability, over a given area, in the direction down-dip from the surface fault trace, is relatively high.

The obvious conclusion from this is that future drilling in the current, producing geothermal field should concentrate on the window between the Fencemaker thrust, and the juncture between the Boyer and Dixie Valley faults. Southwestward from this window, drilling should target areas above, and basinward of, fault-flats that occur along the Dixie Valley fault surface. Northeast of the window, however, it is likely that total subsurface permeability decreases, because severe fault surface irregularity is absent.

Finally, regional geothermal drilling programs should seek to understand the surface geometries of faults that are drilling targets.

REFERENCES

Bally, A.W., Bernoulli, D., Davis, G.A., and Montadert, L., Listric Normal Faults, *Oceanologica Acta, v.4, supplement, p.87-101.*

Barton, C., Hickman, S., 1996, Fracture Permeability and its Relationship to In-situ Stress in the Dixie Valley, Nevada, Geothermal Reservoir, *Proceedings of the eighth international symposium of the continental crust through drilling.*

Bell, J., Katzer, T., 1990, Timing of Late Quaternary faulting in the 1954 Dixie Valley earthquake area, central Nevada, *Geology, v.18, p. 622-625.*

Burke, D.B., 1966, An Aerial Photograph Survey of Dixie Valley, Nevada, *M.S. Thesis, Stanford University.*

_____., 1973, Reinterpretation of the Tobin Thrust; Pre-Tertiary Geology of the Southern Tobin Range, Pershing County, Nevada, *Ph.D. Thesis, Stanford University.*

Burke, D.B., and Silberling, N.J., 1974, The Auld Lang Syne Group of Late Triassic and Jurassic(?) Age, North-Central Nevada, *U.S.G.S. Bulletin 1394E, 14p.*

Busby-Spera, Cathy J., 1988, Speculative tectonic model for the early Mesozoic arc of the southwest Cordilleran United States, *Geology, v.16, p.1121-1125.*

Caine, Jonathan S., 1996, Fault zone architecture and permeability structure, *Geology, v.24, no.11, p.1025.*

Caskey, S.J., Wesnousky, S.G., Zhang, P., and Slemmons, D.B., 1996, Surface Faulting of the 1954 Fairview Peak (Ms=7.2) and Dixie Valley (Ms=6.9) Earthquakes, Central Nevada, *Bull. Seism. Soc. Am., v.86, no.3, pp.761-787.*

Dilek, Y.M., Moores, E.M., 1995, Geology of the Humboldt igneous complex, Nevada, and tectonic implications for the Jurassic magmatism in the Cordilleran Orogen, in *Miller, D.M.;.B., Cathy, ed., Jurassic magmatism and tectonics of the North American Cordillera Geological Society of America Special Paper, v.299, p.229-248): Geological Society of America (GSA), Boulder, CO, United States.*

Dilek, Y.M., Moores, E.M., Humboldt Complex, Nevada, as an Allochthonous Fragment of a Jurassic Arc Terrane, *Geological Society of America, Abstracts with programs, p.A192, 1991.*

Dilek, Y.M., Moores, E.M., and Erskine, M.C., 1988, Ophiolitic Thrust Nappes in Western Nevada: Implications for the Cordilleran Orogen, *Journal of the Geological Society of London, v.145, p. 969-975.*

Duffield, W.A., Sass, J.H., and Sorey, M.L., 1994, Tapping the Earth's natural heat: *U.S.-Geological-Survey-Circular .*

Dula, William F., 1991, Geometric Models of Listric Normal Faults and Rollover Folds, *AAPG Bulletin, v.75, no. 10, p.1609-1625.*

Elison, Mark, 1987, Structural geology and tectonic implications of the East Range, Nevada; *PhD thesis, Northwestern University. Evanston, IL, United States. Pages: 321.*

Elison, Mark, 1989, Structural development during flysch basin collapse: The Fencemaker allochthon, East Range, Nevada; *Journal of Structural Geology.11; 5, Pages 523-538.*

Elison, Mark, 1991, Intracontinental contraction in western North America: Continuity and episodicity, *Geological Soc. Am. Bull., v.103, p. 1226-1238.*

Flynn, T., Buchanan, P.K., 1993; Pleistocene origin of geothermal fluids in the Great Basin, western United States: *Resource Geology Special Issue, no. 16, p.60-68*

Fonseca, J., 1988; The Sou Hills; a barrier to faulting in the central Nevada seismic belt: *Journal of Geophysical Research, B, Solid Earth and Planets, v. 93, p. 475-489*

Gross, M.R., Becker, A., and Gutierrez-Alonso, G., 1997, Transfer of Displacement from Multiple Slip Zones to a Major Detachment in an Extensional Regime: Example from the Dead Sea Rift, Israel, *Geological Society of America Bulletin, v.109, p.1021-1035.*

Hastings, D.D., 1979; Results of exploratory drilling, northern Fallon Basin, western Nevada: in *Basin and Range symposium and Great Basin field conference p. 515-522.*

Hickman, S., Zoback, M., 1996; In situ stress in a fault-hosted geothermal reservoir at Dixie Valley, Nevada: *Proceedings of the eighth international symposium of the continental crust through drilling.*

Honjas, W., 1993; Results of post and pre-stack migrations imaging the Hosgri Fault, offshore Santa Maria Basin, CA :*M.S. Thesis, University of Nevada, 109p.*

Hudson, M.R., Geissman, J.W., 1991; Paleomagnetic evidence for the age and extent of middle Tertiary counterclockwise rotation, Dixie Valley region, west central Nevada: *Journal of Geophysical Research, B, Solid Earth and Planets, v. 96, p. 3979-4006.*

John, David A., 1995; Tilted Middle Tertiary ash-flow calderas and subadjacent granitic plutons, southern Stillwater Range, Nevada: Cross sections of an Oligocene igneous center: *Geological Soc. Am. Bull., v.107, no.2, p.180*

John, David A., 1992; Late Cenozoic volcanotectonic evolution of the southern Stillwater Range, west-central Nevada: *Proceedingsof the Geological Society of Nevada, Walker Lane Symposium, 1992*

Johnson, Maureen G., 1977; Geology and Mineral deposits of Pershing County, Nevada: *Nevada Bureau of Mines and Geology Bulletin 89*

LeBras, R.., Clayton, R.W., 1988, An iterative inversion of back-scattered acoustic waves: *Geophysics, v. 53, p. 501-508.*

Louie, J.N., Clayton, R.W., and Le, B.R.J., 1988, Three-dimensional imaging of steeply dipping structure near the San Andreas Fault, Parkfield, California*: Geophysics, v. 53, p. 176-185.*

Louie, J.N., Qin, J., 1991, Subsurface imaging of the Garlock Fault, Cantil Valley, California: *Journal of Geophysical Research, B, Solid Earth and Planets, v. 96, p. 14,461-14,479.*

Lutz, S.J., Moore, J.N., 1997; Geologic framework of Jurassic reservoir rocks in the Dixie Valley geothermal field, Nevada: Implications from hydrothermal alteration and stratigraphy: *Proceedings, Twenty-second Annual Workshop on Geothermal Reservoir Engineering, Stanford University, Stanford, California 1997.*

Nichols, K.M., 1972, Triassic Depositional History of China Mountain and Vicinity, North-Central Nevada, *Ph.D. Thesis, Stanford University.*

Nosker, S.A., 1981; Stratigraphy and Structure of the Sou Hills, Pershing County, Nevada: *M.S.Thesis, University of Nevada, 60 p.*

Okaya, D.A., Thompson, G.A., 1985, Geometry of Cenozoic extensional faulting: Dixie Valley, Nevada: *Tectonics, v. 4, p. 107-125.*

Oldow, J.S., Bartel, R.L., and Gelber, A.W., 1990, Depositional Setting and Regional Relationships of Basinal Assemblages: Pershing Ridge Group and Fencemaker Canyon Sequence in Northwestern Nevada, *Geological Society of America Bulletin, v.102, p.193-222.*

Page, B., 1964, Geologic Map of a Part of the Stillwater Range, Churchill County, Nevada,

Pullammanappallil, S.K., Louie, J.N., 1993, A Generalized Simulated-Annealing Optimization for Inversion of First Arrival Times: *Bulletin of the Seismological Society of America, v. 84, p. 1397-1409.*

Savage, J.C.L., M.; Svarc, J.L. ; Gross, W.K., 1995, Strain accumulation across the central Nevada seismic zone, 1973-1994: *Journal-of-Geophysical-Research-B-Solid-Earth-and-Planets, v. 100, p. 20257-20269.*

Silberling, N.J., Roberts, R.J., 1962, Pre-Tertiary stratigraphy and structure of northwestern Nevada: *Geol. Soc. America Spec. Paper 72, 58p.*

Silberling, N.J., Wallace, R.E., 1967, Geologic Map of the Imlay Quadrangle, Pershing County, Nevada, *U.S.G.S. Geol. Quad. Map GQ-666.*

_____, 1969, Stratigraphy of the Star Peak Group (Triassic) and Overlying Lower Mesozoic Rocks, Humboldt Range, Nevada, *U.S.G.S Professional Paper 592.*

Silberman, M.L., and McKee, E.H., K-Ar Ages of Granitic Plutons in North-Central Nevada, *Isochron/West, no.1, p.15-32.*

Slemmons, D.B., 1956, Geologic setting for the Fallon-Stillwater [Nev.]: Earthquakes of 1954, in The Fallon Stillwater earthquakes of July 6, 1954, and August 23, 1954: *Seismol. Soc. America Bull., v. 46*

Slemmons, D.B., 1967, Pliocene and Quaternary crustal movements of the Basin-and-Range province, USA [with discussion]: in *Sea level changes and crustal movements of the Pacific during the Pliocene and post Pliocene time. Osaka Univ., J. Geosci., v. 10, p. 91-103.*

Speed, R.C., Jones, T.A., 1969, Synorogenic quartz sandstone in the jurassic mobile belt of western nevada - boyer ranch formation: *Geol. Soc. America Bull., v. 80, p.2551-2584*

Speed, R.C., 1976, Geologic map of the Humboldt Lopolith and surrounding terrane, Nevada: *Geol. Soc. Am., Map Chart Series,Mc-14, p. 4.*

Speed, R.C., 1976, Mesozoic and Cenozoic tectonic evolution of the western Great Basin: Econ. *Geol; 71, v. 3, p. 703.*

Speed, R.C., 1978a, Basinal terrane of the early Mesozoic marine province of the western Great Basin, *in Howell, D.G and McDougall, K., eds., Mesozoic Paleogeography of the Western United States: Society of Economic Paleontoogists and Mineralogists, Pacific Section, Pacific Coast Paleogeography Symposium 2, p.237-252.*

Speed, R.C., 1978b, Paleogeographic and plate tectonic evolution of the early Mesozoic marine province of the western Great Basin, *in Howell, D.G and McDougall, K., eds., Mesozoic Paleogeography of the Western United States: Society of Economic Paleontoogists and Mineralogists, Pacific Section, Pacific Coast Paleogeography Symposium 2, p.253-270.*

Speed, R., Elison, M.W., and Heck, F.R., 1988, Phanerozoic tectonic evolution of the Great Basin: *Rubey colloquium on Metamorphism and crustal evolution of the Western United States, v. 7, p. 573-605.*

Thompson, G.A., Burke, D.B., 1973, Rate and Direction of Spreading in Dixie Valley, Basin and Range Province, Nevada: *Geol. Soc. Am. Bull., Vol.84, No. 2.*

Thompson, G.A., Burke, D.B., 1974, Regional geophysics of the Basin and Range Province: *Annu. Rev. Earth and Planet. Sc., v. 2, p. 213-238.*

Unruh, J.R., Honjas, W., and Pullamannappillil, S., 1998, Re-evaluation of tectonic structure in northern Dixie Valley, Nevada, from re-processed seismic reflection profiles: implications for subsurface permeability; *Proceedings, Twenty-third Annual Workshop on Geothermal Reservoir Engineering, Stanford University, Stanford, California 1998.*

Vetter, U.R., Ryall, A.S., 1983; Systematic change of focal mechanism in the western Great Basin: *Journal of Geophysical Research, v.88, no. B10, p.8237*

Vidale, J.E., 1988, Finite-difference calculation of travel times*: Bulletin of the Seismological Society of America, v. 78, p. 2062-2076.*

Vidale, J.E., 1990, Finite-difference calculation of traveltimes in three dimensions: *Geophysics, v. 55, p. 521-526*

Waibel, A.F., 1987; An overview of the secondary mineralogy of the high temperature geothermal system in Dixie Valley, Nevada: *Geothermal Resource Council Transactions, v.11, October 1987*

Wallace, R.E., 1984a, Patterns and Timing of Late Quaternary Faulting in the Great Basin Province and Relation to some Regional Tectonic Features, *J. Geophys. Res., 89,* 5763-5769.

Wallace, R.E., Whitney, R.A., 1984, Late Quaternary history of the Stillwater seismic gap, Nevada*: Bulletin of the Seismological Society of America, v. 74, p. 301-314.*

Wilden, R., and Speed, R.C., 1974, The Geology and Mineral Deposits of Churchill County, Nevada: Nevada Bureau of Mines and Geology Bulletin 83.

Wernicke, B., 1981, Low Angle Normal Faults in the Basin and Range Province: Nappe Tectonics in an Extending Orogen, *Nature, 291, pp.645-648.*